MOLECULAR PROBES FOR THE DETECTION OF REACTIVE OXYGEN SPECIES

CHEN WEI

(M. Sc.)

A THESIS SUBMITTED

FOR THE DEGREE OF DOCTOR OF PHILOSOPHY

DEPARTMENT OF CHEMISTRY

NATIONAL UNIVERSITY OF SINGAPORE

2013

Declaration

I hereby declare that this thesis is my original work and it has been written by me in its entirety, under the supervision of Associate Prof Huang Dejian, (in the laboratory Food Bioactive Molecules, S13-05-02), Chemistry Department, National University of Singapore, between 4 Aug 2008 and 3 Aug 2013.

I have duly acknowledged all the sources of information which have been used in the thesis.

This thesis has also not been submitted for any degree in any university previously.

The content of the thesis has been partly published in:

1. **Chen, Wei;** Bay, W.-P.; Wong, M.-W.; Huang, Dejian*, Selenium Blue-α and -β: turning on the fluorescence of a pyrenyl fluorophore via oxidative cleavage of the Se–C bond by reactive oxygen species, *Tetrahedron Letters* **2012**, *53*, 3843-3846

Chen Wei	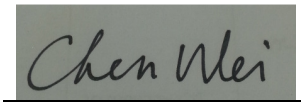	May 14, 2014
Name	Signature	Date

Acknowledgements

First and foremost, I wish to express my sincerest gratitude to my supervisor Professor Huang Dejian, who gave valuable supervision, patient guidance and encouragement throughout the project. I feel honored to have him as my supervisor and have learnt from him his invaluable ideas, profound knowledge, and rich research experience. Without his encouragement, I would not have embarked on my PhD studies.

I also wish to extend my sincere gratitude to NUS research scholarship. The financial support from Science and Engineering Research Council (SERC) of the Agency for Science, Technology and Research (A*Star) of Singapore (Grant Number: 072-101-0015) is greatly appreciated.

Next, I would like to express my sincere gratitude to Professor Wong Ming Wah for his valuable help in the theory calculation of selenium probes. My deepest appreciation to Dr Yao Wei for his help in the synthetic work of benzoxazole-selenium probes and single crystal analysis, and Dr Wang Suhua for his knowledge and expertise in the synthesis of quantum dots. I wish to thank the honours year students Mr Ang Wei Min, Miss Lim Si Ting and Miss Guo Shuen Samantha for their help in doing the synthetic work in the synthesis of molecular probes. Special thanks to Miss Yip Pei Chun for her kind help in the cell imaging laboratory.

Next, I would like to express my heartfelt appreciation to Mr Fu Caili, Miss Quek Yi Ling, Miss Yan Yan and other members of Food Bioactive Molecules group for their advice and assistance rendered throughout the project.

In addition, I would like to express my appreciation to Ms Lee Chooi Lan, Ms Lew Huey Lee, Ms Jiang Xiaohui, and Mr Abdul Rahman bin Mohd Noor for their excellent technical support. I am also grateful to the specialists at NUS Chemical, Molecular and Materials Analysis Centre (CMMAC) for their technical assistance.

Last but not least, I would like to express my sincere appreciation to my parents, my husband, and other family members for their love, their constant

encouragement, and their unwavering support during my PhD studies. From the bottom of my heart, I thank all my friends whose name may not have been mentioned here, but have never hesitated to give me their helping hands whenever I needed help.

Chen Wei

August 2013

Table of Contents

Summary

In the first part of this thesis, design and synthesis of new organoselenium compounds for the detection of ROS were discussed. Four organoselenium probes are included, namely selenium blue-α and -β, benzoxazole selenium, selenium green and selenium-Nile red. Rapid oxidation of non-fluorescent selenium blue-α by hypochlorite yields pyrenylmethanol and turns on blue fluorescence through a Se-C bond cleavage, while slow oxidation of it by excess H_2O_2 leads to pyrenecarboxaldehyde and gives off bluish green fluorescence. Selenium blue-α is a highly selective and sensitive probe for ClO^- detection and its fluorescence can be turned on by the myeloperoxidase (MPO) hypochlorite generation system. The homolog Selenium Blue-β, reacts slower with H_2O_2 and ClO^- giving the same product, vinylpyrene. Benzoxazole selenium (BSe) probe also shows good reactivity and selectivity to ROS. It can react rapidly with one equivalent of ClO^- and generate strong blue fluorescent signals. It has shown some potential in imaging cell membrane oxidative stress.

In the second part, molecularly engineered QDs have been designed and assembled to selectively detect singlet oxygen by the formation of endoperoxides. Polycyclic aromatic hydrocarbon compound dimethylhomoocoerdianthrone (HOCD) was synthesized as it has strong absorbance of visible to NIR light from 550 nm to 700 nm. It has the ability to react with singlet oxygen selectively and gives colorless endoperoxides. CdSe/ZnS core/shell QDs were used as the fluorophore which can give brighter and more stable fluorescence than organic dyes. By grafting the selected polycyclic aromatic hydrocarbons onto the surface of QDs, the fluorescence of QDs can be quenched by Förster resonance energy transfer (FRET). After reacting with singlet oxygen, the efficiency of FRET decreased dramatically and the fluorescence of QDs can be turned on. HOCD shows good selectivity towards singlet oxygen among various ROS. More importantly, the fluorescence of HOCD-QD can be turned on by singlet oxygen.

In an attempt to functionalize the singlet oxygen reactive dye HOCD, a novel addition reaction of amines to polycyclic aromatic hydrocarbon was observed. We unexpectedly discovered amination reaction of $C(sp^2)$-H under mild conditions without the need of any transition metal catalysts. A series of amines react with HOCD easily with high yield. While ethylene diamine and its analogy react with HOCD, extended conjugation system polycyclic aromatic hydrocarbon can be obtained. The reaction condition and mechanism were studied and this reaction provided a new and simple method for the synthesis of NIR molecular probes.

List of Tables

List of Figures

List of Abbreviations

4-ABH	4-aminobenzoic acid hydrazide
ABTS	2,2'-azinobis-(3-ethylbenzothiazoline-6-sulphonate)
ATP	adenosine-5'-triphosphate
ATTA-Eu^{3+}	[4'-(9-anthryl)-2,2':6',2''-terpyridine-6,6''-diyl]bis(methylenenitrilo) tetrakis(acetate)-Eu^{3+}
BODIPY	4,4-difluoro-4-bora-3a,4a-diaza-s-indacene
BSA	bovine serum albumin
CAT	catalase
CBA	coumarin-7-boronic acid
CIE	The International Commission on Illumination
DCFH-DA	dichlorodihydrofluorescein diacetate
DFT	density functional theory
DHE	dihydroethidium
DMAX	9-[2-(3-carboxy-9,10-dimethyl)anthryl]-6-hydroxy-3H-xanthen-3-one

DMEM	Dulbecco's Modified Eagle Medium
DMF	dimethylformamide
DMSO	dimethyl sulfoxide
DNA	deoxyribonucleic acid
mtDNA	mitochondrial DNA
nDNA	nuclear DNA
DPA	9,10-diphenylanthracene
DPAXs	9-[2-(3-carboxy-9,10-diphenyl)anthryl]-6-hydroxy-3H-xanthen-3-ones
EA	ethyl acetate
ED	ethylenediamine
EDC	ethylene dichloride
EDHF	endothelium-derived hyperpolarizing factor
EI	electron ionization
EPO	endoperoxide

ESI	electrospray ionization
ESR	electron spin resonance spectroscopy
FBS	fetal bovine serum
FRET	Förster resonance energy transfer
FTIC	fluorescein isothiocyanate
GPx	glutathione peroxidase
HCD	heterocoerdianthrone
HDA	hexadecylamine
HEPES	4-(2-hydroxyethyl)-1-piperazineethanesulfonic acid
HL-60	human promyelocytic leukemia cells
HOCD	dimethylhomoocoerdianthrone
HPLC	high performance liquid chromatography
IMDM	Iscove's Modified Dulbecco's Medium
LL2	Lewis lung carcinoma cells

MCLA	2-methyl-6-(4-methoxyphenyl)-3,7-dihydroimidazo[1,2-a]pyrazin-3-one hydrochloride
MPO	myeloperoxidase
MS	mass spectrometry
NIR	near-infrared
NMR	nuclear magnetic resonance
N.R.	no reaction
OD	optical density
2-OHE$^+$	2-hydroxyethidium
PBS	phosphate buffered saline
PCM	polarizable continuum model
PDT	photodynamic therapy
PL	photoluminescence
QDs	quantum dots
QY	quantum yield

ROS	reactive oxygen species
SOD	superoxide dismutase
SOSG	Singlet Oxygen Sensor Green®
TBAC	tetrabutylammonium chloride
TBHP	t-butylhydroperoxide
THF	tetrahydrofuran
TOP	trioctylphosphine
TOPO	trioctylphosphine oxide
TPD	N,N'-diphenyl-N,N'-bis(3-methylphenyl)-1,1'-biphenyl-4,4'-diamine
Tris	tris(hydroxymethyl)aminomethane
UV-Vis	ultraviolet–visible

List of Symbols

λ_{em}	emission wavelength
λ_{ex}	excitation wavelength
ΔG	relative free energy
R^2	coefficient of determination
pK_a	acid dissociation constant
pK_b	base dissociation constant
ε	molar extinction coefficient
Φ	fluorescence quantum yield
η	refractive indice

Chapter 1: Introduction

Reactive oxygen species (ROS) include oxygen radicals such as superoxide ($O_2^{\bullet -}$) and hydroxyl radical ($HO^{\bullet}$), and certain nonradicals which are oxidizing agents such as hypochlorous acid (HClO) and hydrogen peroxide (H_2O_2) (***Table 1.1***).[1] They are potent antimicrobial agents due to their strong oxidative damage power.[2] In the meantime, ROS are capable of inflicting oxidative stress to the biological systems and are implicated in aging and the pathology of many conditions, such as cancer, cardiovascular diseases, inflammatory and neurodegenerative diseases.[1,3]

Table 1.1 *Reactive oxygen species produced by phagocytes.* [1]

Free Radicals	**Nonradicals**
Superoxide, $O_2^{\bullet -}$	Hydrogen peroxide, H_2O_2
Hydroxyl, $HO^{\bullet}$	Hypobromous acid, HBrO
Hydroperoxyl, $HO_2^{\bullet}$	Hypochlorous acid, HClO
(protonated superoxide)	Ozone, O_3
Carbonate, $CO_3^{\bullet -}$	Singlet oxygen, $^1O_2$
	Peroxynitrite, $ONOO^-$
	Peroxynitrous acid, ONOOH
	Nitrosoperoxycarbonate, $ONOOCO_2^-$

1.1 ROS in Biological System

Traditionally, ROS have been considered as unavoidable by-products of aerobic metabolism or as the result of exogenous factors such as smoking and air pollution as well as mitochondrial respiration which is believed to be the major intracellular source of accidental ROS.[4, 5] During mitochondrial respiration, a flux of electrons is created by phosphorylation and subsequently used as an energy source for the adenosine-5'-triphosphate (ATP) synthesis.

Through a chain enzymatic complexes (I to IV), electrons are transferred to molecular oxygen (O_2) to form $O_2^{\bullet-}$.[6] Subsequent dismutation of $O_2^{\bullet-}$ by superoxide dismutase (SOD) generates H_2O_2, which produces highly reactive hydroxyl radicals ($HO^{\bullet}$) in the presence of transition metals. Under the catalysis of various peroxidases or metal ions, interconversion of different ROS can take place easily in the physiological conditions (***Figure 1.1***). Alternatively, hydrogen peroxide may be converted into water by the enzymes catalase or glutathione peroxidase. In the glutathione peroxidase reaction, glutathione is oxidized to glutathione disulfide, which in turn can be converted back to glutathione by glutathione reductase in a triphosphopyridine nucleotide (NADPH)-consuming process (***Figure 1.2***). Frequently, different ROS coexist in the reactive environment and make it difficult to identify unequivocally which agent is responsible for a given biological effect.

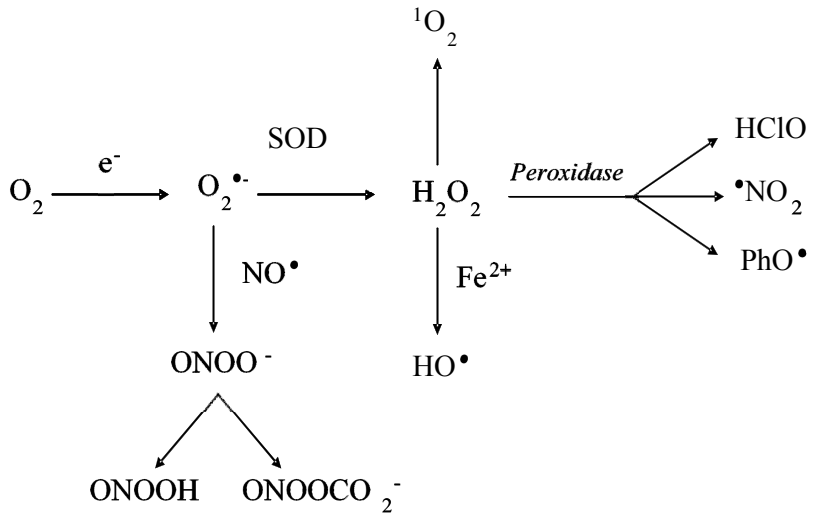

Figure 1.1 *Physiologically relevant ROS.*

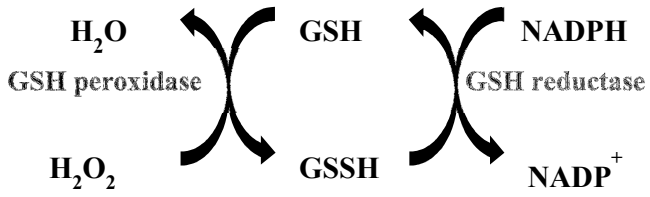

Figure 1.2 *Pathways of ROS clearance. GSH, glutathione; GSSG, glutathione disulfide.*

It is now realized that generation of ROS is a regulated physiological process.[7] In addition to mitochondria respiration, ROS is also generated by various enzymes such as cellular NADPH oxidase (NOXs), xanthine oxidase, nitric oxide synthase and peroxisomal oxidoreductases. Oxidants are also formed in the endoplasmic reticulum during the process of protein folding and disulfide bond formation.[5,8] Many studies have shown that ROS are involved in the redox-dependent regulation of different cellular functions such as energy metabolism and in response to stress or growth signals. For instance, H_2O_2 is directly implicated in the physiological regulation of the signal transduction events which are triggered by activated growth-factor receptors.[9]

Generation of ROS by phagocytes is vital for effective host defence. Large amount of superoxide is produced by NADPH oxidase in phagocytes for use in oxygen-dependent killing mechanisms of invading pathogens. Mutations in the gene coding for the NADPH oxidase cause an immunodeficiency syndrome called chronic granulomatous disease, characterized by extreme susceptibility to infection.[3]

Exposure to free radicals from a variety of sources has led organisms to develop a series of defence mechanisms.[10] There are many defence mechanisms against free radical-induced oxidative stress such as repair mechanisms and enzymatic antioxidant defences. Enzymatic antioxidant defences include superoxide dismutase (SOD), glutathione peroxidase (GPx), catalase (CAT) while non-enzymatic antioxidants are exemplified by ascorbic acid (Vitamin C), α-tocopherol (Vitamin E), glutathione (GSH), carotenoids, flavonoids, and other antioxidants. Under normal conditions, there is a balance between both the activities and the intracellular levels of these antioxidants, which is essential for the survival of organisms and their health.

However, the excessive production of ROS at host tissue will cause oxidative modification of cellular and extracellular components in many conditions.[11] At high concentrations, ROS can be important mediators of damage to cell structures, nucleic acids, lipids and proteins.[12] Oxidative stress has been implicated in various pathological conditions involving cancer, cardiovascular disease, diabetes, neurological disorders and ageing. The

process of ageing is to a large extent due to the damaging consequence of free radical action, such as lipid peroxidation, DNA damage, and protein oxidation.

For example, in various cancer cells, oxidative stress induces a cellular redox imbalance; the redox imbalance thus may be related to oncogenic stimulation. DNA mutation is a critical step in carcinogenesis and elevated levels of oxidative DNA lesions have been noted in various tumors, strongly implicating such damage in the etiology of cancer. To date, more than 100 oxidized DNA products have been identified. DNA damage can result induction of transcription, induction of signal transduction pathways, replication errors, and genomic instability, all of which are associated with carcinogenesis.[13]

In the cases of cardiovascular disease, oxidative stress is associated with increased formation of ROS that modifies phospholipids and proteins leading to peroxidation and oxidation of thiol groups. Mitochondrial creatine kinase activity of rat heart was reported to decrease upon exposure to xanthine plus xanthine oxidase or hydrogen peroxide. Cardiac mitochondria treated with ROS exhibited decreased Ca^{2+} membrane transport, and when it was exposed to 4-hydroxy-2-nonenal a rapid decrease in NAD(P)H state 3 and uncoupled respiration was resulted. In view of these findings, it may be concluded that oxidative stress can alter the activities of different subcellular structures, proteins, and lipids and thus changing myocyte functions.[14]

The process of ageing may be defined as a progressive decline in the physiological functions of an organism after the reproductive phase of life. The free radical theory of ageing was first introduced in 1956 by Denham Harman who proposed the concept of free radicals playing a role in the ageing process.[15] Generally, there are two main theories describing the process of ageing: damage-accumulation theories and genetic theories.[16] As one of the damage accumulation theories, “free radical theory” is based on the fact that the random deleterious effects of free radicals produced during aerobic metabolism cause damage to DNA, lipids, and proteins and accumulate over time. The genesis of ageing starts with oxygen, occupying the final position in the electron transport chain.[17] Even under normal conditions, some electrons

"leak" from the electron transport chain to produce superoxide radicals. Under physiological conditions, about 1–3% of the oxygen molecules in the mitochondria are converted into superoxide. Mitochondrial DNA (mtDNA) is the primary site of radical oxygen damage from such superoxide radical.[18] While the cell repairs much of the damage done to nuclear DNA (nDNA); mtDNA, on the other hand, cannot be readily fixed and over time extensive mtDNA damage shuts down mitochondria, causing cells to die and the organism to age.

1.2 Detection of ROS

Although we are now aware that ROS are capable of inflicting biological damage and are implicated in aging and the pathology of many diseases, effective antioxidant drug has yet been developed and clinical trials of antioxidants have been disappointing. This is perhaps that we do not know enough about mechanisms of oxidant and antioxidant action to design the right interventions.

To figure out the purported multiple roles of ROS as causative agents for oxidative stress, cell signal transduction molecules, and immune response, it is essential to measure ROS accurately. The increasing studies of ROS also need highly specific selectivity ROS detection method. However, this poses a challenge as endogenous ROS are difficult to measure in biological systems because they are produced in small quantities and are relatively unstable. Furthermore, *in vivo* ROS can convert to each other very easily in biological condition (***Figure 1.1***). ROS are also rapidly degraded *in vivo* by interaction with endogenous antioxidants (e.g., superoxide dismutase, catalase, and glutathione) and cellular components such as thiol residues, molecular oxygen, metalloproteins, and other ROS.[2]

Numerous assays provide indirect evidence of ROS activity in biological systems. These indirect indices include changes in endogenous antioxidant levels or an increase in biochemical markers of oxidative damage. For example, indirect evidence of NO synthesis can be obtained by measuring citrulline (a by-product of NO synthesis from L-arginine), NO synthase activity in tissue homogenates, or molecules that serve as second messengers

for NO. Indirect evidence of ROS effects on muscle function has been obtained by testing the effects of anti-ROS enzymes (superoxide dismutase, catalase) and nonspecific antioxidants (thiol donors, spin traps, antioxidant nutrients).[19] Studies using these tools provide complementary information about the actions of ROS. However, none can be used to determine biological production of ROS.

Beside indirect detection methods for ROS, there are few direct detection methods of ROS generation in biological system, which include electron spin resonance spectroscopy (ESR), chemiluminescence and fluorescence assay.

ESR is one of the few techniques that can directly detect molecules with unpaired electrons making it uniquely suited for the measurement of free radicals. The basic principle of ESR involves the exposure of paramagnetic molecules to a magnetic field. This field aligns the magnetic moments of the electron spins of the unpaired electrons in free radicals. Spin traps can be used in conjunction with ESR to identify individual free radical species, enhance the detection of a weak signal, or detect previously undetectable radicals. By binding to specific free radicals producing a more stable radical product that can be detected with ESR. Unfortunately, large concentrations of spin traps are required (10- 100 mM), which may have secondary or non-specific effects unto themselves.[20]

Chemiluminescent probes include luminol, 2-methyl-6-(4-methoxyphenyl)-3,7-dihydroimidazo[1,2-a]pyrazin-3-one hydrochloride (MCLA), and coelenterazine can directly react with ROS and generate luminescence. Chemiluminescence has many advantages such as minute detection limits, speed, ease of use, and simple instrumentation. However the main disadvantage is that presence of impurities can cause a background signal that reduces sensitivity and specificity limits its application. For example, a commonly used chemiluminescence technique for measurement of $O_2^{\bullet-}$ is lucigenin-enhanced chemiluminescence.[21] The validity of this technique has been questioned on the grounds that $O_2^{\bullet-}$ production might be artificially overestimated because of a phenomenon known as redox cycling, in which the lucigenin radical reacts with oxygen to generate $O_2^{\bullet-}$.[22]

Fluorescent probes are most widely used methods either *in vivo* imaging and *in vitro* detection of biomolecules in biological and cell lines; in other words, we can "watch" the behavior of a target biomolecule in living cells in real time. Since the pioneering work on a fluorescent probe for Ca^{2+} was reported by Tsien's group, a variety of fluorescent probes for various biomolecules have been reported to date and some of them have greatly contributed new information related to cellular physiology.[23] They are highly sensitive, fast-responding, easy to handle and capable of giving high resolution image by microscopy. The high sensitivity of detection down to the single molecule by "turn-on" fluorescent probes makes them even more attractive thus fluorescent probes are extensively investigated for imaging and monitoring the ROS generation and trafficking in cells for understanding the mechanisms of ROS action and developing means of controlling the ROS damage.[24, 25]

In the past decade, a number of fluorescent probes have been developed. These new state-of-the-art methods provide new tools for ROS detection. The more commonly used fluorescent probes for ROS included dihydroethidium (DHE), dichlorodihydrofluorescein diacetate (DCFH-DA), 10-acetyl-3,7-dihydroxyphenoxazine (Amplex® Red) and boronate-based probes. The main problems for most fluorescent probes are selectivity and stability. For instance, during the past decades, many researchers used DHE for $O_2^{\bullet-}$ detection, which unfortunately can form two fluorescent products. One is ethidium, which is formed by nonspecific redox reactions, while the other is 2-hydroxyethidium ($2\text{-}OHE^+$), a specific adduct of $O_2^{\bullet-}$. The fluorescence spectra of the two products overlap, therefore it is difficult to use simple fluorescence detection with methods such as confocal microscopy or other fluorescence-based microscopic assays to accurately measure only $2\text{-}OH\text{-}E^+$.[26] Boronate-based fluorescent probes have similar problems. These probes possess a fluorophore that is protected by boronate, and upon exposure to H_2O_2, the boronate undergoes a nucleophilic attack, leading to its removal from the fluorophore and allowing light emission.[27] Some studies show that boronate-based probes such as coumarin-7-boronic acid (CBA) can also react with peroxynitrite

($ONOO^-$) which is generated by overproduction of $O_2^{\bullet-}$ with nitric oxide under inflammatory condition and oxidative stress.[28]

1.3 Key Criteria for ROS Fluorescent Probes

To know better about mechanisms of reactive oxygen species and antioxidant action in biological system, good detection and measuring tools are needed. As a good fluorescent probe for ROS, some criteria are summarized.

- Reactivity and Sensitivity

The probe must be sensitive to the target analytes and sufficiently reactive to compete with intracellular enzymes and other intracellular targets.

- Selectivity

Although probes with less specificity can be used to estimate total ROS production, the probe must have a high degree of specificity to identify specific molecular species. It has become clear that each ROS has its own unique physiological activity. ROS are involved in physiological as well as pathological processes as growth signals, regulators cellular functions and host defence agent. New roles for endogenous NO invigorated research on the elucidation of unknown physiological roles for each ROS. Consequently, novel roles for various ROS have been found such as endothelium-derived hyperpolarizing factor (EDHF) for H_2O_2 and as a second messenger in T cell activation for the hydroxyl radical ($HO^{\bullet}$).[29, 30] For that reason, the development of fluorescent probes capable of detecting a specific ROS with high selectivity is critical to pinpoint the complex ROS chemistry in biological system.

- Optical property

Some optical properties are needed for the fluorescent detection include:

1) High fluorescence intensity. The brightness of the fluorescence emission of a particular fluorophore is proportional to the product of its extinction coefficient and its quantum yield. The brighter the dye, the higher is the sensitivity.

2) Large Stokes shift. Assuming everything else being equal, the wider separation results in higher signal-to-background ratio and increases the overall sensitivity of the detection.

3) Narrow absorption and emission spectra. The absorption and emission spectra of a particular dye usually overlap, resulting in fluorescence quenching. Dyes with smaller spectral overlaps enable multi-color detection of different molecular targets in the same experiment.

4) Good Photostability. Photobleaching is a result of gradual breaking of covalent bonds in the fluorophore molecules upon exposure to intense light. This reduces signal intensity over time and can lead to irreproducible experimental data.

- Turn-on florescence

Comparing with turn-off probes, turn-on fluorescent probes are non- or low-fluorescence, they give strong fluorescence signal while interact with the target analytes. This advantage makes them more important than turn-off probes as the can provide real-time imaging at the site of the ROS generation.

- Biocompatibility

To detect the majority of reactive species, the assay system should have access to the intracellular space since reactivity and charge tend to concentrate endogenous ROS near the sites of synthesis.

In the search of new turn-on fluorescent probes for ROS, two new types of probes are designed and synthesized for the selective detection of ROS, which are organoselenium probes and nanoprobes, a composite of organic chromophores and quantum dots. Each system will be illustrated in detail in this thesis.

Chapter 2: Organoselenium Probes for Ultrasensitive and Selective Detection of Reactive Oxygen Species by Cleaving the Se-C Bond

2.1 Introduction

The image of selenium has changed dramatically over the last century. Initially, it was widely considered very toxic to mammals.[31] After many years studies on selenium deficiency syndromes in experimental animals, selenium biochemistry was emerged when two bacterial enzymes namely formate dehydrogenase and glycine reductase were found containing selenium in 1973.[32] Moreover, the vital role of selenium in biological systems was discovered when selenium is found to be a part of antioxidant enzyme glutathione peroxidase (GPx).[33, 34] Selenium in physiological system can be found in the form of selenocysteine in prokaryotes, formate dehydrogenases, hydrogenases and glycine reductase.[35] It also can bind to a cysteine residue in CO dehydrogenase, of which it forms a redox active center with cofactor-bound molybdenum.[36]

During 1970, increasing number of novel organoselenium compounds and their useful reaction continued to generate more interest in the burgeoning organoselenium research. Recent years, more and more novel functions of selenium in biological systems are discovered, such as anticarcinogenic properties and viral suppression function.[31] In view of its versatility great efforts have been made to the development of synthetic organoselenium compounds that could be used as antioxidants, enzyme inhibitors, anti-infective agents and immunomodulators.[37]

The unique redox properties of selenium are influential in the catalytic activities of organoselenium compounds.[38a] For example, selenium dependent peroxidase, GPx, is a tetrameric enzyme and each of the four identical subunits containing one atom of selenium as a selenocysteine involved in the catalytic activities.[39] GPx utilizes exclusively glutathione (GSH) as reducing substrate to reduce H_2O_2 and a number of bio-organic hydroperoxides

including phospholipid hydroperoxides, fatty acid hydroperoxides, and cholesterol hydroperoxides.[40] The catalytic cycle of GPx involves three steps as shown in ***Figure 2.1***. Selenium center in GPx is utilized in the active center by transferring oxygen from peroxides to give selenol, which is also proposed as the reaction intermediate of GPx mimics including ebselen and its analogues (***Figure 2.1***).[38]

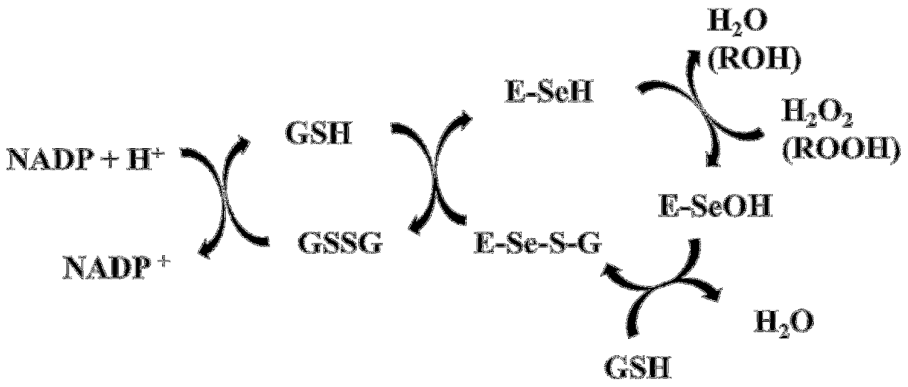

Figure 2.1 *Catalytic cycle of GPx*

The various structures of organoselenium compounds are closely related to their sulfur analogs, but their reactivities are often quite different due to variations on bond lengths, bond strengths, and redox potentials. Selenium forms weaker *C-Se* single bond than sulfur does. The bond dissociation energy of *C-Se* bond is 590.4 kJmol^{-1} whereas that of *C-S* bond is 713.3 kJmol^{-1}.[41a] Many organoselenium reactions, which involve the cleavage of such bonds, take place faster than their sulfurous counterparts and proceed under milder reaction conditions.[41c] The *syn*-elimination of selenoxides was discovered in 1970 and had a major impact on organoselenium chemistry.[41b] This reaction is about three orders of magnitude more rapid than the elimination of the corresponding less polar and less basic sulfoxides. [41a]

In our search of new type turn-on fluorescent probe for ROS, we were inspired by the anioxidative property of organoselenium compounds. We hypothesized that selenium could be a good fluorescent quencher due to its reducing property and large atomic weight (heavy atom effect).[42] To test this

hypothesis, we designed new organoselenium compounds **2.1** and **2.2** containing pyrenyl fluorophores (***Figure 2.2***). When selenium was oxidized to selenoxide, the weak C-Se bond is easy to be cleaved, turning the pyrenyl fluorescence on. We coined a nickname for compound **2.1** and **2.2** as selenium blue probes attributing to the intense blue fluorescence of pyrenyl fluorophores with high quantum yield around 0.4 in water.

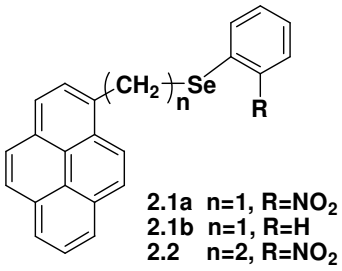

Figure 2.2 *Structures of selenium blue probes*

2.2 Results and Discussion

2.2.1 Synthesis and reactivity of selenium blue-α and selenium blue-β

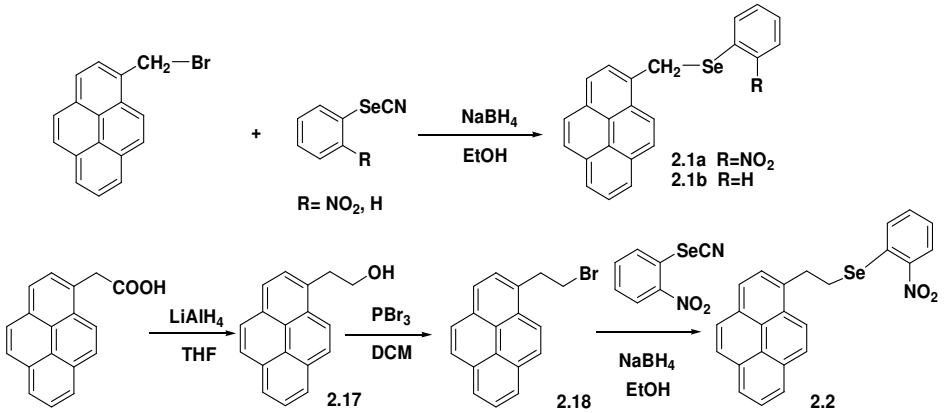

Figure 2.3 *Synthesis of selenium blue probes.*

The organoselenium compound **2.1** and **2.2** were successfully prepared through a simple substitution reaction from corresponding halide and phenyl selenocyanate in the presence of $NaBH_4$ with good yields (***Figure 2.3***).

We named compound **2.1a** as "selenium blue-α" and **2.2** as "selenium blue-β". Selenium blue-α is non-fluorescent likely due to the presence of selenium. The presence of nitrophenyl group may also act as fluorescence quencher. Similarily, the phenyl analogue, **2.1b**, does not give fluorescence, implying the presence of selenium alone is enough to suppress the fluorescence via two possible pathways - either through electron transfer from selenium lone pair to the excited state pyrenyl π orbitals, or heavy atom selenium can facilitate intersystem crossing.[42]

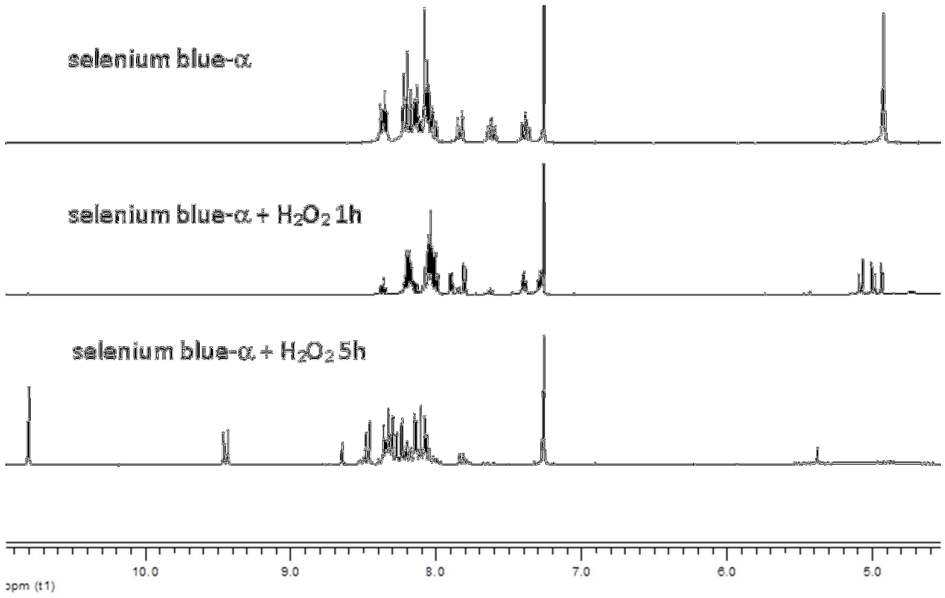

Figure 2.4 *^{1}H NMR of selenium blue-α* ***2.1a*** *and* ***2.1a*** *react with H_2O_2 in $CDCl_3$.*

Reaction of **2.1a** in deuterated chloroform with one equivalent hydrogen peroxide at ambient conditions yielded firstly the oxygenated product **2.3** revealed by ^{1}H NMR spectrum, which has a characteristic AB pattern of the two magnetically inequivalent CH_2 protons at 5.03 ppm due the chiral Se center. As reaction progressed in the presence of excessive H_2O_2, the concentration of **2.3** decreased and new products formed judging from the complex proton NMR signals in the aromatic region. A characteristic singlet showed up at 10.8 ppm indicating an aldehyde proton. (***Figure 2.4***) Indeed, 1-pyrenecarboxaldehyde, **2.4**, was detected by comparing the ^{1}H NMR spectrum

pattern with authentic 1-pyrenecarboxaldehyde. The isolated yield for **2.4** was 85% at preparative scale. (***Figure 2.5***)

The identity of 1-pyrenecarboxaldehyde was further confirmed by EI-MS spectrum, which shows a correct molecular ion peak at *m/z* = 230.0731 for $C_{17}H_{10}O$ (cacld. 230.0732). The Se containing species was identified by MS spectrum as 2-nitrophenylseleninic acid **2.5** (*m/z* = 234, ESI-MS negative mode) with correct isotope distribution for $C_6H_4NO_4Se$. The fluorescence spectroscopy of the diluted reaction solution in water gave an expected strong emission peak (excited at 337 nm) at 470 nm (blue green, ***Figure 2.6***).[43]

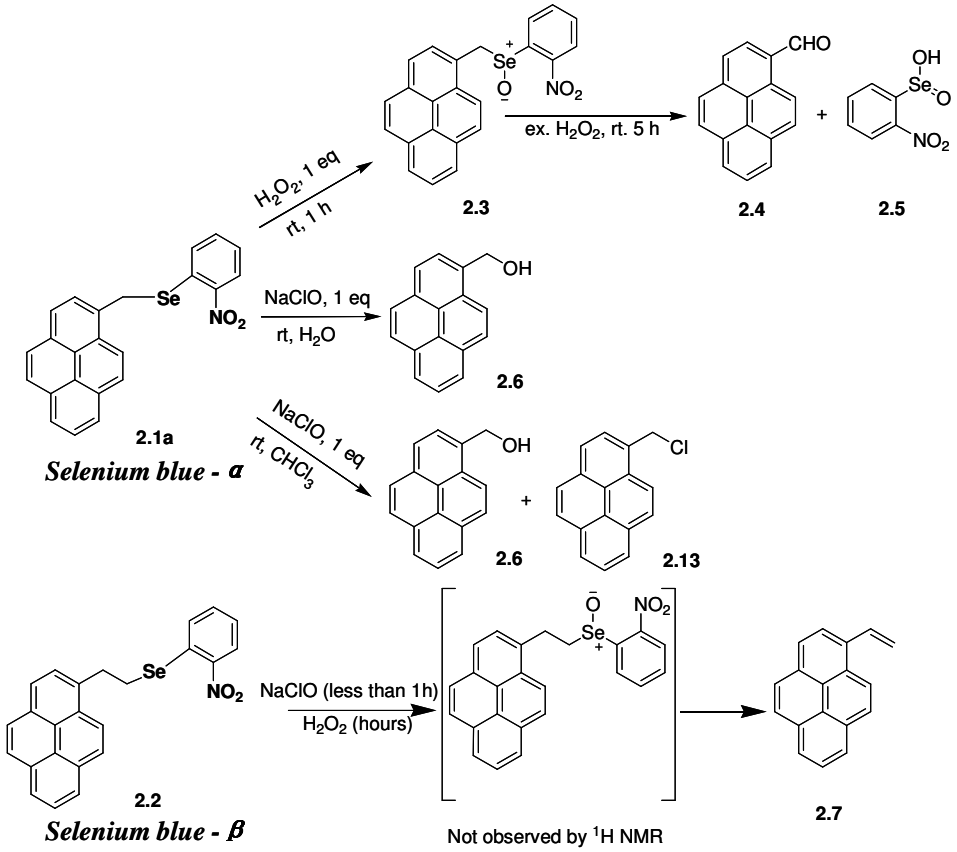

Figure 2.5 *Reaction of* ***2.1a*** *and* ***2.2*** *with hydrogen peroxide and sodium hypochlorite. Solvent: $CHCl_3$ or water.* ***2.1a***, ***2.2*** *and* ***2.3*** *have no fluorescence while* ***2.4***, ***2.6***, *and* ***2.7*** *are highly fluorescent.*

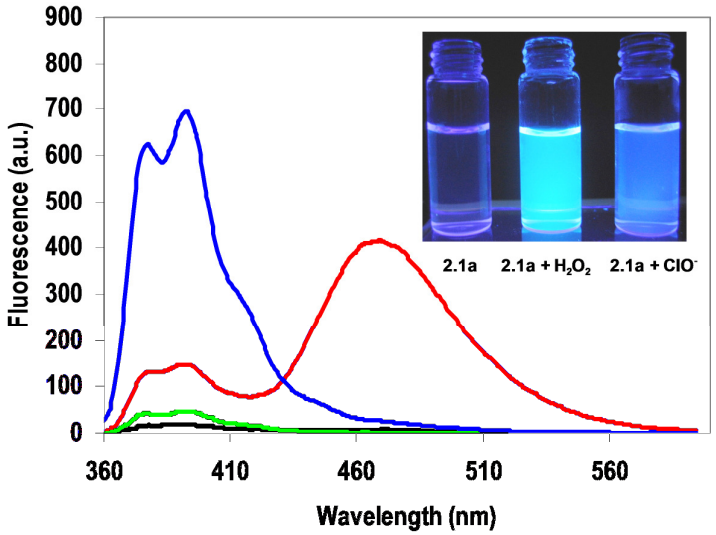

Figure 2.6 *Fluorescence spectra of compound* ***2.1a*** *(black),* ***2.3*** *and* ***2.1a*** *mixture (green),* ***2.1a****+ 1eq NaClO (10 min, blue), and* ***2.1a*** *+ H_2O_2 (10 μM, 5 hours, red) in water. [****2.1a****] = 50 nM, λ_{ex} = 337 nm. The inset is the images of 1 μM of* ***2.1a*** *and its reaction products with ClO^- and H_2O_2 respectively.*

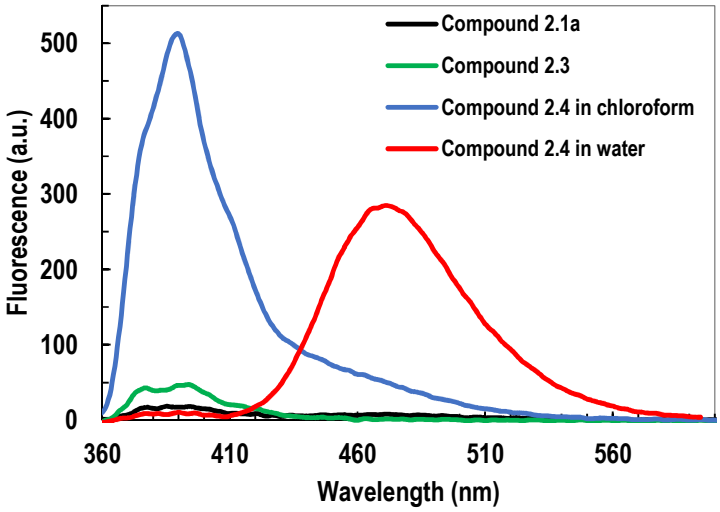

Figure 2.7 *Fluorescence spectra of compound* ***2.4*** *in different solvents.*

The fluorescence behavior of aromatic aldehydes including 1-pyrenecarboxaldehyde **2.4** is highly dependent on the polarity of solvents. In nonpolar solvents such as chloroform, the fluorescence spectrum of structure **2.4** with peaks around 400 nm due to an n-n* transition. However, on increasing the polarity of the solvent media, the π-π level which lies close to the n-π* level, is significantly brought below the n-π* level by solvent relaxation during the lifetime of the excited state. Thus in polar solvents the π-π* state becomes the fluorescence emitting state and a red shift of the λ_{max} can be observed.[44] As such, the fluorescence spectrum of the reaction between selenium blue-α **2.1a** with hydrogen peroxide shows different emission peak in different solvent. For example, the emission band is from 370 nm- 420 nm if the reaction takes place in chloroform, while the emission maximum is at 470 nm if the reaction is in water (***Figure 2.7***).

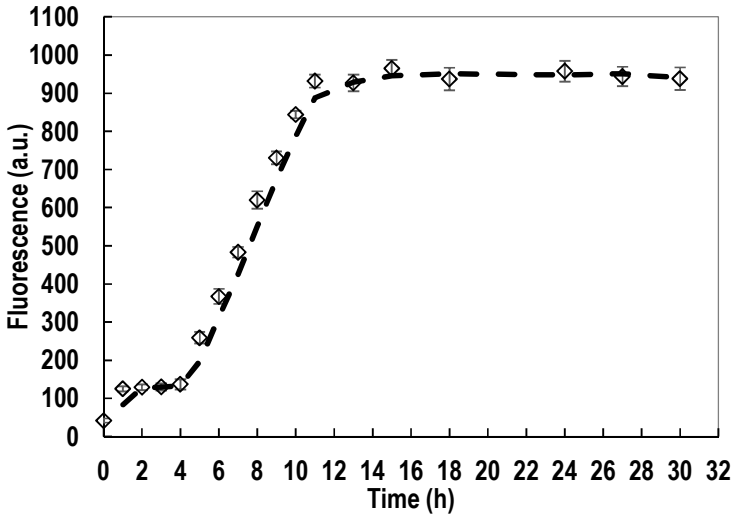

Figure 2.8 *Fluorescence intensity of 0.1 μM compound* ***2.1a*** *reacted with excess H_2O_2 (5 μM) in chloroform (λ_{ex} = 337 nm, λ_{em} = 392 nm)*

The fluorescence of reaction of selenium blue-α **2.1a** with hydrogen peroxide has also been monitored. The fluorescence intensity at 392 nm only increases minimally at the initial stage and then plateaus from one to four hours of the reaction. This phenomenon is in agreement with the NMR finding, as the reaction only forms low fluorescent selenoxide species **2.3**. As the reaction progresses, highly fluorescent aldehyde **2.4** forms and the emission

intensity increases dramatically and reaches the maximum after twelve hours (***Figure 2.8***).

When testing the selectivity of **2.1a** towards different reactive oxygen species, we found that **2.1a** reacted with hypochlorite within minutes at room temperature in water at nM concentration (***Figure 2.9, Figure 2.10***).

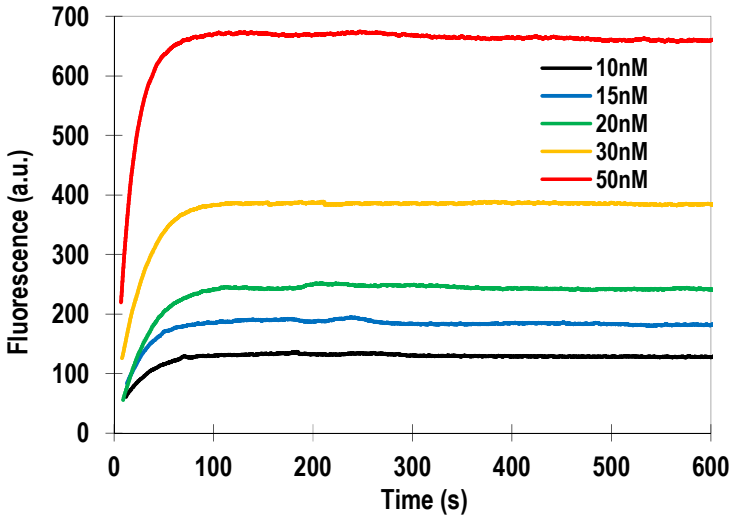

Figure 2.9 *Fluorescence intensity of various concentration compound* ***2.1a*** *react with excess NaClO (6 μM) in water. (λ_{ex} = 337 nm)*

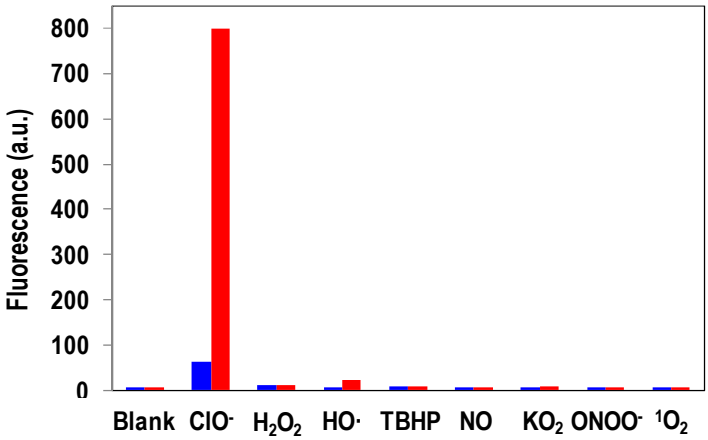

Figure 2.10 *Fluorescence responses of 50 nM* ***2.1a*** *and 1 μM reactive oxygen species (ROS). Bars represent fluorescence intensity at 5 s (blue) and 10 min (red) after the addition of ROS. Data were collected at RT in water, with λ_{ex} = 337 nm and emission at 392 nm. TBHP, t-butylhydroperoxide; $ONOO^-$, peroxynitrite.*

With the attempting to identify the product by NMR using $CDCl_3$ as reaction solvent, to our surprise, the reaction went very slow likely due to the poor solubility of hypochlorite in $CDCl_3$. Nonetheless, after five hours a mixture of chloromethylpyrene **2.13** and pyrenylmethyl alcohol **2.4** were detected by ^{1}H NMR spectroscopy.

The intermediate selenoxide **2.3** was observed in the reaction of selenium blue-α and hydrogen peroxide. In the presence of excess H_2O_2, 1-(hydroperoxymethyl)pyrene, **2.14** might be formed by the nucleophilic substitution and upon elimination,1-pyrenecarboxaldehyde **2.4** was formed (***Figure 2.5***). In our ^{1}H NMR studies, selenium blue-α **2.1a** was treated with H_2O_2 in the presence of tetrabutylammonium chloride (TBAC). During the reaction, the characteristic AB pattern of CH_2 at 5.03 ppm indicated the formation of selenoxide **2.3**. A singlet for the CH_2 proton of chloromethylpyrene (**2.13)** was also found at 5.33 ppm. As the reaction progressed, the selenoxide peak disappeared and that for chloromethylpyrene (**2.13)** increased (***Figure 2.12***). This indicates that selenoxide **2.3** mightly have acted as a good leaving group and was substituted by chloride anion.

In the reaction between selenium blue-α and hypochlorite, selenoxide **2.3** may also play a role as an intermediate. Hypochlorite oxidized probe **2.1a** to selenoxide **2.3** first and was immediately substituted by the chloride anion formed at the site of oxidation to form chloromethyl pyrene. The high concentration of chloride anion generated immediately after oxygen transfer from ClO^- to Se at the site of selenoxide may cause the rapid substitution. This rapid substitution of selenoxide **2.3** may also have caused the observation of the observation of selenoxide intermediate in NMR spectrum to be difficult.

Studies of the stability of chloromethylpyrene **2.13** by HPLC were futile as it is not very stable in aqueous or alcohol solution. The chloride group would be substituted by water or methanol to form pyrenyl methanol **2.6** or methoxymethylpyrene, **2.15** in one hour (***Figure 2.11***). This finding explained why chloromethylpyrene is only been observed in the reaction when chloroform is used as the solvent and not in methanol or water.

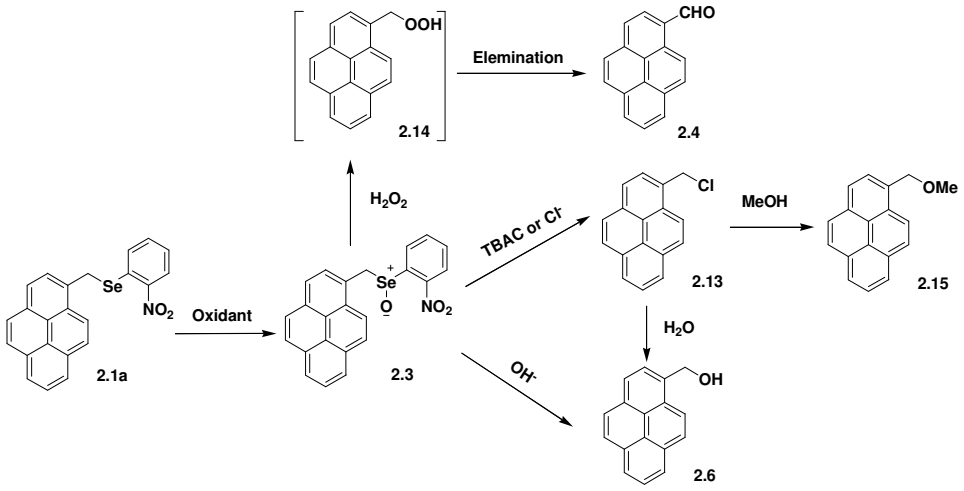

Figure 2.11 *Proposed mechanism of* ***2.1a*** *reacts with hydrogen peroxide and sodium hypochlorite. TBAC = tetrabutylammonium chloride.*

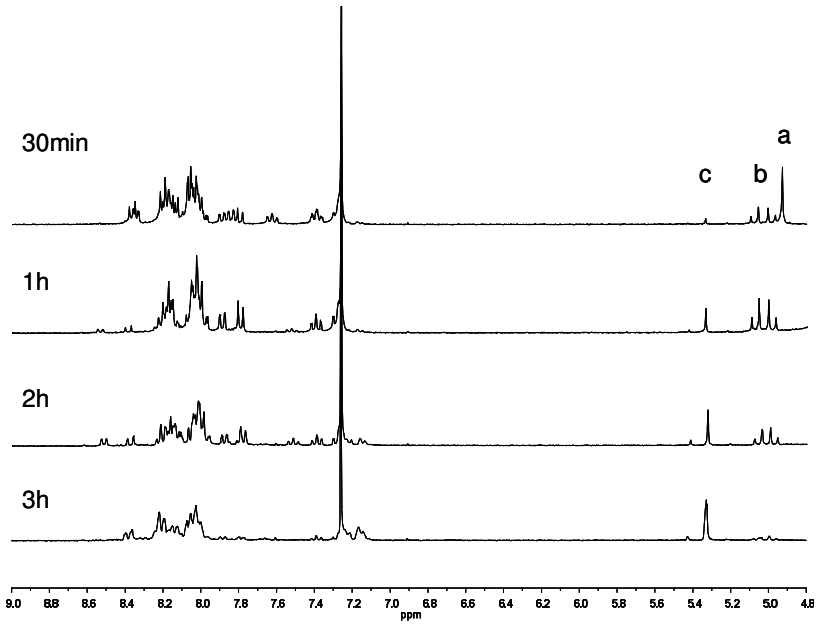

Figure 2.12 *^{1}H NMR of selenium blue-α* ***2.1a*** *reacts with H_2O_2 in the presence of TBAC. (a, b and c represent the CH_2 proton of selenium blue-α, selenoxide and chloromethylpyrene.)*

The pyrenylmethanol **2.6** also shows strong blue fluorescence (***Figure 2.7***). It has two emission peaks, one at 392 nm and the other at 380 nm. This makes selenium blue-α **2.1a** is a highly selective and sensitive probe for rapid detection of ClO^- in PBS buffers or in water (***Figure 2.10***). With molar ratio of 1:1 between **2.1a** and ClO^-, the detection limit can be as low as 5 nM.

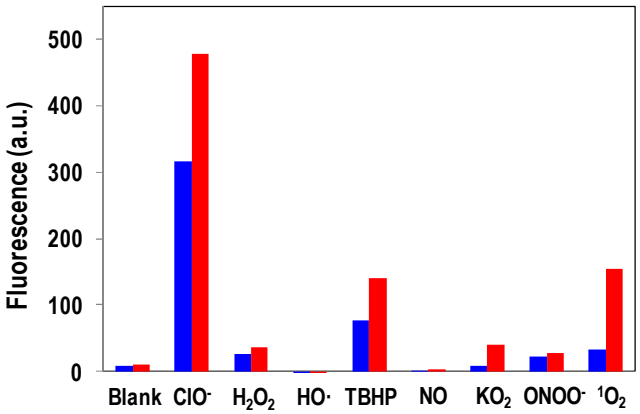

Figure 2.13 *Fluorescence responses of 1 μM* ***2.2*** *on 20 μM reactive oxygen species (ROS). Bars represent fluorescence intensity at 1 h (blue) and 3 h (red) after the addition of ROS. Data were collected at RT in water, with* λ_{ex} *= 365 nm and emission at 390 nm. TBHP, t-butylhydroperoxide; ONOO*$^-$*, peroxynitrite.*

Selenium blue-β, **2.2** has very weak fluorescence and also shows reaction with H_2O_2 and ClO^-, however, it gives rise to different products, vinyl pyrene, **2.7**, possibly through undetectable intermediate selenoxide **2.3** that eliminates ArSe-OH readily (***Figure 2.5***).[45] Comparing with **2.1a**, compound **2.2** showed a relatively slower reaction and took hours to complete. Treatment of **2.2** with different ROS resulted in fluorescence turning on again, a hypochlorite still shows the best response whereas t-butylhydroperoxide (TBHP) and singlet oxygen also turns on the fluorescence but at much less intense signals (***Figure 2.13***).

2.2.2 Influence of biological media on ClO$^-$ detection

Selenium blue-α shows good selectivity and sensitivity towards hypochlorite. However, detection of hypochlorite is not straightforward in biological system as there are many interferences such as the amine groups present in proteins and small organic biomolecules that are reactive towards hypochlorite. The solvents used in *in vitro* detection of hypochlorite may also lead to interferences as some buffer components are amines, such as tris(hydroxymethyl)aminomethane (Tris) and 4-(2-hydroxyethyl)-1-piperazineethanesulfonic acid (HEPES). The amines may react slowly with ClO^- but their high concentration (at mM level) comparing to the probes (at

nM level) have the competitive advantage. We tested the reactivity of selenium blue-α with hypochlorite in various buffer systems and found that the oxidation of the probe was inhibited by the amine containing buffers. (***Figure 2.14***) In pH 7.4 Tris-HCl and HEPES buffers, the conversion of the probe to pyrenyl methanol is only 3% and 23% respectively. The difference between Tris and HEPES may due to the free amino group of Tris which has higher reactivity in the scavenger of hypochlorite. Therefore, one needs to exercise care when choosing a suitable buffer in ROS detection.

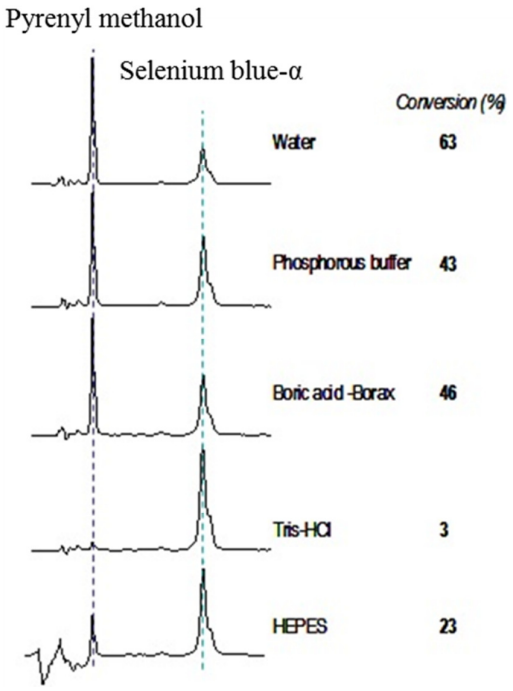

Figure 2.14 *HPLC analysis of selenium blue-α reacts with hypochlorite in water (pH 5.5) and different pH 7.4 buffers. (Concentration of buffer ions: 100 mM).*

2.2.3 Mechanism of the C-Se bond cleavage by hypochlorite

I proposed that oxidative C–Se bond cleavage of **2.1a** involved a two-step process. Firstly, the Selenium in **2.1a** is first oxidized to a selenoxide **2.3**, and the resulting ArSe(O) group becomes a better leaving group, which will be subsequently cleaved in the presence of a nucleophile via substitution. Nucleophilic substitution by H_2O_2 led to unobserved 1-pyrenecarboxylic acid

(Py-CH_2COOH), which decomposed to water and 1-pyrenecarboxyaldehyde (PyCHO, **2.4**). When excess tetrabutylammonium chloride (TBAC) was added to the reaction mixture, there was no PyCHO detected but 1-(chloromethyl)pyrene ($PYCH_2Cl$, **2.13**) was formed as the only product. However, when the reaction was carried out in chloroform, we did not observe the formation of **2.3**. Instead, $PyCH_2Cl$ and 1-pyrenylmethanol ($PyCH_2OH$, **2.6)** were detected. Meanwhile if a nucleophilic solvent was present, products such as methoxymethylpyrene ($PyCH_2OCH_3$ **2.15)** was formed in methanol, and $PyCH_2OH$ was formed in water. I proposed that in the nonprotic solvent such as chloroform, in situ generated Cl^- from ClO^- is a much stronger nucleophile and thus gave rise to $PyCH_2Cl$, which was also found to be reactive towards water (or HO^-) and methanol to give $PyCH_2OH$ and $PyCH_2OCH_3$ respectively.

To further elucidate the mechanism of the reactions of ClO^- with **2.1a** and **2.2**, density functional theory (DFT) calculations were carried out. The calculated relative free energies (ΔG_{298}) of the various reaction pathways are summarized in schematic energy diagrams, as shown in ***Figures 2.15*** and ***2.16***. For both selenium blue derivatives (**2.1a** and **2.2**), the formation of a selenoxide intermediate is the rate-determining step of the overall reaction with ClO^-. This oxidation step is predicted to be strongly exothermic, −195 and −175 $kJ{\cdot}mol^{-1}$ for **2.1a** and **2.2**, respectively. In agreement with the experimental observation, **2.1a** is calculated to have a significantly lower activation barrier of 49 $kJ{\cdot}mol^{-1}$, via transition state **TS1** (cf 84 $kJ{\cdot}mol^{-1}$ in **2.2**, via **TS4**).

Selenoxide intermediate **2.3** can undergo nucleophilic substitution by HO^- or Cl^- to form substitution products **2.6** or **2.13**, respectively. These S_N2 displacement reactions are exothermic and have a moderate energy barrier (**Figure 2.15**). Not surprisingly, HO^- substitution, via **TS2**, is calculated to be more favorable than Cl^- substitution, via **TS3**, both thermodynamically and kinetically. **TS2** has a significantly lower activation barrier than **TS3** (42 kJ mol^{-1}). Hence, we predict that HO^- substitution, leading to pyren-1-ylmethanol **2.6**, is dominant in aqueous medium. This is in excellent accordance with

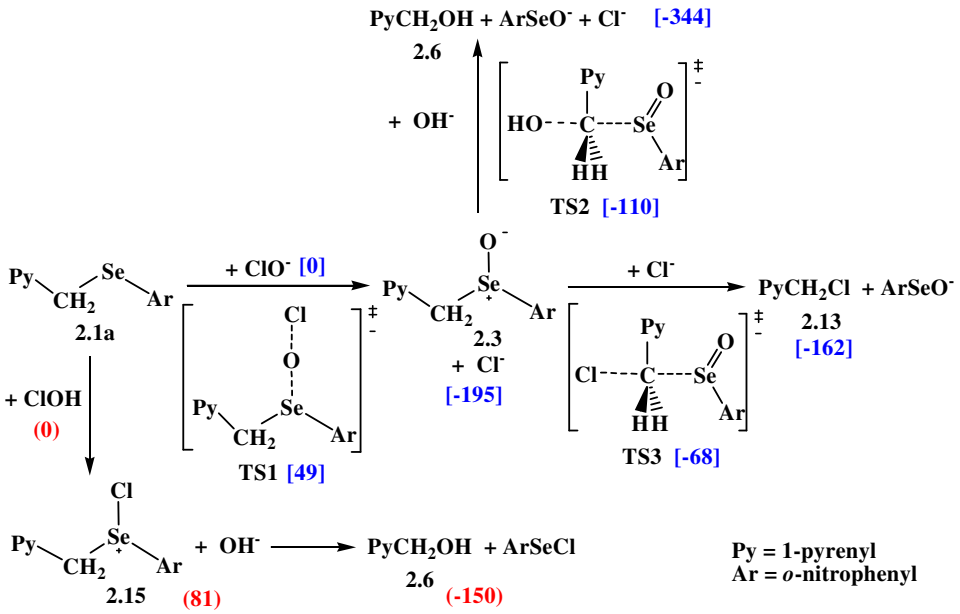

Figure 2.15 *Schematic potential energy diagram showing various reaction pathways of reactions of selenium blue-α (**2.1a**) with ClO^- and HOCl. PCM-B3LYP/6-311+G**//PCM-B3LYP/6-31G* relative free energies (ΔG_{298}) are given in kJ·mol^{-1}. Energies related to ClO^- and HOCl reactions are in square bracket and parenthesis, respectively.*

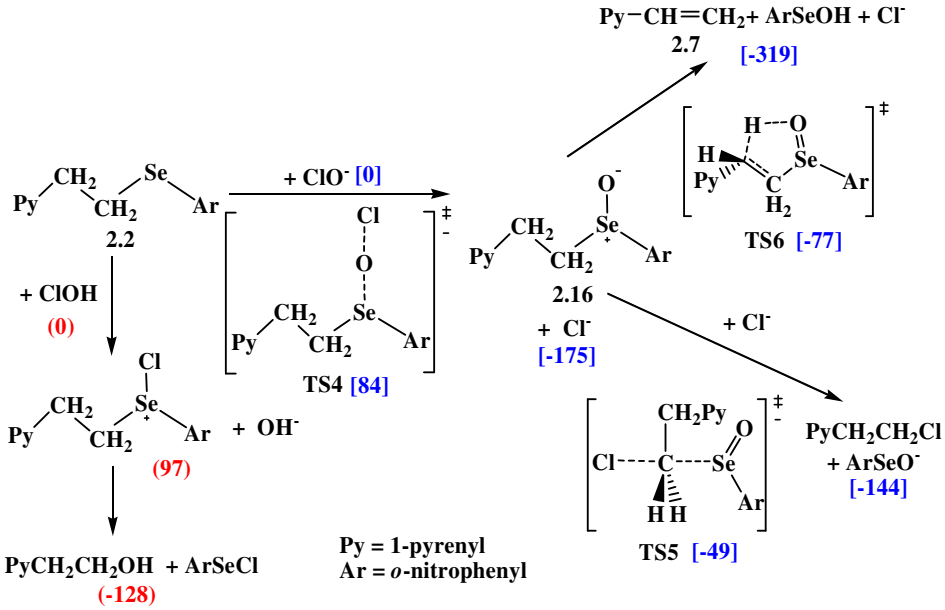

Figure 2.16 *Schematic potential energy diagram showing various reaction pathways of reactions of selenium blue-β (**2.2**) with ClO^- and HOCl. PCM-B310LYP/6-311+G**//PCM-B3LYP/6-31G* relative free energies (ΔG_{298}) are given in kJ·mol^{-1}. Energies related to ClO^- and HOCl reactions are in square bracket and parenthesis, respectively.*

experimental observations. In $CDCl_3$, both **2.6** and **2.13** were observed. In this case, **2.6** is probably formed through reaction of **2.1a** with HOCl, which yields intermediate **2.15** and OH^- (***Figure 2.15***) that are resulted the reaction of 2.1a eoth HOCl. Based on the energies of the intermediates and products, the formation of **2.6** is less favorable than the formation of **2.13**. In the case of **2.2**, selenoxide can readily undergo a well-established Grieco-Sharpless elimination to form vinyl pyrene. [45] This syn elimination reaction is strongly exothermic (–319 $kJ \cdot mol^{-1}$). The calculated activation barrier of 98 $kJ \cdot mol^{-1}$, via a coplanar transition state, is smaller than that of the Cl^- displacement reaction (***Figure 2.16***).

Hence, the formation of vinyl pyrene is calculated to be kinetically and thermodynamically more favorable and in agreement with the experimental findings. These DFT calculations have shed light on the reaction mechanism and confirmed our observation of remarkable reactivity and selectivity of the two organoselenium probes.

Organoselenium-containing fluorescent probes are rare. Previously, an aryl-Se-derived rhodamine probe was reported and used for sensing thiols through substitution of aryl-Se by RS, which turns on the fluorescence; however, the probe was not responsive to reactive oxygen species.[45]

2.2.4 Detection of NaClO concentration and myeloperoxidase activity by selenium blue-α

We further examined the fluorescence response of 0.3 μM selenium blue-α on the hypochlorite concentration, the plot of fluorescence intensity vs. [NaClO] resulted a linear relationship with R^2 value of over 0.999 (***Figure 2.17***). This is in accordance to many organic dyes which typically have one to one stoichiometric ratio when reacting with hypochlorite and result in a linear relationship between [NaClO] and changing in fluorescence.

$$Cl^- + H_2O_2 \xrightarrow{MPO} HClO + OH^- \qquad \textbf{Eq. 2.1}$$

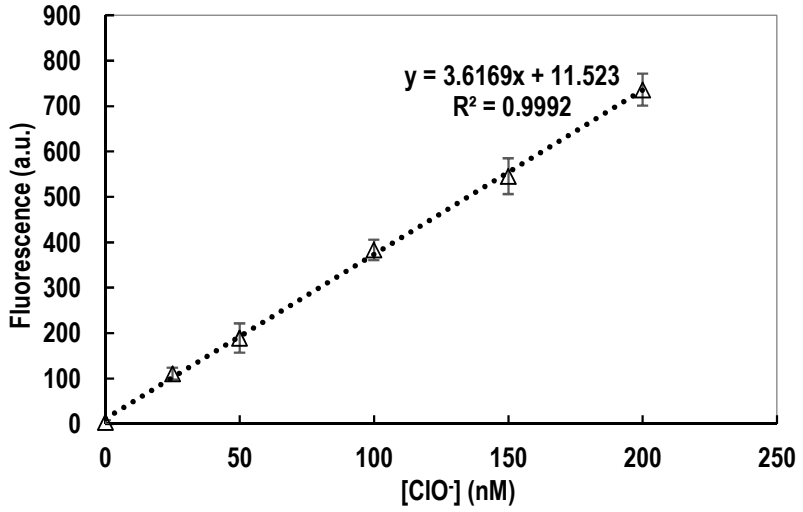

Figure 2.17 *Fluorescent response of 0.3 μM Selenium blue-α* ***2.1a*** *reacted with different concentration of NaClO in water*

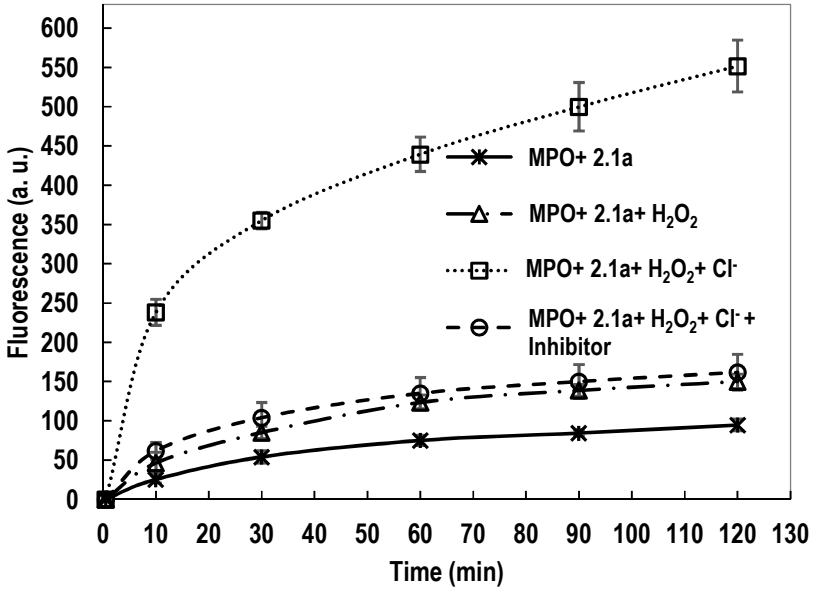

Figure 2.18 *Fluorescent response of 0.4 μM Selenium blue-α* ***2.1a*** *reacted with ClO^- generated by MPO at 37 °C in water. ([MPO] = 0.1UN/mL, [H_2O_2] = 3 μM, [NaCl] = 40 μM) Controlled experiments were conducted by H_2O_2 +MPO and MPO alone to the probe respectively. MPO inhibitor 4-aminobenzoic acid hydrazide (4-ABH) is used as a negative control. (λ_{ex} = 337 nm and emission at 392 nm were recorded)*

With a pK_a of 7.46, hypochlorous acid is present in physiological pH as a mixture of approximately 50% HClO and ClO^- (Here, we use "hypochlorite" refer to this mixture in physiological condition).[47] Hypochlorous acid is well known as household bleach, that remove dyes and stains at certain concentration. It is also a very strong oxidant and disinfectant. Formation of hypochlorous acid from hydrogen peroxide (H_2O_2) and chloride ions (Cl^-) (**Eq. 2.1**) is catalyzed by myeloperoxidase (MPO) that is released by activated phagocytes at sites of inflammation.[48]

The MPO-derived hypochlorite is implicated in the pathogenesis of atherosclerosis and other inflammatory states.[49] The high reactivity of hypochlorite to amino groups or azaaromatics leads the chlorination and oxidation of nucleosides and amino acids which induces DNA, RNA and protein dysfunction.[50] Hence, it is essential to develop a sensitive and selective method for detecting hypochlorite in environmental and biological samples.

The fluorescence of selenium blue-α increases greatly after MPO was incubated with hydrogen peroxide in the presence of chloride anion. To make sure the turn-on fluorescence is indeed induced by hypochlorite, control experiments were done by incubating the MPO-Probe and MPO-Probe-Hydrogen peroxide. Negative control experiment with MPO inhibitor 4-aminobenzoic acid hydrazide (4-ABH) was also carried out.[51] The fluorescence of MPO-Probe-H_2O_2 and negative control shows slightly increase during the reaction. This should be due to the oxidation of the probe by hydrogen peroxide and the selenoxide **2.3** has very weak fluorescence. This suggests that the MPO-generated hypochlorite turned on the fluorescence of the probe successfully (***Figure 2.18***). The reaction was monitored for two hours as longer reaction time may cause the fluorescence turn-on of the probe by hydrogen peroxide (***Figure 2.8***).

2.3 Conclusion

New organoselenium-based fluorescent probes selenium blue-α were designed and synthesized. Rapid oxidation of non-fluorescent selenium blue-α by hypochlorite yielded pyrenyl methanol and turns on blue fluorescence,

while slow oxidation of it by excess H_2O_2 leads to pyren-1-ylaldehyde and gives off bluish green fluorescence. Selenium blue-α is a high selective and sensitive probe for ClO^- detection and the biological hypochlorite generation system MPO-derived ClO^- can turn on the fluorescence of the probe.

However the blue emission wavelength and poor solubility in water of selenium blue-α make it not ideal in imaging of ClO- activity the biological system, especially in the real-time imaging of living cell. Newly designed organoselenium probe with longer emission wavelength will overcome these disadvantages. Future study will be focused on the synthesis and properties of other organoselenium probes in sensing ROS. Moreover, we are interested to embark on the studies on the organoselenium probes with different emission bands that will reveal the quenching mechanism of selenium and reaction mechanisms of organoselenium probes towards hypochlorite.

2.4 Experimental Section

2.4.1 Instruments and Materials

^1H and $^{13}C\{^1H\}$ NMR spectra were recorded in deuterated chloroform with a Bruker AC300 spectrometer (Karlsruhe, Germany) at 300 and 75 MHz, respectively. The electrospray ionization mass spectra were obtained from a Finnigan / MAT LCQ ion trap mass spectrometer (San Jose, CA, USA) equipped with an electrospray ionization (ESI) source. The heated capillary and voltage were maintained at 250 °C and 4.5 kV, respectively. The full-scan mass spectra from *m/z* 50 to 1000 were recorded. LC/MS spectra were acquired using Finnigan/MAT LCQ atmospheric pressure chemical ionization (San Jose, CA, USA) equipped with TSP 4000 HPLC system, which includes UV6000LP PDA detector, P4000 quaternary pump and AS3000 autosampler. High resolution MS spectrum was obtained from Finnigan (MAT 95XL-T) high resolution (60,000), 5KV Double Focusing Reversed Nier-Johnson Geometry Mass Spectrometer. The HPLC analysis was carried out on a Waters HPLC system with a 2996 PDA detector with a C18 column (250 × 4.6 mm, 5 μm, a Shimadzu, Kyoto, Japan). UV-Vis spectra were recorded using a Shimadzu UK1601 spectrophotometer fitted with a quartz cell. Fluorescence analysis was performed using Perkin Elmer LS 55

Luminescence Spectrometer, with excitation/emission slit 10 nm and scan speed 500 nm/min. All solvent used were of reagent grade unless otherwise specified. All chemicals unless indicated were obtained from Sigma Aldrich and used as received.

2.4.2 Synthesis of the organoselenium probes

(2-Nitrophenyl)(pyren-1-ylmethyl)selane, 2.1a: To a suspension of *o*-nitrophenyl selenocyanate (38 mg, 0.17 mmol) in 5.0 mL anhydrous methanol in a two necked round bottom flask under nitrogen, sodium borohydride (7.0 mg, 0.19 mmol) was added. The reaction solution turned dark brown. 1-(Bromomethyl)pyrene (50 mg, 0.17 mmol) was added and the reaction was stirred at r.t. Twenty hours later, the yellow solid in the reaction was filtered and washed by ethanol to give compound **2.1a** (60 mg, 85%). EI-MS for $C_{23}H_{15}NO_2Se$: 417.1. ^{1}H NMR (300 MHz, $CDCl_3$): δ = 8.34 (d, *J* = 1.3 Hz, 1H), 8.21 (d, *J* = 7.6 Hz, 1H), 8.00-8.17 (m, 8H), 7.83 (d, *J* = 8.1 Hz, 1H), 7.62 (td, *J* = 1.5 Hz, 8.1 Hz, 1H), 7.38 (td, *J* = 1.5 Hz, 7.8 Hz, 1H), 4.92 (s, 2H). ^{13}C{^{1}H} NMR (75 MHz, $CDCl_3$): δ = 145.8, 134.7, 133.6, 130.8, 130.5, 130.4, 130.3, 129.6, 128.7, 128.5, 127.7, 127.4, 126.4, 126.2, 125.4, 125.3, 125.0, 124.2, 123.8, 123.5, 28.5.

Phenyl(pyren-1-ylmethyl)selane, 2.1b: Procedure is similar to that of **2.1a** with 75% isolated yield. EI-MS for $C_{23}H_{16}Se$: 372.1. ^{1}H NMR (300 MHz, $CDCl_3$): δ = 8.31 (d, *J* = 9.2 Hz, 1H), 8.00-8.20 (m, 8H), 7.76 (d, *J* = 7.7 Hz, 1H), 7.49-7.72 (m, 2H), 7.22-7.28 (m, 2H), 4.85 (s, 2H). ^{13}C{^{1}H} NMR (75 MHz, $CDCl_3$): δ = 134.0, 132.0, 131.3, 130.9, 130.7, 129.0, 128.7, 127.7, 127.5, 127.2, 126.0, 125.1, 124.8, 124.6, 123.3, 30.5.

2-(1-Pyrenyl)ethanol, 2.17: To a suspension of $LiAlH_4$ (113 mg, 3.0 mmol) in 5.0 mL THF was added a solution of (1-pyrenyl)acetic acid (195 mg, 0.75 mmol) in THF under a N_2 atmosphere. After stirring for 30 min at room temperature, methanol and 10% sulfuric acid was added to the reaction. The mixture was extracted with ether and the ethereal solution was washed with brine and dried over Na_2SO_4. The solvent was removed to give the crude product which was purified by a silica gel column chromatography with dichloromethane to give 2-(1-pyrenyl)ethanol (165 mg, 89%) as yellow solid.

^{1}H NMR (300 MHz, $CDCl_3$): δ = 8.30 (d, *J* = 9.2 Hz, 1H), 7.98-8.19 (m, 7H), 7.91 (d, *J* = 7.8 Hz, 1H), 4.10 (t, *J* = 6.8 Hz, 2H), 3.63 (t, *J* = 6.8 Hz, 2H).

1-(2-Bromoethyl)pyrene, 2.18: Phosphorus tribromide (0.15 mL, 1.6 mmol) was added drop wise to a solution of 2-(1-pyrenyl)ethanol (160 mg, 0.65 mmol) in dichloromethane (10 mL) at 0 ºC. The reaction was allowed to gradually warm to r.t. and stirred for 24 hr. before being cooled and quenched with saturated $NaHCO_3$. The mixture was extracted with dichloromethane and the organic layers pooled and dried over Na_2SO_4. Evaporation under reduced pressure gave crude product which was purified by a silica gel column chromatography with ethyl acetate and hexane to give 1-(2-bromoethyl)pyrene (100 mg, 50%) as yellow solid. ^{1}H NMR (300 MHz, $CDCl_3$): δ = 8.21-8.26 (m, 5H), 8.00-8.19 (m, 3H), 7.90 (d, *J* = 7.9 Hz, 1H), 3.91 (t, *J* = 8.4 Hz, 2H), 3.77 (t, *J* = 8.4 Hz, 2H). EI-MS for $C_{18}H_{13}Br$: *m/z* 308.0.

(2-Nitrophenyl)(2-(pyren-1-yl)ethyl)selane, 2.2: To a suspension of *o*-nitrophenyl selenocyanate (38 mg, 0.17 mmol) in 5 mL anhydrous methanol in a two necked round bottom flask under nitrogen, sodium borohydride (7.0 mg, 0.19 mmol) was added. The reaction solution turned dark brown. 1-(2-Bromoethyl)pyrene (52 mg, 0.17 mmol) was added and the mixture was stirred at r.t. for 24 hrs. before the solvent was removed under reduced pressure. The residue was purified by a silica gel column chromatography with ethyl acetate and hexane to give **2.2** (30 mg, 41%) as yellow solid. ^{1}H NMR (300 MHz, $CDCl_3$): δ = 7.99-8.28 (m, 9H), 7.92 (d, *J* = 7.8 Hz, 1H), 7.49 (dd, *J* = 1.2 Hz, 8.1 Hz, 1H), 7.37 (td, *J* = 1.5 Hz, 7.2 Hz, 1H), 7.23 (td, *J* = 1.2 Hz, 7.8 Hz, 1H), 4.92 (s, 2H). EI-MS for $C_{24}H_{17}NO_2Se$: *m/z* 431.1.

2.4.3 General conditions for detection of various ROS by fluorescence spectroscopy

A probe solution of was prepared by dilution of a methanol solution of probes with water. Reactive oxygen species includes H_2O_2, *t*-butylhydroperoxide (TBHP), and sodium hypochlorite (NaClO) were diluted from the commercially available solution to 1.0 mM in water. Peroxynitrite and nitric oxide were prepared in-house according to established procedures.[52] $^1O_2$ was generated via irradiation of rose Bengal.[53] Hydroxyl radical was

generated by Fenton reaction. Nitric oxide gas was generated by reacting ascorbic acid with sodium nitrite and by purifying with sodium hydroxide and molecular sieves before passing through de-aerated water under inert atmosphere.[54] The content of nitric oxide in the resultant solution was estimated by colorimetric method using ammonium 2,2'-azinobis-(3-ethylbenzothiazoline-6-sulphonate) (ABTS) as an indicator.[55] All reactions were carried out at r.t. The fluorescence was excited at 337 nm and the emission intensities at 392 nm were recorded before ROS addition and 5 s and 10 min after the addition of ROS.

2.4.4 Computation details for the DFT calculations

The density functional theory (DFT) calculations were carried out according to literature.[56] The condense-phase reactions were investigated by an implicit model of water via the polarizable continuum model (PCM).[57] Geometry optimizations were performed with hybrid B3LYP functional in conjunction with 6-31G* basis set in water solvent (ε = 78.4).[58] Higher-level relative energies were computed at PCM-B3LYP/6-311+G** level based on the PCM-B3LYP/6-31G* optimized geometries. Vibrational analysis was performed to verify the nature of stationary points as local minima or transition states. The condense-phase reactions were investigated by an implicit model of water via PCM. The key intermediates coordination parameters and the energy level are shown in appendices.

2.4.5 Detection of NaClO concentration

The standard curve for hypochlorite detection was prepared as follows: Selenium blue-α solution (10.0 μM) was diluted in water at a final concentration of 300 nM. A series of concentrations of sodium hypochlorite (0, 25, 50, 100, 150 and 200 nM) were obtained by dilution and mixed with selenium blue-α solutions with a final volume of 3.0 mL. The fluorescence intensities were measured before and 5 min after the addition of NaClO stock solutions

2.4.6 Myeloperoxidase (MPO) activity measurement

Selenium blue-α **2.1a** was incubated with MPO 37 °C in the presence or absence of H_2O_2 and the fluorescence intensity was measured. For the MPO inhibition experiment, **2.1a** solution was incubated with MPO, H_2O_2 and NaCl in the presence of 4-ABH, a known MPO inhibitor. The spectrofluorometer was maintained at 37 °C with a water circulator during the incubations and fluorescence measurements.

Chapter 3: Reaction-based Organoselenium Probe for Fluorescence Imaging Intracellular Oxidative Stress

3.1 Introduction

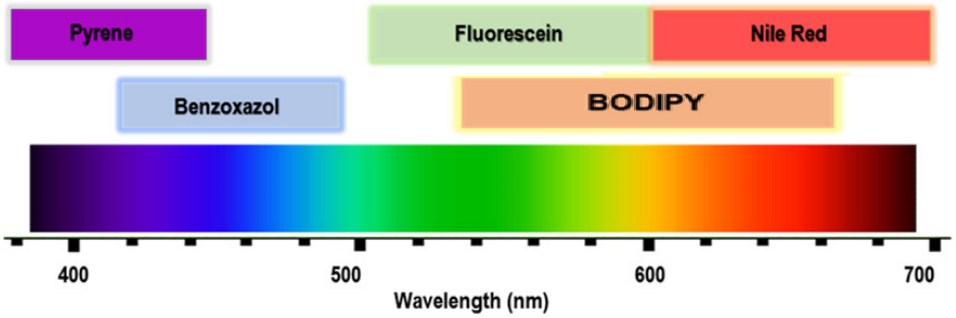

Figure 3.1 *Fluorescent groups chosen for the organoselenium probes.*

To overcome the short pyrene emission wavelength of selenium blue-α, other fluorescent groups with longer emission bands are designed for new organoselenium probes, such as benzoxazole, fluorescein, 4,4-difluoro-4-bora-3a,4a-diaza-*s*-indacene (BODIPY) and Nile red fluorophores (***Figure 3.1***).

Compounds with benzoxazole structural motifs are receiving much attention as therapeutic agents and optical-electronic materials.[59] The benzoxazole ring exhibits noteworthy luminescent properties and the extended configurations have been characterized by optical absorption and emission spectroscopy. Solutions of benzoxazole analogues fluoresce strongly and exhibit emission spectral profiles, which mirror their respective excitation spectra.[60] Based on a previous research done in our group, a novel synthetic method is well established for benzoxazoles, with tolerance for a wide range of functional groups.[61] It involves the one-pot reaction between *o*-nitrosophenol and alkyl bromide to form the benzoxazole ring in reportedly high yields. As such, it opens up a potential mild route to synthesize benzoxazole compounds, which can be tapped upon to serve as fluorescent probes (***Figure 3.2***).

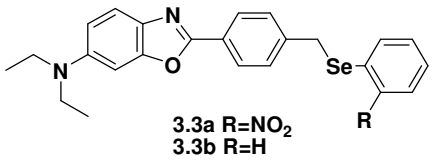

Figure 3.2 *Structures of BSe probes*

Fluorescein is one of the most widely used dyes in biological study, especially in labeling and tracking cells in fluorescence microscopy applications. It has an absorption maximum at 494 nm and emission maximum of 521 nm (in water) which is a typically green fluorescence, with a quantum yield over 0.9 at pH > 8.[62] The sodium salt of fluorescein, is used extensively as a diagnostic tool in the field of ophthalmology and optometry, where topical fluorescein is used in the diagnosis of corneal abrasions, corneal ulcers and herpetic corneal infections.[63] There are many fluorescein derivatives used as fluorescence probe. One of the most famous probes is fluorescein isothiocyanate (FITC) (***Figure 3.3***). FITC is the fluorescein molecule functionalized with an isothiocyanate reactive group (-N=C=S) that is reactive towards nucleophiles including amine and sulfhydryl groups. It is widely used to attach a fluorescent label to proteins via the amine group. The isothiocyanate group reacts with amino terminal and primary amines in proteins. It has been used for the labeling of proteins including antibodies and lectins. Based on the novel synthesis route for fluorescein, selenium green was designed with the structure **3.9** as shown in ***Figure 3.3***.

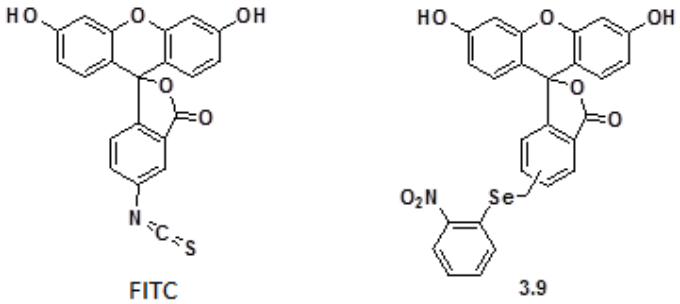

Figure 3.3 *Structure of FITC and designed selenium green probe.*

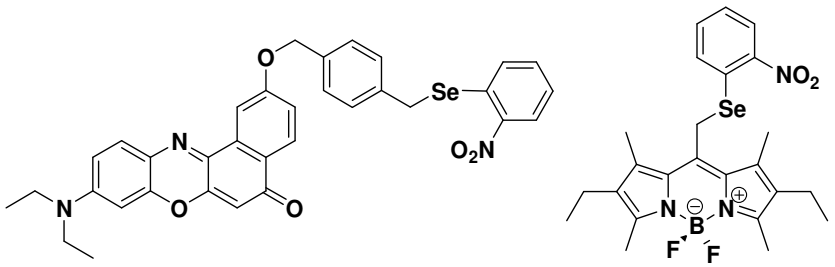

Figure 3.4 *Structure of designed selenium-Nile red and selenium-BODIPY probe.*

Organoselenium probes with even longer wavelength which emit red fluorescence are designed as "selenium red" (***Figure 3.4***). Two types of dyes are involved including 9-diethylamino-5H-benzo[alpha]phenoxazine-5-one (Nile red) and 4,4-Difluoro-4-bora-3a,4a-diaza-*s*-indacene (BODIPY) dyes. Nile red (also known as Nile blue oxazone) has been used in cell biology as a membrane dye which can be readily visualized using an epifluorescence microscope with excitation and emission wavelengths usually shared with red fluorescent protein.[64] BODIPY fluorophore has a high extinction coefficient (>80 000 cm^{-1} M^{-1}), a high fluorescence quantum yield (approaching 1.0), and its derivatives are relatively insensitive to the polarity and pH of their environment and hence are reasonably stable to physiological conditions. Small modifications to their structures enable tuning of their fluorescence characteristics; adapting, these dyes are widely used to label various proteins and DNA sequences.[65] Both Nile red and BODIPY dyes emit orange to near infra-red fluorescence (550- 700 nm). The designed selenium red probes are shown in ***Figure 3.4***.

In this chapter, new organoselenium probes BSe (**3.3a**, **3.3b**), selenium green (**3.9**) and selenium red (**3.12**, **3.13**) were designed. Their sensitivity and selectivity towards ROS were examined. In addition, applications on ROS imaging were explored.

3.2 Results and Discussion

3.2.1 Synthesis and structure of BSe probe

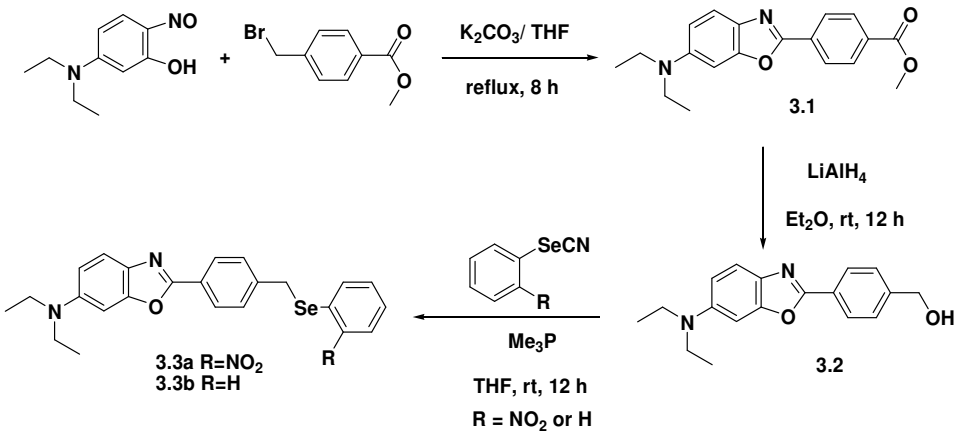

Figure 3.5 *Synthesis of benzoxazole derived selenium probes.*

One-pot reaction of 2-nitrosophenol with bromoalkylbenzoate under mild conditions yielded the coupled product benzoxazole (**Compound 3.1**). $LiAlH_4$ subsequently reduces the ester moiety of **3.1** in an inert environment to form benzoxazole phenylmethanol **3.2**. The alcohol group was reacted with nitrophenyl selenocyanate or phenyl selenocyanate in the presence of trimethylphosphine to attach an aryl selenium moiety to the benzoxazole, forming compounds **3.3a** and **3.3b** respectively (***Figure 3.5***). The structure of compounds **3.2** and **3.3a** are were well characterized by ^{1}H, ^{13}C NMR spectroscopy and mass spectra. The structures of **3.2** and **3.3a** were further verified by X-ray crystallography (***Figure 3.6***).

The X-ray crystal structures of compounds **3.1**, **3.2** and **3.3a** obtained showed the conjugated ring system between benzene and the oxazole to be co-planar. ***Table 3.1*** shows the selected bond lengths and angles of heteroatoms in the compounds. Expectedly, bond lengths of C=N (C1-N1: 1.292-1.296Å) while the bond length of sp^3C-N (C7-N1/C2-N1) of approximately 1.400Å and C-O of the oxazole of all three compounds fall within the normal range as predicted. Further examination of the bond angles around the nitrogen atom in the

oxazole (C1-N1-C7/C1-N1-C2) revealed an approximate angle of 104°, indicating a bent conformation. The observed bond length of sp^3C-Se of

Table 3.1 *Selected bond lengths and angles for compounds* ***3.1****,* ***3.2*** *and* ***3.3a***

Compound 3.1			
Bond angle (°)		**Bond length (Å)**	
C1-O1-C2	103.71	C1-O1	1.382
C1-N1-C7	104.03	C1-N1	1.294
C4-N2-C10	121.88	C4-N2	1.382
C12-C1-N1	127.74	C7-N1	1.402
N1-C1-O1	115.44		
O2-C18-O3	123.08		
Compound 3.2			
Bond angle (°)		**Bond length (Å)**	
C1-O1-C2	104.01	C1 - O1	1.380
C1-N1-C7	104.58	C1-N1	1.292
C4-N2-C10	121.56	C2 -O1	1.379
C12-C1-N1	127.76	C4 - N2	1.373
N1-C1-O1	114.86	C7 - N1	1.398
O2-C18-C15	112.94	C18 - O2	1.420
Compound 3.3a			
Bond angle (°)		**Bond length (Å)**	
C1-O1-C7	104.00	C1-O1	1.388
C1-N1-C2	104.70	C1-N1	1.296
C5-N2-C8	121.40	C2-N1	1.394
C18-Se1-C19	101.07	C5-N2	1.385
C19-C24-N3	120.50	C18-Se1	1.969
O2-N3-O3	123.70	C19-Se1	1.907
		C24-N3	1.468
		O2-N3	1.225
		O3-N3	1.222

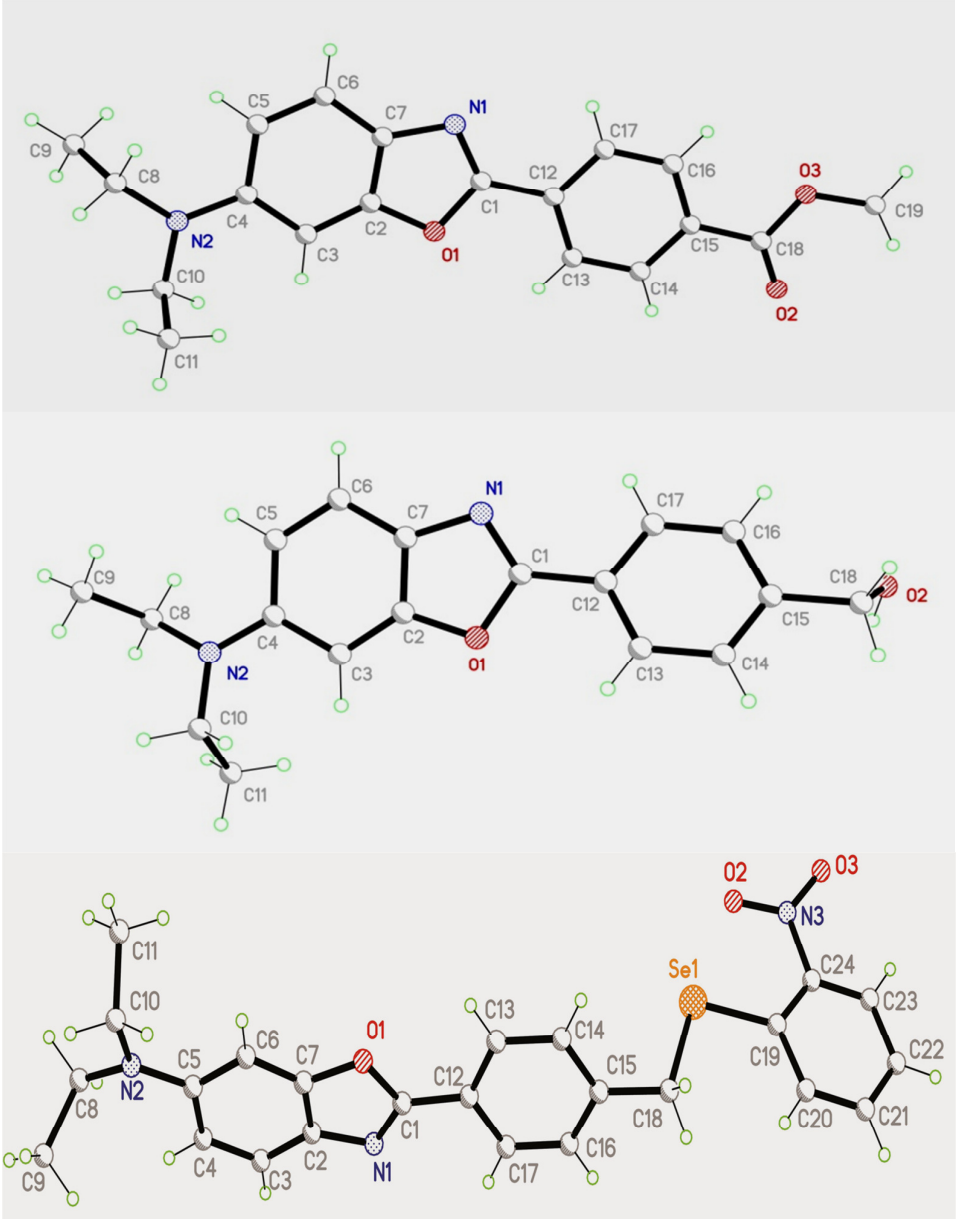

Figure 3.6 *X-ray crystal structure of compound* ***3.1*** *(upper),* ***3.2*** *(middle) and* ***3.3a*** *(bottom).*

compound **3.3a** (see C18-Se1: 1.969Å) is longer than sp^2C-Se bond in the aromatic nitrobenzene ring (see C19-Se1: 1.907Å), implying the selenium moiety was successfully attached to the benzoxazole ring as predicted. All three compounds each have unit-cells that do not bear equal dimensions. Compound **3.1** and **3.3a** show triclinic system where all three vectors are not

mutually orthogonal. Compound **3.2** on the other hand exhibits a monoclinic system where two pairs of vectors are perpendicular.

3.2.2 Optical property, reactivity and selectivity of BSe probes

The UV-Vis absorption spectrum of probe **3.3a** exhibits a maximum absorption at 375 nm while **3.3b** has a slight red shift to 380 nm. Both probes showed almost no fluorescence emission upon excitation at 363 nm. Upon addition of one equivalent ClO^-, the emission intensity of **3.3a** increases significantly. This enhancement can be explained by the formation of the strongly luminescent compound **3.4** which was confirmed by HR-ESIMS (positive mode, $[M+H]^+$ $C_{19}H_{23}N_2O_2$: cacl. 311.1754, found 311.1742). The oxidative Se-C cleavage of BSe probe **3.3a** by hypochlorite is in the same way as in selenium blue-α (***Figure 3.7***). The reactivity of BSe **3.3a** with hypochlorite was monitored by the fluorescence intensity changes of trating 60 nM **3.3a** with one equivalent hypochlorite after one minute (***Figure 3.8***). An emission light around 470 nm appeared due to the oxidative cleavage of Se-C bond of the probe. The observed fluorescent emission intensity increased to more than five times than that of the initial intensity at 5 min. At 30 min, the fluorescent emission intensity increased peaked at 470 nm. Comparing to **3.3a**, the reactivity of BSe probe **3.3b** with hypochlorite is much less. While **3.3b** was treated with hypochlorite, the fluorescence increase was very limited (***Figure 3.9***). This could be due to the strong electron withdrawing *ortho*-nitro group of **3.3a**, which makes the selenium attached to a more electron deficient carbon and the C-Se bond is much easier to cleave comparing to the non-nitro substituted probe **3.3b**.

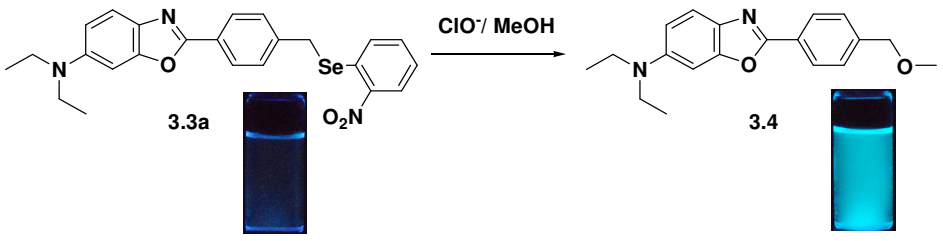

Figure 3.7 *Oxidative C-Se cleavage of BSe probe* ***3.3a*** *by NaClO in methanol.*

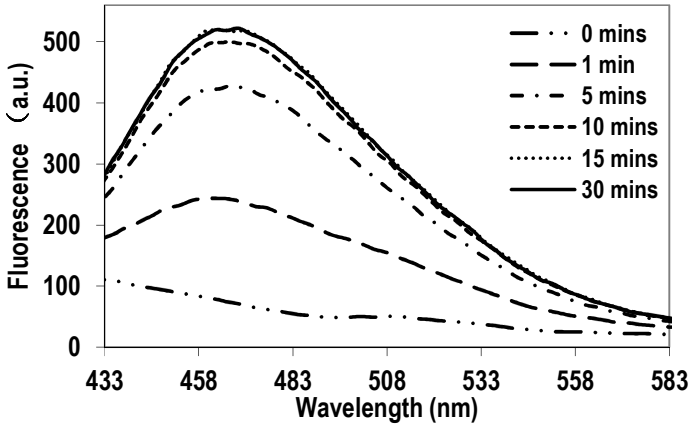

Figure 3.8 *Fluorescence responses (λ_{ex} = 363 nm) of 60 nM probe* ***3.3a*** *upon the addition of 60 nM NaClO in methanol.*

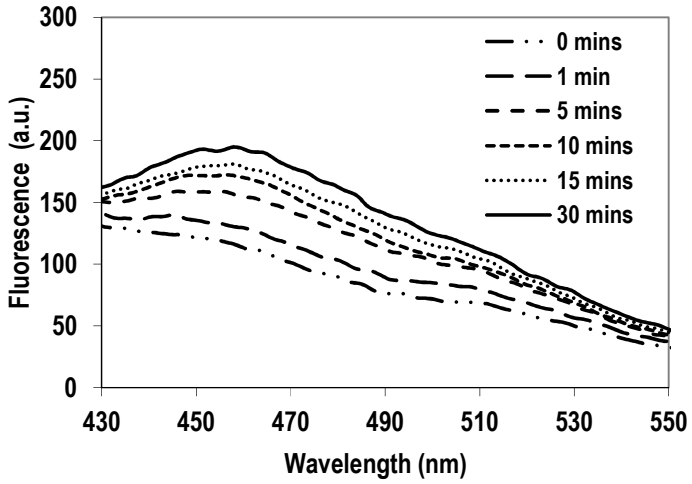

Figure 3.9 *Fluorescence responses (λ_{ex} = 363 nm) of 60 nM probe* ***3.3b*** *upon the addition of 60 nM NaClO in methanol.*

To investigate the selectivity of the probe **3.3a**, the probe was treated with different ROS (**Figure 3.10**). Representative ROS, such as H_2O_2, NO, $^1O_2$, H_2O_2/Fe^{2+}, KO_2, $ONOO^-$, only induced minimum enhancement in the fluorescence spectra of probe **3**. However, upon addition of NaClO to probe **3.3a**, a strong enhancement with a 9-fold increase in fluorescence was observed. Thus, the probe **3.3a** showed high selectivity for NaClO over other ROS examined. This indicates that the probe can be used in detection of ClO^- in nanomolar range.

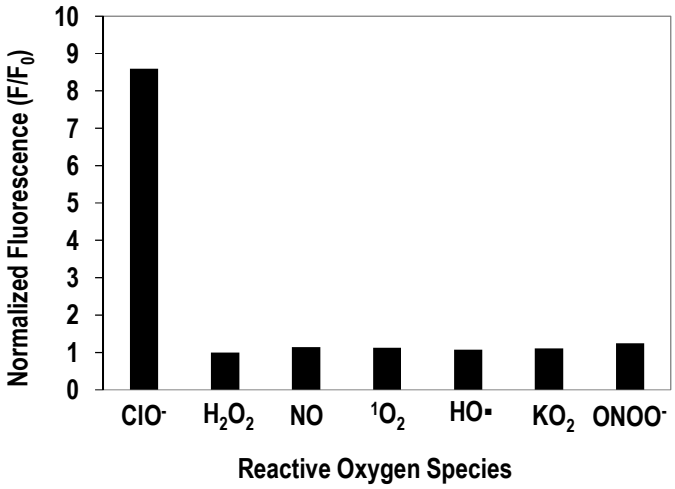

Figure 3.10 *Fluorescence responses of 60 nM BSe probe* ***3.3a*** *and 60 nM ROS. Bars represent normalized fluorescence intensities (F/F_0) at 30 min after the addition of ROS. Data were collected at RT in water/MeOH, with λ_{ex} = 363 nm and emission at 470 nm. $ONOO^-$ = peroxynitrite*

3.2.3 Oxidative stress monitored by BSe probe in vivo

Fluorescent probes have become an excellent tool for ROS imaging in cells due to their high sensitivities and high resolutions in microscopic imaging techniques. BSe probe **3.3a** showed good reactivity towards ROS that were induced in human promyelocytic leukemia cells (HL-60) and Lewis lung carcinoma cells (LL2) with H_2O_2 and ClO^- exogenously. The cellular responses were monitored by BSe probe **3.3a** under laser confocal microscopy and images were taken at 5, 10, 20 and 30 min. HL-60 cells were loaded with **3.3a** for 30 min (at 37 ^oC) and oxidative stress was mediated exogenously. Progressive increase in fluorescence intensity was observed in cells that were subjected to 50 μM H_2O_2 and ClO^-. The changes in fluorescence intensity of probe-loaded cells were due to the oxidation and cleavage of Se-C cleavage at the quenching site of the probe, emitting strong blue fluorescence of benzoxazole moiety (***Figure 3.11***). The results indicated that exogenous H_2O_2 and ClO^- stimuli rapidly increaseed the intracellular oxidative stress. The probe in the cell was then oxidized and thereby indicating an increase in fluorescence intensity of a localized signal compared to control cells. Due to high sensitivity of the probe **3.3a**, the result of its oxidation was visible after only five minutes of incubation with exogenous ROS.

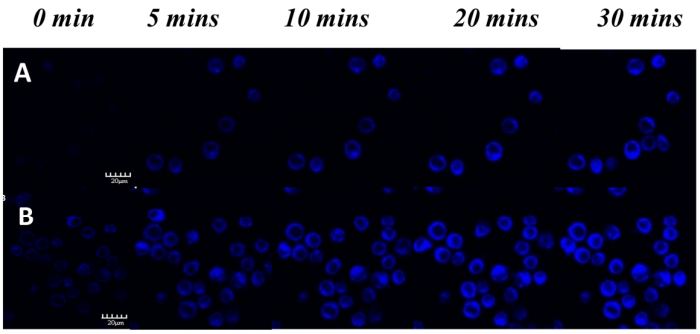

Figure 3.11 *Fluorescence imaging of live promyelocytic leukemia cells (HL-60) stained with probe* ***3.3a****. Fluorescence arises from the ROS-stimulated cleavage of C-Se bond (A) HL 60 cells loaded with 10 µM* ***3.3a*** *and 50 µM NaClO. (B) HL-60 cells loaded with 10 µM* ***3.3a*** *and 50 µM H_2O_2. Filter sets: Excitation 405 nm, Emission 461 nm. Scale bar = 20 µm.*

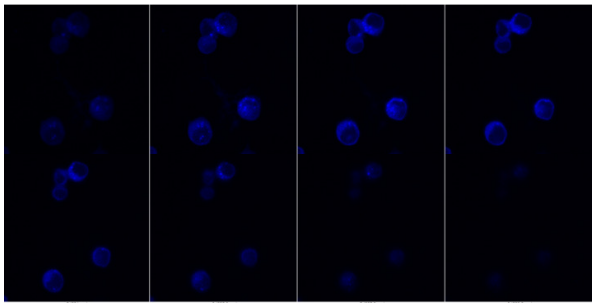

Figure 3.12 *Fluorescence imaging of fixed Lewis lung carcinoma cells (LL2) stained with probe* ***3.3a*** *presented at different Z layers. LL2 cells loaded with 10 µM probe for 30 mins (at 37^{o}C) followed by incubation with 50 µM NaClO for 10 mins (37 ^{o}C). This figure shows site specific property of the probe at the cell membrane, as proven by the Z stack images (Top left to Bottom right). Filter sets: Excitation 405 nm, Emission 461 nm.*

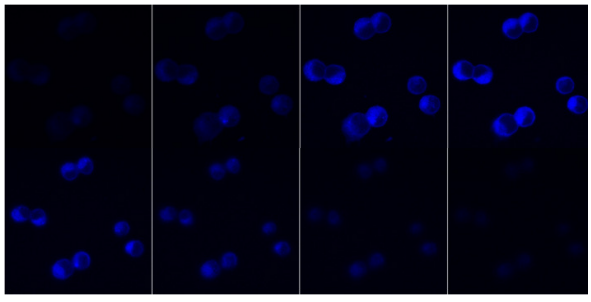

Figure 3.13 *Fluorescence imaging of fixed Lewis lung carcinoma cells (LL2) stained with probe* ***3.3a*** *presented at different Z layers. LL2 cells loaded with 10 µM probe for 30 mins (at 37^{o}C) followed by incubation with 50 µM H_2O_2 for 10 mins (at 37 ^{o}C). This figure shows site specific property of the probe towards the cell membrane, as proven by the Z stack images (Top left to Bottom right). Filter sets: Excitation 405 nm, Emission 461 nm.*

Furthermore, we visualized the intracellular site of oxidative stress mediated by H_2O_2 and ClO^- with BSe probe **3.3a** under laser confocal microscopy. ***Figure 3.11*** and ***Figure 3.12*** clearly showed that probe **3.3a** exhibits selective binding towards the cell membrane, where the major sites of oxidative stress are. Both Z-stack diagrams offer good evidence that the nucleus of the cells remained unstained from the cross-section view. The high reactivity of the radicals $HO^{\bullet}$, $O_2^{\bullet-}$ and H_2O_2 is reflected by their half-lifes of 10^{-9} s, 10^{-6} s and 10^{-5} s respectively. The short lifespan of the radicals makes studies of probing oxidative stress a challenge as this limits the distance it can diffuse and thereby its reactivity with the probe. Hence it is of great importance to achieve high sensitivity of the probe and specific site selection, when imaging of intracellular damages by oxidative stress is of concern.

3.2.4 Synthesis of selenium green and selenium red

In order to obtain an organoselenium probe with longer emission wavelength, fluorescein, BODIPY and Nile red dyes are chosen to be introduced to the selenium moiety (***Figure 3.3***, ***Figure 3.4***).

When 4-methylphthalic anhydride (Compound **3.5**) and resorcinol were used to form fluorescein, the reaction did not provide any selectivity and the products obtained were a mixture of 4'- and 5'-methylfluorescein (Compound **3.6**).[66] The two isomers were very different to isolate and were not distinguishable in the emission spectrum. Hence, the mixture was used without further separation in the synthesis of organoselenium probe. Compound **3.7**, which is less polar, was obtained by the acetylation of **3.6** and was easily isolated. The bromination of **3.7** yielded compound **3.8**, which was directly reacted with ArSeCN to form the organoselenium compound **3.9**. The acetyl groups were hydrolyzed during work-up (***Figure 3.14***). We named compound **3.9** "selenium green" because of its green fluorescence due to fluorescein group.

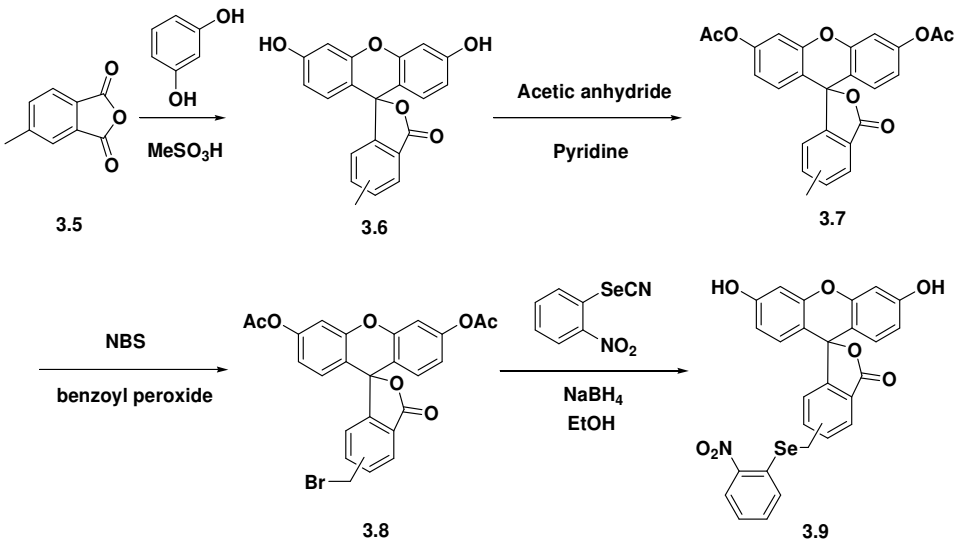

Figure 3.14 *Synthesis of selenium green* ***3.9****.*

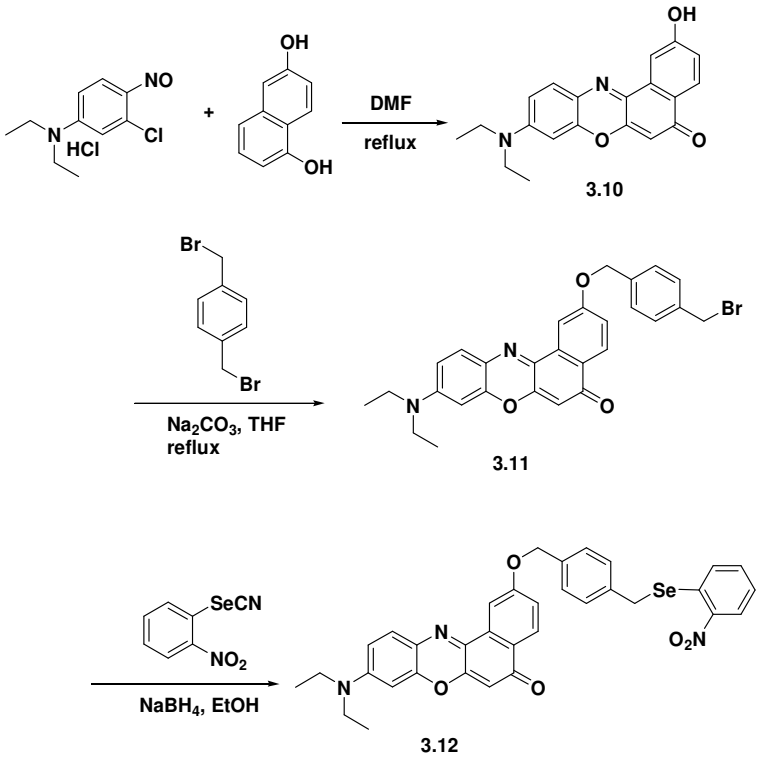

Figure 3.15 *Synthesis of selenium- Nile red.*

2-Hydroxy Nile red, Compound **3.10** was synthesized according to the literature.[67] Under basic condition, compound **3.10** reacted with 1, 4-bis(bromomethyl)benzene, linking the Nile red moiety to a bromomethyl group through a benzyloxy bond. A substitution of the halide group of **3.11** yielded the desired compound selenium- Nile red, **3.12** (***Figure 3.15***).

Previous study showed that the more substitution on the BODIPY core would lead to a red-shifted absorption and emission maxima. Hence, to obtain a longer emission, hepta-alkylated BODIPY core was chosen for the selenium-BODIPY. However, when the 8-chloromethyl BODIPY (compound **3.14**) was treated with sodium borohydride and selenocyanate to synthesize the selenium-BODIPY, compound **3.13**, the chloromethyl group was reduced to a methyl group resulting in compound **3.15** (***Figure 3.16***).

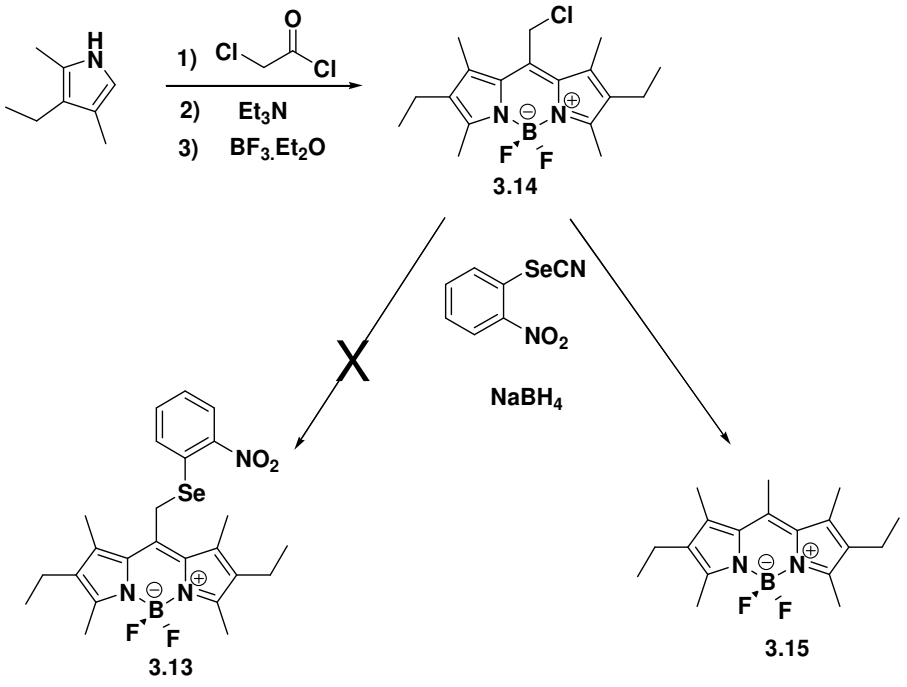

Figure 3.16 *Synthesis of selenium-BODIPY.*

3.2.5 Comparison of optical property and quantum yield of organoselenium probes

We found that the selenium quenching effect was much less with selenium green **3.9** and selenium-Nile red **3.12** than that of selenium blue-α, β and BSe probes. For example, selenium green at concentration of 100 nM showed F_{512} more than 450 (λ_{ex} = 460 nm). When selenium green was treated with one equivalent ClO^-, the fluorescence increased immediately but only marginally (less than two fold). It is noteworthy that the fluorescence after the reaction showed a very poor stability in water and after seven minutes of the reaction, the fluorescence intensity went even lower than the original intensity of the probe (***Figure 3.17***).

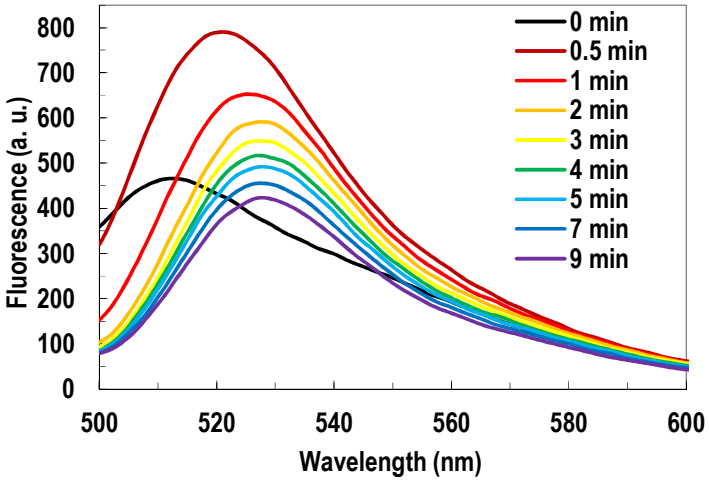

Figure 3.17 *Fluorescence responses (λ_{ex} = 460 nm) of 100 nM probe* ***3.9*** *upon the addition of 100 nM NaClO in water. (0 min spectrum is taken without NaClO)*

In comparison with selenium green, the quenching effect of selenium in selenium- Nile red probe **3.12** is even weaker. Probe **3.12** did not show any significant difference in the fluorescence with its non-selenium analogue.

To understand the quenching effect of selenium atom in all the synthesized organoselenium probes, the quantum yield (QY) of the all the probes and their non-selenium analogues were measured (***Table 3.2***). The presence of selenium atom in the pyrene and benzoxazoles greatly reduced the QY of the fluorophore. The selenium blue-α, -β and BSe probes all showed no

fluorescence (QY< 0.01). In the case of selenium green probe which has a fluorescein group, the selenium also has quenching effect but to a smaller extent. The QY of the probe is 0.31 compared to QY_{FL-CH3}= 0.54 and QY_{FL}= 0.95. While selenium incorporated with the red light emit dye Nile red, there is very small quenching effect observed.

Table 3.2 *Quantum yields of organoselenium probes and their non-selenium analog.*

Compound	Solvent	λ_{em} (nm)	Φ
Pyrene	cyclohexane	380	0.34
$PyCH_2OH$[a], 2.6	EtOH	390	0.42
Selenium blue-α, 2.1a	EtOH	NA	<0.01
Selenium blue-β, 2.2	EtOH	NA	<0.01
BSe, 3.3a	EtOH	NA	<0.01
3.4	EtOH	470	0.56
Fluorescein	0.1N NaOH	514	0.95
FL-CH_3[b], 3.6	0.1N NaOH	510	0.54
Selenium green, 3.9	0.1N NaOH	513	0.31
3.12	MeCN	610	0.62
3.10	MeCN	617	0.57

a) Py= pyrene
b) FL= fluorescein

3.3 Conclusion

In this chapter, we have presented the synthesis, optical properties, and reactivity of three organoselenium probes: BSe, selenium green and selenium-Nile red. BSe probe shows very good reactivity towards ROS. Its biological applications, such as being a new cell membrane-targeting fluorescent probe to detect oxidative stress of living cells have been developed.

Compared to selenium blue-α, BSe probes also process very good reactivity and selectivity to ROS detection. Moreover, BSe probes show superior properties that are suitable for the application in biological system, such as longer fluorescence emission wavelength (λ_{em} = 470 nm) than selenium blue-α (λ_{em} = 392 nm). Upon reacting with ROS, **3.3a** also emits strong blue fluorescence of benzoxazole group which is deemed more suitable for a fluorescence detector in biological research, especially in the real-time imaging of living cell. Besides that, BSe probes are more soluble in polar solvent due to their N, N-dimethylaminobenzoxazole groups which can easily form cationic centers to make the probes soluble in aqueous media. It is found that BSe probe **3.3a** exhibits in vivo sensitivity for oxidative stress in both leukemia and carcinoma cells. This probe also shows specific binding towards cell membrane, which is the major site of oxidative stress. Hence this probe offers an excellent insight of oxidative stress in biological system due to its target-selective property and high sensitivity.

The quenching effect of selenium atom in selenium green and selenium-Nile red probes are, however, not satisfactory. The quantum yields of the two probes are too high to make them good fluorescent probes for ROS detection.

3.4 Experimental Section

3.4.1 Instruments and Materials

^{1}H and $^{13}C\{^{1}H\}$ NMR spectra were recorded in deuterated chloroform with a Bruker AC300 spectrometer (Karlsruhe, Germany) at 300 and 75 MHz, respectively. The electrospray ionization mass spectra were obtained from a Finnigan / MAT LCQ ion trap mass spectrometer (San Jose, CA, USA) equipped with an electrospray ionization (ESI) source. The heated capillary

and voltage were maintained at 250 ^{o}C and 4.5 kV, respectively. The full-scan mass spectra from *m/z* 50 to 1000 were recorded. High resolution MS spectrum was obtained from Finnigan (MAT 95XL-T) high resolution (60,000), 5 KV Double Focusing Reversed Nier-Johnson Geometry Mass Spectrometer. UV-Vis spectra were recorded using a Shimadzu UK1601 spectrophotometer fitted with a quartz cell. Fluorescence analysis was performed using Perkin Elmer LS 55 Luminescence Spectrometer, with excitation/emission slit 10 nm and scan speed 500 nm/min.

All solvent used were of reagent grade unless otherwise specified. All chemicals unless indicated were obtained from Sigma Aldrich and used as received. Experiments involving moisture and/or air sensitive components were performed under a positive pressure of nitrogen in oven-dried glassware equipped with a rubber septum inlet. Dried solvents and liquid reagents were transferred by oven-dried syringes or hypodermic syringe cooled to ambient temperature in a desiccator. Anhydrous THF was freshly distilled from Na/benzophenone.

3.4.2 Synthesis of the organoselenium probes

Methyl 4-(6-(diethylamino)benzo[d]oxazol-2-yl)benzoate, 3.1: A solution of 5-diethylamino-2-nitrosophenol (0.252 g, 1.3 mmol) and methyl-4-bromomethylbenzoate (0.303 g, 1.3 mmol) in THF (10 mL) in presence of K_2CO_3 (0.359 g, 2.6 mmol) was heated to reflux for 8 h and filtered. The THF was evaporated under reduced pressure and the residual material was purified by flash chromatography eluting with 1:4 EA/hexane to afford compound 3.1 as yellow solid (0.337 g, 80%). ^{1}H NMR (300 MHz, $CDCl_3$): δ = 1.22 (t, 6H, CH_2CH_3), 3.42 (q, 4H, CH_2CH_3), 3.95 (s, 3H, $COOCH_3$), 6.78 (m, 1H, Ph–H), 6.81 (d, 1H, Ph–H), 7.56 (d, 1H, Ph–H), 8.15 (d, 2H, Ph–H), 8.22 (d, 2H, Ph–H) ppm. ^{13}C{^{1}H} NMR (75 MHz, $CDCl_3$): δ = 12.61, 45.22, 52.37, 92.88, 110.86, 120.38, 126.69, 130.14, 131.47, 131.82, 132.34, 147.48, 153.28, 159.39, 166.62 ppm. MS (ESI, positive mode): 325.1 [M+H]. HRMS: calcd. for $C_{19}H_{20}N_2O_3Na^+$ 347.1367; found 347.1352.

(4-(6-(Diethylamino)benzoxazol-2-yl)phenyl)methanol, 3.2: A mixture of **3.1** (0.804 g, 2.48 mmol) and $LiAlH_4$ (0.282 g, 7.44 mmol) in dry Et_2O (20

mL) was stirred for 12 h in an inert environment. H_2O (0.25 mL), NaOH (0.25 mL, 3.0 mol/L) and H_2O (0.75 mL) were successively added to quench the reaction and filtered. Evaporation of the solvent under reduced pressure and the residual material was purified by flash chromatography eluting with 1:1 EA/hexane to afford compound **2** as a yellow solid (0.654 g, 89%). ^{1}H NMR (300 MHz, $CDCl_3$): δ = 1.21 (t, *J* = 7.0 Hz, 6H, CH_2CH_3), 3.43 (q, *J* = 7.1 Hz, 4H, CH_2CH_3), 4.76 (s, 2H, CH_2Ph), 6.76 (d, *J* = 8.7 Hz,1H, Ph–*H*), 6.82 (s, 1H, Ph–*H*), 7.48 (d, *J* = 8.4 Hz, 1H, Ph–*H*), 7.53 (d, *J* = 8.7 Hz, 1H, Ph–*H*), 8.15 (d, *J* = 8.4 Hz, 2H, Ph–*H*) ppm. ^{13}C{^{1}H} NMR (75 MHz, $CDCl_3$): δ = 12.38, 45.07, 64.61, 93.11, 110.50, 119.69, 126.67, 126.93, 132.05, 143.56, 146.85, 152.72, 160.34 ppm. MS (ESI, +C): 297.2 $[M+H]^+$. HRMS calculated for $C_{18}H_{20}N_2O_2$ 297.1598, found 297.1594

N,N-diethyl-2-(4-((2-nitrophenylselanyl)methyl)phenyl)benzoxazol-6-amine, 3.3a: A solution of **3.2** (0.317 g, 1.07 mmol) in 10 mL of THF containing o-nitrophenyl selenocyanate (0.267 g, 1.18 mmol) under N_2 was treated drop wise with trimethylphosphine (2.14 mL, 2.14 mmol, 1.0 M in toluene) at room temperature. After the reaction was stirred for 12 h, the solvent was removed under reduced pressure. The residual material was crystallized from ethanol to give the desired compound **3.3a** as a yellow solid (0.426 g, 83%). ^{1}H NMR (300 MHz, $CDCl_3$): δ = 1.21 (t, *J* = 7.0 Hz, 6H, CH_2CH_3), 3.43 (q, *J* = 7.1 Hz, 4H, CH_2CH_3), 4.22 (s, 2H, CH_2Ph), 6.75 (d, *J* = 8.7 Hz, 1H, Ph–*H*), 6.82 (s, 1H, Ph–*H*), 7.33 (t, *J* = 7.5 Hz, 1H, Ph–*H*), 7.57 (m, 5H, Ph–*H*), 8.11 (d, *J* = 8.4 Hz, 2H, Ph–*H*), 8.31 (d, *J* = 8.4 Hz, 1H, Ph–*H*) ppm. ^{13}C{^{1}H} NMR (75 MHz, $CDCl_3$): δ = 12.64, 31.03, 45.26, 93.19, 110.64, 120.05, 125.89, 126.54, 127.11, 127.38, 129.33, 129.86, 132.40, 133.95, 134.25, 138.35, 146.51, 147.16, 153.05, 160.15 ppm. MS (ESI, +C): 482.1 $[M+H]^+$. HRMS ($C_{24}H_{24}N_3O_3Se$): 482.0977, found 482.0961.

N,N-diethyl-2-(4-(phenylselanylmethyl)phenyl)benzoxazol-6-amine, 3.3b: A solution of **3.2** (0.654 g, 2.21 mmol) in 20 mL of THF containing phenyl selenocyanate (0.269 mL, 2.21 mmol) under N_2 was treated drop wise with trimethylphosphine (4.42 mL, 4.42 mmol, 1.0 M in toluene) at room temperature and pressure. After the reaction was stirred for 12 h, the solvent was removed under reduced pressure. The residual material was purified by

flash chromatography eluting with 1:10 EA/Hexane to afford compound **3.3b** as a yellow oil (0.760 g, 79%). ^{1}H NMR (300 MHz, $CDCl_3$): δ = 1.25 (t, *J* = 7.0 Hz, 6H, CH_2CH_3), 3.46 (q, *J* = 7.0 Hz, 4H, CH_2CH_3), 4.16 (s, 2H, CH_2Ph), 6.80 (d, *J* = 8.7 Hz, 1H, Ph–*H*), 6.86 (s, 1H, Ph–*H*), 7.32 (m, 5H, Ph–*H*), 7.50 (m, 2H, Ph–*H*), 7.57 (d, *J* = 9.0 Hz, 1H, Ph–*H*), 8.06 (d, *J* = 8.4 Hz, 2H, Ph–*H*) ppm. $^{13}C\{^{1}H\}$ NMR (75 MHz, $CDCl_3$): δ = 12.44, 32.05, 45.11, 93.11, 110.44, 119.81, 126.22, 126.86, 127.60, 129.01, 129.22, 129.65, 134.08, 141.46, 146.90, 152.80, 160.31 ppm. MS (ESI, positive mode): 437.1 $[M+H]^+$. HRMS calculated for $C_{24}H_{24}N_2OSeNa$ 459.0946, found 459.0958.

4'(5')-Methylfluorescein, 3.6: 4-Methylphthalic anhydride (0.81 g, 5 mmol) was added to a solution of resorcinol (1.1 g, 10 mmol) in methanesulfonic acid (5 mL). The resulting mixture was heated under dry nitrogen at 85 °C for 36 h. The cooled mixture was poured into 7 volumes of ice water followed by filtration. The residue was dried at 60 °C *in vacuo* to give yellow solid **7** (1.5 g, 87%). ESI/MS *m/z* 347 $[M+H]^+$. ^{1}H NMR (300 MHz, DMSO-d_6): δ = 7.86 (d, *J* = 7.9 Hz, 1H, 5-isomer), 7.78 (s, 1H, 4-isomer), 7.60 (d, *J* = 7.7 Hz, 1H, 4-isomer), 7.50 (d, *J* = 7.9 Hz, 1H, 5-isomer), 7.14 (d, *J* = 7.7 Hz, 1H, 4-isomer), 7.06 (s, 1H, 5-isomer), 6.67 (s, 4H), 6.55 (s, 8H), 2.49 (s, 3H), 2.38 (s, 3H) ppm.

4(5)-Methylfluorescein diacetate, 3.7: 4(5)-Methylfluorescein, **3.6** (1 g, 2.9 mmol) was heated with Ac_2O (3.5 g, 34 mmol) and pyridine (0.6 g, 7.7 mmol) for 5 min at 80 °C. The solution was poured into ice water and followed by filtration. The precipitate was recrystallized from absolute ethanol to yield yellow solid (1.1 g, 90%). ESI/MS *m/z* 431 $[M+H]^+$. ^{1}H NMR (500 MHz, DMSO-d_6): δ = 7.92 (d, *J* = 8.2 Hz, 1H, 5-isomer), 7.85 (s, 1H, 4-isomer), 7.62 (d, *J* = 7.6 Hz, 1H), 7.55 (d, *J* = 7.6 Hz, 1H), 7.26-7.27 (m, 4H), 7.19 (s, 1H, 5-isomer), 6.86-6.96 (m, 8H), 7.06 (s, 1H, 5-isomer), 2.45 (s, 3H), 2.37 (s, 3H) 2.27 (s, 12H) ppm. $^{13}C\{^{1}H\}$ NMR (75 MHz, $CDCl_3$): δ = 169.2, 168.7, 153.6, 152.0, 151.6, 151.4, 150.2, 146.7, 140.5, 136.4, 131.2, 128.9, 126.4, 125.0, 124.9, 124.2, 123.7, 123.4, 117.6, 116.6, 110.3, 81.5, 81.1, 22.0, 21.2, 21.0 ppm.

4(5)-Bromomethyl fluorescein diacetate, 3.8: A mixture of 4(5)-methylfluorescein diacetate, **3.7** (178 mg, 0.4 mmol), N-bromosuccinimide (71 mg, 0.4 mmol) and benzoyl peroxide (1 mg, 0.004 mmol) was refluxed in 100 mL CCl_4 for 3 hr. The formed succinimide was removed from the reaction solution by filtration. The solvent was evaporated and the crude product was used in the next step without any purification.

4(5)-(2-Nitrophenylselanyl)methyl fluorescein, **3.9**: To a suspension of *o*-nitrophenyl selenocyanate (25 mg, 0.14 mmol) in 5.0 mL anhydrous methanol in a two necked round bottom flask under nitrogen, sodium borohydride (6.0 mg, 0.15 mmol) was added. The reaction solution turned dark brown. 4(5)-bromomethyl fluorescein diacetate**, 3.8** (70 mg, 0.14 mmol) was added and the reaction was stirred at r.t. for 16 hr. The solvent was evaporated and the crude product was purified by a silica gel column chromatography with ethyl acetate and hexane to give **3.9** (18 mg, 20%) as yellow solid. ESI/MS *m/z* 588 $[M\text{-}Ac]^-$. ^1H NMR (300 MHz, $CDCl_3$): δ = 7.99-8.28 (m, 9H), 7.92 (d, *J* = 7.8 Hz, 1H), 7.49 (dd, *J* = 1.2 Hz, 8.1 Hz, 1H), 7.37 (td, *J* = 1.5 Hz, 7.2 Hz, 1H), 7.23 (td, *J* = 1.2 Hz, 7.8 Hz, 1H), 4.92 (s, 2H) ppm.

9-(diethylamino)-2-hydroxy-5*H*-benzo[a]phenoxazin-5-one, 3.10: 5-Diethylamino-2-nitrosophenol hydrochloride (1.14 g, 4.96 mmol) and 1, 6-dihydroxynaphthalene (0.19 g, 4.94 mmol) were heated under reflux in DMF (100 ml) for 4 h. The DMF was removed under reduced pressure. The crude mixture was purified by flash chromatography (ethyl acetate–isopropanol, 100–50%) to yield a dark green solid (1.1 g, 65%).

2-(4-(bromomethyl)benzyloxy)-9-(diethylamino)-5*H*-benzo[a]phenoxazin-5-one, 3.11: A mixture of **1** (0.120 g, 0.35 mmol) and 1,4-bis(bromomethyl)benzene (0.185 g, 0.70 mmol) in THF (20 mL) in presence of Na_2CO_3 (0.074 g, 0.70 mmol) was heated to reflux for 12 h and filtered. The THF was evaporated under reduced pressure and the residual material was purified by flash chromatography(1:10 EA/Hexane-EA) to afford compound **2** as a purple solid (0.156 g, 86%). ^1H NMR (300 MHz, $CDCl_3$): δ = 1.22 (t, *J* = 7.5 Hz, 6H, CH_2CH_3), 3.39 (q, *J* = 7.0 Hz, 4H, CH_2CH_3), 4.17 (s,

2H, BrCH_2Ph), 4.24 (s, 2H, OCH_2Ph), 6.76 (d, J = 9.0 Hz,1H, Ph–H), 6.82 (s, 1H, Ph–H), 7.37 (m, 3H, Ph–H), 7.54 (m, 6H, Ph–H), 8.11 (d, J = 9.0 Hz, 2H, Ph–H), 8.29 (d, J = 9.0 Hz, 2H, Ph–H) ppm. $^{13}C\{^1H\}$ NMR (75 MHz, $CDCl_3$): δ = 12.72, 33.20, 45.17, 69.85, 96.33, 105.22, 107.01, 109.74, 118.41, 124.82, 125.93, 127.21, 128.09, 134.11, 136.86, 137.78, 139.67, 139.67, 146.86, 150.88, 152.08, 161.26, 183.10 ppm.

2-(4-((2-nitrophenylselanyl)methyl)benzyloxy)-9-(diethylamino)-5*H*-benzo[a]phenoxazin-5-one, 3.12: To the solution of o-Nitrophenyl selenocyanate (0.057 g, 0.25 mmol) in 10 mL of anhydrous ethanol, sodium borohydride (0.011 g, 0.28 mmol) was added, and the solution was stirred at room temperature for 30 min. The final reaction solution was treated with compound **2** (0.130 g, 0.25 mmol) and stirred for 12 h. The precipitate was removed by filtration over a Celite plug and washed by cold ethanol to give a purple solid (0.129 g, 81%). ^1H NMR (300 MHz, $CDCl_3$): δ = 1.27 (t, J = 7.5 Hz, 6H, CH_2CH_3), 3.46 (q, J = 7.0 Hz, 4H, CH_2CH_3), 4.21 (s, 2H, OCH_2Ph), 5.25 (s, 2H, SeCH_2Ph), 6.30 (s, 1H, Ph–H), 6.46 (d, J = 3.0 Hz, 1H, Ph–H), 6.64 (q, J = 4.0 Hz,1H, Ph–H), 7.21(d, J = 3.0 Hz, 1H, Ph–H), 7.32 (m, 1H, Ph–H), 7.47 (m, 6H, Ph–H), 7.58 (s, 1H, Ph–H), 7.61 (s, 1H, Ph–H), 8.15 (d, J = 3.0 Hz, 1H, Ph–H), 8.22 (d, J = 9.0 Hz, 1H, Ph–H), 8.28 (m, 1H, Ph–H) ppm. $^{13}C\{^1H\}$ NMR (75 MHz, $CDCl_3$): δ = 12.53, 30.70, 45.00, 69.88, 96.26, 105.23, 107.02, 109.50, 118.39, 124.66, 125.53, 125.86, 126.31, 127.78, 128.12, 129.07, 129.50, 131.02, 133.70, 134.02, 134.45, 135.52, 135.68, 139.84, 146.19, 146.82, 150.72, 152.04, 161.25, 183.12 ppm.

8-Chloromethyl-1, 3, 5, 7- tetramethyl- 2, 6- diethyl- 4, 4-difluoro-4-bora-3a, 4a-diaza-sindacene, 3.14: To an anhydrous dichloromethane solution containing 3-ethyl-2,4-dimethyl-1*H*-pyrrole (0.29 mL, 2.14 mmol, 1 eq.) and under an atmosphere of argon, a solution of the 2-chloroacetyl chloride (120 mg, 1.07 mmol 0.5 eq.) in anhydrous dichloromethane is added drop wise. The reaction mixture is heated under reflux for 3h. After completion of the reaction (TLC analysis), the reaction mixture is evaporated to dryness under vacuum. The residue was then disolved in anhydrous toluene (75 mL) containing triethylamine (10 g, 10.7 mmol, 5 eq.). The mixture is stirred at room temperature for 15 minutes and kept under an argon

atmosphere while $BF_3.Et_2O$ is added drop wise (1.8 mL, 14.5 mmol, 6.8 eq.) The reaction mixture is then stirred at 80°C for 45 minutes until complete conversion of **3.14**. After cooling down to room temperature, the crude reaction mixture was concentrated under vacuum. The residue is purified by column chromatography on silica gel using dichloromethane/methanol eluting system (95:5, v/v). Orange solid **3.14** (300 mg, 80%) was obtained and stored in the dark. ^{1}H NMR (300 MHz, $CDCl_3$): δ = 1.06 (t, *J* = 7.6 Hz, 6H, CH_2CH_3), 2.40 (q, *J* = 7.6 Hz, 4H, CH_2CH_3), 2.46 (s, 6H, Ar-CH_3), 2.51 (s, 6H, Ar-CH_3), 4.83 (s, 2H, CH_2Cl) ppm. ^{13}C {^{1}H} NMR (75 MHz, $CDCl_3$): δ = 12.56, 12.71, 14.76, 17.19, 37.96, 131.00, 133.58, 134.44, 136.41, 155.02 ppm. HRMS calculated m/z for $C_{18}H_{24}N_2{}^{11}B_1{}^{35}ClF_2$ 352.1689, found 352.1702.

8-Methyl-1, 3, 5, 7- tetramethyl- 2, 6- diethyl- 4, 4-difluoro-4-bora-3a, 4a-diaza-sindacene, 3.15: To a suspension of *o*-nitrophenyl selenocyanate (38 mg, 0.17 mmol) in 5.0 mL anhydrous methanol in a two necked round bottom flask under nitrogen, sodium borohydride (7.0 mg, 0.19 mmol) was added. The reaction solution turned dark brown. **3.14** (60 mg, 0.17 mmol) was added and the reaction was stirred at r.t. One day later the crude reaction mixture was concentrated under vacuum. The residue is purified by column chromatography on silica gel using hexane/ethyl acetate eluting system (9:1, v/v). Orange solid **3.15** obtained. (46 mg, 85%) and stored in the dark. ^{1}H NMR (300 MHz, $CDCl_3$): δ = 1.04 (t, *J* = 7.5 Hz, 6H, CH_2CH_3), 2.33 (s, 6H, Ar-CH_3), 2.40 (t, *J* = 7.5 Hz, 4H, CH_2CH_3), 2.50 (s, 6H, Ar-CH_3), 2.60 (s, 3H, CH_3) ppm. EI-MS for $C_{18}H_{25}BF_2N_2$: 318.1.

3.4.3 Crystal structure analyses

Single crystals of **3.2** and **3.3a** suitable for X-ray structural analysis were obtained from DCM/n-hexane mixture. Diffraction data of **3.2** and **3.3a** were collected at 223 K with a Bruker SMART-CCD diffractometer equipped with graphite-monochromated Mo-K_α radiation (λ = 0.71073 Å). Details of the crystal data, data collections, and structure refinements are summarized in ***Table 3.4***. The structure was solved by direct methods and refined by full-matrix least-squares on F^2. All non-hydrogen atoms were

refined anisotropically and the hydrogen atoms were included in idealized position. All calculations were performed using the SHELXTL crystallographic software packages.[111] Crystallographic data (excluding structure factors) for the structures reported have been deposited with the Cambridge Crystallographic Data Centre as supplementary publication no. CCDC-779445 for **3.2**, CCDC-779446 for **3.3a**. These data can be obtained free of charge from The Cambridge Crystallographic Data Centre via www.ccdc.cam.ac.uk/data_request/cif.

Further examination of its volume and density revealed consistent physical data where the densest per unit cell (compound **3.3a**) bears the smallest volume (***Table 3.3***).

Table 3.3 *Unit cell properties of crystals*

Compound / Crystal Properties			3.1	3.2	3.3a
Crystal system			Triclinic	Monoclinic	Triclinic
Unit cell dimensions	**Unit cell axes dimensions (Å)**	**a**	7.389	12.006	7.578
		b	11.242	16.628	8.982
		c	11.275	7.677	16.956
	Inclination angles of axes (°)	**α**	104.357	90.000	96.725
		β	101.867	102.216	102.128
		γ	108.828	90.000	108.860
Other unit cell properties	**Calculated density, D_c (mg/m^3)**		1.320	1.314	1.525
	Volume (Å^3)		815.980	1498.000	1046.070
	Space Group		P-1	P2(1)/c	P-1
	Z (formula units/cell)		2	4	2

Table 3.4 *Crystallographic data and structural refinements details for* ***3.2*** *and* ***3.3a***

	3.2	**3.3a**
Formula	$C_{18}H_{20}N_2O_2$	$C_{24}H_{23}N_3O_3Se$
Fw	296.36	480.41
Cryst. Syst.	Monoclinic	Triclinic
Space group	P2(1)/c	P-1
a (Å)	12.006(3)	7.5778(7)
b (Å)	16.628(4)	8.9812(9)
c (Å)	7.6772(18)	16.9557(16)
α (deg)	90	96.725(2)
β (deg)	102.216(5)	102.128(2)
γ (deg)	90	108.860(2)
V (Å^3)	1498.0(6)	1046.07(17)
Z	4	2
D_{calcd} (g·cm^{-3})	1.314	1.525
F(000)	632	492
θ range for data collection	1.74 to 27.50^o	2.45 to 27.50^o
Limiting indices	$-15 \leq h \leq 15$	$-9 \leq h \leq 9$
	$-18 \leq k \leq 21$	$-11 \leq k \leq 11$
	$-9 \leq l \leq 9$	$-22 \leq l \leq 17$
Reflns collected	10023	7317
Independent reflections	3437	4769
Goodness-of-fit on F^2	1.181	1.043
Final *R* indices [$I > 2\sigma(I)$]	$R_1 = 0.0724$	$R_1 = 0.0406$
	$wR_2 = 0.1684$	$wR_2 = 0.1003$
R indices (all data)	$R_1 = 0.0846$	$R_1 = 0.0520$
	$wR_2 = 0.1746$	$wR_2 = 0.1051$
R_{int}	0.0413	0.0254
Largest diff. peak, hole [e·Å^{-3}]	0.481, –0.384	0.769, –0.335

3.4.4 Detection of various ROS by fluorescence spectroscopy

A probe solution of was prepared by dilution of a methanol solution of probes with water. Reactive oxygen species includes H_2O_2, *t*-butylhydroperoxide (TBHP), and sodium hypochlorite (NaClO) were diluted from the commercially available solution to 1.0 mM in water. Peroxynitrite and nitric oxide were prepared in-house according to established procedures.[52]

$^1O_2$ was generated via irradiation of rose Bengal.[53] Hydroxyl radical was generated by Fenton reaction. Nitric oxide gas was generated by reacting ascorbic acid with sodium nitrite and by purifying with sodium hydroxide and molecular sieves before passing through de-aerated water under inert atmosphere.[54] The content of nitric oxide in the resultant solution was estimated by colorimetric method using ammonium 2,2'-azinobis-(3-ethylbenzothiazoline-6-sulphonate) (ABTS) as an indicator.[55] All reactions were carried out at r.t.

3.4.5 Confocal microscopic imaging of cellular HClO activity by BSe probe

Fluorescence confocal microscopic imaging studies were performed with Olympus Fluoview FV1000 equipped with PlanApo 60X/ 1.00 WLSM 0.17 (Water lens). Excitation of Se loaded cells at 405 nm was carried out with 20 mW solid state laser, and emission was collected using at 461 nm. For live HL-60 cell imaging, live cell imaging chamber supplemented with 5% CO_2 air and stage heater at 37^{o}C were utilized.

Cell culture: The HL-60 cell line was a kind donation from Centre for Life Sciences (Singapore). HL-60 was cultured in IMDM supplemented with 10% FBS and 1% Antibiotic:Antimycotic solution in a 37 ^{o}C incubator in a humidified atmosphere of 5% CO_2. The LL2 cell line was a donation from Department of Pharmacology (National University of Singapore, Singapore). LL2 was cultured in DMEM supplemented with 10% FBS and 1% Antibiotic:Antimycotic solution in a 37 ^{o}C incubator in a humidified atmosphere of 5% CO_2. The medium was replaced with fresh solution every other day and cells were plated at an appropriate density according to each experiment. Cell density was determined with haemocytometer stained with trypan blue. Prior to experiment, the HL-60 was cultured in FBS free media for 24 hours.

Intracellular oxidative stress fluorescence imaging in living HL-60 cells: For loading of probe, HL-60 cells at a concentration of $1x10^6$ cells/ml in serum-free media without phenol red, were cultured in 8-wells chambered glass and incubated with the probe **3.3a** (final concentration of 10 μM) for 30

mins at 37 °C, 5% CO_2. Excess probes were removed with PBS thrice by centrifugation (for 3 mins at 700 x g). Washed cells were then treated with H_2O_2 and NaOCl (with final concentration of 50 μM) to mediate intracellular oxidative stress. Fluorescence images were taken immediately after addition of ROS for a period of 30 mins under the condition of 37 ^oC and 5%CO_2.

Intracellular oxidative stress fluorescence imaging in fixed LL2 cells: LL2 Cells at a concentration of $1x10^5$ cells/ml were cultured in DMEM media supplemented with 10% FBS and 1% antibiotic:antimycotic on 22-mm glass coverslips 24 hours, at 37 ^oC, 5% CO_2 air, before imaging, Cells were washed thrice with PBS for 5 mins per wash for every single treatment thereafter. Prior to loading of cells with Probe **3.3a**, fixation with 4% paraformaldehyde (prepared in PBS) at 37 ^oC for 30 mins was carried out. Next, permeabilization of cells with 0.2% Triton-X-100 (prepared in PBS) on ice for 5 mins follows. Finally blocking of cells with 5% BSA (prepared in PBS) at 37 ^oC for 30 min was performed. Staining of fixed cells with Se probe was carried out at 37 ^oC for 30 min. Intracellular oxidative stress with exogenous ROS (50 μM H_2O_2 and NaClO diluted in PBS) was mediated from 0 to 30 min and images were taken under similar conditions as mentioned in previous section.

3.4.6 Fluorescence Quantum Yield (Φ) Measurements

In a general procedure, all samples of analytes dissolved in correspond solvent having different absorbance between 0.01-0.1 at the excitation wavelength were prepared. Fluorescence spectrum was measured using prepared samples with slit width at 2.5 nm for both excitation and emission and scan speed at 500 nm / min. Fluorescence quantum yield was calculated by plotting the magnitude of the integrated fluorescence intensity against the absorbance of the solution. Fluorescence quantum yields (Φ) were estimated by integrating the area under the fluorescence curves using the equation,

$$\boldsymbol{\phi_{sample} = \phi_{ref}\ \frac{OD_{ref} \times A_{sample} \times \eta^2_{sample}}{OD_{sample} \times A_{sampleref} \times \eta^2_{ref}}}$$

Where A was the area under the fluorescence spectral curve, OD was optical density of the compound at the excitation wavelength and η was the

refractive indices of the solvent. Quinine sulfate was used as quantum yield standard ($\Phi_{\text{quinine sulfate}}$ is 0.51 in 1.0 N H_2SO_4) for measuring the blue fluorescence compounds. Fluorescein was used as quantum yield standard ($\Phi_{\text{fluorescein}}$ is 0.95 in 0.1 N NaOH) for measuring the green fluorescence compounds.

Chapter 4: Molecularly Engineered Quantum Dots for Detection of Singlet Oxygen

4.1 Introduction

4.1.1 Singlet oxygen

Molecular orbital theory predicts two low-lying excited singlet oxygen states, O_2 ($^1\Delta_g$) and O_2 ($^1\Sigma_g^+$) that differ in the spin and the occupancy of oxygen's two degenerate antibonding π_g-orbitals. The O_2 ($^1\Sigma_g^+$) state is very short-lived and relaxes quickly to the lowest lying excited state, O_2 ($^1\Delta_g$) that is referred to as $^1O_2$. The energy difference between the ground and singlet states is 94.3 kJ/mol corresponding to an observable transition in the near-infrared region at 1270 nm.[68]

Singlet oxygen is rapidly deactivated in water with a lifetime of less than 4 μs.[68] However, in the presence of organic molecules in biological system, this highly reactive molecule is still a very strong oxidant and has significant reactivity towards electron rich organic molecules including nucleic acid, protein and lipids.[69] It also plays an important role in the cell cascade and induction of gene expression.[70] Futher more, studies have shown that $^1O_2$ is implicated in the genotoxic effect of solar irradiation UVA (320- 380 nm) and is likely to play an important role in the cell signal transduction cascade associated with apoptosis.[70a,71]

It is believed that the generation of $^1O_2$ by the reaction of H_2O_2 with HClO constitutes an important defence mechanism against microorganisms. (***Eq. 4.1***) This mechanism contribute the most $^1O_2$ formation during phagocytosis.[72, 73]

$$HClO + H_2O_2 \rightarrow {}^1O_2 + Cl^- + H_2O + H^+ \qquad \textit{Eq. 4.1}$$

$^1O_2$ can also be generated in biological system by photoexcitation upon exposure of endogenous photosensitizer (porphyrins, flavins, quinones, etc.) to UVA.[74] In the photodynamic therapy (PDT), singlet oxygen is the primary oxidant generated in the presence of sensitizers. It induces tumor cell death, as well as, gives rise to several other ROS including superoxide anion, hydrogen peroxide and hydroxyl radical. These various ROS contribute to the

biochemical and morphological changes after PDT. Although there are many ROS involved in the PDT process, the overall efficacy is dependent on the amount of singlet oxygen generated.

4.1.2 Detection of singlet oxygen: endoperoxides formation

Monitoring of the faint $^1O_2$ luminescence at 1270 nm is a very specific and noninvasive method. However, this method is troublesome because of the extremely low emission quantum yield of 6.5×10^{-7} in water.[68] Moreover, it is inapplicable in biological system as the medium contains efficient physical quenchers such as amines or phenols. Specific chemical trapping by substrates for $^1O_2$ can be much more sensitive than the luminescence technique, thereby rendering this method hard to apply in biological system.

One of the most widely used methods is the formation of endoperoxides (EPOs) through a [4+2] cycloaddition of $^1O_2$ on aromatic hydrocarbon systems. The first widely used $^1O_2$ trap is 9,10-diphenylanthracene (DPA), that reacts rapidly with $^1O_2$ specifically to form a thermostable endoperoxide at a rate of $k = 1.3\times10^6$ M^{-1} s^{-1}.[75-77] The decrease in absorbance at 355 nm is used as a measure of the formation of the endoperoxide. However, DPA as well as its derivatives are not very sensitive as probes because the detection is based on the measurement of absorbance. Hence, to improve the sensitivity, great efforts were carried out to effect conjugation of DPA with xanthene probes, resulting in new fluorescent probes for $^1O_2$, such as 9-[2-(3-carboxy-9,10-diphenyl)anthryl]-6-hydroxy-3*H*-xanthen-3-ones (DPAXs) and 9-[2-(3-carboxy-9,10-dimethyl)anthryl]-6-hydroxy-3H-xanthen-3-one (DMAX) (***Figure 4.1***). [78, 79] The fluorescence properties of fluorescein derivatives DPAXs and DMAX are controlled by a photo-induced electron transfer (PET) process from the DPA and 9,10-dimethylanthracene moiety to the xanthene ring. Although DPAXs and DMAX are fluorescein derivatives, they are barely fluorescing, while their products upon formation of EPOs, DPAX endoperoxides (DPAX-EPs) and DMAX endoperoxides (DMAX-EPs) on the other hand, are strongly fluorescent. However, DPAX-EP and DMAX-EPs are very sensitive to pH because of the fluorescein group.

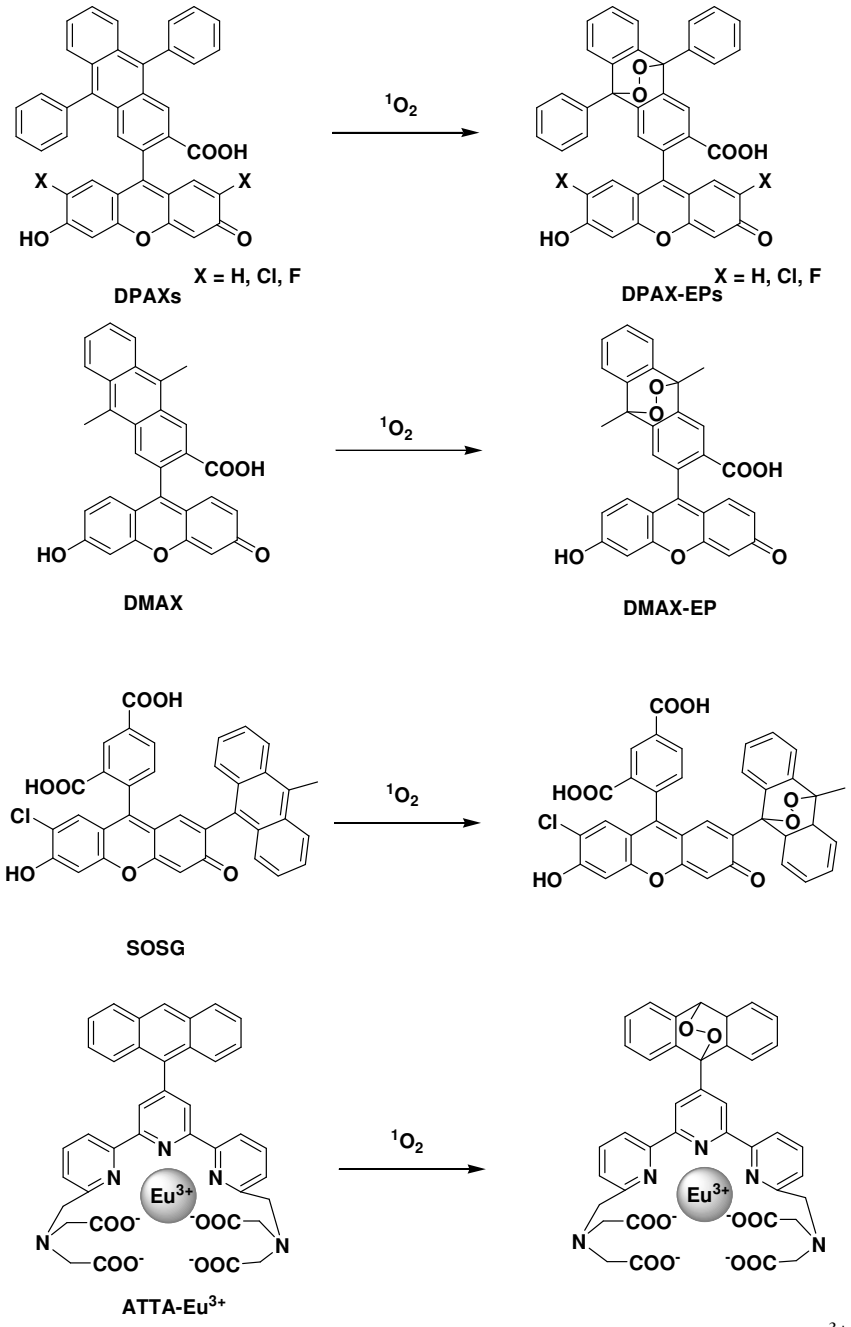

Figure 4.1 *Sensing mechanism of DPAXs, DMAX, SOSG and ATTA-Eu^{3+}.*

Currently, the only commercially available probe Singlet Oxygen Sensor Green® (SOSG), which is highly selective for $^1O_2$ detection and does not show any appreciable response to hydroxyl and superoxide radicals, is used to monitor $^1O_2$ production in biological systems.[80] SOSG exhibits weak blue fluorescence peaks at 395 nm and 416 nm. In the presence of singlet oxygen, the anthracene moiety converts to the corresponding endoperoxide, leading to

an increase in green fluorescence at 525 nm. This probe has been utilized to monitor $^1O_2$ production in diatoms and leaves during photo-oxidative stress, pathogen attack and wounding (***Figure 4.1***).

Besides the normal fluorescent probes, the formation of endoperoxide by singlet oxygen is also been used in some other selective singlet oxygen detection methods. An Eu^{3+} chelate-based phosphorescence probe, [4'-(9-anthryl)-2,2':6',2''-terpyridine-6,6''-diyl]bis(methylenenitrilo) tetrakis(acetate)-Eu^{3+} (ATTA-Eu^{3+}), also take advantage of its 9-anthryl group as a specific reactive moiety for singlet oxygen (***Figure 4.1***). The specific formations of endoperoxides enable all the mentioned probes show very good selectivity to singlet oxygen among other ROS. Similaryly, in our searching of new fluorescent probes for identifying specifically singlet oxygen, via formation of endoperoxides, we expected aromatic hydrocarbon systems, which serve as a highly selective trap for only singlet oxygen.

4.1.3 Quantum dot as fluorescent biological labels

Organic fluorescent dyes have already been commonly used in biological study for a long time. However, the intrinsic photophysical properties of organic fluorophores, namely their broad absorption/emission profiles and low photobleaching threshold, have limited their effectiveness in long-term imaging and simultaneous detection of multiple signals that would otherwise require complex instrumentation and processing.[81] The use of quantum dots (QDs) in biology is the fastest moving and the most exciting interfaces of nanotechnology. Enticing properties of QDs such as high quantum yield, high molar extinction coefficients (~10–100 times that of organic dyes), broad absorption but narrow and symmetric photoluminescence (PL) spectra (full-width at half-maximum ~25–40 nm) spanning the UV to near-infrared region, large effective Stokes shifts, high resistance to photobleaching and exceptional resistance to chemical degradation are of particular interest to biologists.. In comparison to molecular dyes, QDs are more superior than the conventional molecular dyes due to their ability in size-tuning of fluorescent emission, and their broad excitation spectra, allowing excitation of mixed QDs populations at a single wavelength far away (>100 nm) from their respective emissions.[82]

Not only can QDs be biofunctionalized in cellular labeling; it can be molecularly engineered as chemosensors through grafting on their surface with a layer of organic molecules that are responsive towards analytes that can switch the luminescence on/off.[83]

4.1.4 Design of QDs for the sensing of singlet oxygen

In order to detect $^1O_2$ selectively and sensitively, the functional moiety of the probe should react with $^1O_2$ directly, rapidly, and stoichiometrically; the spectroscopic property of the probe should also change dramatically for easy monitoring.

Dimethylhomoocoerdianthrone (HOCD) is a intensely blue compound (λ_{max} = 653 nm) which can selectively react with $^1O_2$ to form a colorless HOCD endoperoxide (HOCDPO), that has no absorbance at 653 nm (***Figure 4.2***). The reaction is reversible but the number of reversible photocycles is limited by the irreversible side reaction in which homolytic rupture of the peroxide bridge of HOCDPO forms rearranged product. This phenonmenon is unlikely and in fact, HOCDPO has one of the lowest tendencies compared to other endoperoxides because the reverse reaction requires the presence of sensitizer to produce singlet oxygen before the reaction can proceed. Furthermore, the half-life for the decay of HOCDPO into HOCD and O_2 is determined to be 170 years at 293 K, making HOCDPO thermally stable at room temperature.[84]

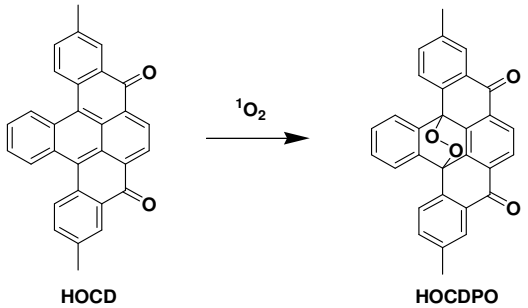

HOCD (Blue color) **HOCDPO** (Colorless)

Figure 4.2 *When HOCD reacts with singlet oxygen, the blue HOCD fades rapidly upon exposure to* $^1O_2$.

The best available QDs for biological applications as the fluorophore are made of CdSe cores over coated with a layer of ZnS passives the core surface, protects it from oxidation, prevents leeching of Cd/Se into surrounding solution and also produces a substantial improvement in the PL yield.[85,86] The CdSe/ZnS core/shell QDs emits from 450 nm to 650 nm, providing a good energy transfer donor for HOCD. Grafting HOCD as the ligand onto the surface CdSe/ZnS QDs by covalent bond and/or *van der waals'* force can quench the fluorescence of QDs by Förster resonance energy transfer (FRET). After the reaction with singlet oxygen, the formation of colorless HOCDPO would change the absorbance of the ligand and the fluorescence of QDs can be turned on.

4.2 Results and discussion

4.2.1 Synthesis of HOCD

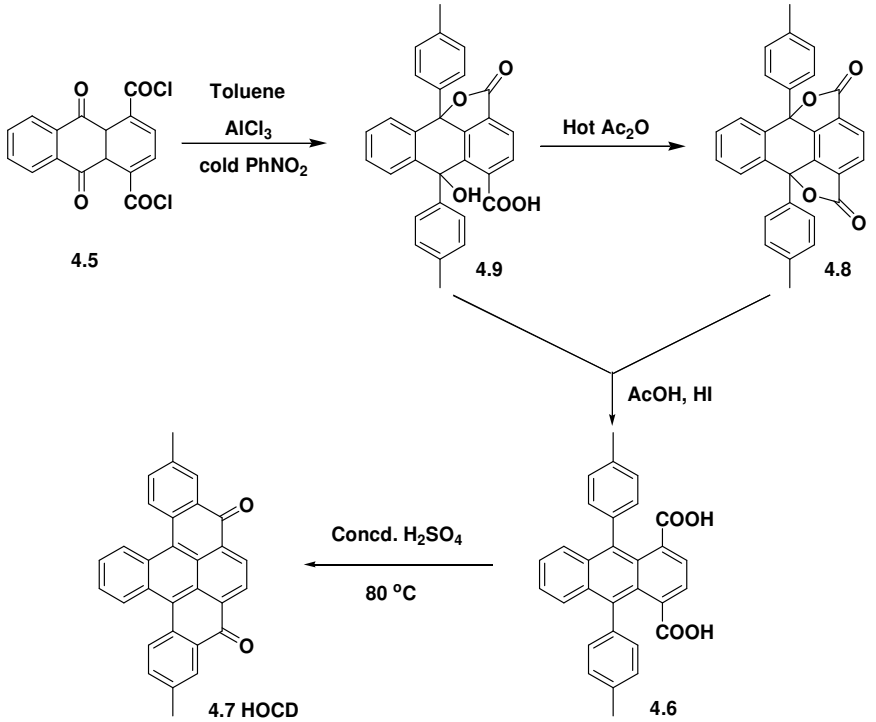

Figure 4.3 *Synthesis of HOCD by Scholl et al. (EDC: ethylene dichloride)*

No other synthetic method for HOCD was reported since Scholl et al disclosed the synthesis of HOCD and its analogies such as heterocoerdianthrone (HCD) in 1930s' (***Figure 4.3)***.[87] Phthalic anhydride **4.1**

and *p*-xylene **4.2** were used as starting materials to form 1,4-dimethyl anthraquinone **4.3** (DMA) through a *Friedel-Crafts* reaction. DMA, under the catalysis of activated manganese dioxide, can be easily oxidized to diacid **4.4** which was subsequently treated with thionyl chloride to form acyl chloride **4.5**. While treating **4.5** and *p*-xylene in the presence of aluminum chloride in nitrobenzene, we increased the reaction temperature to accelerate the reaction. Surprisingly, the products obtained from the reaction are different from previous report. In Scholl's method, **4.5** reacted with *p*-xylene in the presence of aluminum chloride in cold nitrobenzene gave 9, 10-dihydroxy-9,10-di-*p*-tolylanthracene-1,4-dicarboxylic acid monolactone (Compound **4.9**). Subsequently di-*p*-tolyanthracene-1,4-dicarboxylic acid (Compound **4.6**) was obtained from the treatment of **4.9** with acetic acid and hydrogen iodine. Conversion of dicarboxylic acid **4.6** to HOCD **4.7** was then been obtained under the treatment of concentrated H_2SO_4. However, while we treated **4.5** and toluene in the presence of aluminum chloride in nitrobenzene at 100 °C, after the usual work-up with water, dicarboxylic acid **4.6**, 9, 10-dihydroxy-9,10-di-*p*-tolylanthracene (Compound **4.10**) but only trace amount HOCD was obtained.

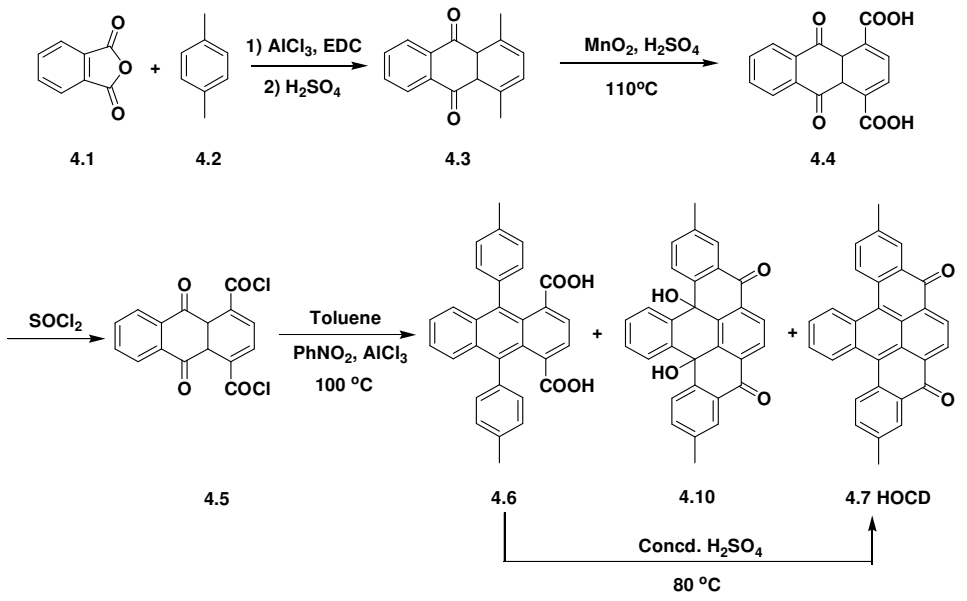

Figure 4.4 *Synthesis of HOCD (EDC: ethylene dichloride)*

This phenomenon has also been found in the synthesis of HOCD analogues, the cycloalkylated HCD derivatives by Hayashi et al.[88] Hayashi treated acyl chloride with indane/tetralin instead of benzene that was reported by Scholl. When the acyl chloride was treated with benzene in the same *Friedel-Crafts* conditions, the reaction proceeded in the similar manner as Scholl's.[87] However, when the acyl chloride was treated with indan or tetralin, the desired product were obtained more conveniently than Scholl's route. Unlike Scholl's multi-step reaction, the cyclization took place during the reaction while hydrogen peroxide was eliminated upon work-up to produce the desired HCD analogues (***Figure 4.5***). Therfore, we rationalized that toluene in our case is similar to the indan or tetralin in Hayashi's cases, in which the stronger electrophilic ability induced by the electron donating alkyl group might have facilitated the substitution and cyclization than benzene in Scholl's synthesis. When the reaction was quenched with water, $AlCl_3$ was hydrolyzed and generated strong hydrochloric acid. Scholl et al reported products monolactone **4.9** and dilactone **4.8** were not stable in this strong acidic environment and hence the hydrolyzed products were formed. It is also noteworthy that di-carboxylic acid **4.6** can be quantitatively converted to the desired HOCD **4.7** by the treatment of concentrated H_2SO_4. Hence, the overall yield from diacid **4.4** to HOCD is 36%.

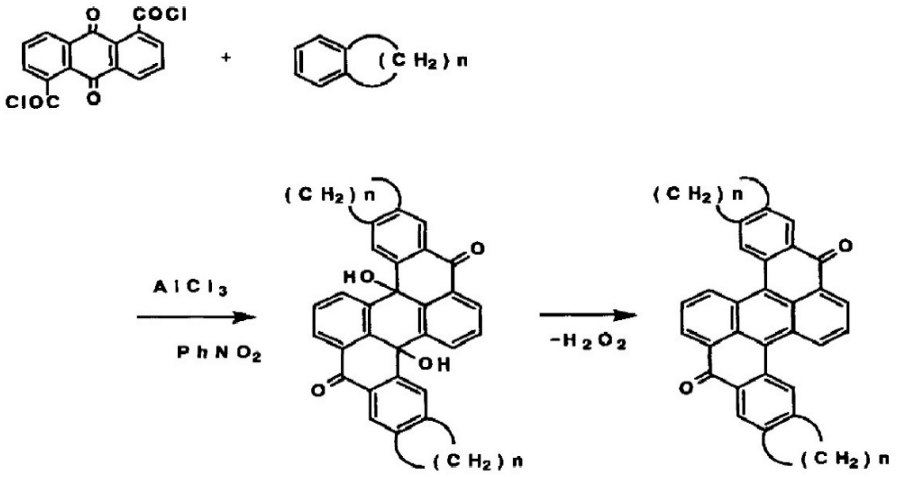

Figure4.5 *Synthesis of HCD derivatives by Hayashi et al.*[88]

While the *Friedel-Crafts* reaction occurred in the presence of light, an interesting by-product 4,4'-dimethylbiphenyl, **4.17** was obtained in 10% yield. We suppose that in the presence of photons, oxygen and the HOCD or the intermediates in the reaction mixture catalyzed the coupling reaction of two toluene molecules. This observation warrants further investigation which will not be discussed in this thesis as it is beyond the scope of this project.

4.2.2 Reactivity of HOCD with ROS

HOCD shows a strong and wide absorbance peak from 500-700 nm with a maximum around 653 nm, due to the presence of conjugated π system. When HOCD reacts with singlet oxygen, the formation of colorless HOCDPO is confirmed by EI-MS (m/z = 442.1) (***Figure 4.6).*** The blue color would fade with the loss of delocalization of the π electrons over the entire HOCDPO system (***Figure 4.2***).

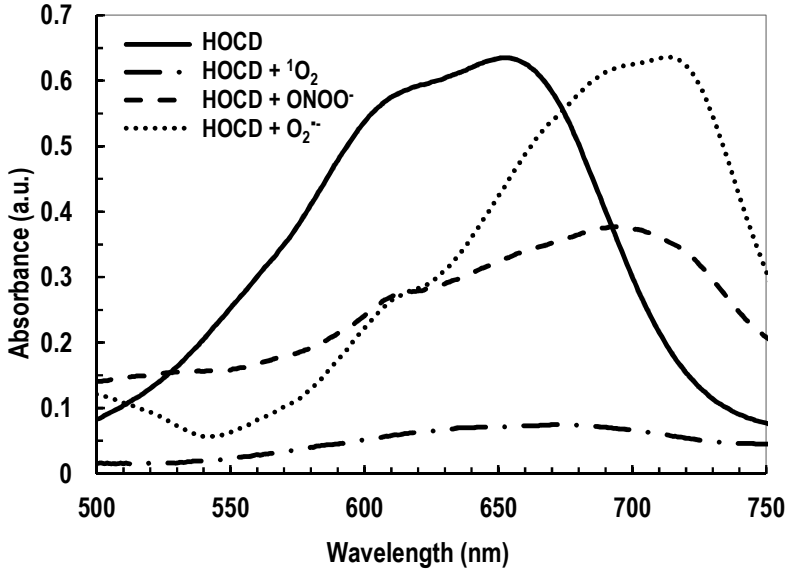

Figure 4.6 *Absorbance of the reaction between HOCD and ROS. 0.15 mM HOCD was treated with various ROS in DMF*

While studying the reactivity of HOCD towards different ROS such as hypochlorite, hydrogen peroxide and nitric oxide by monitoring UV-Vis, we found that HOCD has a very good sensitivity and selectivity toward $^1O_2$ (***Figure 4.6***). The reaction of HOCD with $^1O_2$ decreased the most significantly

compared to the other ROS tested. The absorbance at 653 nm of HOCDPO after reaction is only less than 10% of HOCD. When HOCD was reacted with $O_2^{\bullet-}$, there was a red shift of 50 nm observed. While, reaction with peroxynitrite ($ONOO^-$) showed a decrease of about 50%, which is not enough to bleach the blue color of HOCD (***Figure 4.7***).

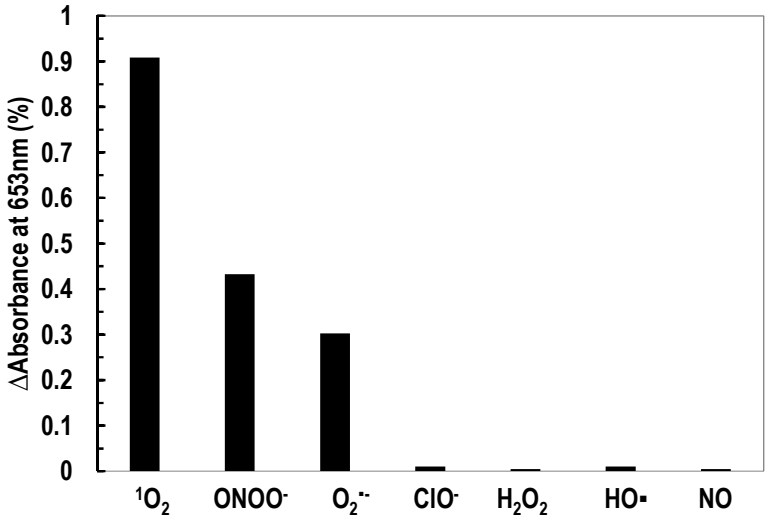

Figure 4.7 *Absorbance decrease at 653 nm while 0.15 mM HOCD was treated with various ROS in DMF. 10 eq. ROS was added, whereas excess $O_2^{\bullet-}$ and 1 eq. of $ONOO^-$ was introduced.*

4.2.3 Quenching and turning on the fluorescence of QDs by HOCD and $^1O_2$

The spectroscopic property of HOCD makes it a good quencher for the QDs fluorescence ***(Figure 4.8).*** It has a very broad absorption band from 500 nm to 700 nm, which covers the emission band of CdSe/ZnSe QDs (λ_{em} = 610 nm), and an extinction coefficiency of 4353 $M^{-1}cm^{-1}$ at 653 nm. When HOCD reacted with singlet oxygen, the blue color was bleached and the colorless HOCDPO does not have any absorption above 500 nm, thereby allowing the fluorescence of QDs to be turned on.

Different concentrations of HOCD were added to the hydrophobic trioctylphosphine oxide (TOPO) and trioctylphosphine (TOP) capped CdSe/ZnS QDs (λ_{em} = 610 nm) to examine the quenching ability of HOCD

(***Figure 4.9***). As shown in ***Figure 4.10***, HOCD can quench the fluorescence of QDs. When the concentration of HOCD increases, the QDs fluorescence decreases, verifying our hypothesis of the quenching effect of HOCD molecules.

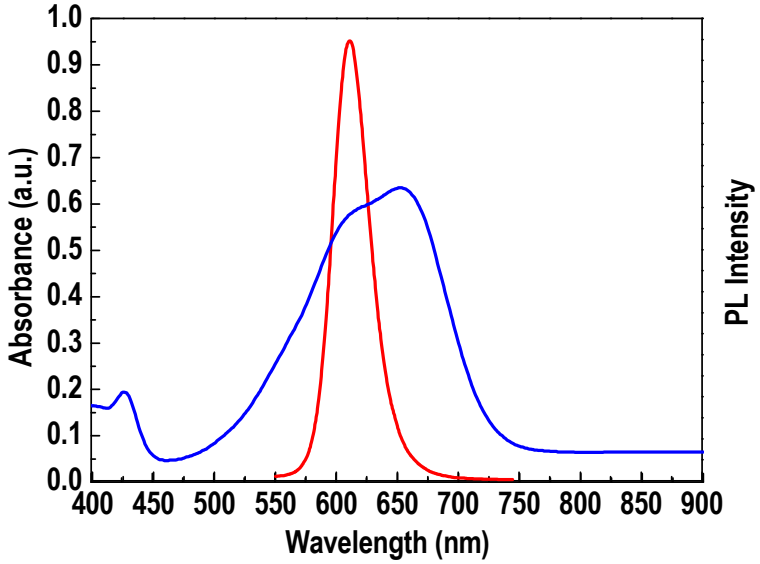

Figure 4.8 *UV-vis absorption spectra of HOCD (blue) and the photoluminescence spectra of CdSe/ZnS QDs (red). The PL intensities were normalized with respect to the absorbance.*

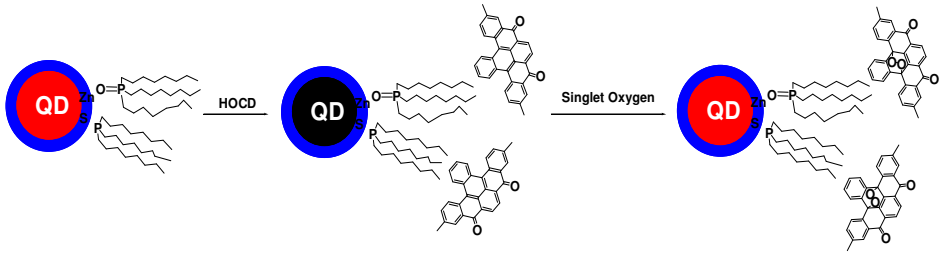

Figure 4.9 *Quenching and turning on fluorescence mechanism by HOCD.*

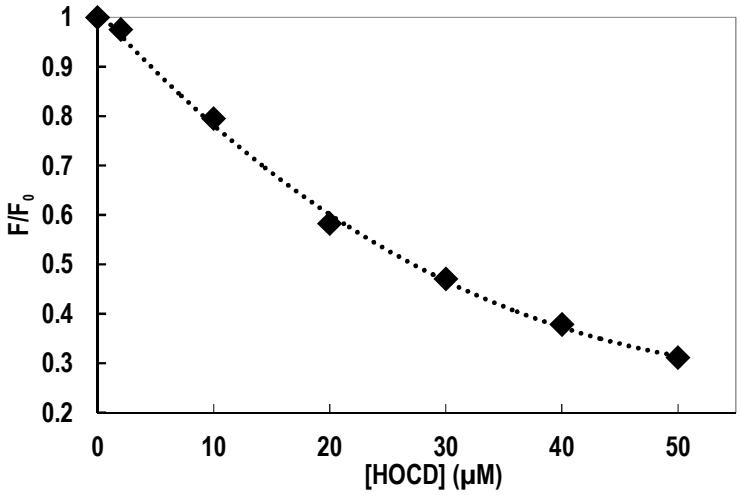

Figure 4.10 *Quenching of fluorescence intensity of CdSe/ZnS QDs at 610 nm with the addition of HOCD, λ_{ex}=450 nm.*

The turn-on mechanism was also successfully identified by adding singlet oxygen to the HOCD-QD solution. Singlet oxygen was generated by the exposure of photo sensitizer rose Bengal under irradiation. Under irradiation, photo sensitizer catalyzed the triplet oxygen to singlet state and the generated singlet oxygen decolourized the deep blue HOCD-QD solution into colorless HOCDPO-QD solution. As, the energy transfer quenching of QDs by HOCD was decreased, the CdSe fluorescence was gradually turned on (***Figure 4.11, Figure 4.12***).

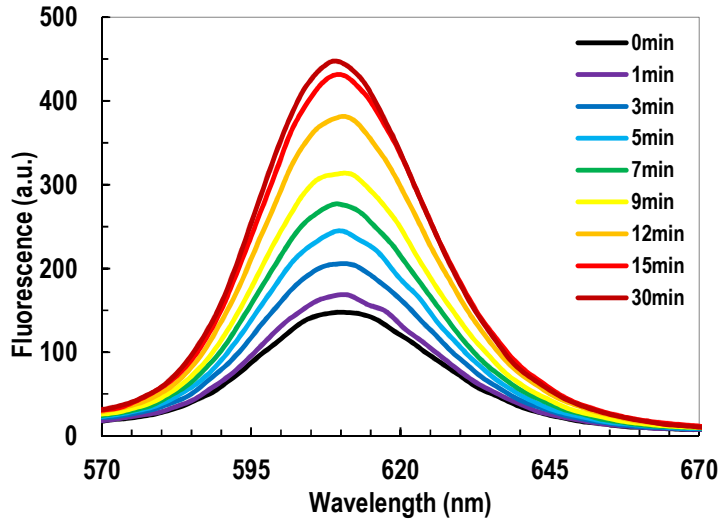

Figure 4.11 *Fluorescence enhancement of HOCD-QD solution by singlet oxygen (λ_{ex}=450 nm).*

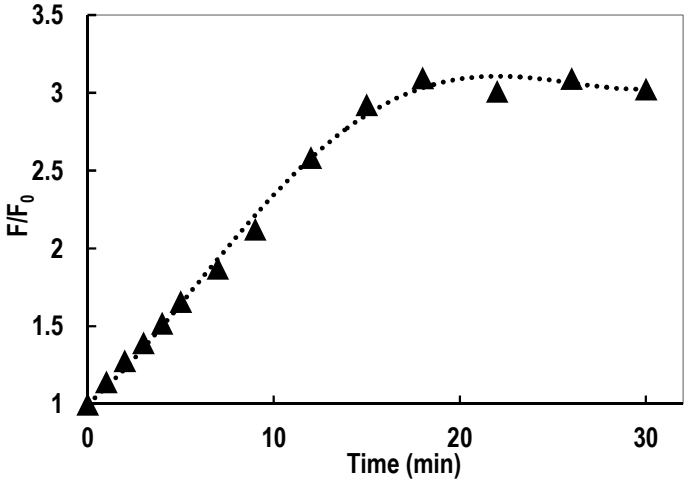

Figure 4.12 *Increments of fluorescence intensity at 610 nm of the HOCD-QD nano probe during the generation of singlet oxygen (λ_{ex} =450 nm).*

4.2.4 Hydrophilic QDs for the detection of singlet oxygen

Previous results identified the "turn-on" mechanism of HOCD-QD by singlet oxygen is promising. Unfortunately, the quenching efficiency of HOCD in solution is not very satisfactory. The high concentration of HOCD required for efficient quenching in solution will consume high concentration of singlet oxygen, leading to low sensitivity of the detection. For instance, 50 μM HOCD can only quench approximately 75% of the QDs fluorescence. Moreover, hydrophobic QDs and HOCD are lipid soluble and thus, are not suitable to be applied in the aqueous biological environment.

In order to make the molecularly engineered probe more biocompatible, hydrophilic QDs are designed (***Figure 4.13***). Previously synthesied hydrophobic TOPO/TOP capped CdSe/ZnS QDs are only soluble in organic solvent, such as chloroform and toluene. Water soluble QDs can be prepared as QD micelles that are synthesized by vigourous stirring a concentrated suspension of TOPO/TOP QDs in chloroform in chloroform in to an aqueous solution of surfactant cetyltrimethylammonium bromide (CTAB). After ten minutes of sonication an oil-in-water microemulsion was formed. Evaporation of chloroform upon heating transfers the QDs into the aqueous phase by an interfacial process driven by the hydrophobic *van der Waals* interactions between the primary alkane of the stabilizing ligand and the secondary alkane

of the surfactant, resulting in thermodynamically defined interdigitated bilayer structures. The synthesized hydrophilic QD micelles shows luminescence property similar to hydrophobic QDs, with a slight red shift (***Figure 4.14***).

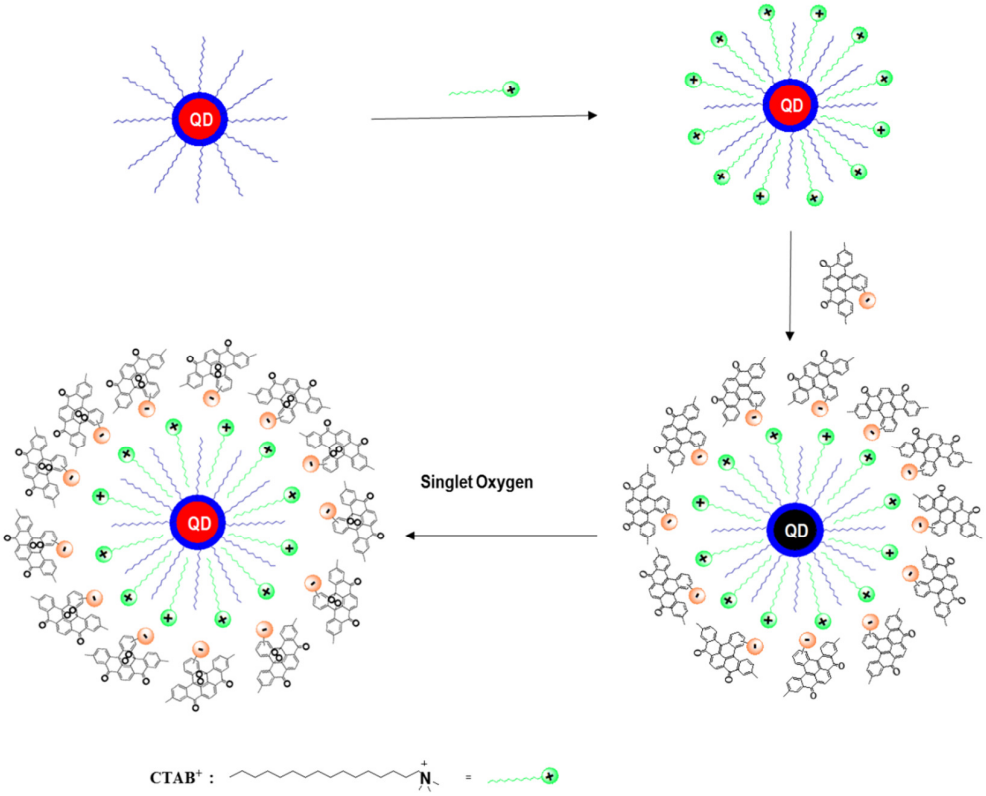

Figure 4.13 *Molecularly engineered hydrophilic QDs.*

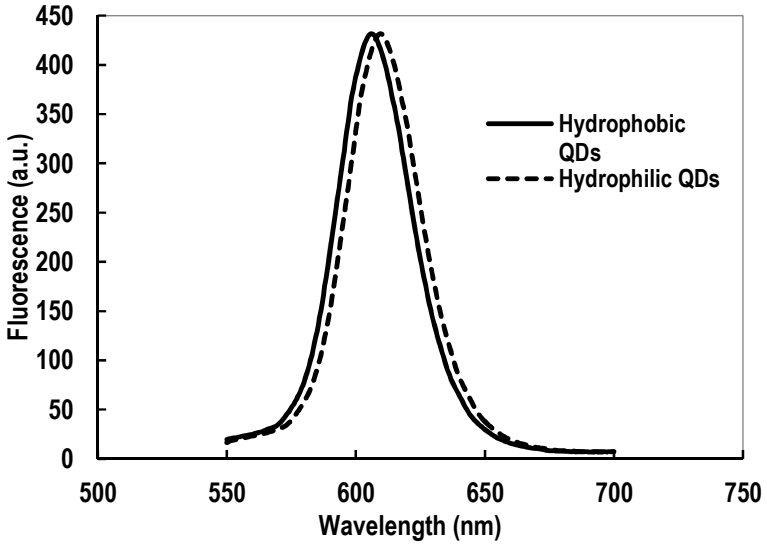

Figure 4.14 *Fluorescence comparison of hydrophilic QDs in water and hydrophobic QDs in chloroform.*

The CTAB cation on the hydrophilic QD surface made it positively charged. A complementary and more effective quencher HOCD is prepared by subjecting HOCD with excess chlorosulfonic acid in anhydrous dichloromethane, yielding negatively-charged HOCD-sulfonic acid (HSa, HSb, compound ***4.11a, 4.11b*** upon subsequent treatment with water (***Figure 4.13*** and ***Figure 4.15***). There are two different HOCD-sulfonic acid obtained at different temperatures. When chlorosufuric acid reacts with HOCD at 0 °C, the obtained HOCD-sulfonic acid HSb (**4.11b**) is soluble in dichloromethane and non-polar solvents. On the other hand, when the reaction takes place at room temperature in dichloromethane, the main product HSa (**4.11a)** precipitates from the solvent and has good solubility in water and polar solvent. The two products are identified by ESI-MS and NMR. They have the same peak of 489.3 in the negative ESI mode which shows both products have only one sulfonic acid group substituted on HOCD. The NMR spectra of the two HOCD-sulfonic acid strctures further supported this result. Both products have eleven aromatic protons indicating that one of the HOCD aromatic proton has been replaced. HSa and HSb are structural isomers which have different $-SO_3H$ substitution positions and hence, the different physical properties. Proton and carbon NMR spectra are, however, insufficient to identify the exact position of the substitution. The most precise method to image the exact structure is X-ray crystallography but despite numerous solvent combinations for crystal growth, we were unable to obtain good crystals to identify the positions of sulfonic acid groups of HSa and HSb.

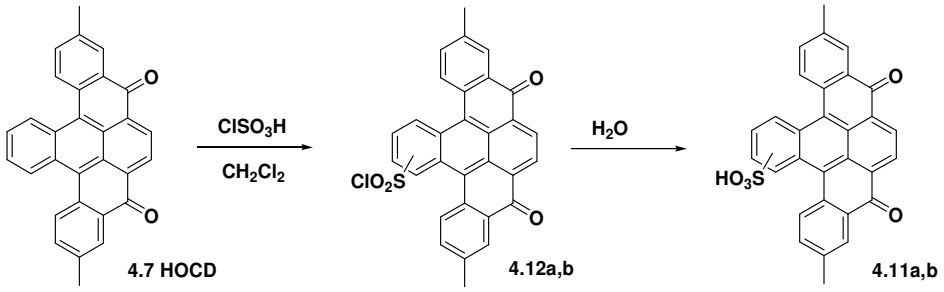

Figure 4.15 *Synthesis of HOCD-sulfonic acid, HSa* ***4.11a****, HSb* ***4.11b****.*

The HOCD-sulfonic acid HSa, which has good solubility in polar and aqueous solvents, is more suitable as the quencher for hydrophilic QDs. Similar to HOCD, the UV-*vis* spectra of HSa shows it also has an intense absorbance at green to red light range. With respect to HOCD, the absorbance of HSa has a blue shift around 30 nm with a maximum at 626 nm. The absorbance range is from 450 nm to 700 nm which also covers the fluorescence of CTAB-QDs (***Figure 4.16***).

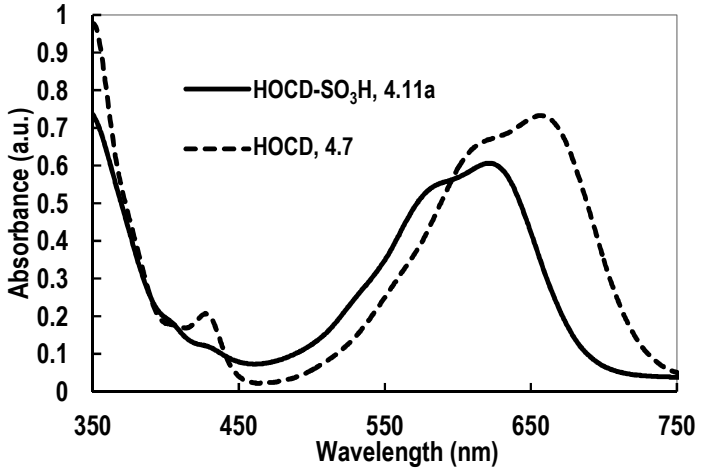

Figure 4.16 *Absorbance of 0.1 mM HOCD in DCM and 0.1 mM HOCD-SO_3H* ***4.11a*** *in acetone.*

When negatively-charged HOCD derivative HSa is exposed to positive-charged CTAB-QDs, the ion-pair QDs are formed. Comparing with HOCD, HSa shows better quenching efficiency. With 25 μM HSa, more than 90% of the CTAB-QDs fluorescence have been quenched whereas 50 μM HOCD can only quench 75% hydrophobic QDs fluorescence (***Figure 4.17***). There are two quenching processes usually encountered, which are namely collisional (dynamic or biomolecular) quenching and static (complex formation) quenching. Collisional quenching occurs when the excited fluorophore contacts with a molecule that can facilitate non-radiative transitions to the ground state. In the simplest case of collisional quenching, the following relation, called the Stern-Volmer equation holds with the following relation: $I_0/I = 1 + K_{sv}[\text{Quencher}]$ (where K_{sv} is the Stern-Volmer quenching constant). A plot of I_0/I versus [Quencher] should yield a straight line. In another hand, in some cases, the fluorophore can form a stable complex with another

molecule. Static quenching happens when the ground-state of the complex is non-fluorescent. In these cases, the relation: $I_0/I = 1 + K_a[\text{Quencher}]$ can be observed (where K_a is the association constant of the complex). When both static and dynamic quenching are occurring at the same time, the following relation holds:$I_0/I = (1 + k_q\tau_0[\text{Quencher}])\ (1 + \text{Ka}[\text{Quencher}])$ (Where k_q is the bimolecular quenching rate constant and τ_0 is the excited state lifetime in the absence of quencher.) Based on Stern-Volmer plot of the quenching effect of HSa, an upward curvature is observed (***Figure 4.17***). This phenomenon indicates that the quenching effect of HSa is possibly due to both dynamic and static quenching as I_0/I versus [HSa] have the $[\text{HSa}]^2$ term.

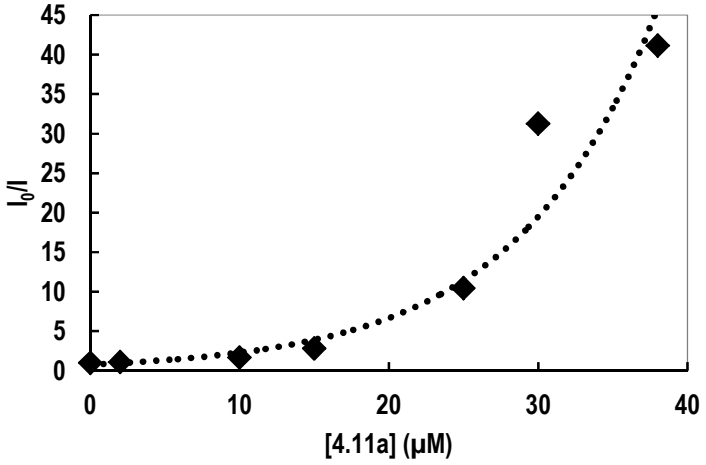

Figure 4.17 *Quenching effect of HOCD-SO_3H* ***4.11a*** *for CTAB-QDs at 610 nm λ_{ex}=450 nm.*

The ion-pair HSa-CTAB-QDs probe shows good selectivity to singlet oxygen comparing with other ROS (***Figure 4.18***). Hydrogen peroxide-hypochlorite singlet oxygen generation system was used to verify the fluorescent of the ion-pair probe was indeed being turned on by singlet oxygen. When large excess of hypochlorite was added to a solution of 30 μM HSa with CTAB-QDs in water, no fluorescence increase observed. However after hydrogen peroxide was added to the solution, the fluorescence was turned on immediately due to the generation of singlet oxygen (***Figure 4.19***).

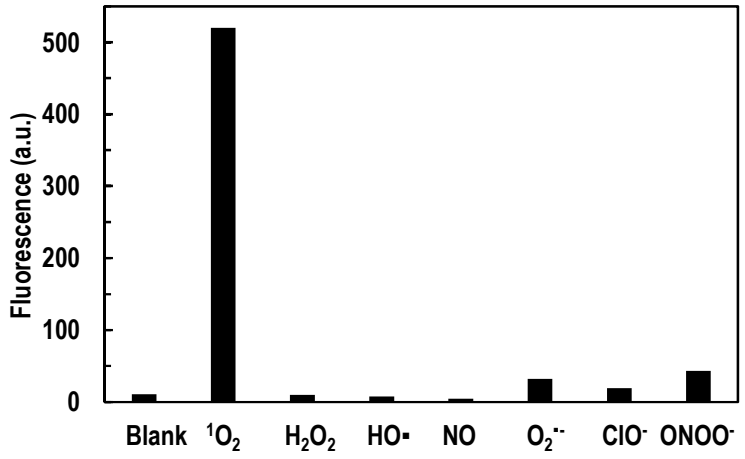

Figure 4.18 *Fluorescence responses of 30 μM HSa* ***4.11a*** *and CTAB-QDs with 100 μM reactive oxygen species (ROS). Bars represent fluorescence intensity at 610 nm 1 min after the addition of ROS. Data were collected at RT in water, λ_{ex} = 450 nm.*

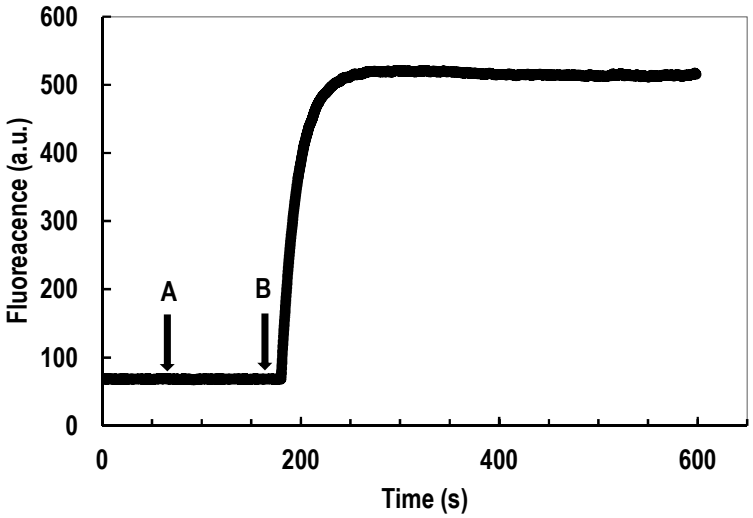

Figure 4.19 *Fluorescence responses of 30 μM HSa* ***4.11a*** *and CTAB-QDs with singlet oxygen. 500 μM hypochlorite was added to the solution at 60 s (A), and 100 μM hydrogen peroxide was added at 180 s (B).*

4.2.5 Trials for the synthesis of covalent bonding QD probe

Hydrophilic ion-pair HSa-CTAB-QDs shows selectivity to singlet oxygen. Comparing with HOCD-hydrophobic QDs, the quencher HSa is more efficient owing to stronger binding of positive-negative ionic interaction than *Van der waal's* interaction in the hydrophobic HOCD-QDs probe. With 25 μM HOCD, 90% of the CTAB-QDs fluorescence can be quenched. However, this quenching effect is still at micro molar level which is not as sensitive as desired. In addition, the ionic interaction is subject to ion exchange in biological systems. To overcome such limitations, covalent bonding of HOCD on the surface of QDs could be a good choice. Moreover, the binding of HOCD molecules on the QDs surface may prevent the oxidation of CdSe core by singlet oxygen and thereby increase the stability of QDs.

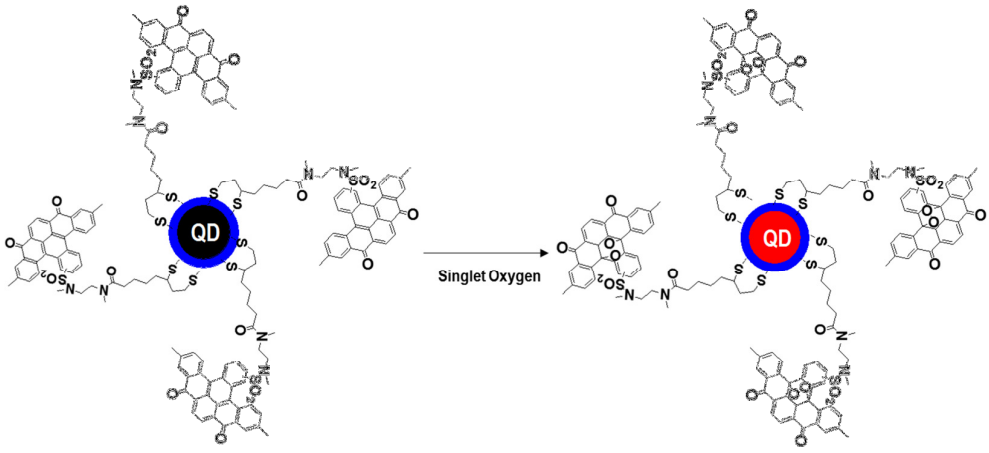

Figure 4.20 *Design of covalent bonding HOCD-QDs probe for the detection of singlet oxygen.*

As such, a nanocomposite containing covalently grafted HOCD onto the surface of QDs by 'cap exchange' is designed as shown in ***Figure 4.20***. This 'cap exchange' involves the substitution of the native TOP/TOPO shell of hydrophobic QDs with bifunctional ligand lipoic acid through the thiol groups, that serves as surface anchors to bind to the fluorescent quencher HOCD derivatives. In order to obtain the HOCD-lipoic acid ligand, N, N'-dimethyl ethylene diamine was chosen as a linker as its two amine groups can react with HOCD sulfonic acid **4.11** and lipoic acid respectively. The reduced dithiol

group of lipoic acid moiety can easily coordinate to the zinc sulfate shell and exchange the TOPO and TOP ligands from the surface of hydrophobic QDs.

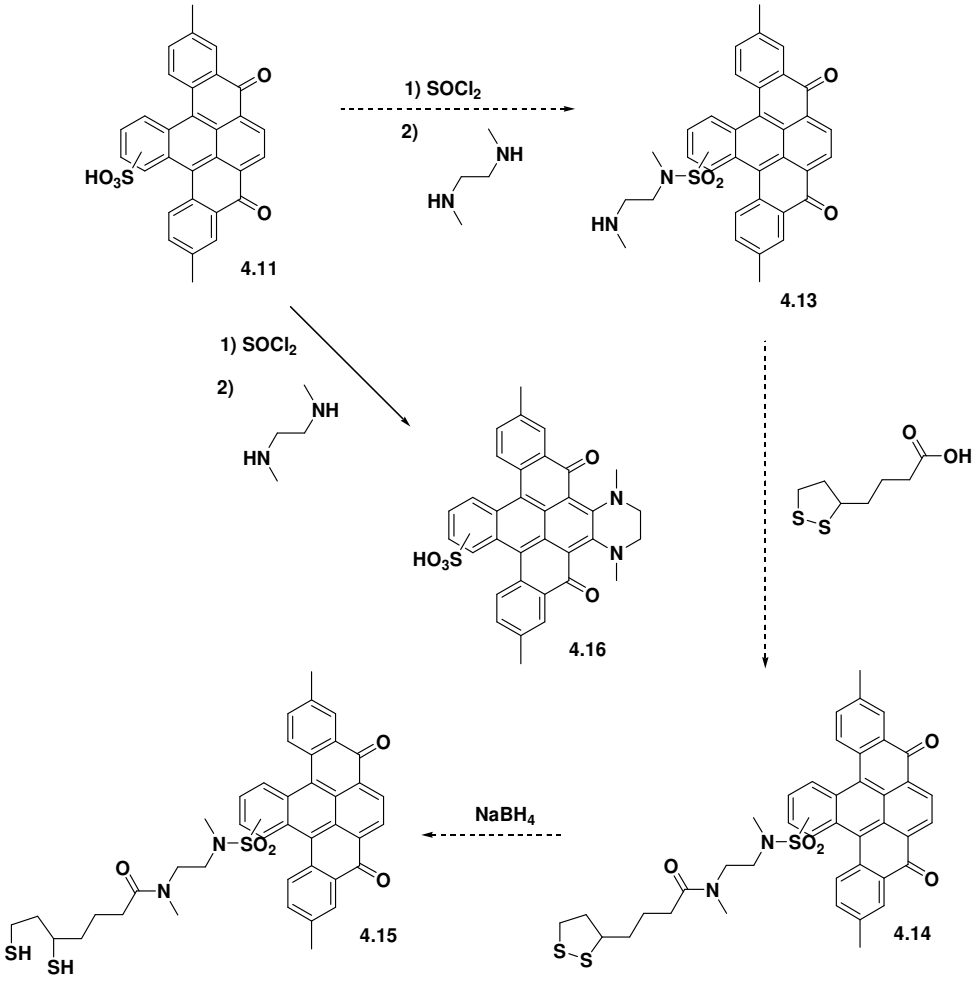

Figure 4.21 *Synthetic route designed for the covalent bonded QD probe.*

However, we did not obtain the desired probe through the suggested route. When we attempted to prepare the HOCD-ethylene diamine sulfonamide in common conditions, the reaction did not give rise to the desired product **4.13** and instead, amination reaction of $C(sp^2)$-H happened, obtaining a cycloaddition product **4.16** in quantitative yield (***Figure 4.21***). The elucidation of the structure of **4.16** is verified by the NMR and MS spectra. The serendipitous discovery is significant and therefore, further studied on the reaction were carried out before pursuing nanocomposites containing QDs

with covalently linked HOCD. Detailed account of the reaction is described in **Chapter 5**.

4.3 Conclusion

Molecularly-engineered QDs have been designed and synthesized to selectively detect singlet oxygen by the formation of endoperoxides. Polycyclic aromatic hydrocarbon compounds namely the HOCD and its derivatives were synthesized as they have strong absorbance of visible light, have the ability to react with singlet oxygen selectively and give colorless endoperoxides. CdSe/ZnS core/shell QDs are suitable to be used as the fluorophores because they can give brighter and more stable fluorescence than organic dyes. By grafting the selected polycyclic aromatic hydrocarbon compounds onto the surface of QDs, the fluorescence of QDs can be quenched by Förster resonance energy transfer (FRET). After reacting with singlet oxygen, the efficiency of FRET decreased dramatically and the fluorescence of QDs can be turned on. In order to make the molecularly-engineered QDs probe water-soluble and more sensitive to singlet oxygen, hydrophilic ion pair HSa-CTAB-QDs are synthesized. The hydrophilic QDs probe also showed good selectivity towards singlet oxygen among various ROS. The sensitivity to singlet oxygen is also improved due to the ion pair interaction.

4.4 Experimental Section

4.4.1 Instruments and Materials

^{1}H and $^{13}C\{^{1}H\}$ NMR spectra were recorded in deuterated chloroform with a Bruker AC300 spectrometer (Karlsruhe, Germany) at 300 and 75 MHz, respectively. High resolution MS spectrum was obtained from Finnigan (MAT 95XL-T) high resolution (60,000), 5KV Double Focusing Reversed Nier-Johnson Geometry Mass Spectrometer. UV-Vis spectra were recorded using a Shimadzu UK1601 spectrophotometer fitted with a quartz cell. Fluorescence analysis was performed using Perkin Elmer LS 55 Luminescence Spectrometer, with excitation/emission slit 10 nm and scan speed 500 nm/min. All solvent used were of reagent grade unless otherwise specified. Phthalic anhydride was purchased from Alfa Aesar. Anhydrous aluminum chloride was

purchased from Fluka. Sodium bicarbonate was purchased from Sino Chemical Co. (Pte) Ltd. All chemicals unless indicated were obtained from Sigma Aldrich and used as received.

4.4.2 Synthesis of HOCD and its derivatives

1,4-Dimethylanthraquinone, 4.3: Aluminum chloride (34.8 g, 0.261 mol) and 150 ml DCM were added to a 250 ml round bottom flask. The reaction mixture was immersed in ice bath before phthalic anhydride (14.8 g, 0.1 mol) and p-xylene (12.9 ml, 0.105 mol) were added. The reaction mixture was allowed to stir for 1 hour before the ice bath was removed though stirring continued overnight. The reaction mixture was then added to cold diluted hydrochloric acid slowly with stirring. The mixture obtained was separated with a separation funnel. The organic layer was collected, rotary evaporated to dryness and washed with deionized water. The pale yellow solid was vacuumed dry at 100 °C for 2 hours and dichloromethane were added to a 250 ml round bottom flask and immersed in ice bath before drop wise addition of concentrated sulphuric acid (105.8 ml, 1.97 mol). The reaction mixture was allowed to stir in ice bath for 1 hour before the temperature was increased to 60 °C for another 3 hours. The reaction mixture was then added slowly into ice water and chloroform was used for extraction. The organic layer was washed with 10% ammonia, dried with anhydrous Na_2SO_4 and rotary evaporated to dryness. 1,4-Dimethylanthraquinone **4.3** was obtained as yellow solid, yield: 60% (14.23 g). ^{1}H NMR ($CDCl_3$): δ = 8.13-8.16 (m, 2H), 7.69-7.72 (m, 2H), 2.77 (s, 6H) ppm. $^{13}C\{^1H\}$ NMR (75 MHz, $CDCl_3$): δ = 185.83, 140.14, 137.30, 134.07, 133.35, 132.74, 126.44, 23.71 ppm. FAB-MS: m/z 236.0.

9,10-Dioxo-9,10-dihydroanthracene-1,4-dicarboxylic acid, 4.4: To a stirred suspension of 1,4-dimethylanthraquinone (1.3 g, 5.51 mmol) in concentrated sulphuric acid (45.9 ml) and deionized water (15.7 ml) at 80 °C, MnO_2 (6.88 g, 79.1 mmol) was added in portions. The temperature was increased to 110 °C after 15 minutes. Four hours later, the reaction mixture was poured into water slowly after cooling. The resulting solid was separated, dissolved in diluted ammonium hydroxide and the solution was filtered.

Hydrochloric acid was added to the filtrate and 0.641 g of pale yellow solid 9,10-dioxo-9,10-dihydroanthracene-1,4-dicarboxylic acid **4.4** was separated, yield: 39%. ^{1}H NMR (DMSO-d_6): δ = 13.32 (br, 2H), 8.15-8.18 (m, 2H), 7.95-7.98 (m, 2H), 7.87 (s, 2H) ppm. ^{13}C{^{1}H} NMR (75 MHz, DMSO-d_6): δ (ppm): 181.56, 169.86, 136.83, 134.86, 132.70, 132.32, 129.90, 126.83 ppm. ESI-MS: m/z 295.0 $[M-H]^-$.

Dimethylhomoocoerdianthrone, 4.7: 9,10-Dioxo-9,10-dihydro-anthracene-1,4-dicarboxylic acid (0.4 g, 1.34 mmol) was mixed with 2 mL thionyl chloride and reflux for 3 hours. The excess thionyl chloride was removed by distillation under reduced pressure. The residue was used directly without any purification. 10 eq $AlCl_3$ was added to the residue with 1 mL toluene (9 mmol), 4 mL nitrobenzene at 0 ℃. The reaction was kept under nitrogen and stirred for 30 min before the temperature was increase to r.t. for 3 days with stirring. Water (10 mL) was added to the reaction and extracted with ethyl acetate. The organic layer was concentrated and 0.55 g brown color solid was obtained. ESI-MS shows the brown solid is a combination of 9,10-di *p*-tolylanthracene-1,4-dicarboxylic acid **4.6**, 9, 10-dihydroxy-9,10-di-*p*-tolylanthracene **4.10**, and HOCD **4.7**. Compound **4.6** was identified by ESI-MS with $[M-H]^-$ = 445.1. Compound **4.10** was identified with EIMS for $C_{30}H_{20}O_4$: 444.1.

The brown solid (0.55 g) without purification was added to 4 mL concentrated H_2SO_4 and was kept at 80 ℃ for 1hour. 4 mL ice water was added to quench the reaction. Blue precipitate forms, filtered and purified the blue solid by column chromatography ($CHCl_3$) get compound **4.7 (**200 mg, yield 36%). ^{1}H NMR ($CDCl_3$): ^{1}H NMR (300 MHz, $CDCl_3$) δ = 8.79 (s, 2H), 8.74 (dd, *J* = 6.6, 3.2 Hz, 2H), 8.28 (s, 2H), 8.25 (d, *J* = 8.3 Hz, 2H), 7.57 (t, *J* = 6.5 Hz, 4H), 2.55 (s, 6H) ppm. HREIMS: cacld. $C_{30}H_{15}O_2$ 410.1307, found 410.1294.

4,4'-Dimethylbipheny **4.17** (180 mg, 11% based on total amount of toluene added) was also been separated by column chromatography ($CHCl_3$) ^{1}H NMR (300 MHz, $CDCl_3$) δ = 7.30 (d, *J* = 8.2 Hz, 4H), 7.04 (d, *J* = 8.2 Hz, 4H), 2.15 (s, 6H) ppm. The structure was confirmed by comparing the data with that of authentic compound purchased commercially. EIMS: *m/z* = 182.1.

3,10-Dimethyl-5,8-dioxo-5,8-dihydronaphtho[1,2,3,4-rst]pentaphene

sulfonic acid, 4.11a: To a solution of **4.7** (50 mg, 0.122 mmol) in 2 mL anhydrous dichloromethane, chlorosulfonic acid (40 µM, 0.60 mmol) was added dropwise at room temperature. The reaction was kept at room temperature overnight and dark blue percipitate formed. The percipiate was filtered and washed with dichloromethane and hexane. The blue solid obtained was then recrystalized from actone get pure **4.11a** (36 mg, yield 60%),^{1}H NMR (acetone-d_6): δ = 8.66 (s, 1H), 8.14 (s, 2H), 8.03 (d, *J* = 9.0 Hz, 1H), 7.79 (s, 1H), 7.67 (s, 1H), 7.57 – 7.42 (m, 3H), 7.26 (d, *J* = 8.0 Hz, 1H), 7.10 (d, *J* = 8.0 Hz, 1H), 2.39 (s, 3H), 2.34 (s, 3H) ppm. HR-ESIMS: negative mode [M-H]$^-$ cacld. $C_{30}H_{17}O_5S$ 489.0802, found 489.0795.

3,10-Dimethyl-5,8-dioxo-5,8-dihydronaphtho[1,2,3,4-rst]pentaphene sulfonic acid, 4.11b: To a solution of **4.7** (25 mg, 0.06 mmol) in 2 mL anhydrous dichloromethane, chlorosulfonic acid (20 µM, 0.30 mmol) was added dropwise at 0 °C. The reaction was kept at 0 °C for 5 hours and room temprature for 2 more hours. 10 mL water was added to the solution and the DCM layer was separated. The organic layer was washed with water, dried with anhydrous Na_2SO_4 and rotary evaporated to dryness. Column separation gave blue solid **4.11b** (16 mg, 54%) ^{1}H NMR (300 MHz, $CDCl_3$) δ = 9.36 (d, *J* = 1.8 Hz, 1H), 8.86 (d, *J* = 9.4 Hz, 1H), 8.73 (q, *J* = 7.5 Hz, 2H), 8.25 (s, 2H), 8.08 (d, *J* = 8.2 Hz, 1H), 8.03 – 7.94 (m, 2H), 7.61 (ddd, *J* = 17.4, 8.2, 1.6 Hz, 2H), 2.56 (d, *J* = 1.3 Hz, 6H) ppm. ^{13}C NMR (75 MHz, $CDCl_3$) δ = 184.22, 184.18, 142.80, 141.38, 140.84, 135.37, 134.92, 134.02, 133.65, 132.34, 131.90, 131.81, 131.76, 130.94, 130.63, 130.46, 130.37, 130.20, 129.97, 129.78, 129.39, 129.14, 122.43, 22.07 ppm. HR-ESIMS: nagative mode [M-H]$^-$ cacld. $C_{30}H_{17}O_5S$ 489.0802, found 489.0820.

4.16: Vacumn dried **4.11a** (29 mg, 0.06 mmol) was disolved in 2 mL $SOCl_2$ and the solution was refluxed for two hours. $SOCl_2$ was then removed under vacumn. The residue was then disolved in 2 mL anhydrous dimethylformamide and added to N, N'-dimethylethylenediamine (55 mg, 0.62 mmol) in 5 mL anhydrous dimethylformamide dropwise at 0 °C. The reaction was kept at 0 °C for one hours and room temprature overnight. 10 mL water was added to the solutin and the dichloromethane layer was separated. The organic layer was washed with water, dried with anhydrous Na_2SO_4 and

rotary evaporated to dryness. Column separation gave purple solid **4.16** (32 mg, 93%). ^{1}H NMR (500 MHz, $CDCl_3$) δ = 9.34 (d, *J* = 1.5 Hz, 1H), 8.79 (d, *J* = 8.9 Hz, 1H), 8.47 (d, *J* = 8.2 Hz, 1H), 8.40 (d, *J* = 8.2 Hz, 1H), 8.30 (d, *J* = 11.3 Hz, 2H), 7.96 (dd, *J* = 8.9, 1.6 Hz, 1H), 7.56 – 7.44 (m, 2H), 3.97 (s, 4H), 3.13 (s, 6H), 2.55 (s, 3H), 2.53 (s, 3H) ppm. ^{13}C NMR (126 MHz, $CDCl_3$) δ = 179.63, 149.18, 148.98, 141.50, 137.41, 137.34, 133.89, 133.82, 133.59, 132.88, 132.60, 129.77, 129.59, 128.42, 127.95, 127.57, 127.47, 125.27, 123.85, 122.93, 122.62, 121.94, 105.93, 51.17, 45.95, 22.04 ppm. ESIMS: negative mode $[M-H]^-$ 573.29.

4.4.3 Synthesis of hydrophobic QDs

The starting hydrophobic core/shell CdSe/ZnS QDs were synthesized according to literatures.[89] Briefly, 0.064 g of CdO, 5.91 g of TOPO and 6.02 g of HDA were added to a flask. The mixture was kept under vacuum and then slowly heated to 110 °C for 2 h followed by filling with nitrogen. 0.064 g of selenium powder was dissolved in 6.0 mL of TOP in a Schlenk flask and then pumped for 2 h at room temperature. The cadmium precursor solution was heated at 340 °C until a colorless solution formed. The solution was then cooled to 300 °C and stabilized for 2 h. At this temperature, selenium precursor solution was rapidly injected into the cadmium solution to form CdSe nanoparticles followed by rapidly reducing the temperature to 270 °C in a few seconds. Two ml of $ZnEt_2$ in hexane (1 M) and 0.45 mL of $(TMS)_2S$ were dissolved in 6.0 mL of TOP in a Schlenk flask. The ZnS precursor solution was added drop wise to the crude CdSe QDs solution at 230 °C to form a ZnS shell over CdSe cores. The reaction mixture was naturally cooled to about 80 °C followed by addition of about 10 mL of toluene in order to prevent solidification at room temperature. The raw QDs were purified using precipitation method and dissolved in toluene for future use. The purified QDs had a maximum emission at 610 nm.

4.4.4 Synthesis of hydrophilic QDs

The starting hydrophilic QDs were synthesized according to literatures. [90] Hydrophobic QDs were first precipitated three times with methanol to remove any free octadecylamine present in the solution and then redispersed in

chloroform. The CTAB solution was prepared by dissolving 0.4 g of CTAB in 10 ml of Millipore water. The solution containing CTAB and the QDs in chloroform (10:1 v/v) was then mixed vigorously until an emulsion was formed. Sonication of the emulsion was carried out in an ultrasonic cleaner. Then, the emulsion was heated at 80 °C for 10 min (until complete evaporation of chloroform). The CTAB QD suspension was filtrated through a 0.2 mm pore regenerated cellulose membrane. Unincorporated free CTAB was removed by cooling the CTAB QD suspension at 4 °C and dialyzing it against water.

4.4.5 UV-Vis analysis of HOCD reaction with different ROS

HOCD (0.15 mM) in dimethylformamide (DMF) was mixed with various ROS of different proportions including 1:1, 1:2 and 1:10. Reactive oxygen species includes H_2O_2 and sodium hypochlorite (NaClO) were diluted from the commercially available solution to 1.0 mM in water. Peroxynitrite and nitric oxide were prepared in-house according to established procedures. $^1O_2$ was generated via irradiation of rose Bengal. Hydroxyl radical was generated by Fenton reaction. All reactions were carried out at r.t. and monitored by Shimadzu UK1601 spectrophotometer fitted with a quartz cell.

4.4.6 Fluorescence analysis of QDs with HOCD and singlet oxygen.

A QDs solution of was prepared by dilution of a toluene solution of probes with dichloromethane. $^1O_2$ was generated via irradiation of rose Bengal. All reactions were carried out at r.t. The fluorescence was excited at 450 nm and the emission intensities at 613 nm were recorded.

4.4.7 Fluorescein analysis of HSa-CTAB-QD reaction with different ROS

Reactive oxygen species includes H_2O_2, *t*-butylhydroperoxide (TBHP), and sodium hypochlorite (NaClO) were diluted from the commercially available solution to 1.0 mM in water. Peroxynitrite and nitric oxide were prepared in-house according to established procedures.[91] $^1O_2$ was generated via irradiation of rose Bengal.[53] Hydroxyl radical was generated by Fenton

reaction. Nitric oxide gas was generated by reacting ascorbic acid with sodium nitrite and by purifying with sodium hydroxide and molecular sieves before passing through de-aerated water under inert atmosphere.[54] The content of nitric oxide in the resultant solution was estimated by colorimetric method using ammonium 2,2'-azinobis-(3-ethylbenzothiazoline-6-sulphonate) (ABTS) as an indicator.[55] All reactions were carried out at r.t. The fluorescence was excited at 450 nm and the emission intensities at 610 nm were recorded before ROS addition and 1 min after the addition of ROS.

Chapter 5: Novel C-N Coupling without Catalyst

5.1 Introduction

Formation of C(sp2)-N bond between aromatic carbon and amine is a highly important organic reaction in the synthesis of arylamines. An arene-nitrogen linkage is included in nitrogen or oxygen heterocycles such as indoles[92] and benzofurans,[93] isodityrosine-based natural products such as vancomycin,[94] conjugated polymers such as polyanilines,[95] readily oxidized triarylamines used in electronic applications such as N,N'-diphenyl-N,N'-bis(3-methylphenyl)-1,1'-biphenyl-4,4'-diamine (TPD)[96] These arylamines are of molecules with medicinally importance, of molecules with structurally interesting properties in organic synthesis, and of materials with important electronic and mechanical properties.

Conventionally, arylamines are prepared by nitration and reduction. However these methods are incompatible with many functional groups and often involve protection and deprotection steps. Currently, there are three main methods for the formation of C(sp2)-N bond as shown in ***Figure 5.1***, which include:

1) Buchwald-Hartwig amination

   Palladium-catalyzed coupling chemistry has proven to be a powerful method for formation of a new C-C bond via substitution of an aryl halide or triflate with a carbon nucleophile.[97] The first example of a palladium catalyzed C–N cross-coupling reaction was published in 1983 by Migita and coworkers.[98] Reports were virtually uncited for a decade, until the establishment of Buchwald–Hartwig catalyst in 1994.[99,100] Under the influence of palladium catalysts, aryl halides or triflates react with primary or secondary amines to give arylamines. The scope of the Buchwald–Hartwig amination has since then expanded to include a wide variety of aryl and amine coupling partners, and the conditions are modified and improved accordingly. Various ligand systems have also been developed, each with its own capabilities and limitations, and the choice of conditions requires

consideration of the steric and electronic properties of both couping partners.

2) Ullmann Reaction

There are two different transformations referred to as the Ullmann Reaction. The "classic" Ullmann Reaction is the synthesis of symmetric biaryls via copper-catalyzed coupling. The "Ullmann-type" Reactions include copper-catalyzed nucleophilic aromatic substitution between various nucleophiles including amines with aryl halides. However, these copper-mediated substitutions occur at high temperatures,[101] and diarylation occurs as undesirable side reactions often give products from diarylation. Moreover, these reaction are typically substrate specific.

3) Chan-Lam Coupling

Similar as Suzuki coupling, the Chan–Lam coupling involes alkyl, alkenyl or aryl boronic acid reacting with a N–H or O–H containing compound in the presence of Cu(II) complexes and under basic condition to form a new carbon–nitrogen bond.[102]

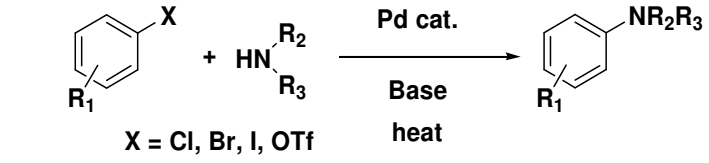

1) Buchwald-Hartwig amination

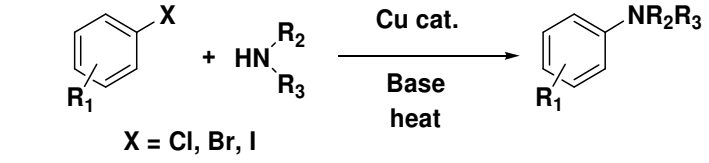

2) Ullmann Reaction

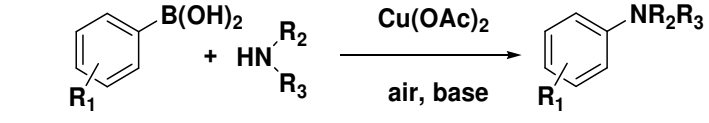

3) Chan-Lam Coupling

Figure 5.1 *Reported synthetic methods for arylamines.*

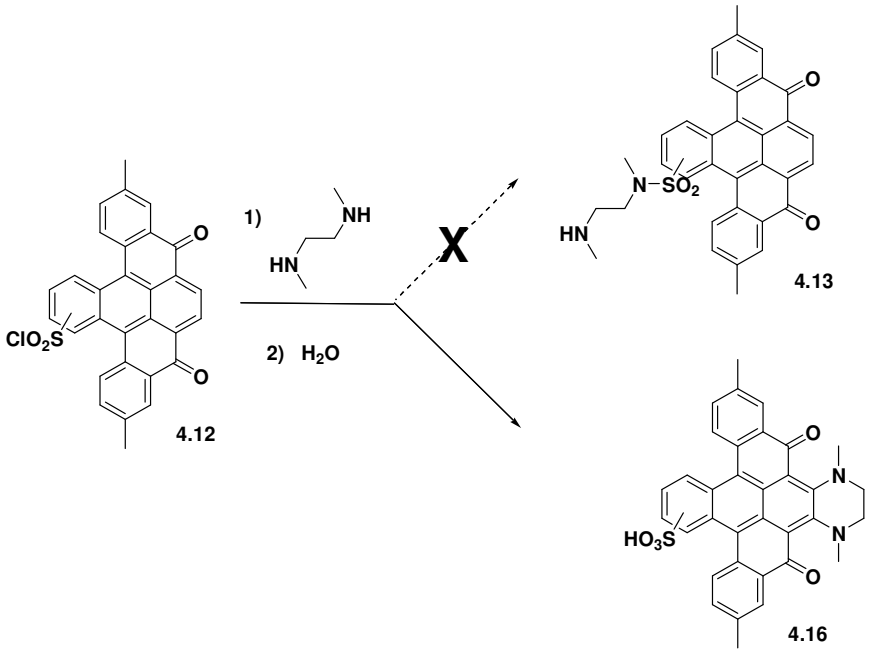

Figure 5.2 *Unexpected amination reaction of C(sp^2)-H under mild conditions.*

Although great progress has being made in developing catalysts to improve reaction scope, most reactions still require harsh conditions such as high temperatures, strong basic conditions, and long reaction time. More importantly, these reactions are catalyzed by transition metal complexes that are not environmental sustainable and cause purification of product challenging.

In an attempt to functionalize a singlet oxygen reactive dye dimethylhomoocoerdianthrone (HOCD), we unexpectedly discovered amination reaction of C(sp^2)-H under mild conditions without the presence of transition metal catalysts (***Figure 5.2***). As described in **Chapter 4**, thr reaction of HOCD sulfonyl chloride **4.12** with dimethylethylenediamine did not yield expected sulfonamide **4.13**. Instead compound **4.16** was obtained exclusively. More detailed studies on this reaction will be discussed in this chapter.

5.2 Results and Discussion

5.2.1 Reactivity of HOCD

Reaction of HOCD sulfonyl chloride **4.12** with dimethylethylenediamine under room temperature yielded compound **4.16** almost quantitatively. We next tested the reactivity of HOCD sulfonic acid **4.11b** with ethylenediamine. At room temperature, same addition product **4.16** formed with 96% yield. We rationalized that the reaction happened because of the electron withdrawing property of $-SO_3^-$ group, which facilitates Michael addition of ethylenediamine. A subsequent dehydrogenation gives the observed product. We then treated HOCD with ethylenediamine. As expected, the reaction also proceeded albeit much slower to give product **5.1**, a purple color solid which its structure is confirmed by ^1H NMR and MS spectra. Attempts to grow single crystals and resolve the structure by X-ray diffraction were not successful **5.1** has the tendency to crystalize as long needles that are not suitable for single crystal diffraction (***Figure 5.3***).

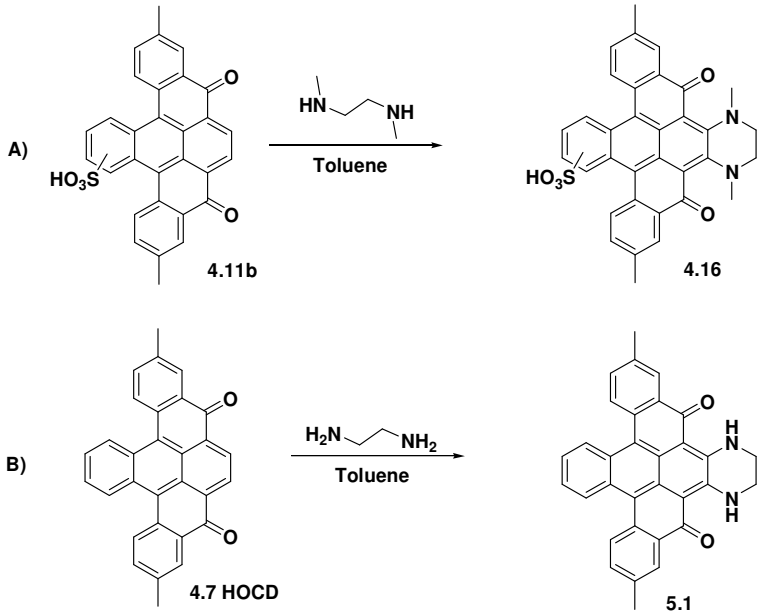

Figure 5.3 *Reaction of HOCD and HOCD sulfonic acid with ethylenediamine*

Table 5.1 *Reactivity of HOCD with amines and diamines (20 eq. amines)*

Entry	Amine	Product	T (°C)	Yield (%)
1	Ethylenediamine	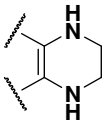 (**5.1**)	r.t.	97
2	N-Methylethylenediamine	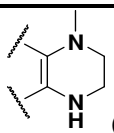 (**5.2**)	r.t.	94
3	N,N'-Dimethylethylenediamine	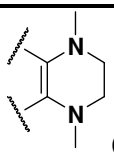 (**5.3**)	r.t.	91
4	Hexadecylamine	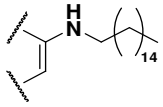 (**5.4**)	r.t.	69
5	(±)-trans-1,2-Diaminocyclohexane	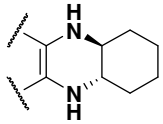 (**5.5**)	50	44
6	Propylamine	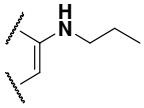 (**5.6**)	50	48
7	Isopropylamine		reflux	N.R.
8	Cysteamine	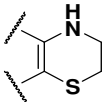 (**5.7**)	r.t.	26
9	L-Cysteine		reflux	N.R.
10	Piperazine	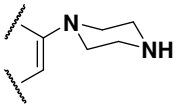 (**5.8**)*	r.t.	33
11	Allylamine		reflux	N.R.
12	(1S,2S)-1,2-Bis(2-hydroxyphenyl)ethylenediamine		reflux	N.R.
13	*o*-Phenylenediamine		reflux	N.R.
14	Ethanolamine		reflux	N.R.
15	**5.13a**		reflux	N.R.
16	**5.13b**		reflux	N.R.

(*: Compound **5.8** is not stable and decomposed during the column separation)

A series of amines and diamines was screened to determine the scope and limitations of the amination reaction as shown in ***Table 5.1***. All of them are characterized by ^{1}H and ^{13}C NMR spectra and mass spectra. As observed, the amination of HOCD is a rather general reaction. Ethylenediamine as well as its analogues all showed good yields (> 90%). Monoamines reacted with HOCD primarily gave monoamine addition product. For example, propylamine reacted with HOCD to give product **5.6** in an average yield of 48%. The reaction was slower than diamines and 20% of HOCD **4.7** was recycled after twelve hours reaction. Isopropylamine did not give any product even after heating. This may be due to the bulky isopropyl group, hindering the amination of $C(sp^2)$-H.

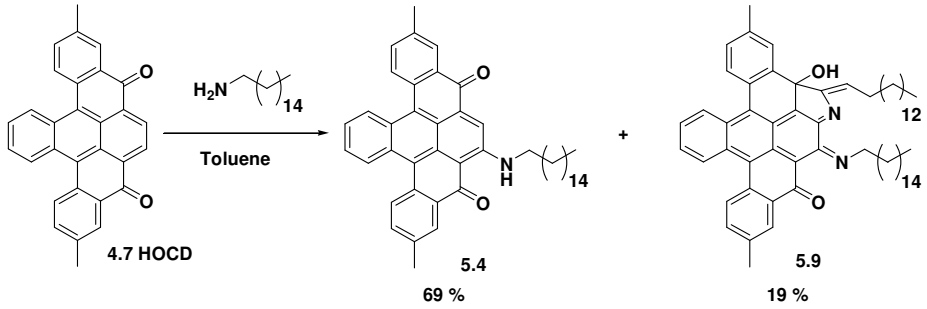

Figure 5.4 *Reaction of HOCD with hexadecylamine.*

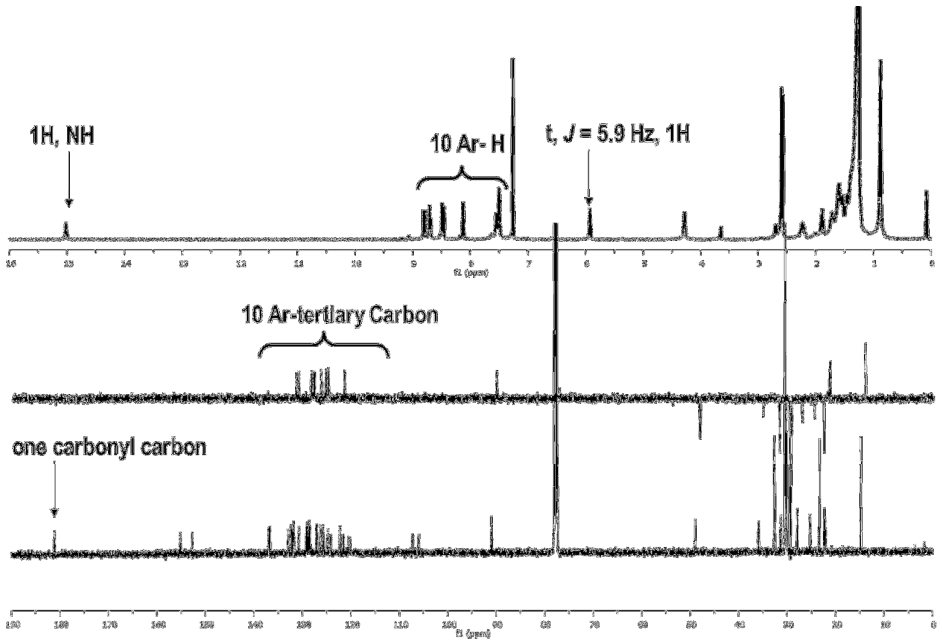

Figure 5.5 *^{1}H, ^{13}C and DEPT135-NMR of compound **5.9**.*

Monoamine with long alkyl chain such as hexadecylamine reacted with HOCD slowly resulting a monoamine addition product **5.4** as a major product, alongside with an unknown compound **5.9**. Based on the ^{1}H, ^{13}C and DEPT135-NMR spectra, this compound **5.9** contains ten aromatic protons and ten aromatic tertiary carbons which indicate two of the HOCD aromatic proton were substituted. This is possibly attributed to the addition of two amine molecules to HOCD. However, the fact that there is only one carbonyl carbon, one amine proton and one triplet proton signal at 5.92 ppm (***Figure 5.5***) implies that the methylene carbon which next to the amine group may have attacked carbonyl carbon and a subsequent dehydrogenation formed a five membered heterocyclic structure as shown in Figure **5.4**. Moreover, both MALDI-TOF (positive mode) and EI-MS supported the molecular weight of the compound being 884.6 in accordance with two amine chain being added to HOCD upon dehydrogenation. However, the proposed structure shows in ***Figure 5.6*** is not very stable. X-ray crystallography identification of the structure of compound **5.9** is needed in the further work.

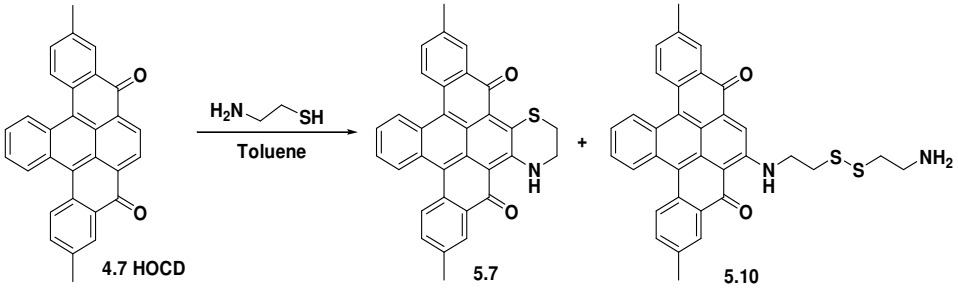

Figure 5.6 *Reaction of HOCD with cysteamine*

Sulfur-containing amines like cysteamine also reacts with HOCD to give cycloaddition product **5.7** but alongside with cystamine addition product **5.10**. This is due to the oxidation of cysteamine during the reaction. However, this reaction did not proceed with cysteine, even upon heating. This may be due to the electron withdrawing CO_2^- group, which weakens the nucleophilicity of the NH_2 group (***Figure 5.6***). Zhuang et al. reported an addition reaction of a thiol to the polymethine bond of the cyanine dye. [114] However, the formation

of thiol-cyanine adduct is through thiyl radical intermediates that does not include any dehydrogenation as occurred in our cases.

In line with our project, we would like to take advantage of this novel reaction to link HOCD derivatives with NIR fluorescence dye as new fluorescent probes for the detection of singlet oxygen.

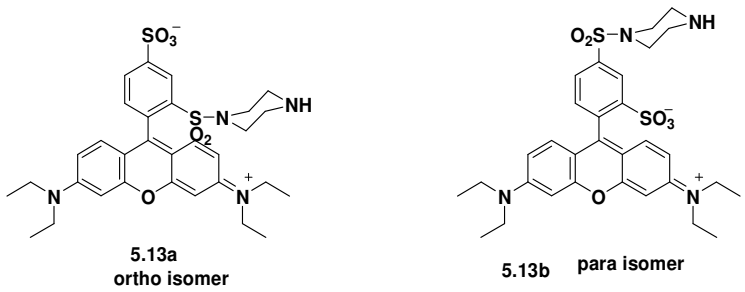

Figure 5.7 *Structure of sulforhodamine B piperazine derivatives* ***5.13a*** *and* ***5.13b****.*

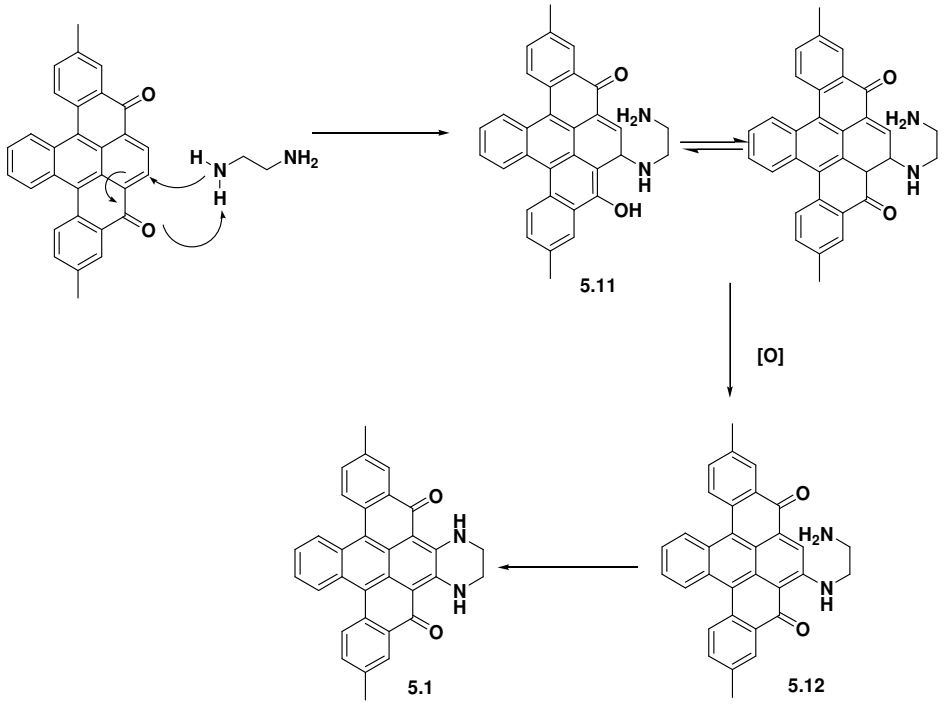

Figure 5.8 *Proposed mechanism of amination of HOCD by ethylenediamine*

Recently, fluorescent probes containing sulforhodamine B for selective detection of nitric oxide were published by our group.[107] The sulforhodamine B piperazine derivatives **5.13a** and **5.13b** have been used as the fluorophore that emit light at around 600 nm. Based on FRET theory, HOCD could be a

good quencher for them. However, when we tried to link HOCD with the sulforhodamine B piperazine derivatives via the amination reaction, no product was formed. This may be attributed to the low nucleophilicity of the piperazine nitrogen of **5.13a** and **5.13b**.

Based on our observations, we propose the reaction mechanisms to involve a 1,4-Michael addition of amine with HOCD (***Figure 5.8***). Oxygen containing amines such as ethanolamine and aryl amines such as phenylenediamine show no reactivity to HOCD. This is due to the low nucleophilicity of oxygen and aryl amine.

Nucleophilicities of amines are generally related to their basicities as well as solvent and steric effects.[112] In addition, amines with aryl substituents are abnormally weak nucleophiles due to the mesomeric effect.[113] When the reaction is carried out in non-polar solvents like toluene, the nucleophilicity is primarily related to the basicity of amines. We obtained some pKb values of the amines from the supplier and found that the reactivities of amines in highly accordance with the basicities (***Table 5.2***). The stronger the base is, the higher yield of product obtained. This finding also supported the proposed mechanism.

Table 5.2 *Reactivity and pKb of selected amines*

Amines	**Yield (%)**	**pKb**
Ethylenediamine	97	4.11
Hexadecylamine	69	3.33
(±)-trans-1,2-Diaminocyclohexane	44	3.47
Propylamine	48	3.29
Cysteamine	26	3.53
Piperazine	33	4.19
Allylamine	N.R.	4.47
o-Phenylenediamine	N.R.	9.54
Ethanolamine	N.R.	4.5

5.2.2 Optical properties of amination products

The International Commission on Illumination (CIE) recommended the division of infrared (IR) radiation into the three bands. IR-A, which is well-known as near-infrared (NIR) light is electromagnetic radiation with wavelengths from 700 nm to 1400 nm.[103] Conventionally, NIR light is considered to be less useful portion of the spectrum comparing with IR or UV/Vis for chemical composition testing. The broad and overlapping peaks in NIR make it more difficult to determine chemical components. With the advent of brighter light sources and more sensitive detectors, the benefits of NIR became more apparent, especially in the bioimaging applications. Dyes active in the NIR region have attracted ongoing attention due to their diverse applications in biomedical, materials and related fields. Due to their advantages that include enhanced tissue penetration depth, minimal interfering absorption and autofluorescence from biological samples, low light scattering as well as inexpensive laser diode excitation. [104] However, there are only a few classes of NIR dyes that are readily available, such as phthalocyanines[105] and cyanine dyes.[106]

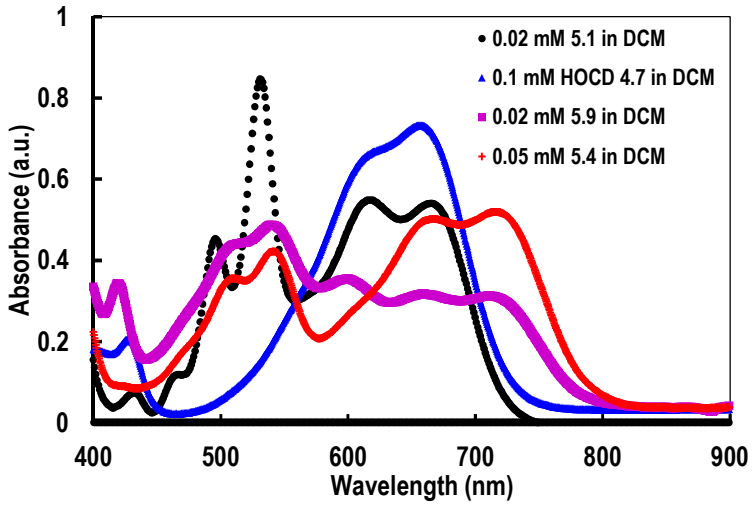

Figure 5.9 *UV-vis spectra of HOCD and its aminated derivatives*

Introducing an amine moiety to organic dyes normally causes a red shift in the UV-*vis* absorbance. The unpaired electrons on nitrogen atom of electron-donating amine groups increase the number of delocalized electrons of the π system and therby enhancing the conjugation system. Thus, amine substituted aromatic rings in most cases have lower transition energies and show red shifts on the UV-*vis* spectrum compared to the original molecules. The amination of different amine group on polyaromatic HOCD ring also shows different extent of red shift. HOCD ring shows a broad visible light absorbance range from 550 – 700 nm. The red shift facilitate the HOCD amination products to absorb NIR light readily. The UV-vis absorbances of compound **5.1**, **5.4** and **5.9**, represennting cycloaddition product, monoamine addition product and diamine product respectively showed new absorbance bands around 500 nm and 530 nm. Although HOCD ethylenediamine product **5.1** does not show much red shift of the conjugation system (approximate 10 nm), compound **5.9** and **5.4** showed significant red shifts of 70 nm comparing with HOCD. The absorbance band of **5.4** ranges from 580 nm to 800 nm with an absorbance maximum at 727 nm. Compound **5.9** shows a new absorbent peak at 605 nm, mainly due to the formation of new conjugation system (***Figure 5.9***), while having a very broad absorbance band, and thus, has the potential of becoming promising photonic materials.

In the meantime, hyperchromic effect has also been observed in all three compounds. Based on Beer-Lambert Law: $\boldsymbol{A = \varepsilon c l}$, with the same path length l, the aminated products give similar absorbance at much lower concentration at λ_{max} than that of HOCD. This indicates that the aminated products have much higher absorbance coefficiencies than HOCD.

Based on the findings, HOCD aminated products are good NIR dyes as they are not only absorb light of longer wavelength but also have higher absorbent intensities.

5.2.3 Optimization studies of amination

In the general procedure for amination reaction of HOCD, reaction proceeds easily under mild conditions in the absence of any transition metal catalysts. Using the model reaction of HOCD **4.7** and ethylenediamine

(Reaction B, ***Figure 5.3***), a series of reaction conditions have been studied to understand the mechanism and the factors influencing the amination reaction.

We first determined the molar equivalence of ethylenediamine needed for the reaction. Large excess amine was used to ensure the completion of reaction in twelve hours. When we monitored the reaction by proton NMR with stoichiometric amount of amine, the reaction did not occur even with heating at 50 °C for seven days in either deuterated chloroform or toluene (***Figure 5.10***). On contrary, with twenty equivalents of ethylenediamine at room temperature, the aromatic proton at 8.79 ppm of HOCD decreased significantly while methylene proton of product **5.1** at 3.93 ppm increased accordingly after five hours. The reaction completed in twelve hours as no HOCD protons can be detected in the proton NMR spectrum. This observation indicated to us the importance of excess of amines in the amination reaction.

In order to unravel the mystery as to why excess amine are vital for the reaction, we first examined if it plays a role as a base since basic conditions are favoured in a typical Michael addition. When stoichiometric amount of ethylenediamine reacted with HOCD **4.7** in the presence of excess N,N,N′,N′-tetramethylethylenediamine as base, the reaction proceeded smoothly, converting half of HOCD to desired product **5.1** after five hours (***Figure 5.11***). This finding indicated that the presence of base is preferred in HOCD amination reaction and as such large excess amines may act as both substrate and catalyst.

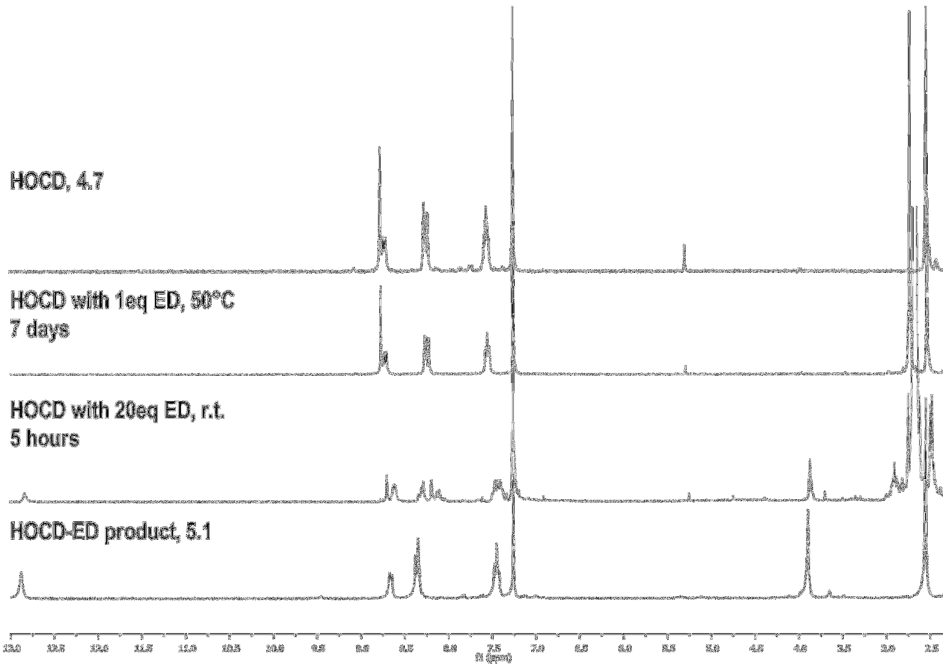

Figure 5.10 *^{1}H-NMR of HOCD-ethylenediamine reaction. (ED: ethylenediamine, Solvent: $CDCl_3$)*

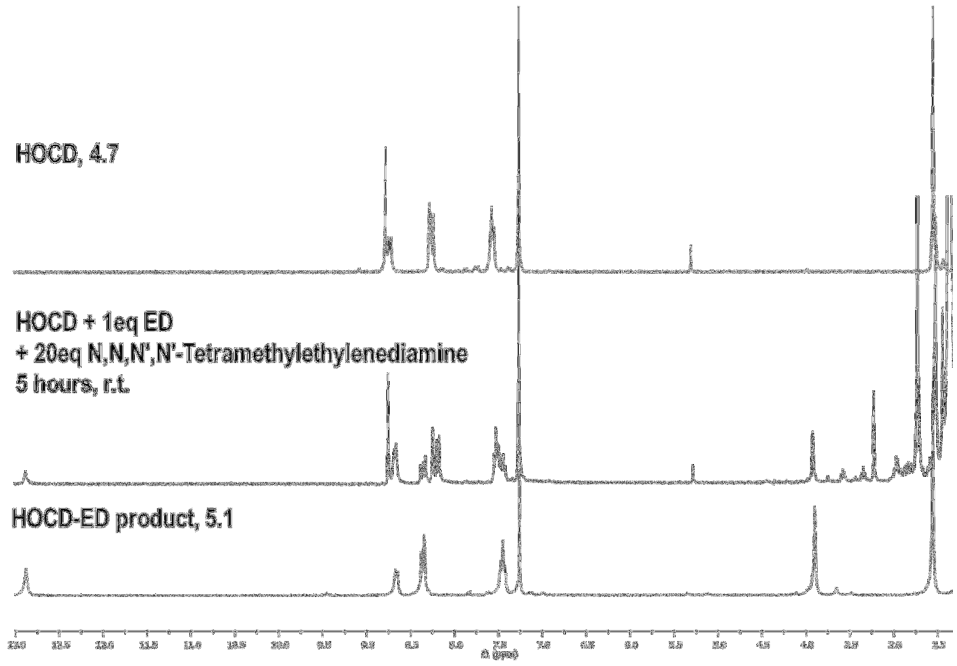

Figure 5.11 *^{1}H-NMR of HOCD-ethylenediamine reaction in the presence of base. (ED: ethylenediamine, Solvent: $CDCl_3$)*

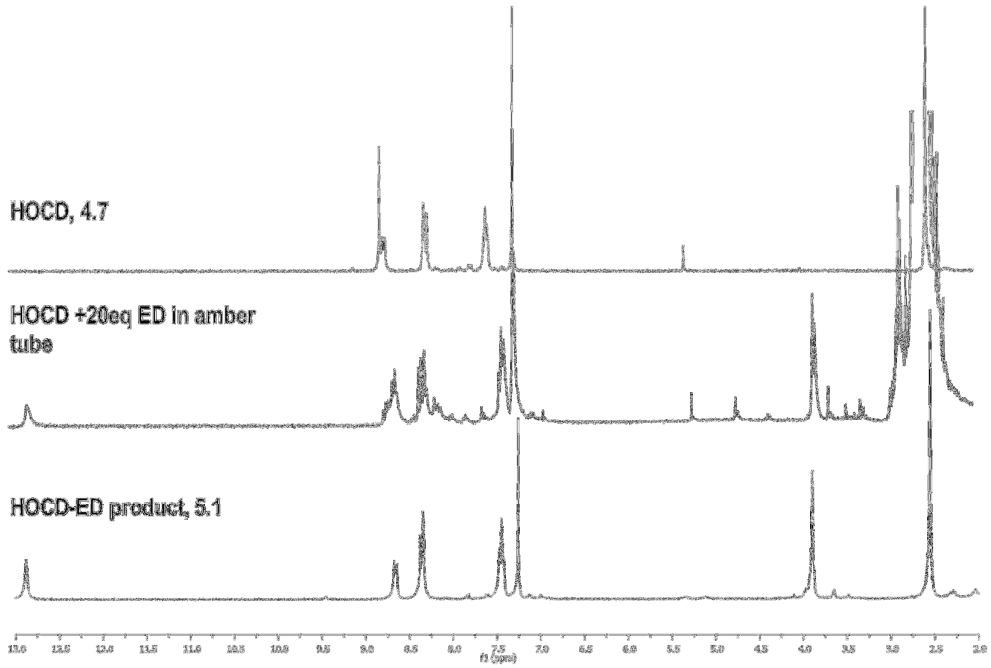

Figure 5.12 *^{1}H-NMR of HOCD-ethylenediamine reaction in amber tube. (ED: ethylenediamine, Solvent: $CDCl_3$)*

As starting material HOCD **4.7** and the product **5.1** are organic dyes that have strong absorbances of visible light, these molecules are easily excited to more active states by photons. In order to examine whether light is involved in the reaction, the reactionwas carried out in amber NMR tube. From the NMR spectra, there were no significant difference between reactions with or without light (***Figure 5.12***).

In the proposed mechanism, dehydrogenation is a very important step in the formation of tetrahydroquinoxaline (***Figure 5.8***). Molecular oxygen-assisted oxidative dehydrogenation is one of the most convenient methods. We next tested the influence of molecular oxygen. As expected, the reaction did not proceed in the absence of oxygen. When HOCD and 20 equivalents of ethylenediamine were mixed under argon, no reaction was observed even after four days (***Figure 5.13***).

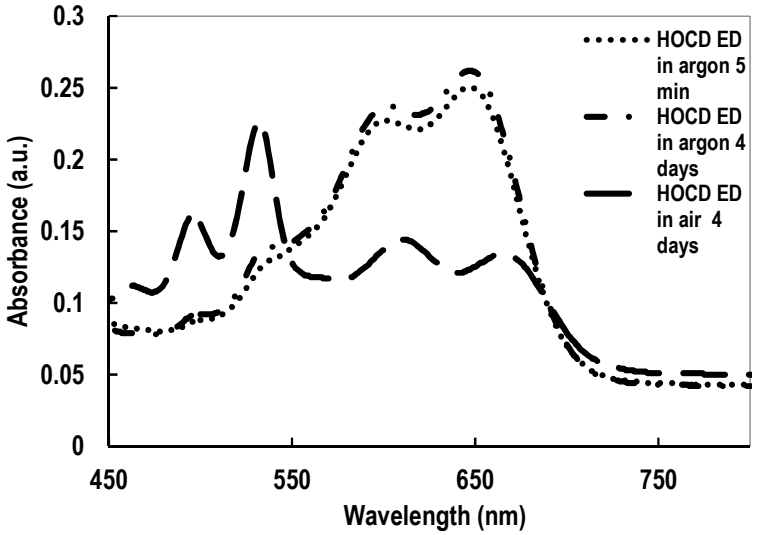

Figure 5.13 *UV-vis spectra of 0.05 mM HOCD react with 20 eq. ethylenediamine in air and argon. (Solvent: toluene)*

The involvement of singlet oxygen in amination reaction was also examined by carrying out the reaction in the presence of singlet oxygen. When singlet oxygen is generated in the reaction mixture, the blue color HOCD solution will be bleached, indicating the formation of HOCDPO. Treating the endoperoxides with 365 nm UV gave blue solution other than the purple color of the amination product **5.1**. After a few cycles of such treatment, amination reaction did not show any difference with or without singlet oxygen. This result shows that singlet oxygen in the system only reacts with HOCD and does not participate in the amination reaction (***Figure 5.14***).

In conclusion, we found that molecular oxygen and basic environment are vital for the HOCD amination. While the presence of light and singlet oxygen do not have any influence on the reaction. These also supported our proposed amination mechanism that involves the 1-4 Michael addition of amine with HOCD to give rise to intermediate product, which is then dehydrogenated by O_2 to give monoaminated product, **5.12**. This monoaminated compound **5.12** then undergoes an intramolecular Michael addition followed by dehydrogentation to yield the expected product. The fact that extended conjugation system is required for the C-H bond amination to occur seems indicate that the extended conjugation may favor the dehydrogenation reaction.

Monoamines such as ethylamine may have weaker nucleophilicity and thus the Michael addition need longer time with lower yield. Ethanolamine and aryl amines show no reactivity to HOCD likely due to the low nucleophilic ability of oxygen and aryl amine.

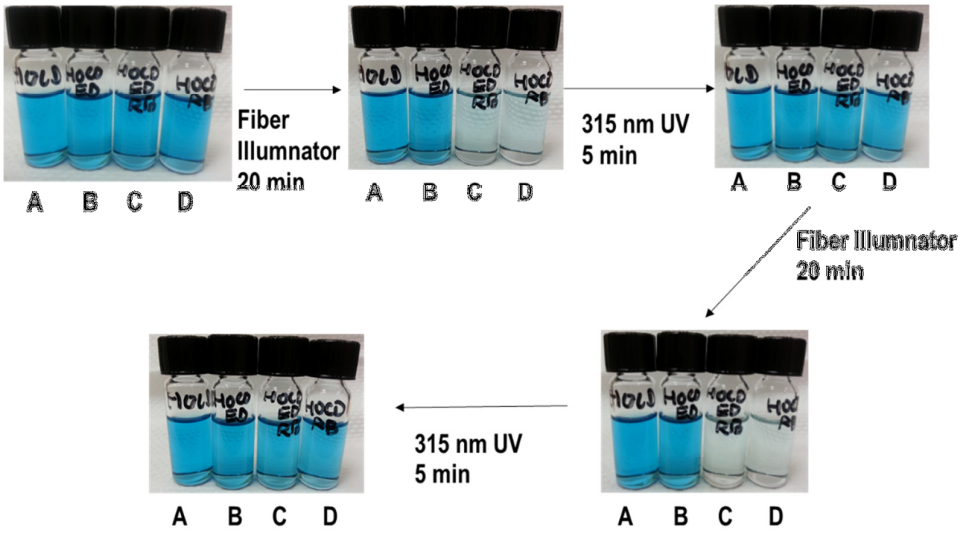

Figure 5.14 *HOCD-ethylenediamine reaction with or without singlet oxygen: A) HOCD 0.15 mM in dichloromethane; B) HOCD 0.15 mM + Ethylenediamine 14 mM in dichloromethane; C) HOCD 0.15 mM + Ethylene diamine 14 mM + Rose Bengal 0.14 μM in dichloromethane; D) HOCD 0.15 mM + Rose Bengal 0.14 μM in dichloromethane.*

5.2.4 Synthesis of NIR absorbent Ru complex

Extensive studies have been done on the spectroscopic properties of ruthenium complexes and their changes in absorption and photoluminescence when the ligands replaced. $[Ru(bipy)_2]^{2+}$ complexes such as $[Ru(bipy)_3]^{2+}$ (λ_{em} = 611 nm) , $[Ru(bipy)_2(en)]^{2+}$ (λ_{em} = 682 nm) [108] and $[Ru(bipy)_2(dien)]^{2+}$ (λ_{em} = 675 nm), has phosphorescence wavelengths of around near the NIR range of acetonitrile at room temperature.[109] When HOCD-amine ligand is coordinated to photoluminescence materials such as $Ru(bipy)_2^{2+}$, photooxidation on the non-innocent ligand can act as a "switch", which can turn on/off the phosphorescence of $Ru(bipy)_2^{2+}$. This phosphorescence wavelength lies in the absorption range of HOCD and HOCD-amine. Based on FRET theory, the donor chromophore (ruthenium moiety) in the electronically excited state transfers energy to an acceptor chromophore (HOCD-amine moiety) via non-

radiative dipole-dipole coupling, resulting in the loss of phosphorescence of the Ru(II) complex.[110] When the endoperoxide is formed, absorption band will shift away from this range, "switching on" the phosphorescence of the complex, indicating the presence of singlet oxygen.

HOCD-amine derivatives with one free NH group was designed in the Ru complex (***Figure 5.15***). Compound **5.2** has a strong absorbent band from 450 nm to 750 nm. The red shift after amination of HOCD is around 10 nm. We would expect the absorbent band to disappear upon reaction with singlet oxygen as the conjugation is broken due to formation of endoperoxide. Since this absorption band is responsible for the loss of phosphorescence in the Ru(II) complex, absorption of singlet oxygen would allow phosphorescence to be observed.

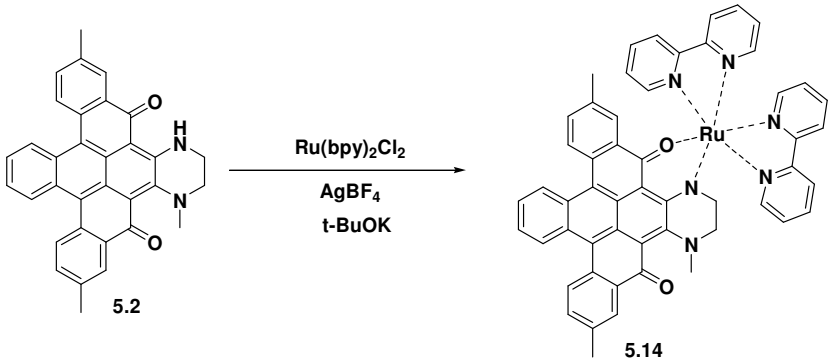

Figure 5.15 *Preparation of HOCD-Ruthenium complex*

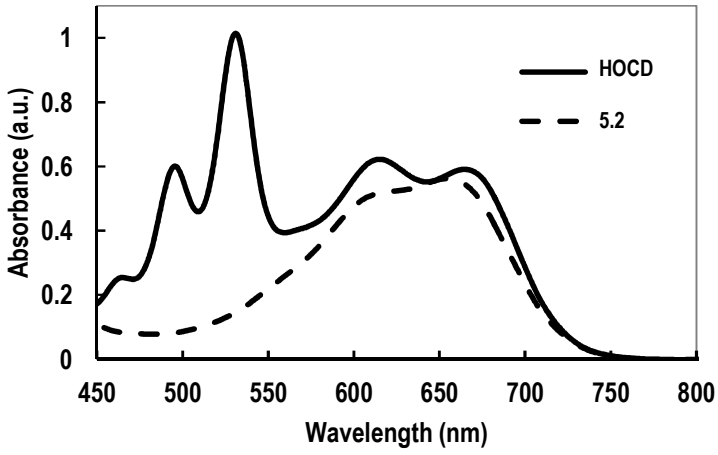

Figure 5.16 *UV-vis absorbance of HOCD and compound* ***5.2***

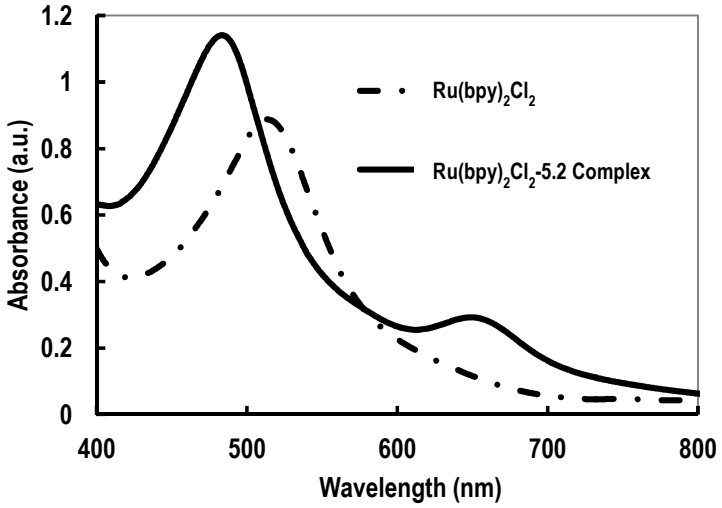

Figure 5.17 *UV-vis absorbance of $Ru(bpy)_2Cl_2$ and its complex* ***5.14*** *in water.*

After the complexation reaction of HOCD-amine **5.2** and $Ru(bpy)_2Cl_2$, aqueous extract of reaction shows reddish-brown color and has an additional absorbance band at 650 nm (***Figure 5.17***). Although **5.2** also has absorbance wavelength at 650 nm, this compound is not soluble in water. Thus, the appearance of the 650 nm absorbance band in the aqueous extract solely reflects the production of Ruthenium metal with the HOCD amine analogue during the reaction. We expect the product to be water-soluable is due to the ionic nature of the complex.

The spectroscopic data obtained indicate the formation of HOCD-Ru complex with strong absorbance at NIR range. The structure of the compound, however, needs to be fully characterized before exploring its potential as a dinglet oxygen probe.

5.3 Conclusion

A novel C-N Coupling reaction of HOCD was discovered. The reaction proceeds in mild conditions in the absence of transition metal catalyst. The reaction condition, mechanism and scope were investigated. A series of HOCD-amine derivatives were easily prepared through this reaction from a variety of amines and diamines. The bathochromic shift (red shift) and hyperchromic effect were observed in the HOCD derivatives render these prepared compounds good NIR dyes.

Based on the highly selective and sensitive reaction between HOCD and singlet oxygen, the HOCD-amine compounds could be used in a singlet oxygen probes. Preliminary study shows that HOCD-amines can coordinate with transition metal and this finding provides insights for new NIR singlet oxygen probes and NIR photocatalysts.

5.4 Experimental Section

5.4.1 Instruments and Materials

^{1}H and $^{13}C\{^{1}H\}$ NMR spectra were recorded in deuterated chloroform with a Bruker AC300 spectrometer (Karlsruhe, Germany). High resolution MS spectrum was obtained from Finnigan (MAT 95XL-T) high resolution (60,000), 5KV Double Focusing Reversed Nier-Johnson Geometry Mass Spectrometer. UV-Vis spectra were recorded using a Shimadzu UK1601 spectrophotometer fitted with a quartz cell. MALDI-TOF mass spectra were collected on a Brucker microTOF-QII mass spectrometer (Singapore) equipped with delayed extraction and a N_2 laser set at 337 nm. The length of one laser pulse was 3 ns. The measurements were carried out using the following conditions: positive polarity, linear flight path with 21 kV acceleration voltage, and 100 pulses per spectrum. 1,8,9-trihydroxyanthracene as the matrix was used to enhance ion formation. All solvent used were of reagent grade unless otherwise specified. All chemicals unless indicated were obtained from Sigma Aldrich and used as received. Anhydrous THF was obtained by distillation in the presence of Na metal before use.

5.4.2 Synthesis of HOCD derivatives and fluorescent dyes

General procedure for synthesis of amination products HOCD and HOCD sulfonic acid. To a solution of HOCD **4.7** (20 mg, 0.049 mmol) or HOCD sulfonic acid **4.11b** (15 mg, 0.031 mmol) in toluene, 20 equivalent amine was added. The reaction was kept in the temperature as listed in ***Table 5.1*** for twelve hours before 10 mL water and 10 mL dichloromethane was added. The separated organic layer was washed with 5% $NaHCO_3$ (10 mL, two times) and water (10 mL, two times) to remove the excess amines, dried

over $NaSO_4$, and rotary evaporated to dryness. The residue was then purified with silica gel column chromatography and gave pure amination products.

4.16: Column separation by chloroform gave purple solid **4.16** (17 mg, 96 %). ^{1}H NMR (500 MHz, $CDCl_3$) δ = 9.34 (d, *J* = 1.5 Hz, 1H), 8.79 (d, *J* = 8.9 Hz, 1H), 8.47 (d, *J* = 8.2 Hz, 1H), 8.40 (d, *J* = 8.2 Hz, 1H), 8.30 (d, *J* = 11.3 Hz, 2H), 7.96 (dd, *J* = 8.9, 1.6 Hz, 1H), 7.56 – 7.44 (m, 2H), 3.97 (s, 4H), 3.13 (s, 6H), 2.55 (s, 3H), 2.53 (s, 3H) ppm. ^{13}C NMR (126 MHz, $CDCl_3$) δ = 179.63, 149.18, 148.98, 141.50, 137.41, 137.34, 133.89, 133.82, 133.59, 132.88, 132.60, 129.77, 129.59, 128.42, 127.95, 127.57, 127.47, 125.27, 123.85, 122.93, 122.62, 121.94, 105.93, 51.17, 45.95, 22.04 ppm. ESIMS: nagative mode $[M-H]^-$ 573.29.

5.1: Column separation by dichloromethane gave purple solid **5.1** (22 mg, 97%). ^{1}H NMR (300 MHz, $CDCl_3$) δ = 12.92 (s, 2H), 8.74 (dd, *J* = 6.5, 3.2 Hz, 2H), 8.44 (d, *J* = 8.2 Hz, 2H), 8.38 (s, 2H), 7.52-7.50 (m, 4H), 3.93 (s, 4H), 2.57 (s, 6H) ppm. ^{13}C NMR (126 MHz, $CDCl_3$) δ = 184.18, 146.54, 142.09, 137.12, 134.24, 133.99, 132.86, 132.14, 130.64, 129.68, 129.28, 128.99, 127.94, 127.71, 127.55, 127.27, 125.57, 125.38, 121.71, 121.01, 106.16, 38.92, 22.06 ppm. EIMS: *m/z* = 466.2.

5.2: Column separation by dichloromethane gave purple solid **5.2** (22 mg, 94%). ^{1}H NMR (500 MHz, $CDCl_3$) δ = 12.89 (s, 1H), 8.84 – 8.72 (m, 2H), 8.49 (d, *J* = 8.3 Hz, 1H), 8.39 (s, 1H), 8.36 (d, *J* = 8.2 Hz, 1H), 8.18 (s, 1H), 7.55 – 7.45 (m, 4H), 3.97 (t, *J* = 5.4 Hz, 2H), 3.94 – 3.87 (m, 2H), 3.05 (s, 3H), 2.58 (s, 3H), 2.56 (s, 3H) ppm. ^{13}C NMR (126 MHz, $CDCl_3$) δ = 182.98, 149.19, 136.74, 136.47, 133.73, 133.05, 132.02, 131.69, 129.17, 128.89, 128.66, 126.97, 126.51, 126.28, 125.03, 124.73, 122.26, 121.04, 104.20, 51.84, 45.82, 38.45, 21.39, 21.31ppm. EIMS: *m/z* = 480.3.

5.3: Column separation by pure dichloromethane gave purple solid **5.3** (22 mg, 91%).^{1}H NMR (500 MHz, $CDCl_3$) δ = 8.79 (dd, *J* = 6.5, 3.4 Hz, 2H), 8.46 (s, 1H), 8.44 (s, 1H), 8.33 (s, 2H), 7.53 – 7.45 (m, 4H), 3.95 (s, 4H), 3.13 (s, 6H), 2.56 (s, 6H) ppm. ^{13}C NMR (126 MHz, $CDCl_3$) δ = 179.65, 149.00, 137.21, 133.96, 133.65, 132.40, 129.58, 129.40, 127.60, 125.30, 123.11, 122.07, 106.07, 51.16, 45.89, 22.02 ppm. EIMS: *m/z* = 494.3.

5.4: Column separation by dichloromethane gave purple solid **5.4** (22 mg, 69%). ^{1}H NMR (500 MHz, $CDCl_3$) δ = 12.34 (s, 1H), 8.77 (d, *J* = 8.5 Hz, 1H), 8.65 (d, *J* = 8.5 Hz, 1H), 8.46 (s, 2H), 8.33 (s, 1H), 8.17 (s, 2H), 7.60 – 7.42 (m, 4H), 3.74 (dd, *J* = 12.8, 6.6 Hz, 2H), 2.58 (s, 3H), 2.51 (s, 3H), 1.90 (dt, *J* = 14.8, 7.3 Hz, 2H), 1.41 (d, *J* = 7.5 Hz, 2H), 1.25 (m, 24H), 0.87 (t, *J* = 5.5 Hz, 3H) ppm. ^{13}C NMR (126 MHz, $CDCl_3$) δ = 185.56, 183.52, 154.58, 138.96, 138.96, 137.85, 135.87, 134.87, 132.83, 132.57, 131.93, 130.95, 129.54, 128.27, 127.79, 127.57, 127.41, 125.88, 123.04, 119.31, 106.96, 44.05, 44.05, 32.61, 30.39, 30.22, 30.05, 27.84, 25.14, 23.37, 22.73, 22.14, 21.87, 21.20, 14.79 ppm. EIMS: *m/z* = 649.5.

5.5: Column separation by dichloromethane gave purple solid **5.5** (11 mg, 44%). ^{1}H NMR (500 MHz, $CDCl_3$) δ = 12.75 (s, 2H), 8.64 (dd, *J* = 6.2, 3.3 Hz, 2H), 8.36 (d, *J* = 8.1 Hz, 2H), 8.33 (s, 2H), 7.46 (d, *J* = 8.1 Hz, 2H), 7.42 (dd, *J* = 6.2, 3.3 Hz, 2H), 3.44 (d, *J* = 9.3 Hz, 2H), 2.55 (s, 6H), 2.30 (d, *J* = 11.6 Hz, 2H), 1.98 (d, *J* = 8.5 Hz, 2H), 1.61 (d, *J* = 15.1 Hz, 2H) ppm. ^{13}C NMR (126 MHz, $CDCl_3$) δ = 183.59, 146.23, 136.52, 133.43, 132.22, 131.52, 129.13, 126.94, 126.61, 124.81, 105.43, 77.26, 77.00, 76.75, 54.16, 30.10, 24.13, 21.37 ppm. EIMS: *m/z* = 520.4.

5.6*:* Column separation by dichloromethane gave purple solid **5.6** (11 mg, 48%). ^{1}H NMR (500 MHz, $CDCl_3$) δ = 12.38 (s, 1H), 8.79 (dd, *J* = 8.5, 2.1 Hz, 1H), 8.68 (dd, *J* = 8.5, 2.8 Hz, 1H), 8.47 (s, 2H), 8.36 (d, *J* = 2.3 Hz, 1H), 8.18 (s, 2H), 7.59 – 7.41 (m, 4H), 3.73 (dd, *J* = 12.8, 6.8 Hz, 2H), 2.59 (s, 3H), 2.52 (s, 3H), 1.94 (dt, *J* = 7.3, 6.8 Hz, 3H), 1.18 (t, *J* = 7.3 Hz, 3H) ppm. EIMS: *m/z* = 467.3.

5.7: Column separation by pure dichloromethane gave purple solid **5.7** (6 mg, 26%).^{1}H NMR (500 MHz, $CDCl_3$) δ = 14.11 (s, 1H), 8.72 (d, *J* = 8.5 Hz, 1H), 8.67 (d, *J* = 8.4 Hz, 1H), 8.42 (m, 1H), 8.26 (s, 1H), 8.20 (d, *J* = 8.1 Hz, 1H), 7.74 (m, 1H), 7.55 – 7.44 (m, 4H), 4.17 (dt, *J* = 10.6, 3.8 Hz, 2H), 3.13 (t, , *J* = 5.4 Hz 2H), 2.58 (s, 3H), 2.53 (s, 3H) ppm. ^{13}C NMR (126 MHz, $CDCl_3$) δ = 184.83, 183.02, 150.79, 137.91, 137.11, 133.58, 133.40, 132.60, 132.13, 131.84, 130.96, 130.72, 129.59, 128.76, 128.24, 127.23, 127.12,

126.67, 126.55, 125.10, 123.04, 121.12, 104.19, 77.35, 77.10, 76.84, 40.86, 25.12, 21.58, 21.39 ppm. EIMS: *m/z* = 483.2.

5.9: Column separation by dichloromethane gave red brown solid **5.9** (8 mg, 19%). ^{1}H NMR (500 MHz, $CDCl_3$) δ = 15.02 (s, 1H), 8.80 (d, *J* = 8.7 Hz, 1H), 8.70 (t, *J* = 8.8 Hz, 2H), 8.49 (s, 1H), 8.47 (d, *J* = 8.3 Hz, 1H), 8.12 (s, 1H), 7.55 (d, *J* = 1.9 Hz, 1H), 7.52 – 7.47 (m, 3H), 5.92 (t, *J* = 5.9 Hz, 1H), 4.27 (dd, *J* = 7.3, 5.4 Hz, 2H), 2.60 (s, 3H), 2.57 (s, 3H), 2.22 (td, *J* = 14.7, 6.6 Hz, 2H), 1.89 (dd, *J* = 14.8, 7.4 Hz, 2H), 1.70 (d, *J* = 13.8 Hz, 2H), 1.26 (m, 48H), 0.88 (t, *J* = 6.9 Hz, 6H) ppm. ^{13}C NMR (126 MHz, $CDCl_3$) δ = 181.12, 155.19, 155.14, 152.78, 136.89, 136.63, 133.01, 132.88, 132.31, 132.13, 131.79, 130.73, 129.14, 128.96, 128.61, 128.45, 127.07, 126.17, 125.66, 124.79, 124.10, 122.27, 121.53, 120.52, 107.21, 106.00, 90.92, 77.95, 77.70, 77.44, 48.97, 35.86, 32.62, 31.33, 30.41, 30.36, 30.29, 30.20, 30.13, 30.06, 27.87, 25.32, 23.38, 22.29, 22.10, 14.79 ppm. EIMS: *m/z* = 884.8. MALDITOF-MS (positive mode) $[M+H]^+$ = 885.6.

Synthesis of 5.13a and 5.13b: Compound **5.13a** and **5.13b** were prepared by literature methods.[107] Briefly, to a stirred solution of sulforhodamine B (14.5g, 25.0 mmol) in anhydrous CH_2Cl_2 (220 mL) at 0 °C, was slowly added oxalyl chloride (10.7 mL, 125 mmol) and DMF (0.35 mL) in sequence. The resulting mixture was stirred at r.t. for 16 h and then concentrated *in vacuo*. To the resulting slurry, benzene (150 mL) was added and the volatiles were removed *in vacuo*. To the residue, diethyl ether (150 mL) was added to give a mixture, which was filtered and washed with ethyl acetate (50 mL) and dried under vacuum to give crude sulforhodamine B mono sulfonyl chloride. A solution of crude sulforhodamine B sulfonyl chloride (1.10 g, 1.91 mmol) and piperazine (0.82 g, 9.5 mmol) in 15 mL anhydrous DMF was stirred overnight under argon. The solvent was evaporated, and the residue was treated with column chromatography ($MeCN/MeOH/NH_4OH$, 80:20:1) was to give **1** (200 mg, 16.8%) and **2** (50 mg, 4.2%). Spectral data for **1**: ^{1}H NMR (300 MHz, CD_3OD, *δ* (ppm): 8.55 (d, *J* = 1.5 Hz, 1H), 8.05 (dd, *J* = 7.8, 1.5 Hz, 1H), 7.59 (d, *J* = 7.8 Hz, 1H), 7.06 (q, *J* = 9.0 Hz, 4H), 6.96 (d, *J* = 2.1, 2H), 3.69 (q, *J* = 6.0 Hz, 8H), 3.13 (t, *J* = 3.0 Hz, 4H), 2.94 (t, *J* = 3.0 Hz, 4H), 1.32 (t, *J* = 6.0 Hz, 12H). ^{13}C{^{1}H} NMR (300 MHz, CD_3OD, *δ* (ppm)): 157.90, 156.05,

155.60,145.87, 137.26, 134.63, 132.11, 131.08, 128.58, 127.01, 113.75, 113.55, 95.50, 46.30, 45.31,44.41, 11.29. ESI-MS: *m/z* 627 $[M + H]^+$, *m/z* 649 $[M + Na]^+$. Spectral data for **2**: ^1H NMR (300 MHz, CD_3OD, δ = 8.54 (d, *J* = 1.2 Hz, 1H), 8.25 (dd, *J* = 6.0, 1.2 Hz, 1H), 7.58 (d, *J* = 6.0 Hz, 1H), 7.09 (q, *J* = 6.9 Hz, 4H), 6.98 (d, *J* = 1.8 Hz, 2H), 3.69 (q, *J* = 6.0 Hz, 8 H), 2.93 (t, *J* = 3.6 Hz, 4H), 2.68 (t, *J* = 3.6 Hz, 4H), 1.31 (t, *J* = 6.0 Hz, 12H) ppm. $^{13}C\{^1H\}$ NMR (300 MHz, CD3OD, δ = 157.79, 155.87, 154.49, 147.90, 138.76, 132.69, 131.83, 131.76, 129.98, 127.08, 114.16, 113.79, 95.80, 45.52, 45.45, 44.40, 11.42 ppm. ESI-MS: *m/z* 627 $[M + H]^+$, *m/z* 649 $[M + Na]^+$.

Synthesis of Ru complex 5.14: To a solution of $Ru(bpy)_2Cl_2$ (8 mg, 0.041 mmol) in anhydrous THF, $AgBF_4$ (8 mg, 0.016 mmol) was added. (Reaction vessel 1) The resulting mixture was stirred under argon at room temperature overnight. Color changed from orange to reddish-brown was observed.

To a solution of **5.2** (10 mg, 0.021 mmol) in anhydrous THF t-BuOK (2 mg, 0.018 mmol, was added. (Reaction vessel 2) Reaction was left to stir at room temperature under with exclusion of light overnight. No color change was observed.

Reaction vessel 1 was added drop wise to reaction vessel 2 in argon. The mixture was allowed to stir at room temperature for four days. Color change from purple to dark blue. The reaction was then quenched with water and extracted with dichloromethane. The aqueous layer gave a reddish color while the organic layer was slightly purple.

5.4.3 UV-Vis analysis of HOCD amination reaction with ethylenediamine.

HOCD (0.05 mM in 4 mL toluene) was mixed with 20 eq. ethylenediamine in air or in argon. The reactions were carried out at room temperature and monitored by Shimadzu UK1601 spectrophotometer fitted with a quartz cuvette at 5min, 1, 2, 5, 24, 48, and 96 h. All solvent and reagent used in the reaction in argon have been Freeze-Pump-Thaw degased before use.

References

[1] Halliwell, B.; Whiteman, M. *British Journal of Pharmacology* **2004**, *142*, 231–255.

[2] Nathan, C. *Nature* **2002**, *420*, 846–852.

[3] (a) Halliwell, B.; Gutteridge, J.M.C. *Free Radicals in Biological and Medicine*; Oxford University Press: Oxford, **2007**; (b) Winterbourn, C. C. *Nat. Chem. Biol.* **2008**, *4*, 278–286.

[4] Droge W. *Physiol. Rev*. **2002**, *82*, 47–95.

[5] Giorgio, M.; Trinei, M.; Migliaccio, E.; Pelicci, P. G. *Nat. Rev. Mol. Cell Biol.* **2007**, *8*, 722–728.

[6] Balaban, R. S.; Nemoto, S.; Finkel, T. *Cell* **2005**, *120*, 483–495.

[7] Nathan, C. *J. Clin. Invest.* **2003**, *111*, 769–778.

[8] Lambeth, J. D. *Nat. Rev. Immunol. Rev.* **2007**, *219*, 88–102.

[9] (a) Valko, M. et al. *Int. J. Biochem. Cell Biol.* **2007**, *39*, 44–84; (b) Stone, J. R.; Yang, S. *Antioxid. Redox Signal.* **2006**, *8*, 243–270.

[10] Cadenas, E. *Biofactors*, **1997**, *6*, 391–397.

[11] Brennan, M. L.; Hazen, S. L. *Amino Acids*, **2003**, *25*, 365-374.

[12] Valko, M.; Rhodes, C. J.; Moncol, J.; Izakovic, M.; Mazur, M. *Chem. Biol. Interact.*, **2006**. *160*, 1–40.

[13] Marnett, L. J. *Carcinogenesis*, **2002**, *21*, 361–370.

[14] Hayashi, H.; Iimuro, M.; Matsumoto,Y.; Kaneko, M. *Eur. J. Pharmacol.*, **1998**, *349*, 133–136.

[15] Harman, D., *J. Gerontol.*, **1956**, *11*, 298–300.

[16] Hayflick, L., *Exp. Gerontol.*, **1998**, *33*, 639–653.

[17] Valko, M., Izakovic, M., Mazur, M., Rhodes, C. J., Telser, J., *Mol. Cell. Biochem.*, **2004**, *266*, 37–56.

[18] Cadenas, E., & Davies, K. J. A., *Free Radic. Biol. Med.*, **2000**, *29*, 222–230.

[19] Belvisi, M., Barnes, P.J, Larkin, S., Yacoub, M., Tadjkarimi, S., Williams, T.J., Mitchell, J.A., *Eur. J. Pharmacol*., **1995**, *283*, 255–258.

[20] Andrade, F.H., Moody, M.R., Stamler, J.S., Reid, M.B., Cytochrome c reduction assay detects nitric oxide release by rat diaphragm. In: Moncada, S., Stamler, J., Gross, S., Higgs, E.A., editors. *The biology of nitric oxide*. London: Portland Press, **1996**. p 45.

[21] Dikalov. S.; Griendling, K. K.; Harrison, D. G., *Hypertension*, **2007**, *49* 717–727.

[22] Vasquez-Vivar, J.; Hogg, N.; Pritchard, K. A. Jr.; Martasek, P.; Kalyanaraman, B. *FEBS Lett.,* **1997**, *403*, 127–130.

[23] (a) Tsien, R. Y. *Biochemistry,* **1980**, *19*, 2396–2404 (b) Grynkiewicz, G.; Poenie, M.; Tsien, R. Y. 3440–3450 (c) Minta, A.; Kao, J. P. Y.; Tsien, R. Y. *J. Biol. Chem*., **1989**, *264*, 8171–8178 (d) Tsien, R. Y., Pozzan, T. *Methods Enzymol.*, **1989**, *172*, 230–244.

[24] De Silva, A. P.; Gunaratne, H. Q. N.; Gunnlaugsson, T.; Huxley, A. J. M.; McCoy, C. P.; Rademacher, J. T.; Rice, T. E. *Chem. Rev.* **1997**, 97, 1515–1566.

[25] Wardman, P. *Free Radical Biol. Med.* **2007**, *43*, 995–1022.

[26] Zielonka, J. and Kalyanaraman, B. *Free Radic. Biol. Med.,* **2010**, *48*, 983–1001.

[27] Chang, M. C.; Pralle, A.; Isacoff, E. Y., Chang, C. J. *J. Am. Chem. Soc.* **2004**, *126,* 15392–15393.

[28] Zielonka, J.; Zielonka, M.; Sikora, A.; Adamus, J.; Joseph, J.; Hardy, M.; Ouari, O.; Dranka, B. P.; Kalyanaraman, B. *J. Biol. Chem.* **2012**, *287*, 2984–2995.

[29] Iida, Y.; Katusic, Z. S. *Stroke*, **2000**, *31*, 2224–2229.

[30] Tatla, S.; Woodhead, V.; Foreman, J.C.; Chain, B. M. *Free Radic. Biol. Med.*, **1999**, *26*, 14–24.

[31]*Selenium: its molecular biology and role in human health*; Hatfield, D. L., Berry, M. J.; Gladyshev, V. N., Eds. New York, NY: Springer, **2006**.

[32](a) Andreesen, J. R.; Ljungdahl, L. *J. Bacteriol.,* **1973**, *116*, 867−873. (b) Turner, D. C.; Stadtman, T. C. *Arch. Biochem. Biophys.,* **1973**, *154*, 366−381.

[33]Rotruck, J. T.; Pope, A. L.; Ganther, H. E.; Swanson, A. B.;Hafeman, D. G.; Hoekstra, W. G. *Science* **1973**, *179*, 588−590.

[34]Michiels, C.; Raes, I.; Toussaint, O.; Remacle, J. *Free Radical Biol. Med.* **1994**, *17*, 235−248.

[35]Flohe, L.; Andreesen, J. R.; Brigelius-Flohe´, R.; Maiorino, M.; Ursini, F.; *IUBMB Life* **2000**, *49*, 411−420.

[36]Dobbek, H.; Gremer, L.; Meyer, O.; Huber, R. *Proc. Natl. Acad. Sci.* **1999**, *96*, 8884−8889.

[37](a) Muller, A.; Cadenas, E.; Graf, P.; Sies, H. *Biochem. Pharmacol.* **1984**, *33*, 3235−3239. (b) Wendel, A.; Fausel, M.; Safayhi, H.; Tiegs, G.; Otter, R. *Biochem. Pharmacol.* **1984**, *33*, 3241−3245. (c) Sies, H.; Masumoto, H. *Adv. Pharmacol.* **1997**, *38*, 2229−2246.

[38](a) Mugesh, G.; du Mont, W. W.; Sies, H. *Chem. Rev.* **2001**, *101*, 2125−2180; (b) Sies, H. *Free Radical Biol. Med.* **1993**, *14*, 313−323; (c) Bjornstedt, M.; Xue, J.; Huang, W.; Åkesson, B.; Holmgren, A. *J. Biol. Chem.* **1994**, *269*, 29382-29384.

[39]Flohe, L. *Glutathione peroxidase brought into focus. In Free radicals in biology. Volume V* edited by William A. Pryor. London Academic Press, c**1982**, 223−254

[40]Maiorino, M.; Gregolin, C.; Ursini, F. *Methods Enzymol.* **1990**, *186*, 448−457.

[41](a) *Handbook of Chemistry & Physics (90th Edition)* Lide, D. R. Eds. CRC Press : Chapman & Hall, **1999**; (b) Sharpless, K. B.; Lauer, R. F. *J. Am. Chem. Soc.* **1973**, *95*, 2697−2698; (c) Jones, D. N.; Mundy, D.; Whitehouse, R. D. *Chem. Commun.* **1970**, 86−87.

[42]Lower, S. K.; El-Sayed, M. A. *Chem. Rev.* **1966,** *66*, 199–241.

[43]Ellison, E. H; Moodley, D.; Hime, J. *J. Phys. Chem. B* **2006**, *110*, 4772–4792.

[44]Kalyanasundaram, K.; Thomas, J. K. *J. Phys. Chem.*, **1977**, *81*, 2176–2180.

[45](a) Grieco, P. A.; Gilman, S.; Nishizawa, M. *J. Org. Chem*. **1976**, *41*, 1485–1486. (b) Sharpless, K. B.; Young, M. W. *J. Org. Chem.* **1975**, *40*, 947–949.

[46](a) Tang, B.; Xing, Y.; Li, P.; Zhang, N.; Yu, F., Yang, G. *J. Am. Chem. Soc.* **2007**, *129*, 11666–11667. (b) Tang, B.; Yin, L.; Wang, X.; Chen, Z.; Tong, L.; and Kehua Xu, K. *Chem. Commun.*, **2009**, 5293–5295

[47]Morris, J. C. *J. Phys. Chem.* **1966**, *70,* 3798–3805.

[48]Harrison, J. E.; Schultz, J. *J. Biol. Chem.* **1976**, *251*, 1371–1374.

[49]Berliner, J. A.; Heinecke, J. W. *Free Radical Biol. Med.* **1966**, *20*, 707–728.

[50]Henderson, J. P.; Byun, J.; Heinecke, J. W. *J. Biol. Chem.* **1999**, *274,* 33440 –33448.

[51]Kettle, A. J.; Gedye, C. A.; Winterbourn, C. C. *Biochem. J.,* **1997**, *321*, 503–508.

[52]Beckman, J. S.; Beckman, T. W.; Chen, J.; Marshall, P. A.; Freeman, B. A. *Proc. Natl. Acad. Sci*. **1990**, *87*, 1620–1624.

[53]Hevesi, L.; Krief, A. *Angew. Chem.* **1976**, *88*, 413.

[54]Bunton, C. A. *Nature* **1959**, *183*, 163–165.

[55]Nims, R. W.; Cook, J. C.; Krishna, M. C.; Christodoulou, D.; Poore, C. M. B.; Miles, A. M.; Grisham, M. B.; Wink, D. A. *Method Enzymol.* **1996***, 268*, 93–105.

[56]Frisch, M. J. et al. Gaussian 03; Gaussian, Inc., Wallingford CT, **2004**.

[57]Cossi, M.; Barone, V.; Cammi, R.; Tomasi, *J. Chem. Phys. Lett*., **1996**, *255*, 327–335.

[58](a) D. A. Becke, *J. Chem. Phys.,* **1993**, *98*, 5648–5652. (b) Lee, C.; Yang, W.; Parr, R. G. *Phys. Rev. B*, **1988**, *37*, 785–789.

[59](a) Aiello, S.; Geoffrey Wells, G.; Stone, E. L.; Kadri, H.; Bazzi, R.; David, R.; Bell, D. R.; Malcolm, F. G.; Stevens, M. F. G.; Matthews, C. S.; Bradshaw, T. D.; Andrew, D.; Westwell, A. D. *J. Med. Chem.* **2008**, *51*, 5135–5139. (b) Razavi, H.; Palaninathan, S. K.; Powers, E. T.; Wiseman, R. L.; Purkey, H. E.; Mohamedmohaideen, N. N.; Deechongkit, S.; Chiang, K. P.; Dendle, M. T. A.; Sacchettini, J. C.; Kelly, J. W. *Angew. Chem., Int. Ed.* **2003**, *42*, 2758–2761. (c) Taki, M.; Wolford, J. L.; O'Halloran, T. V. *J. Am. Chem. Soc.* **2004**, *126*, 712–713. (d) Seo, J.; Kim, S.; Park, S. Y. *J. Am. Chem. Soc.* **2004**, *126*, 11154–11155. (e) Ohshima, A.; Momotake, A.; Nagahata, R.; Arai, T. *J. Phys. Chem. A* **2005**, *109*, 9731–9736.

[60]Reiser, A.; Leyshon, L. J.; Saunders, D.; Mijovic, M. V.; Bright, A.; Bogie, J. *J.A.C.S.*, **1972**, *94*, 2414–2421.

[61]Yao, W.; Huang, D. *Org. Lett*., **2010**, *12*, 736–738.

[62]Lakowicz, J.R. *Principles of Fluorescence Spectroscopy*, 3rd Ed., New York: Springer, **c2006**.[24] Du, H.; Fuh, R. A.; Li, J.; Corkan, A.; Lindsey, J. S. *Photochemistry and Photobiology,* **1998**, *68*, 141–142.

[63]Kwiterovich, K. A.; Maguire, M. G.; Murphy, R. P.; Schachat, A. P.; Bressler, N. M.; Bressler, S. B.; Fine, S.L. Ophthalmology, 1991, 98, 1139–1142.

[64]Greenspan, P.; Mayer, E. P.; Fowler, S. D. ***J. Cell Biol.*** **1985**, *100*, 965–973.

[65](a) Karolin, J.; Johansson, L. B.-A.; Strandberg, L.; Ny, T. *J. Am. Chem. Soc.* **1994**, *116*, 7801–7806. (b) Yee, M.-c.; Fas, S. C.; Stohlmeyer, M. M.; Wandless, T. J.; Cimprich, K. A. *J. Biol. Chem.* **2005**, *280*, 29053–29059. (c)Loudet, A.; Burgess, K. *Chem. Rev*. **2007,** *107*, 4891–4932.

[66]Sun, W. C.; Gee, K. R.; Klaubert, D. H.; Haugland, R. P. *J. Org. Chem.* **1997**, *62*, 6469–6475.

[67]Briggs, M. S. J.; Bruce, I., Miller, J. N., Moody, C. J., Simmonds, A. C., Swann, E. *J. C. S. Perkin Transactions 1: Organic and Bio-Organic*

Chemistry, **1997**, 1051–1058.

[68]Schweitzer, C.; Schmidt, R. *Chem. Rev.* **2003,** *103*, 1685–1757.

[69]Cadet, J.; Pouget, J. P.; Ravanat, J. L. *Methods Enzymol.* **2000**, *319*, 143–153.

[70](a)Ryter, S.W.; Tyrrell, R.M. *Free Radical Biol. Med.* **1998**, *24*, 1520–1534. (b) S. Basu-Modak and R. M. Tyrrell, *Cancer Res*., **1993**, *53*, 4505–4510.

[71]Wagner, D.; Przybyla, D.;op den Camp, R.; Kim, C., et al. *Science* **2004**, *306*, 1183–1185.

[72]Miyamoto, S.; Ronsein, G. E.; Prado, F. M.; Uemi, M.; Corrêa, T. C.; Toma, I. N.; Bertolucci, A.; Oliveira, M. C. B.; Motta, F.D.; Medeiros, M. H. G.; Mascio, P. D. *IUBMB Life*, **2007**, 59, 322–331.

[73]Hampton, M. B.; Kettle, A. J.; Winterbourn, C. C. *Blood* **1998**, *92*, 3007–3017.

[74]Baier, J.; Maisch, T.; Maier, M.; Engel, E.; Landthaler, M.; Baumler, W. *Biophys. J.* **2006**, *914*, 1183–1185.

[75]Corey, E. J.; Taylor, W. C. *J. Am. Chem. Soc.* **1964**, *86*, 3881–3882.

[76]Wasserman, H. H.; Scheffer, J. R.; Cooper, J. L. *J. Am. Chem. Soc.* **1972**, *94*, 4991–4996.

[77]Turro, N. J.; Chow, M. F.;Rigaudy, J. *J. Am. Chem. Soc.* **1981**, *103*, 7218–7224.

[78]Umezawa, N.; Tanaka, K.; Urano, Y.; Kikuchi, K.; Higuchi, T.; Nagano, T. *Angew. Chem. Int. Ed.* **1999**, *38*, 2899–2901.

[79]Tanaka, K.; Miura, T.; Umezawa, N.; Urano, Y.; Kikuchi, K.; Higuchi, T.; Nagano, T. *J. Am. Chem. Soc.* **2001**, *123,* 2530–2536.

[80]Flors, C.; Fryer, M. J.; Waring, J.; Reeder, B.; Bechtold, U.; Mullineaux, P. M.; Nonell, S.; Wilson, M. T.; Baker, N. R. *J. Exp. Bot*., **2006**, *57*, 1725–1734

[81]Schrock, E. *et al. Science* **1996**, *273***,** 494–497.

[82] Mendintzi, I. L.; Uyeda, H. T.; Goldmani, E. R.; Mattoussi, H. *Nat. Mater.* **2005**, *4*, 435–446.

[83] Wang S. H.; Han M. Y.; Huang D. J. *J. Am. Chem. Soc.* **2009**, *131,* 11692–11694.

[84] Schmidt, R.; Drews, W.; Brauer, H. D. *J. Phys. Chem.* **1982**, *86*, 4909–4913.

[85] Dabbousi, B. O. *et al. J. Phys. Chem. B* **1997***, 101***,** 9463–9475.

[86] Hines, M. A.; Guyot-Sionnest, P. *J. Phys. Chem.* **1996**, *100*, 468–471.

[87] Scholl, R.; Meyer, K. *Justus Liebigs Ann. Chem.* **1934**, *512*, 112–124.

[88] Motoyoshiya, J.; Masunaga, T.; Harumoto, D.; Ishiguru, S.; Narita, S.; Hayashi, S. *Bull. Chem. Soc. Jpn.,* **1993**, *66*, 1166–1171.

[89] Talapin, D. V.; Rogach, A. L.; Kornowski, A.; Haase, M.; Weller, H. *Nano Lett*. **2001**, *4*, 207–211.

[90] Kim, J. H.; Park, J.; Won, N.; Chung, H. K.; Kim, S. *J. Exp. Nanosci.* **2009**, *4*, 105–112.

[91] Beckman, J. S.; Beckman, T. W.; Chen, J.; Marshall, P. A.; Freeman, B. A. *Proc. Natl. Acad. Sci*. **1990**, *87*, 1620–1624.

[92] Glennon, R. A. *J. Med. Chem.* **1987**, *30*, 1–12.

[93] Barton, D. H. R.; Donnelly, D. M. X.; Finet, J.; Guiry, P. J.; Kielty, J. M.; *Tetrahedron Lett.* **1990**, *46*, 6637–6640.

[94] Boger, D. L.; Yohannes, D.; *Tetrahedron Lett.* **1989**, *30*, 2053–2056.

[95] Lu, F.-L.; Wudl, F.; Nowak, M.; Heeger, A. J. *J. Am. Chem. Soc*. **1986**, *108*, 8311–8313.

[96] Strukelj, M.; Jordan, R. H.; Dodabalapur, A. *J. Am. Chem. Soc*. **1996**, *118*, 1213–1227.

[97] Stille, J. K. *Angew. Chem. Int. Ed. Engl.* **1986**, *25*, 508–524.

[98] Kosugi,M.; Kameyama, M.; Migita, T. *Chemistry Letters* 1983, **12**, 927–928.

[99] Paul,F.; Patt, J.; Hartwig, J.F. *J. Am. Chem. Soc.* **1994**, *116*, 5969–5970

[100] Guram, A.S.; Buchwald, S.L. *J. Am. Chem. Soc.* **1994**, *116*. 7901–7902

[101] Lindley, J. *Tetrahedron* **1984**, *40*, 1433–1456.

[102] Chan, D. M. T.; Monaco, K. L.; Li, R.; Bonne, D.; Clark, C. G.; Lam. P. Y. S. *Tetrahedron Letters*, **2003**, *44*, 3863–3865.

[103] Byrnes, James *Unexploded Ordnance Detection and Mitigation*. Springer. **2009**. pp. 21–22.

[104] Escobedo, J. O.; Rusin, O.; Lim, S.; Strongin, R.M. *Curr. Opin. Chem. Biol.* **2010**, *14*, 64–70

[105] Dandliker WB and Hsu M-L. WO Patent 91/18007, 1991.

[106] Fischer GM, Isomäki-Krondahl M, Göttker-Schnetmann I, Daltrozzo E, Zumbusch A. *Chem. Eur. J.* **2009**, *15*, 4857–4864.

[107] Yan, Y.; Krishnakumar, S.; Yu, H.; Ramishetti, S.; Deng, L.-W.; Wang, S.; Huang, L.; Huang, D. *J. Am. Chem. Soc.* **2013**, *135*, 5312–5315.

[108] Tyson, D. S.; Luman, C. R.; Zhou, X.; Castellano, F. N., *Inorganic Chemistry* **2001,** *40*, 4063–4071.

[109] Aydin, N.; Schlaepfer, C.-W., *Polyhedron* **2001,** *20*, 37–45.

[110] Jie, Z. "Spectroscopy-based quantitative fluorescence resonance energy transfer analysis". *Ion Channels: Methods and Protocols. Methods in Molecular Biology* **2006,** *337*, 65–77.

[111] G. M. Sheldrick, *SHELXTL-97*, Program for the Refinement of Crystal Structures; University of Gottingen: Germany, 1997.

[112] H. K. Hall Jr. *J. Am. Chem. Soc.*, **1957**, *79*, 5441–5444.

[113] H. K. Hall Jr.; Schultz, C. J. *J. Org. Chem.*, **1960**, *27*, 4643–4646.

[114] X. Zhuang, et al. *J. Am. Chem. Soc.*, **2009**, *131*, 18192–18193.

Appendices

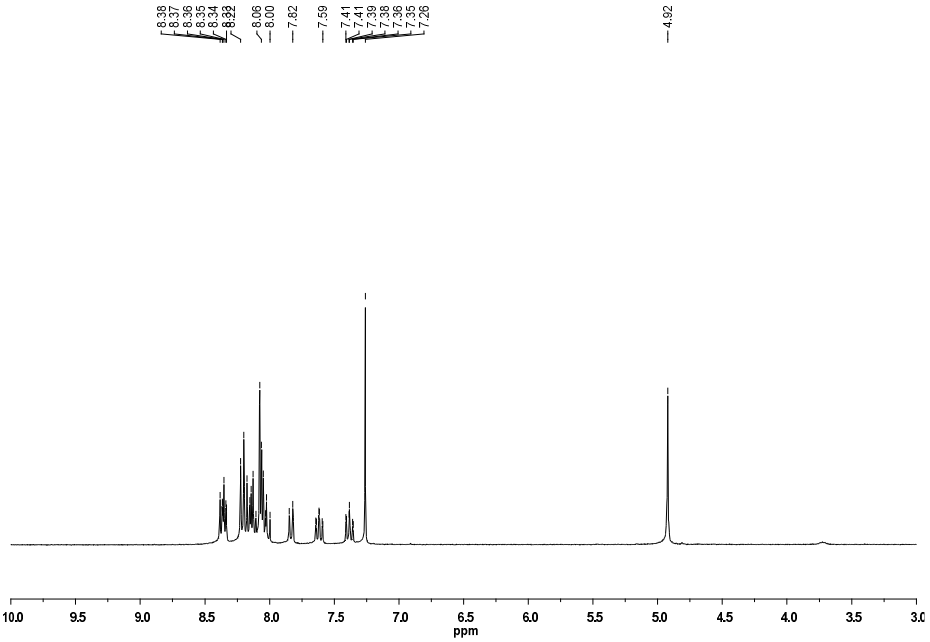

Figure A1 ^{1}H-NMR of selenium blue-α **2.1a**

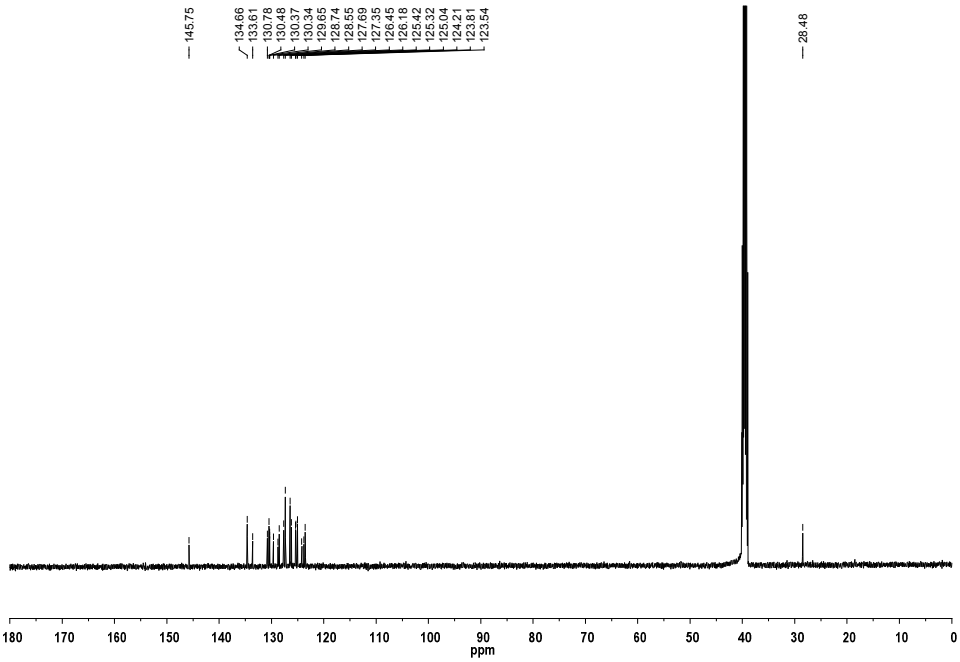

Figure A2 ^{13}C-NMR of selenium blue-α **2.1a**

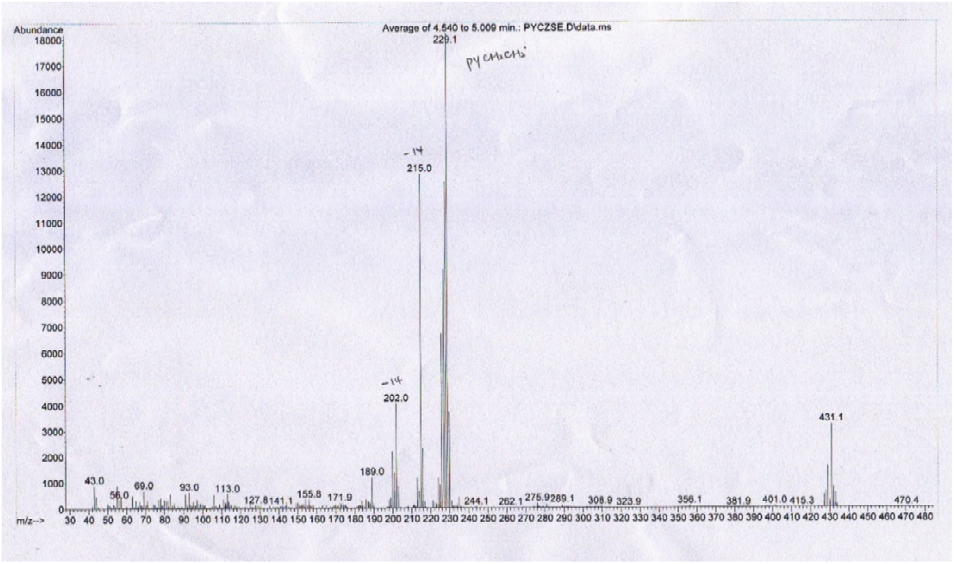

Figure A3 EIMS of selenium blue-α **2.1a**

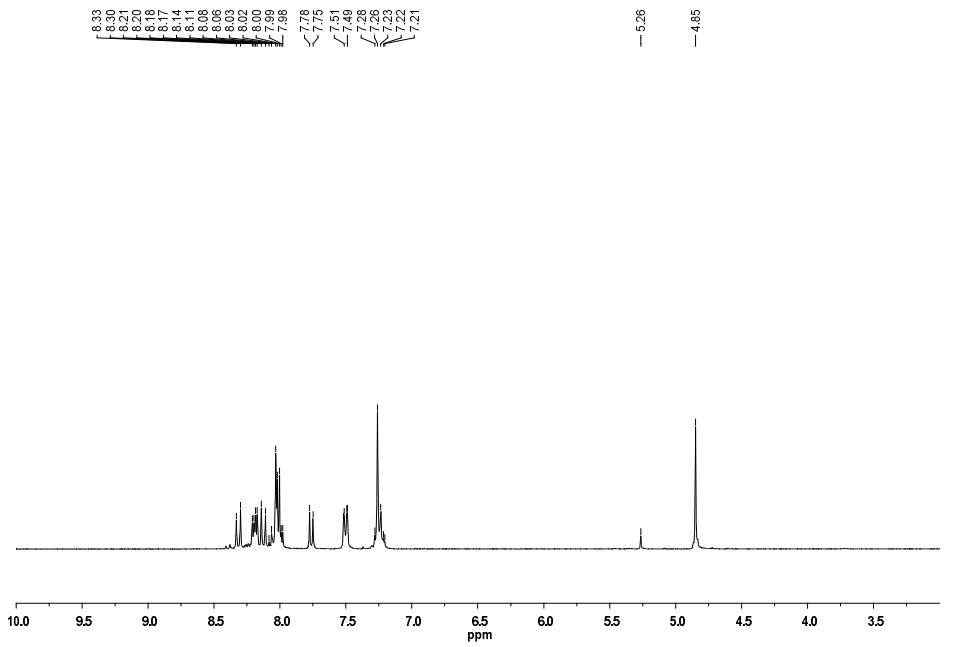

Figure A4 ^{1}H-NMR of phenyl (pyren-1-ylmethyl)selane, **2.1b**

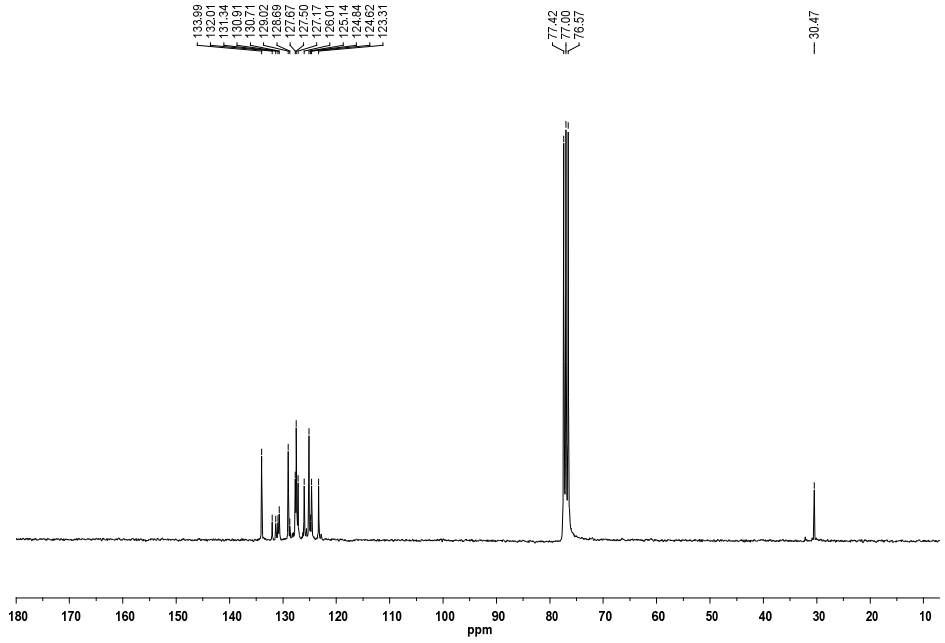

Figure A5 ^{13}C-NMR of phenyl (pyren-1-ylmethyl)selane, **2.1b**

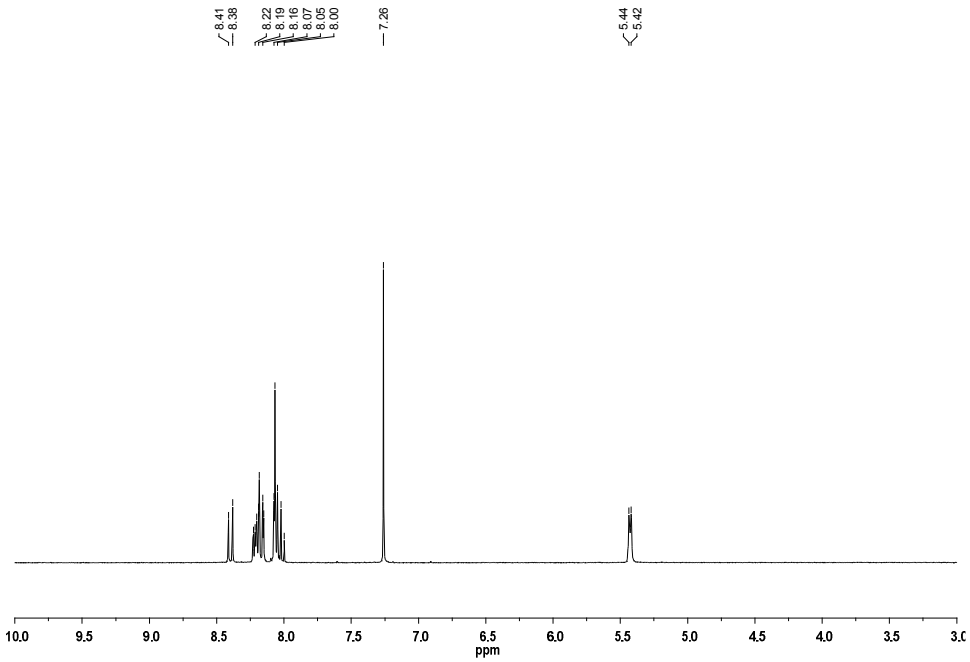

Figure A6 ^{1}H-NMR of pyrenyl methanol, **2.6**

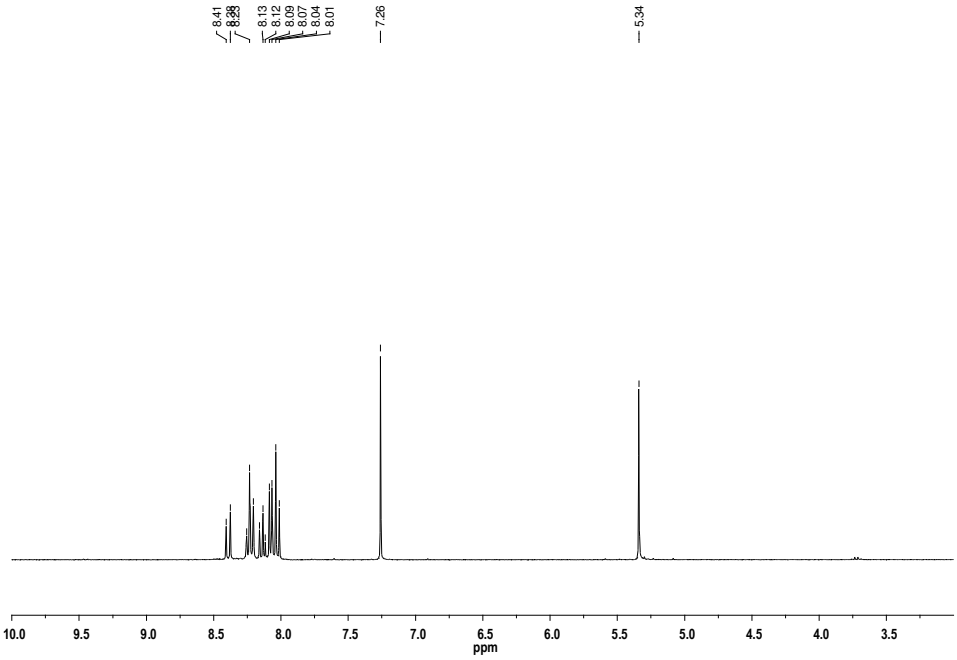

Figure A7 ^{1}H-NMR of chloromethyl pyrene, **2.13**

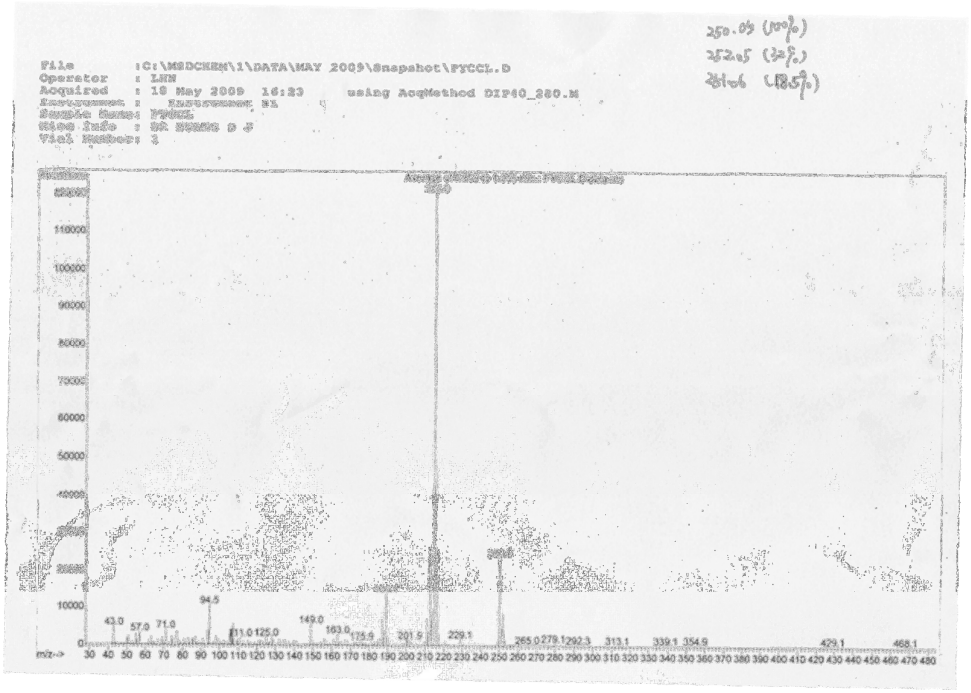

Figure A8 EI-MS of chloromethyl pyrene, **2.13**

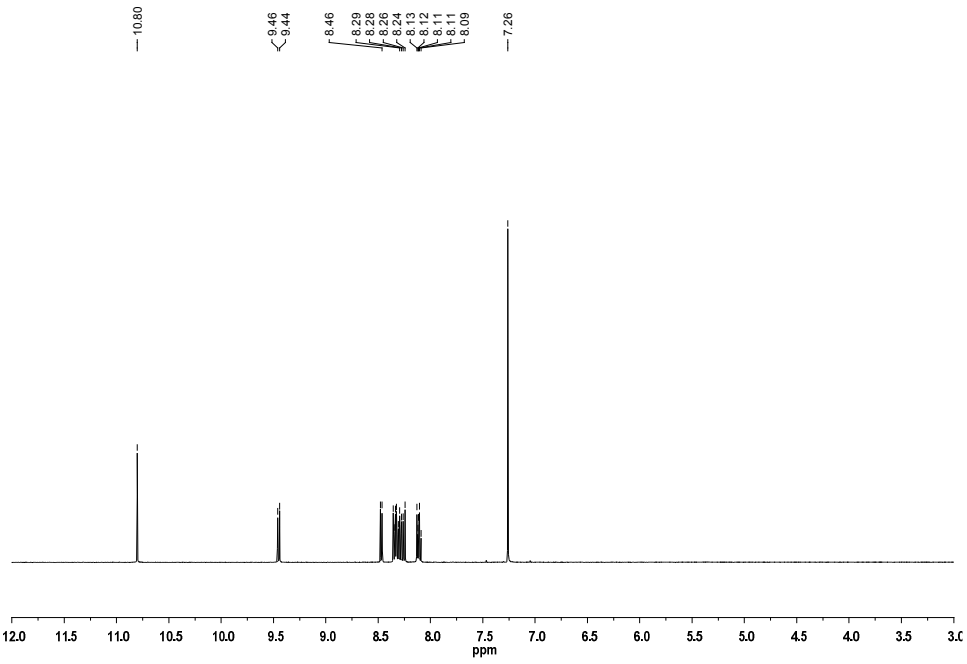

Figure A9 [1]H-NMR of 1-pyrenecarboxaldehyde, **2.4**

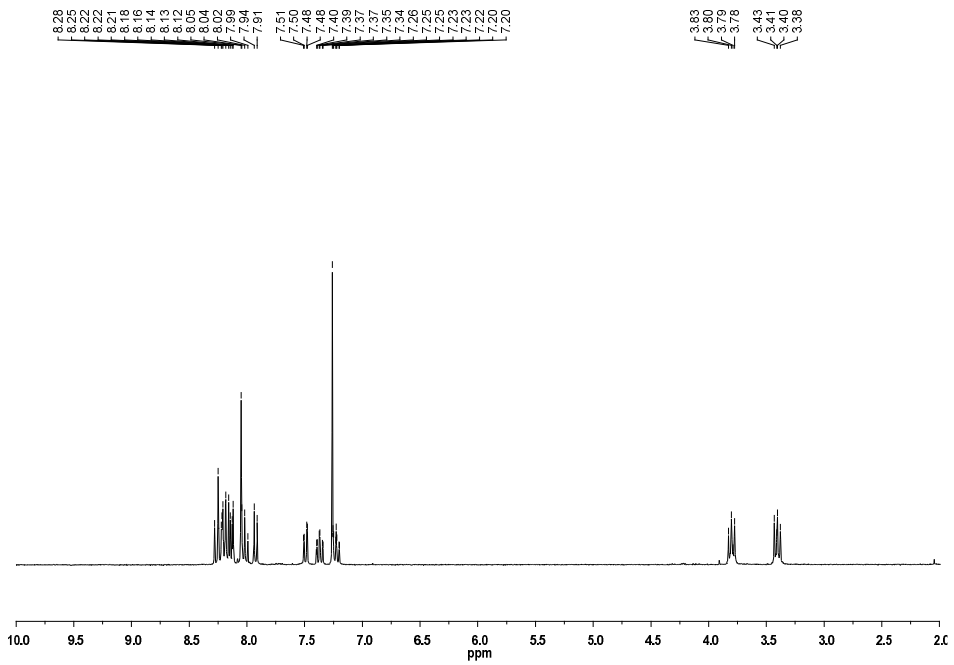

Figure A10 [1]H-NMR of selenium blue-β, **2.2**

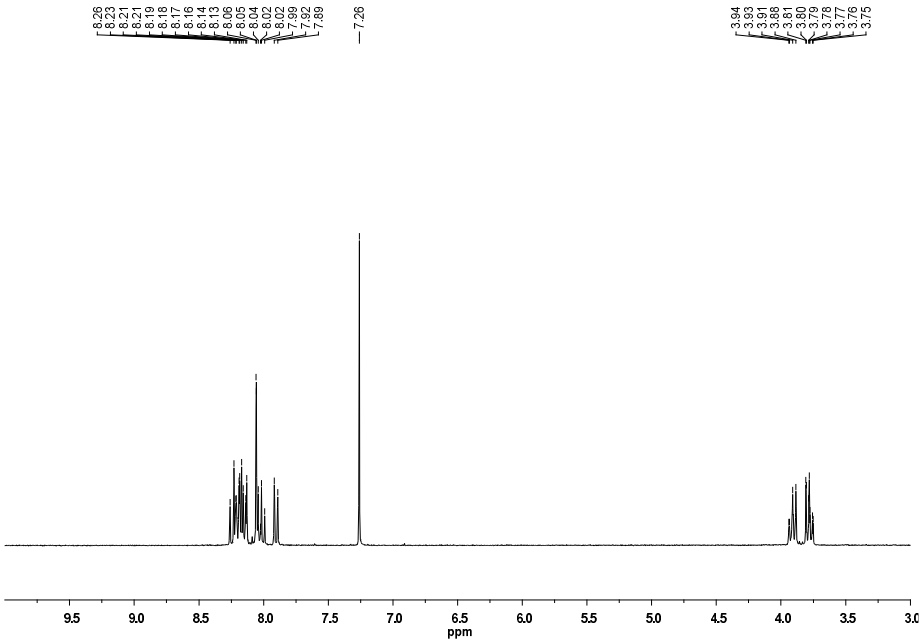

Figure A11 ^{1}H-NMR of 1-(2-bromoethyl)pyrene, **2.18**

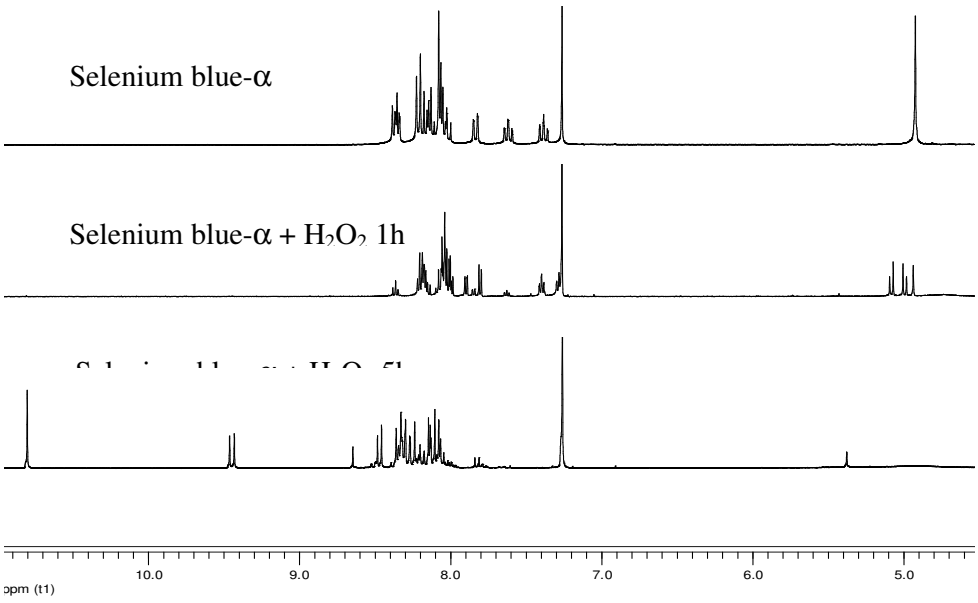

Figure A12 ^{1}H NMR of selenium blue-α 2,1a and 2,1a react with H_2O_2 in $CDCl_3$

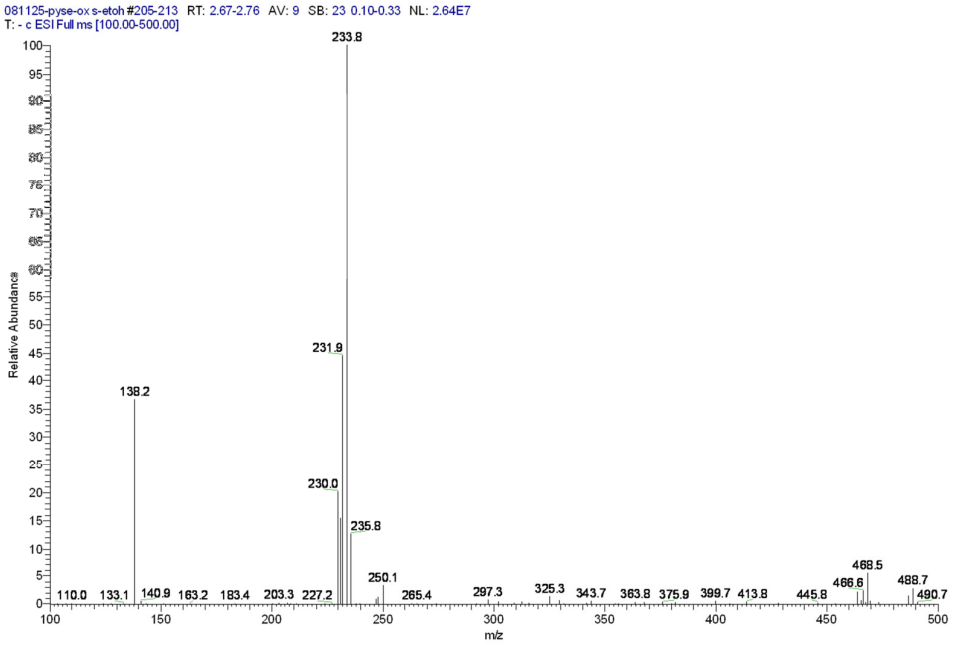

Figure A13 ESI spectra of 2-nitrophenylseleninic acid **2.5**

Table A1 key intermediates coordination parameters and the energy level of DFT calculation

Cartesian coordinates and total energies (in Hartrees) of all PCM-B3LYP/6-31G* optimized geometries (Py = 1-pyrenyl and Ar = o-nitrophenyl). Number of imaginary frequency is in square bracket.

$PyCH_2SeAr$ (**2.1b**) -3489.54988 [0]				$PyCH_2CH_2SeAr$ (**2.2**) -3528.86159 [0]			
C	-5.308241	-4.899719	0.943037	C	-5.080727	-4.927657	1.329829
C	-3.944640	-4.981012	1.225889	C	-3.737675	-4.817020	1.690078
C	-3.077123	-3.929936	0.880525	C	-2.949155	-3.760897	1.200601
C	-3.604306	-2.770536	0.233911	C	-3.536208	-2.794935	0.326881
C	-5.003846	-2.697572	-0.052606	C	-4.914652	-2.917785	-0.036439
C	-5.834141	-3.772164	0.310855	C	-5.664678	-3.990341	0.476424
C	-1.668069	-3.977307	1.153052	C	-1.563980	-3.612141	1.549586

C	-2.738273	-1.690846	-0.125262	C	-2.750709	-1.713630	-0.182180
C	-1.335859	-1.762420	0.161550	C	-1.368851	-1.589396	0.179168
C	-0.840539	-2.949094	0.810775	C	-0.813467	-2.582287	1.064617
C	-0.500024	-0.673198	-0.197010	C	-0.610987	-0.508359	-0.338254
C	-1.063363	0.439023	-0.841029	C	-1.233137	0.413396	-1.190598
C	-2.422276	0.512574	-1.124632	C	-2.573919	0.299740	-1.546505
C	-3.283749	-0.540208	-0.775341	C	-3.355982	-0.757167	-1.055753
C	-4.694248	-0.493659	-1.050999	C	-4.743925	-0.904971	-1.403457
C	-5.517036	-1.523669	-0.705991	C	-5.489357	-1.936584	-0.917544
H	-6.584203	-1.475640	-0.920698	H	-6.539728	-2.037200	-1.189147
H	-5.092882	0.391418	-1.545956	H	-5.188630	-0.166735	-2.070165
H	-1.265345	-4.863152	1.643455	H	-1.117359	-4.346759	2.219041
H	-5.967207	-5.722198	1.216785	H	-5.678252	-5.751514	1.717049
H	-3.538011	-5.863687	1.718446	H	-3.285789	-5.550984	2.356485
H	-6.899827	-3.714622	0.091607	H	-6.714066	-4.082513	0.198308
H	0.219806	-3.034035	1.028672	H	0.230228	-2.510249	1.358793
H	-0.415750	1.269312	-1.118539	H	-0.647016	1.244599	-1.582175
H	-2.829495	1.393842	-1.618878	H	-3.027200	1.035956	-2.209423
C	0.974315	-0.669492	0.076710	C	0.864546	-0.334823	-0.029578
H	1.377925	0.341625	0.088077	H	1.134958	0.718816	-0.166143
H	1.249166	-1.187505	0.996347	H	1.079447	-0.580954	1.017229
C	3.762368	-1.446523	-0.792024	C	1.731373	-1.199400	-0.958760
C	4.603330	-0.330659	-0.975605	H	1.496969	-2.261218	-0.854230

C	4.336487	-2.579446	-0.198684
C	5.943236	-0.339174	-0.579732
C	5.669594	-2.594934	0.218400
H	3.719733	-3.464832	-0.064872
C	6.475129	-1.470442	0.032913
H	6.551646	0.545715	-0.744524
H	6.074723	-3.490116	0.687661
H	7.513682	-1.470706	0.358173
N	4.138546	0.909198	-1.604255
O	4.948101	1.537729	-2.292428
O	2.977790	1.272980	-1.414134
Se	1.941701	-1.615362	-1.420625

$PyCH_2Se(O)Ar$ (**2.3**) -3564.72787 [0]

H	1.502631	-2.000791	-1.433168
C	0.598784	-1.400617	-1.522871
H	0.308843	-1.922996	-3.590852
C	-0.072662	-1.361284	-2.738994
C	-1.038374	0.092501	-0.508474
C	-1.252297	-0.612448	-2.880898
C	0.135257	-0.699928	-0.397811
C	-1.742828	0.121875	-1.756262
C	-1.979709	-0.566145	-4.120132
H	1.620646	-0.898849	-2.000944
C	4.439397	-2.144427	-1.806958
C	4.832304	-3.417352	-1.371526
C	4.757552	-1.800577	-3.135859
C	5.480060	-4.316801	-2.221754
H	4.622145	-3.702813	-0.343624
C	5.421901	-2.683826	-3.990894
C	5.771808	-3.952378	-3.537021
H	5.756178	-5.302389	-1.850262
H	5.645818	-2.371832	-5.007179
H	6.272876	-4.647107	-4.208300
N	4.426174	-0.493516	-3.711028
O	5.210611	-0.019519	-4.538456
O	3.388285	0.065463	-3.357005
Se	3.654875	-0.969690	-0.486956

$PyCH_2CH_2Se(O)Ar$ (**2.16**) -3604.02598 [0]

C	6.576776	-1.510598	1.602022
C	5.431844	-2.205439	1.212094
C	4.365455	-1.535931	0.586590
C	4.462928	-0.130262	0.350688
C	5.641976	0.572779	0.754101
C	6.682869	-0.137351	1.376984

C	-3.125867	0.161082	-4.240703	C	3.171629	-2.216452	0.169110
H	-1.591190	-1.132065	-4.966319	C	3.388200	0.569319	-0.282238
H	-3.668740	0.186273	-5.185157	C	2.203647	-0.132210	-0.682923
C	-3.648830	0.912955	-3.131971	C	2.145337	-1.550626	-0.432896
C	-4.829065	1.669527	-3.234384	C	1.149852	0.585117	-1.303035
C	-2.942662	0.888099	-1.888131	C	1.294820	1.962517	-1.515494
C	-5.311813	2.392015	-2.142089	C	2.442360	2.650058	-1.131749
H	-5.365907	1.686394	-4.182340	C	3.504507	1.976101	-0.509567
H	-6.227753	2.972545	-2.240785	C	4.702251	2.656756	-0.095832
C	-4.628403	2.377680	-0.926265	C	5.723508	1.987803	0.508680
H	-5.006823	2.945872	-0.077100	H	6.624959	2.515558	0.818419
C	-3.444258	1.633850	-0.778035	H	4.773533	3.728692	-0.277683
C	-1.562648	0.871521	0.583788	H	3.100068	-3.289640	0.343442
H	-1.012535	0.910757	1.518029	H	7.393931	-2.043295	2.085825
C	-2.708185	1.600592	0.453866	H	5.353323	-3.277467	1.389561
H	-3.082332	2.183552	1.295170	H	7.579407	0.399892	1.684371
C	0.890712	-0.841269	0.883646	H	1.263794	-2.109749	-0.734932
H	1.538702	-1.717877	0.873066	H	0.483190	2.507221	-1.997024
H	0.270650	-0.845415	1.783359	H	2.523701	3.720973	-1.314376
Se	2.123021	0.750801	1.267772	C	-0.151792	-0.077924	-1.713619
O	1.186192	1.683439	2.310486	H	-0.635813	0.530103	-2.485868
C	3.261747	-0.222637	2.554733	H	0.024335	-1.066874	-2.154167
C	4.847983	-1.407585	4.545086	C	-1.116503	-0.197733	-0.526138

C	3.000105	0.024724	3.897577	H	-0.779554	-0.915255	0.229265
C	4.336611	-1.057739	2.222195	H	-1.321373	0.767826	-0.064103
C	5.134417	-1.650590	3.203941	C	-3.893416	-0.552503	0.485539
C	3.781411	-0.572439	4.891514	C	-4.098726	-1.694417	1.262924
H	2.179089	0.694267	4.145732	C	-4.550742	0.626065	0.858741
H	5.959449	-2.293164	2.910313	C	-4.903437	-1.650485	2.405191
H	3.557603	-0.380264	5.939892	H	-3.636568	-2.635959	0.964940
H	5.459890	-1.868916	5.317782	C	-5.394586	0.673414	1.968865
N	4.647324	-1.333357	0.825951	C	-5.557870	-0.467757	2.753305
O	5.668915	-1.958192	0.550901	H	-5.033143	-2.548120	3.007324
O	3.853546	-0.914600	-0.032055	H	-5.895407	1.604848	2.220598
				H	-6.200516	-0.429611	3.630701
$PyCH_2Cl$ (**2.13**) -1114.67872 [0]				N	-4.357981	1.889006	0.135117
C	-4.826578	-5.089523	0.333866	O	-5.340725	2.617840	-0.009963
C	-3.439971	-5.081064	0.484182	O	-3.225525	2.170915	-0.250001
C	-2.715235	-3.880303	0.381875	Se	-2.884293	-0.876647	-1.179672
C	-3.413106	-2.662034	0.121262	O	-3.381258	0.255591	-2.314996
C	-4.834652	-2.681565	-0.032829				
C	-5.518384	-3.904467	0.077785	$PyCH{=}CH_2$ (**2.7**) -693.16547 [0]			
C	-1.288043	-3.831581	0.528797	C	-5.335558	-4.629914	0.092990
C	-2.694443	-1.431105	0.014428	C	-3.940657	-4.620920	0.072220
C	-1.271113	-1.410661	0.171409	C	-3.232373	-3.406937	0.037119
C	-0.599813	-2.658292	0.427422	C	-3.953992	-2.174223	0.022329

C	-0.587900	-0.171976	0.067860	C	-5.384571	-2.194719	0.047778
C	-1.311085	0.999110	-0.198301	C	-6.051383	-3.432117	0.081723
C	-2.692871	0.983618	-0.353502	C	-1.797683	-3.355471	0.022312
C	-3.408712	-0.220271	-0.250374	C	-3.251209	-0.928969	-0.016042
C	-4.838084	-0.269814	-0.401227	C	-1.817913	-0.905159	-0.047634
C	-5.519847	-1.445035	-0.297077	C	-1.126487	-2.168984	-0.013417
H	-6.603045	-1.468444	-0.413024	C	-1.139614	0.346166	-0.089335
H	-5.366989	0.661429	-0.601532	C	-1.903785	1.528072	-0.096516
H	-0.755604	-4.762294	0.723039	C	-3.291125	1.509089	-0.056943
H	-5.373680	-6.027374	0.415907	C	-3.993384	0.292501	-0.019716
H	-2.903644	-6.008522	0.682506	C	-5.429184	0.243047	0.006682
H	-6.601523	-3.917514	-0.039580	C	-6.096049	-0.945305	0.038178
H	0.481445	-2.671902	0.534865	H	-7.185218	-0.969285	0.057874
H	-0.773892	1.943929	-0.277723	H	-5.976889	1.185046	0.000878
H	-3.230779	1.909519	-0.553190	H	-1.245856	-4.294824	0.046231
C	0.890738	-0.066853	0.248214	H	-5.869848	-5.578394	0.119611
H	1.201952	0.959308	0.444226	H	-3.385128	-5.558133	0.083941
H	1.292308	-0.725592	1.018215	H	-7.140691	-3.445109	0.099751
Cl	1.834897	-0.543495	-1.293816	H	-0.040298	-2.182061	-0.004653
				H	-1.391962	2.485497	-0.162710
$PyCH_2OH$ (**2.6**) -730.29344 [0]				H	-3.849062	2.444839	-0.071955
C	-4.785677	-5.090883	0.318909	C	0.332043	0.420019	-0.147366
C	-3.397616	-5.067310	0.454556	H	0.846599	-0.427759	-0.599227

C	-2.687344	-3.857753	0.352772	C	1.083573	1.438248	0.297661
C	-3.403141	-2.645975	0.107539	H	2.165057	1.421069	0.190296
C	-4.826475	-2.680809	-0.030384	H	0.657831	2.310687	0.788769
C	-5.494624	-3.912440	0.078917				
C	-1.257870	-3.793046	0.482286	$PyCH_2Se(Cl)Ar^+$ (**2.15**) -3949.55694 [0]			
C	-2.700001	-1.405331	0.002986	H	0.235391	2.796774	-0.445149
C	-1.275825	-1.368940	0.142265	C	-0.661683	2.181806	-0.387974
C	-0.585359	-2.611212	0.379897	H	-1.922962	3.848804	0.104526
C	-0.601566	-0.125600	0.053243	C	-1.871420	2.777153	-0.081653
C	-1.340777	1.037383	-0.186889	C	-1.727575	-0.020629	-0.581557
C	-2.726819	1.010944	-0.331498	C	-3.049138	2.007242	-0.011792
C	-3.430499	-0.199230	-0.238243	C	-0.558846	0.796534	-0.637784
C	-4.861665	-0.264939	-0.375081	C	-2.981075	0.601992	-0.270803
C	-5.528537	-1.448831	-0.276235	C	-4.314365	2.603147	0.306417
H	-6.612628	-1.483911	-0.381027	C	-5.453160	1.853826	0.362971
H	-5.404172	0.661882	-0.559994	H	-4.344997	3.674234	0.501990
H	-0.713039	-4.719915	0.660660	H	-6.408562	2.318294	0.605459
H	-5.320898	-6.035721	0.400588	C	-5.426086	0.442159	0.103869
H	-2.848735	-5.989955	0.640911	C	-6.589505	-0.345561	0.153780
H	-6.578887	-3.937621	-0.025867	C	-4.177563	-0.176842	-0.214822
H	0.497780	-2.600365	0.448545	C	-6.536872	-1.715906	-0.105348
H	-0.815355	1.989388	-0.257502	H	-7.539031	0.129158	0.398835
H	-3.274796	1.934181	-0.516933	H	-7.448313	-2.309708	-0.062712

C	0.896010	-0.029640	0.233068
H	1.184004	1.031300	0.274659
H	1.187971	-0.483854	1.193163
O	1.555407	-0.691859	-0.850972
H	2.517119	-0.711999	-0.641063

HOCl -535.9510804 [0]

O	-0.030421	0.000000	-0.047522
Cl	0.012266	0.000000	1.678423
H	0.938029	0.000000	-0.288686

OCl^- -535.454212 [0]

O	0.000000	0.000000	-0.003204
Cl	0.000000	0.000000	1.753204

OH^- -75.859425 [0]

O	0.000000	0.000000	0.109003
H	0.000000	0.000000	-0.872023

$ArSeO^-$ -2910.39255 [0]

C	3.850200	-1.408554	-1.036915
C	4.653958	-0.239949	-1.045961
C	4.423096	-2.576995	-0.483045
C	-5.324074	-2.328509	-0.419176
H	-5.285555	-3.398168	-0.622559
C	-4.135807	-1.578120	-0.478214
C	-1.725898	-1.432135	-0.850549
H	-0.797550	-1.935692	-1.102599
C	-2.872424	-2.171434	-0.801828
H	-2.839377	-3.239704	-1.013655
C	0.769174	0.262045	-0.952170
H	1.437173	0.966249	-1.448509
H	0.831815	-0.731260	-1.394518
Se	1.920125	-0.031195	0.853236
C	3.609428	-0.614309	0.102313
C	6.145663	-1.246217	-0.917389
C	3.975765	-1.945506	-0.053039
C	4.524957	0.388380	-0.260947
C	5.790545	0.090709	-0.764733
C	5.242062	-2.252935	-0.567282
H	3.300931	-2.750156	0.219624
H	6.468416	0.897342	-1.034027
H	5.518378	-3.299176	-0.689228
H	7.126953	-1.501646	-1.312288
N	4.132858	1.764041	-0.113903
O	4.906748	2.671892	-0.343949

C	5.968507	-0.240267	-0.527513
C	5.708310	-2.577173	0.024224
H	3.802087	-3.469948	-0.478614
C	6.494062	-1.399452	0.004066
H	6.541054	0.681432	-0.559844
H	6.122646	-3.493197	0.444353
H	7.505608	-1.407297	0.404768
N	4.136282	0.958737	-1.585306
O	4.826400	2.004964	-1.605622
O	2.961962	0.926544	-2.039558
Se	2.078427	-1.545632	-1.701268
O	1.688881	-3.201526	-1.397316

ArSeCl -3295.28240 [0]

C	3.895309	1.429125	1.066791
C	4.674579	0.255732	1.026465
C	4.460737	2.597791	0.542306
C	5.970146	0.218526	0.490479
C	5.746616	2.569371	0.008195
H	3.902015	3.526634	0.549681
C	6.506123	1.386739	0.021424
H	6.520981	0.718434	0.488456
H	6.167886	3.489543	0.394666
O	2.942603	1.971879	0.265643
Cl	1.072647	-2.040365	1.371007

$PyCH_2CH_2Cl$ -1153.99285 [0]

C	-4.797423	-5.110600	0.359319
C	-3.413860	-5.085376	0.535023
C	-2.699864	-3.878932	0.428439
C	-3.404777	-2.670961	0.137198
C	-4.823768	-2.707930	-0.041002
C	-5.496549	-3.936724	0.074416
C	-1.276341	-3.812003	0.605188
C	-2.696443	-1.433843	0.023654
C	-1.274256	-1.394591	0.201182
C	-0.599354	-2.633438	0.497570
C	-0.595809	-0.154910	0.085091
C	-1.331737	1.002071	-0.203466
C	-2.712184	0.971893	-0.377541
C	-3.419371	-0.235609	-0.269575
C	-4.845884	-0.302116	-0.442717
C	-5.517626	-1.482344	-0.333974
H	-6.598391	-1.518942	-0.467858
H	-5.380646	0.621001	-0.664649
H	-0.739053	-4.732623	0.831513

H	7.508779	1.387862	0.443548	H	-5.336291	-6.052964	0.444768
N	4.104302	0.930311	1.557280	H	-2.871901	-6.004112	0.757120
O	4.703977	1.999244	1.566688	H	-6.577185	-3.962753	-0.062372
O	2.927116	0.823231	2.026601	H	0.477615	-2.633585	0.643862
Se	2.155367	1.279386	1.835683	H	-0.805123	1.952465	-0.287930
Cl	1.507338	3.489896	1.566576	H	-3.254979	1.890822	-0.596383
				C	0.911008	-0.040994	0.229696
ArSeOH	-2910.88989	[0]		H	1.171758	0.984253	0.514114
C	3.874677	-1.395359	-1.248270	H	1.292691	-0.699069	1.017489
C	4.641712	-0.227289	-1.080921	C	1.603292	-0.376104	-1.092541
C	4.407386	-2.595559	-0.755926	H	1.418364	-1.403455	-1.411320
C	5.894420	-0.233616	-0.448639	H	1.311197	0.310739	-1.889168
C	5.648359	-2.610388	-0.127371	Cl	3.427014	-0.223016	-0.944677
H	3.839464	-3.511632	-0.881260				
C	6.397825	-1.431793	0.029850	$PyCH_2CH_2OH$	-769.60810	[0]	
H	6.443729	0.697903	-0.347758	C	-4.793912	-5.112645	0.371678
H	6.042395	-3.554683	0.246153	C	-3.407983	-5.085324	0.528317
H	7.367538	-1.457352	0.522216	C	-2.697338	-3.877634	0.413095
N	4.122018	1.013167	-1.574540	C	-3.408481	-2.670561	0.132274
O	4.759462	2.059452	-1.442063	C	-4.829928	-2.709964	-0.027378
O	3.002298	0.973785	-2.137545	C	-5.499029	-3.940035	0.096722
Se	2.176036	-1.356598	-2.119030	C	-1.271269	-3.808167	0.570516
O	1.826474	-3.159444	-2.012112	C	-2.703830	-1.431627	0.011837

H	1.325251	-3.293512	-1.168396	C	-1.279698	-1.388867	0.173495
				C	-0.598669	-2.627707	0.456865
TS1	-4024.99668 [1]			C	-0.601831	-0.148590	0.056596
C	1.000830	-1.011085	-0.480480	C	-1.346796	1.005973	-0.219891
H	1.359723	-1.733562	0.251150	C	-2.728869	0.973799	-0.382479
C	3.877202	-1.161833	-1.286763	C	-3.433150	-0.234770	-0.270292
C	4.729837	-0.062760	-1.467248	C	-4.861513	-0.303950	-0.426238
C	4.362321	-2.255873	-0.558214	C	-5.529903	-1.485401	-0.310385
C	6.025373	-0.045294	-0.938545	H	-6.612181	-1.523956	-0.430532
C	5.636378	-2.228730	0.008980	H	-5.400763	0.618521	-0.640147
H	3.669035	-3.110896	-0.509322	H	-0.729405	-4.728630	0.786435
C	6.472795	-1.124736	-0.183839	H	-5.329924	-6.056027	0.464134
H	6.654500	0.817049	-1.124833	H	-2.861571	-6.003330	0.742427
H	5.983073	-3.081676	0.587776	H	-6.581404	-3.967817	-0.025160
H	7.473587	-1.105265	0.241040	H	0.480181	-2.622884	0.585170
N	4.338460	1.140924	-2.222406	H	-0.823799	1.958328	-0.304550
O	5.235155	1.738576	-2.831894	H	-3.275602	1.892346	-0.593528
O	3.164522	1.495226	-2.200950	C	0.901758	-0.029777	0.194335
Se	2.121625	-1.465661	-2.083727	H	1.158489	0.995824	0.485411
Cl	1.726089	-5.232558	-0.194308	H	1.286588	-0.685963	0.983983
O	1.933943	-3.546309	-1.253567	C	1.651004	-0.347481	-1.105637
H	0.014779	-1.349961	-0.804607	H	1.432836	-1.379422	-1.423677
C	1.019902	0.401233	0.005933	H	1.296529	0.323223	-1.904516

C	0.266351	1.439893	-0.600129	O	3.040243	-0.166795	-0.856963
C	1.799360	0.708328	1.131220	H	3.523822	-0.338964	-1.695439
C	0.298153	2.757199	-0.044970				
C	-0.538247	1.222968	-1.771071	**TS3**	-4064.31423	[1]	
C	1.846065	1.988555	1.670258	C	0.677793	-0.305812	-0.224723
H	2.377302	-0.088467	1.591765	H	-0.344366	-0.029895	-0.500822
C	-0.472242	3.808204	-0.632249	H	1.220751	0.598089	0.053302
C	1.099622	3.033153	1.105621	C	3.254816	-1.304074	-1.462157
C	-1.273064	2.223769	-2.332820	C	4.298151	-0.369617	-1.316591
H	-0.538688	0.240049	-2.227826	C	3.583490	-2.664217	-1.358212
H	2.459826	2.187496	2.546385	C	5.613592	-0.773480	-1.057576
C	-1.274420	3.550068	-1.786087	C	4.889189	-3.070642	-1.087494
C	-0.445544	5.124236	-0.071424	H	2.742136	-3.355858	-1.474523
C	1.109142	4.363414	1.644918	C	5.908005	-2.125544	-0.931533
H	-1.868620	2.031088	-3.222424	H	6.379273	-0.013539	-0.958975
C	-2.027022	4.596720	-2.346672	H	5.107521	-4.131237	-0.989788
C	-1.215088	6.137796	-0.666528	H	6.926640	-2.437186	-0.714491
C	0.372131	5.363393	1.086024	N	4.093818	1.074552	-1.452657
H	1.725830	4.557678	2.520168	O	5.067037	1.764836	-1.787738
C	-1.996433	5.874199	-1.791093	O	2.970887	1.533613	-1.238981
H	-2.634826	4.396803	-3.226307	Se	1.402520	-0.976338	-1.952713
H	-1.193131	7.137693	-0.238274	Cl	0.385298	-5.063188	-1.250292
H	0.390871	6.366310	1.507368	O	0.767123	-3.130362	-1.616643

H	-2.584417	6.672037	-2.238725	C	0.683121	-1.398746	0.865008
				H	1.594030	-1.299484	1.467582
TS2	-4025.064078	[1]		H	0.725125	-2.368405	0.345106
C	-5.826222	-4.623542	0.310889	C	-0.529093	-1.299923	1.761938
C	-4.495001	-4.964905	0.545980	C	-1.786630	-1.820617	1.354680
C	-3.476090	-3.998916	0.441781	C	-0.435405	-0.650904	2.999710
C	-3.816987	-2.658907	0.091530	C	-2.925490	-1.648801	2.206117
C	-5.183154	-2.320089	-0.155250	C	-1.955030	-2.527300	0.107993
C	-6.169061	-3.315802	-0.037479	C	-1.535511	-0.489139	3.836616
C	-2.096394	-4.314911	0.659572	H	0.532032	-0.260895	3.309622
C	-2.797269	-1.664501	-0.013508	C	-4.202175	-2.154453	1.810441
C	-1.432591	-2.003664	0.243649	C	-2.796075	-0.973875	3.460163
C	-1.116610	-3.365040	0.562170	C	-3.177665	-3.008404	-0.258376
C	-0.436239	-0.974729	0.151719	H	-1.096404	-2.699701	-0.545932
C	-0.828338	0.332362	-0.238550	H	-1.425048	0.020618	4.791986
C	-2.143871	0.649954	-0.503304	C	-4.340936	-2.839320	0.563675
C	-3.155872	-0.329038	-0.385401	C	-5.343942	-1.980298	2.655043
C	-4.531578	-0.017441	-0.632795	C	-3.958342	-0.816699	4.289534
C	-5.504664	-0.969752	-0.519217	H	-3.276123	-3.554518	-1.193368
H	-6.547782	-0.717111	-0.707854	C	-5.606996	-3.327253	0.192545
H	-4.787579	1.003376	-0.913945	C	-6.587631	-2.483634	2.239286
H	-1.833089	-5.344869	0.899733	C	-5.175183	-1.294163	3.906967
H	-6.602977	-5.381536	0.396703	H	-3.843980	-0.300846	5.241241

H	-4.229364	-5.987452	0.812392	C	-6.713875	-3.149302	1.019895
H	-7.210230	-3.053894	-0.223275	H	-5.710094	-3.851146	-0.754943
H	-0.078601	-3.661681	0.682824	H	-7.454847	-2.349151	2.882723
H	-0.060987	1.102234	-0.310441	H	-6.045778	-1.165400	4.547206
H	-2.418208	1.662432	-0.796174	H	-7.684025	-3.534453	0.713816
C	0.930524	-1.197983	0.473146				
H	1.646568	-0.415484	0.257890	**TS4** -4064.36729 [1]			
H	1.330835	-2.165827	0.740031	C	-1.173351	-1.836615	0.538299
C	3.766476	-2.163266	-1.567583	H	-1.724142	-2.764350	0.514352
C	4.193936	-1.250030	-2.556253	H	-1.549797	-1.059946	1.188160
C	4.659799	-2.437477	-0.515307	C	-3.565995	0.673401	-0.639172
C	5.456483	-0.631298	-2.499993	C	-4.424743	1.033291	0.417874
C	5.905200	-1.830123	-0.454207	C	-2.924276	1.711679	-1.332185
H	4.328312	-3.142401	0.243178	C	-4.640416	2.373492	0.778134
C	6.311259	-0.920379	-1.450858	C	-3.129853	3.040900	-0.980988
H	5.736831	0.064897	-3.284389	H	-2.263305	1.432852	-2.149082
H	6.576001	-2.060112	0.372859	C	-3.992303	3.378031	0.077007
H	7.289442	-0.446814	-1.399244	H	-5.311187	2.599229	1.601464
N	3.329562	-0.931248	-3.649477	H	-2.618609	3.827878	-1.534168
O	3.699073	-0.129611	-4.525856	H	-4.152413	4.419698	0.347267
O	2.209864	-1.486720	-3.678763	N	-5.104386	0.009795	1.165904
Se	2.082930	-3.076597	-1.536673	O	-5.861391	0.323241	2.094737
O	2.220277	-4.000869	-0.083209	O	-4.896212	-1.175232	0.838096

Cl	1.183291	-0.577184	2.883266	Se	-3.232726	-1.124766	-1.249505
				O	-2.090637	-0.848205	-2.509546
TS5 -3603.97794 [1]				Cl	0.012184	-2.750732	2.462380
C	-0.309589	-1.427775	-1.451167	C	-0.116223	-1.581114	-0.463593
H	-1.324481	-0.721368	-1.909583	H	0.367890	-2.528328	-0.707530
H	-0.161764	-2.123442	-2.292515	H	-0.661485	-1.278856	-1.410243
C	-0.957450	-2.023279	-0.339694	C	0.876379	-0.483015	-0.132218
H	-1.266459	-3.064587	-0.361666	C	2.280439	-0.663088	-0.228156
H	-0.892510	-1.571446	0.647382	C	0.380732	0.777918	0.227593
C	-3.993123	-0.146346	0.519034	C	3.151804	0.444366	0.054605
C	-5.055381	-0.739485	1.215987	C	2.896981	-1.912223	-0.603135
C	-3.654292	1.168605	0.860779	C	1.216803	1.851258	0.511961
C	-5.732517	-0.055966	2.225157	H	-0.693989	0.927570	0.276782
H	-5.369831	-1.748238	0.952456	C	4.572128	0.294231	-0.040134
C	-4.357971	1.883352	1.834232	C	2.610674	1.711660	0.432753
C	-5.392141	1.264869	2.529277	C	4.249454	-2.052912	-0.694034
H	-6.540539	-0.551036	2.757951	H	2.273371	-2.774477	-0.817500
H	-4.067711	2.906464	2.049908	H	0.791744	2.815113	0.790375
H	-5.927594	1.810565	3.301263	C	5.139784	-0.960711	-0.419180
N	-2.506471	1.848231	0.261455	C	5.436596	1.399916	0.241920
O	-2.593883	3.063682	0.066938	C	3.501735	2.805059	0.712088
O	-1.504911	1.177409	0.027146	H	4.680374	-3.012241	-0.979338
Se	-3.350037	-1.294748	-0.916485	C	6.536695	-1.089013	-0.509591

O	-2.566150	-0.330728	-2.117660	C	6.828158	1.226159	0.139404
C	0.833375	-0.452642	-1.288780	C	4.852967	2.658071	0.621655
C	0.808721	0.756719	-1.997666	H	3.066661	3.762020	0.999181
C	1.981841	-0.762135	-0.510777	C	7.369693	-0.004789	-0.232371
C	1.856533	1.668410	-1.946177	H	6.962816	-2.048896	-0.799663
H	-0.069308	0.993702	-2.591853	H	7.483008	2.069865	0.355044
C	3.062533	0.180377	-0.441382	H	5.518017	3.494305	0.835252
C	2.993008	1.410454	-1.164868	H	8.450081	-0.119664	-0.306468
H	1.795326	2.600064	-2.505273				
C	4.222113	-0.102618	0.347611				
C	4.323715	-1.335550	1.062071				
C	5.292324	0.844636	0.423564				
C	5.181395	2.075279	-0.311811				
H	5.999027	2.790793	-0.249757				
C	3.244268	-2.275748	0.950572				
H	3.329293	-3.225471	1.475337				
C	4.083924	2.342442	-1.073012				
H	4.011382	3.275078	-1.629304				
C	2.137100	-2.003523	0.204293				
H	1.349479	-2.746433	0.135691				
C	5.469733	-1.593804	1.833728				
H	5.541815	-2.534667	2.375720				
C	6.418763	0.544507	1.208988				

H	7.230300	1.267248	1.266120
C	6.503877	-0.660861	1.906053
H	7.383838	-0.875181	2.508205

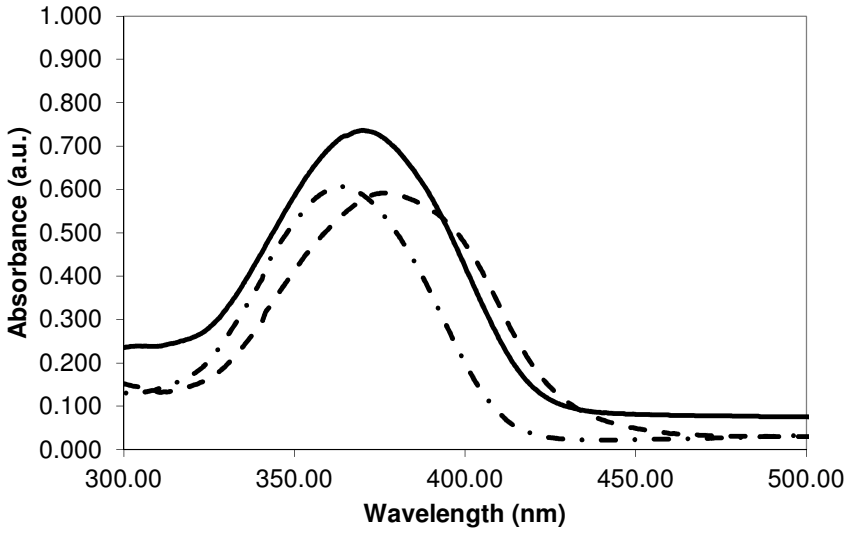

Figure A14 Uv-vis spectra of **3.2** (dash dot), **3.3a** (dash) and **3.3b** (solid) in methanol.

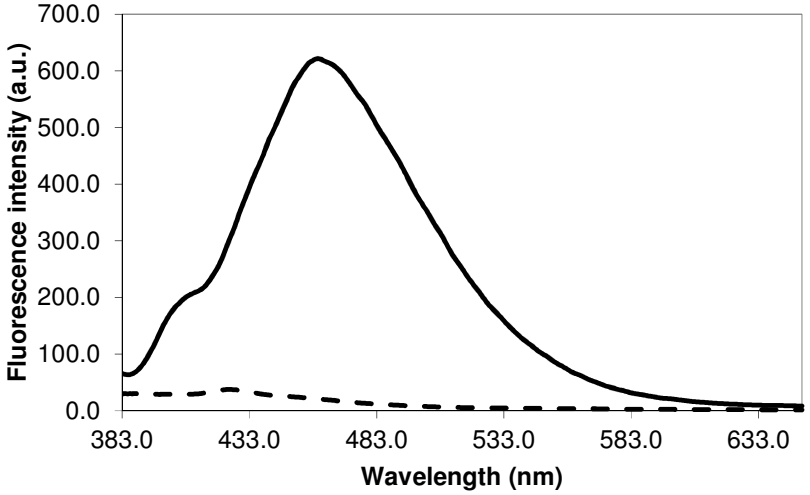

Figure A15 Fluorescence spectra of **3.2** (solid) and **3.3a** (dash) in methanol.

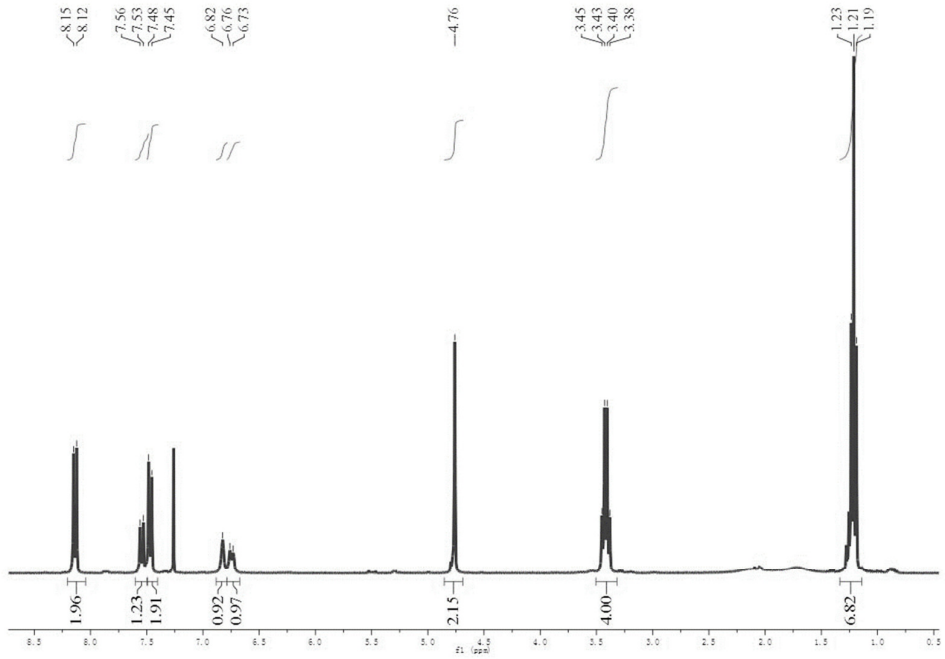

Figure A16 ^{1}H NMR spectrum of (4-(6-(diethylamino)benzoxazol-2-yl)phenyl)methanol, **3.2**

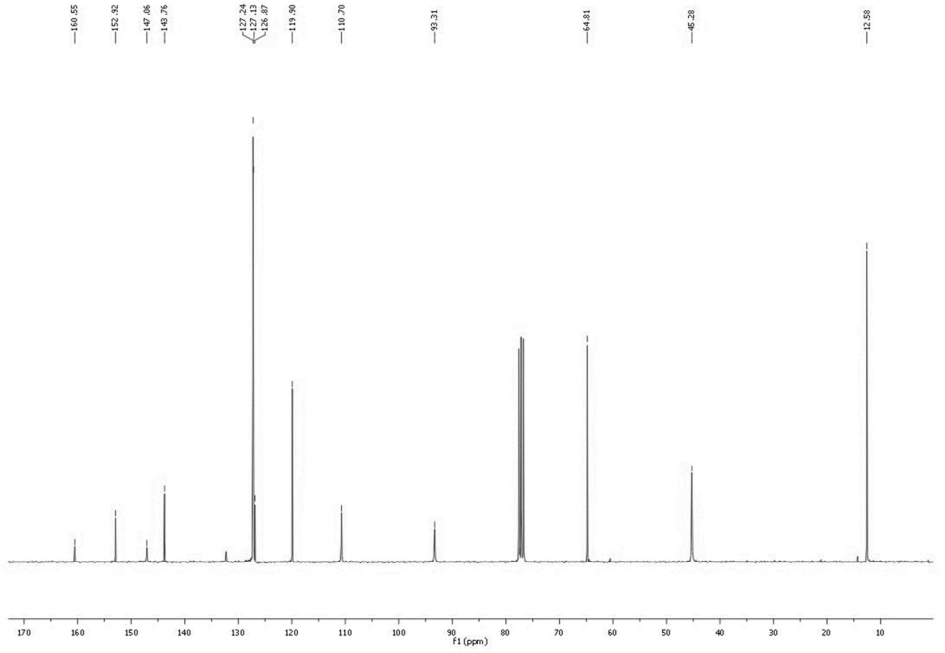

Figure A17 ^{13}C NMR spectrum of (4-(6-(diethylamino)benzoxazol-2-yl)phenyl)methanol, **3.2**

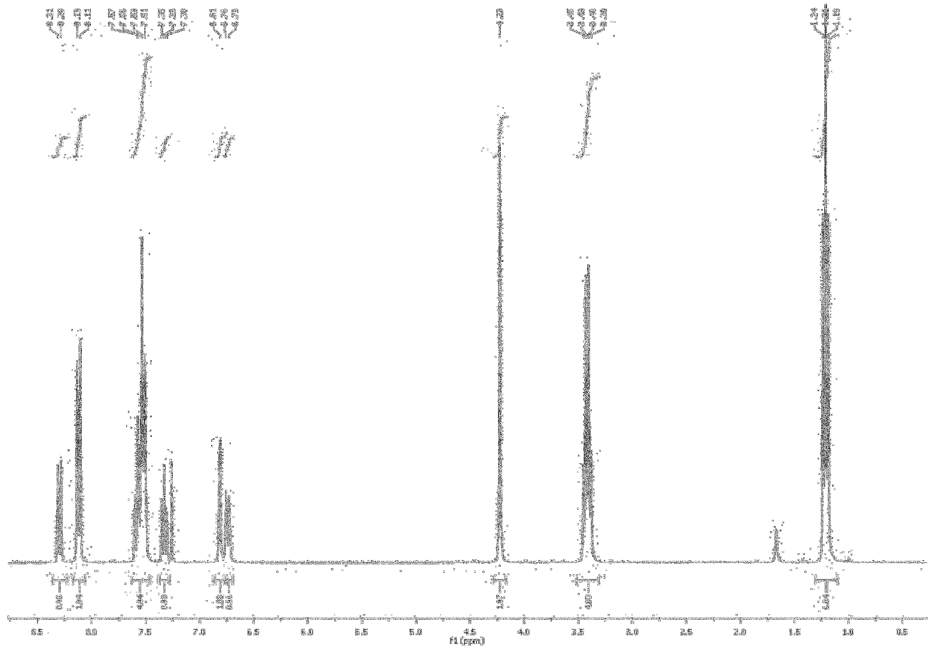

Figure A18 ^{1}H NMR spectrum of N,N-diethyl-2-(4-((2-nitrophenylselanyl)methyl)phenyl)benzoxazol-6-amine, **3.3a**

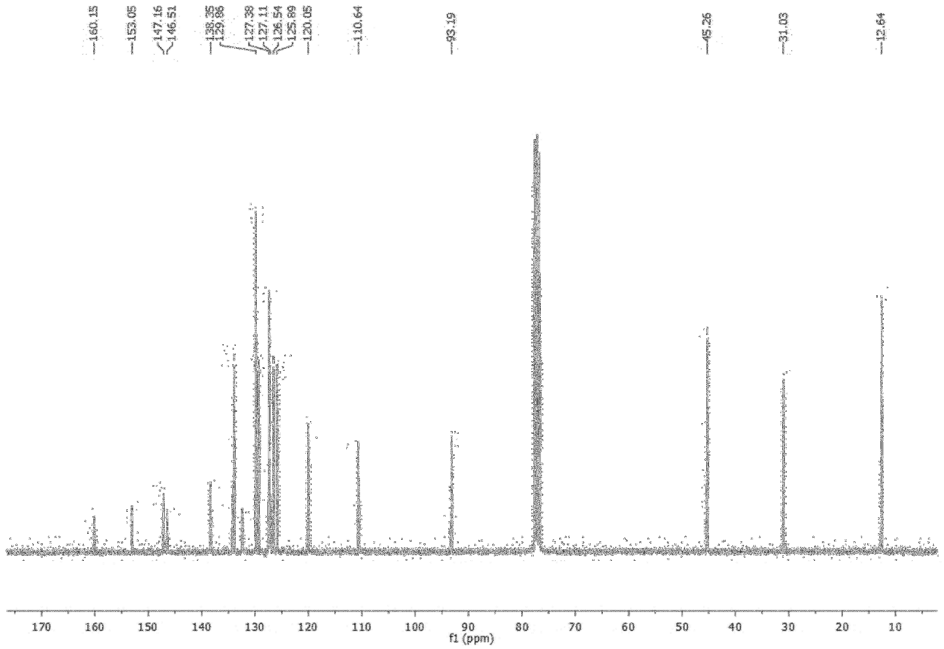

Figure A19 ^{13}C NMR spectrum of N,N-diethyl-2-(4-((2-nitrophenylselanyl)methyl)phenyl)benzoxazol-6-amine, **3.3a**

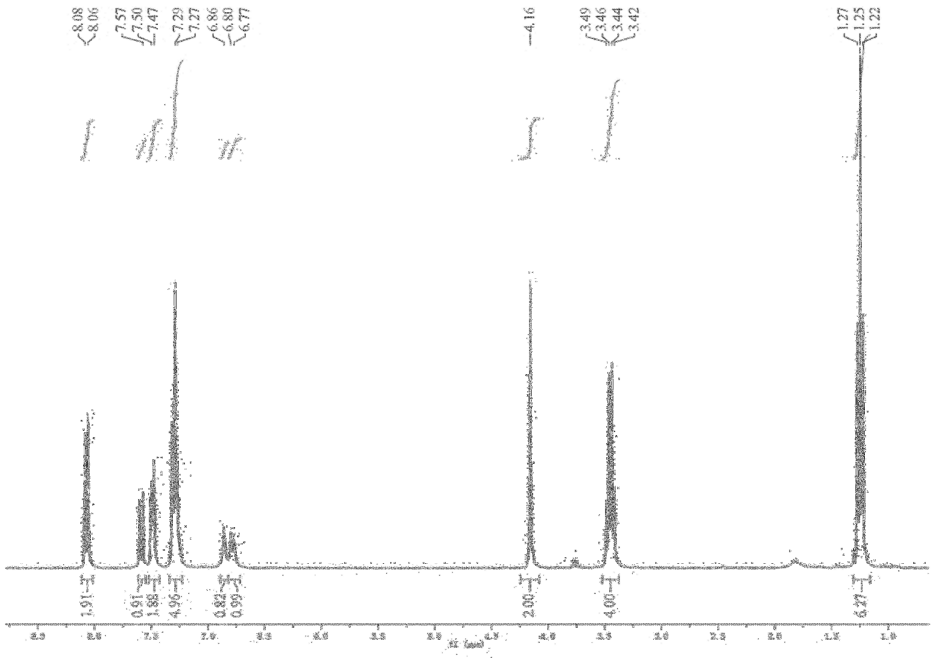

Figure A20 ^{1}H NMR spectrum of N,N-diethyl-2-(4-(phenylselanylmethyl) phenyl)benzoxazol-6-amine, **3.3b**

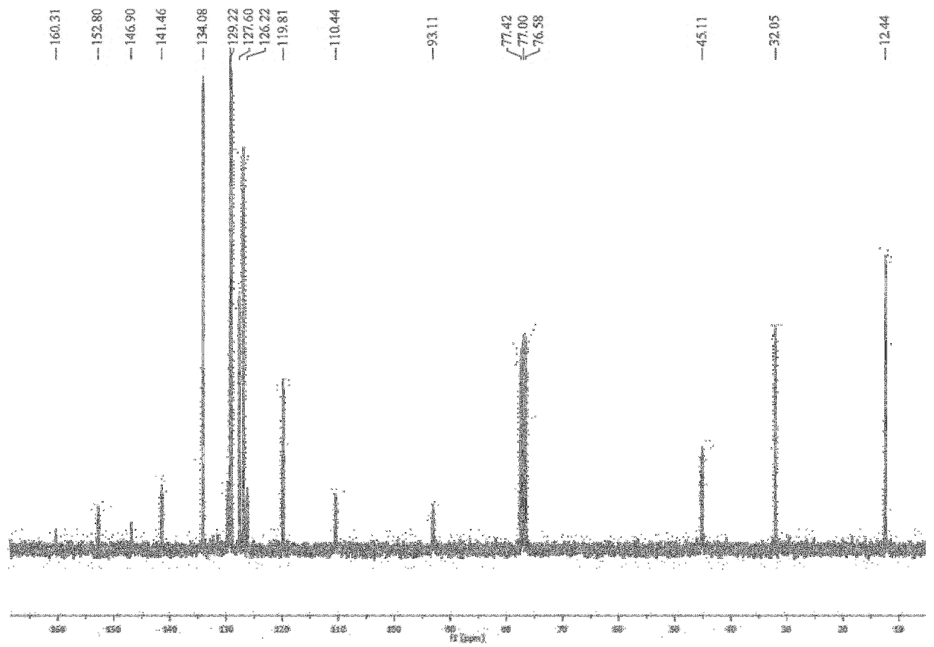

Figure A21 ^{13}C NMR spectrum of N,N-diethyl-2-(4-(phenylselanylmethyl) phenyl)benzoxazol-6-amine, **3.3b**

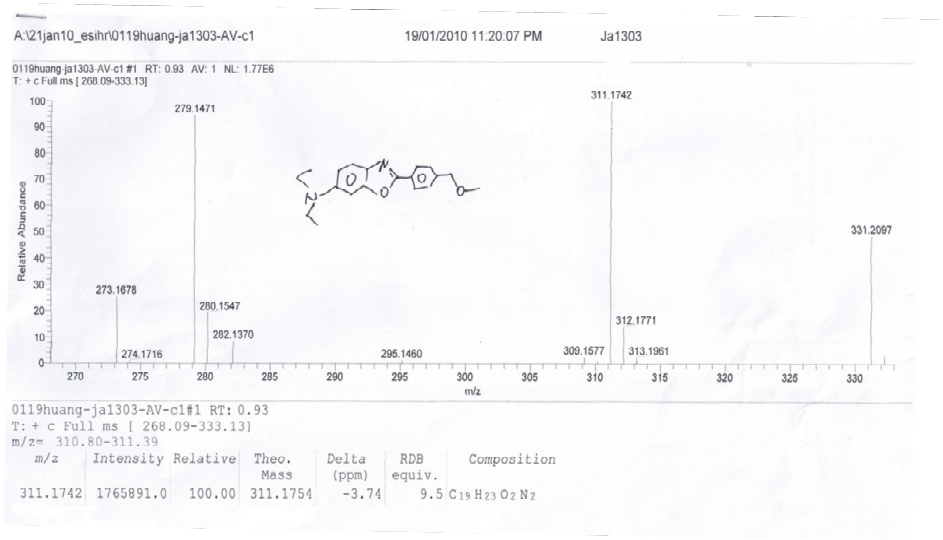

Figure A22 The HRMS spectrum of compound **3.4**

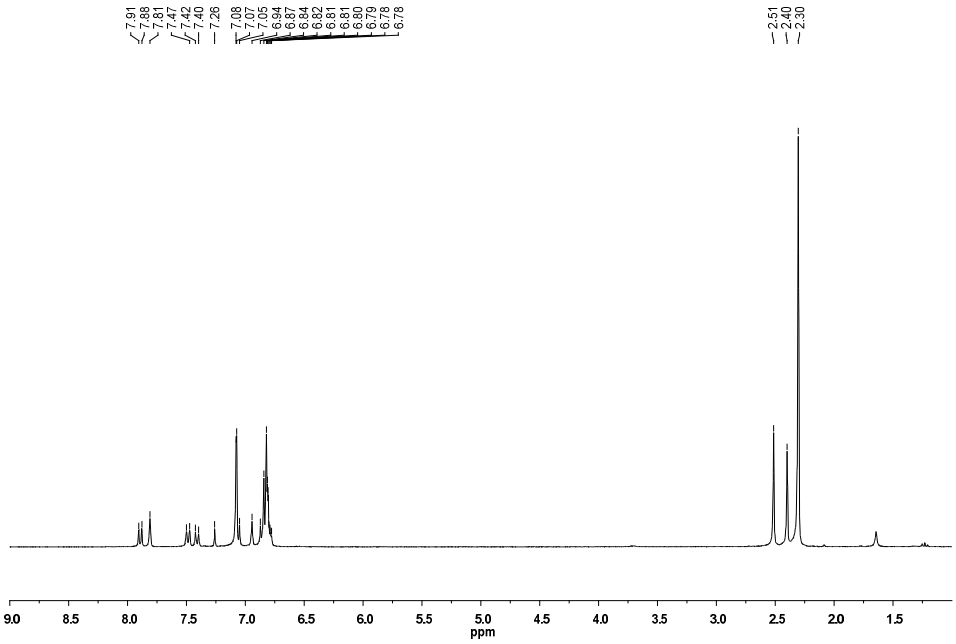

Figure A23 ^{1}H NMR of 4(5)-methylfluorescein diacetate, **3.7**

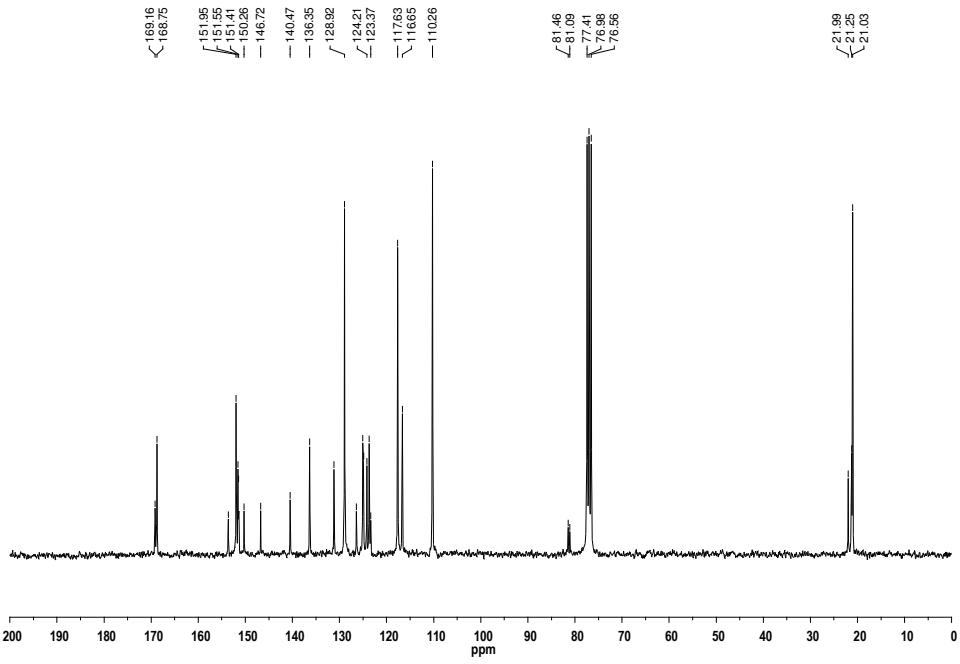

Figure A24 ^{13}C NMR of 4(5)-methylfluorescein diacetate, **3.7**

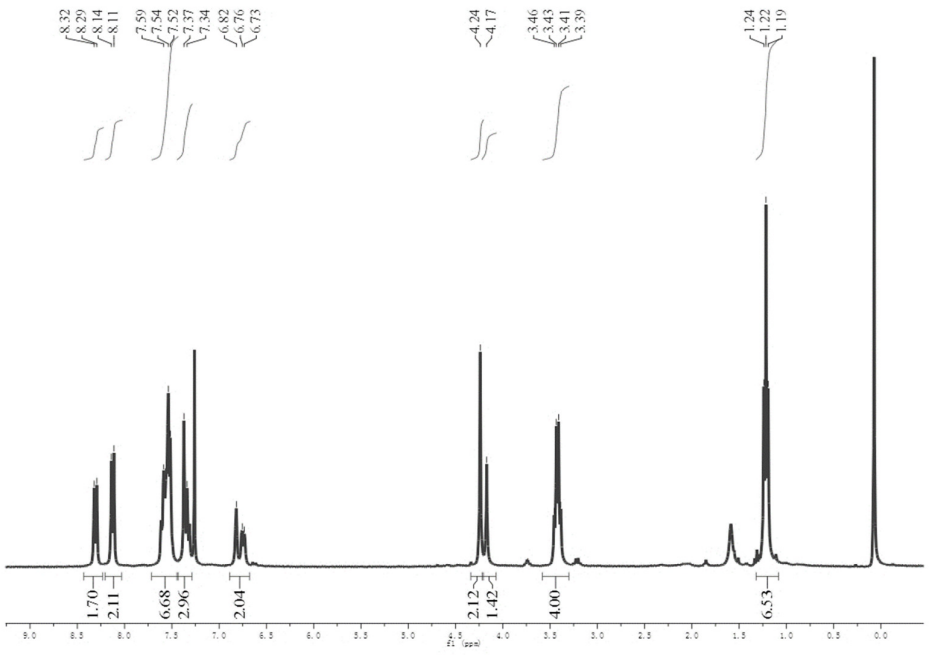

Figure A25 ^{1}H NMR spectrum of 2-(4-(bromomethyl)benzyloxy)-9-(diethylamino)-5H-benzo[a]phenoxazin-5-one, **3.11**

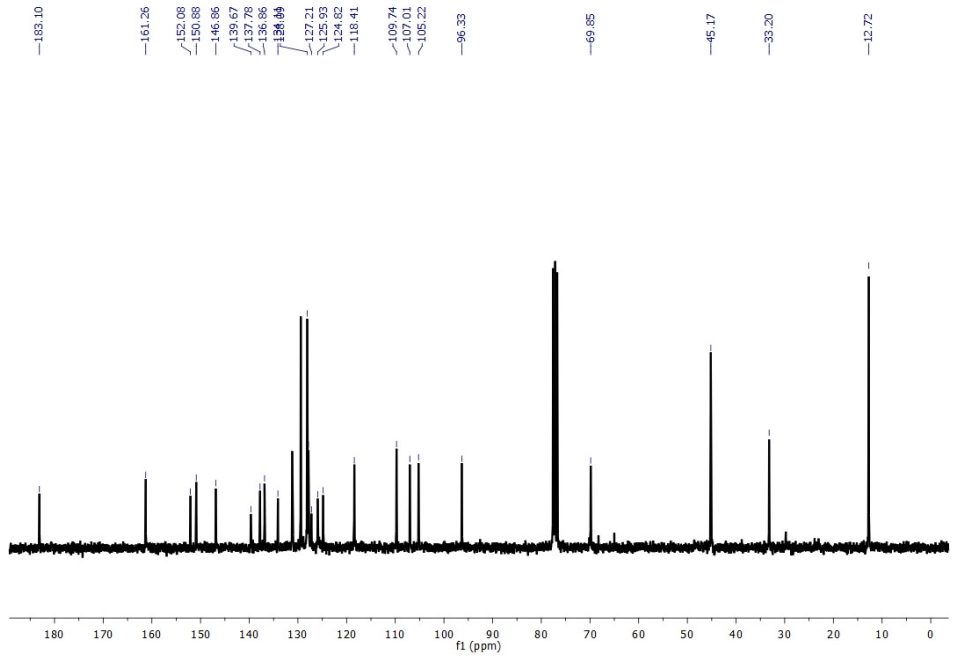

Figure A26 ^{13}C NMR spectrum of 2-(4-(bromomethyl)benzyloxy)-9-(diethylamino)-5H-benzo[a]phenoxazin-5-one**, 3.11**

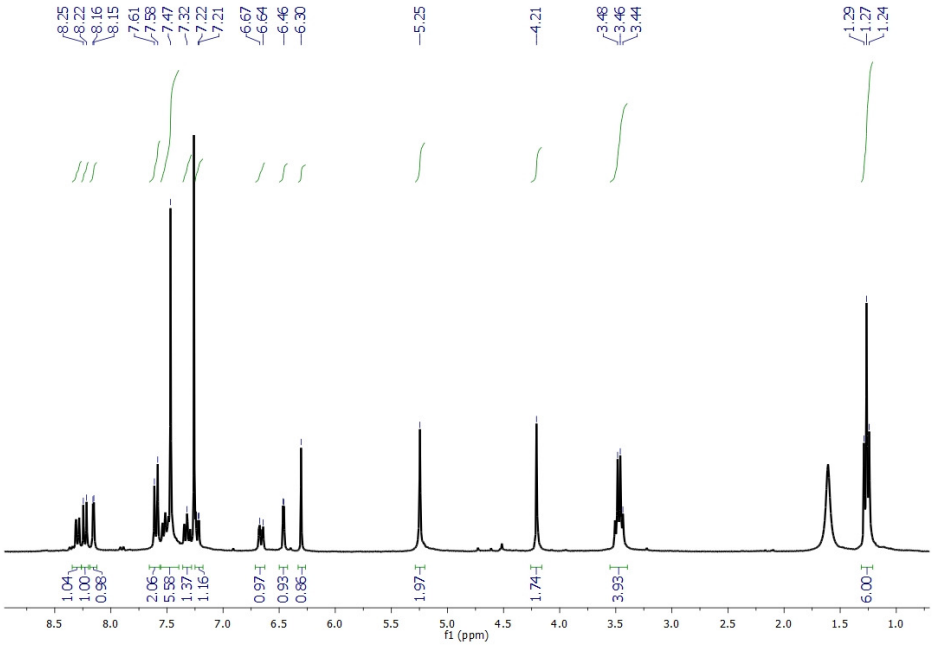

Figure A27 ^{1}H NMR spectrum of 2-(4-((2-nitrophenylselanyl)methyl) benzyloxy)-9-(diethylamino)-5H-benzo[a]phenoxazin-5-one, **3.12**

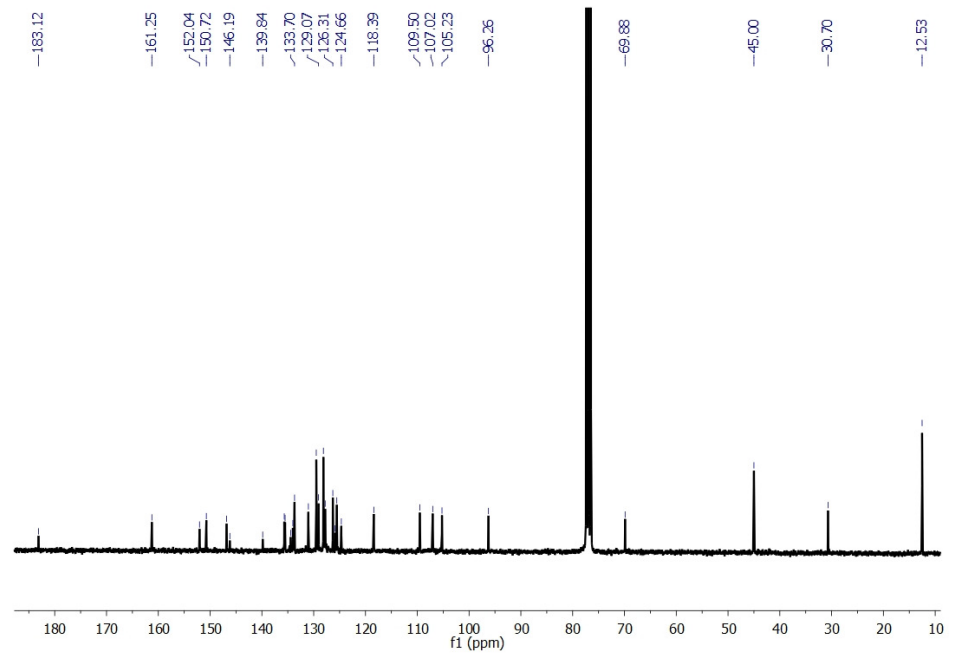

Figure A28 ^{13}C NMR spectrum of 2-(4-((2-nitrophenylselanyl)methyl) benzyloxy)-9-(diethylamino)-5H-benzo[a]phenoxazin-5-one, **3.12**

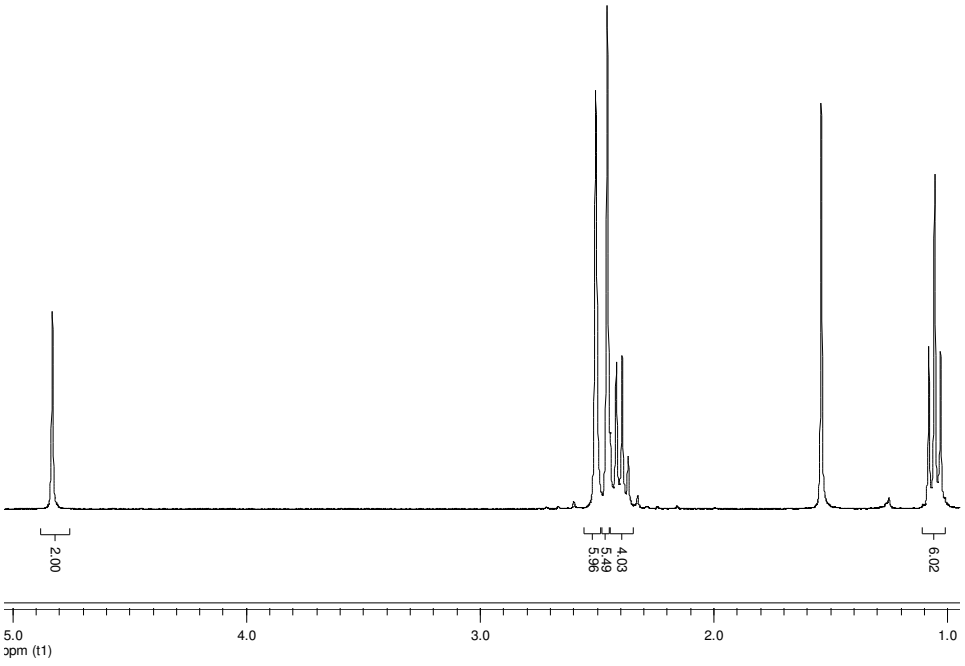

Figure A29 ^{1}H NMR spectrum of 8-chloromethyl-1, 3, 5, 7- tetramethyl- 2, 6-diethyl- 4, 4-difluoro-4-bora-3a, 4a-diaza-sindacene**, 3.14**

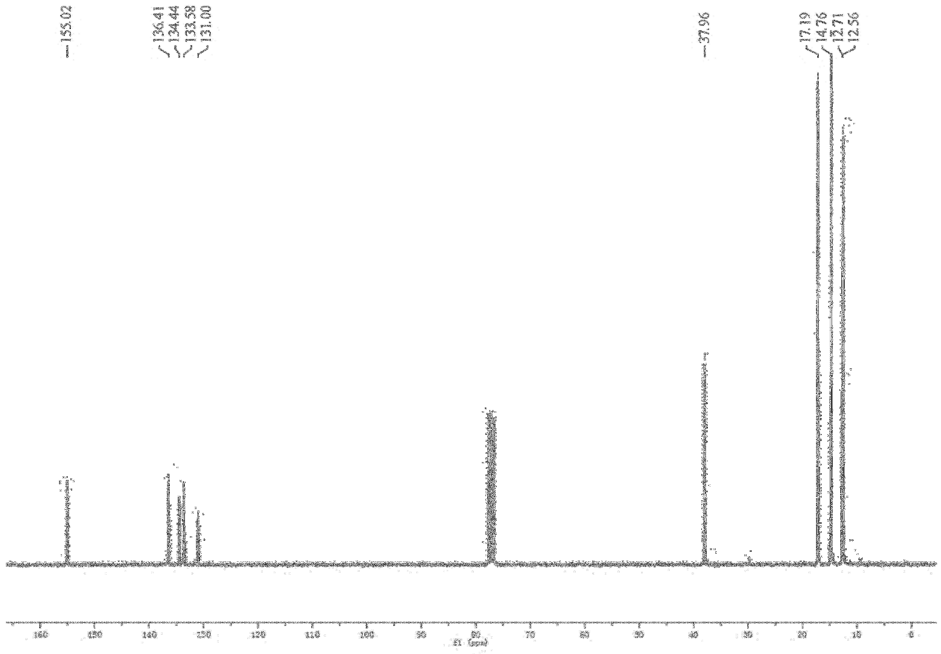

Figure A30 ^{13}C NMR spectrum of 8-chloromethyl-1, 3, 5, 7- tetramethyl- 2, 6- diethyl- 4, 4-difluoro-4-bora-3a, 4a-diaza-sindacene**, 3.14**

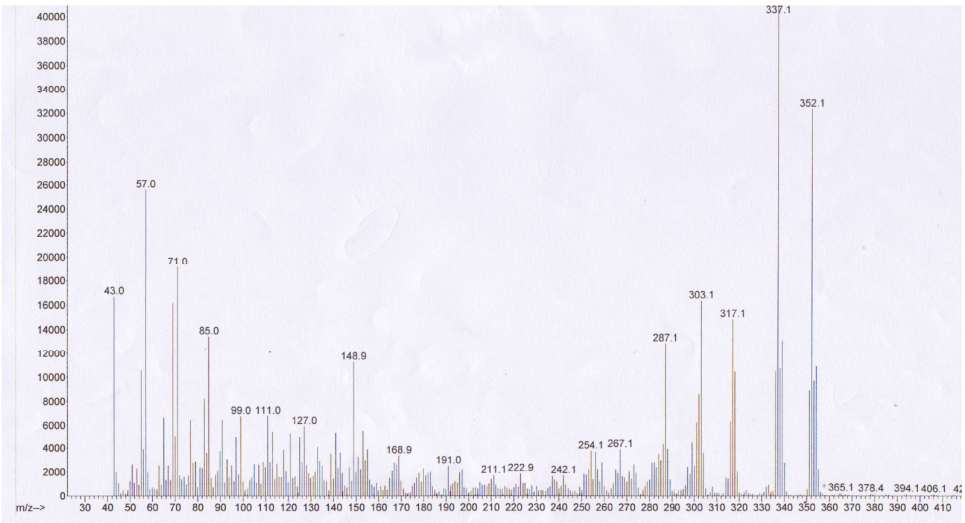

Figure A31 EIMS spectrum of 8-chloromethyl-1, 3, 5, 7- tetramethyl- 2, 6-diethyl- 4, 4-difluoro-4-bora-3a, 4a-diaza-sindacene**, 3.14**

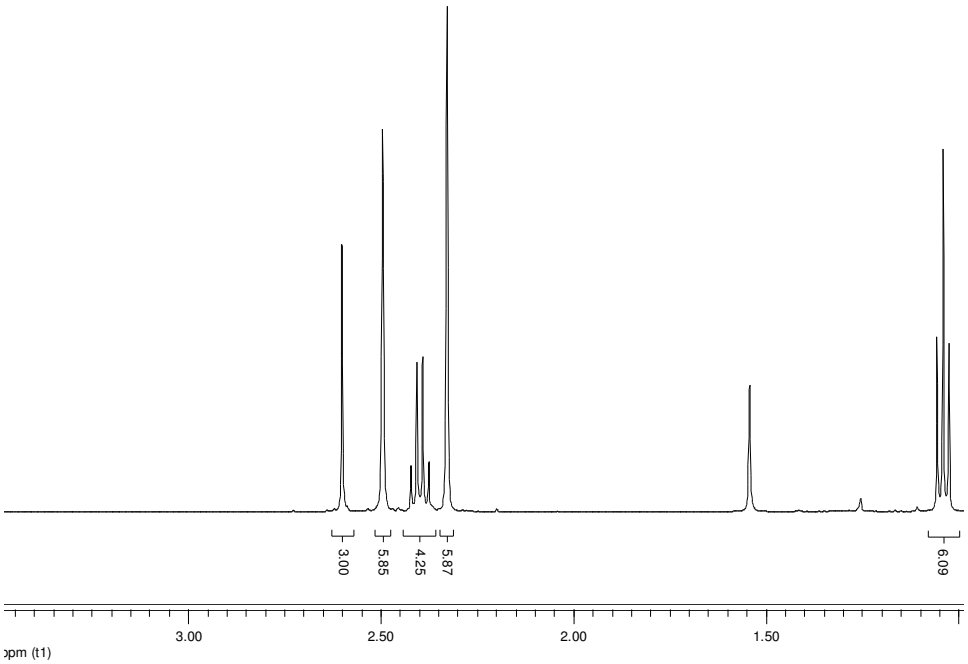

Figure A32 ^{1}H NMR spectrum of 8-methyl-1, 3, 5, 7- tetramethyl- 2, 6-diethyl- 4, 4-difluoro-4-bora-3a, 4a-diaza-sindacene**, 3.15**

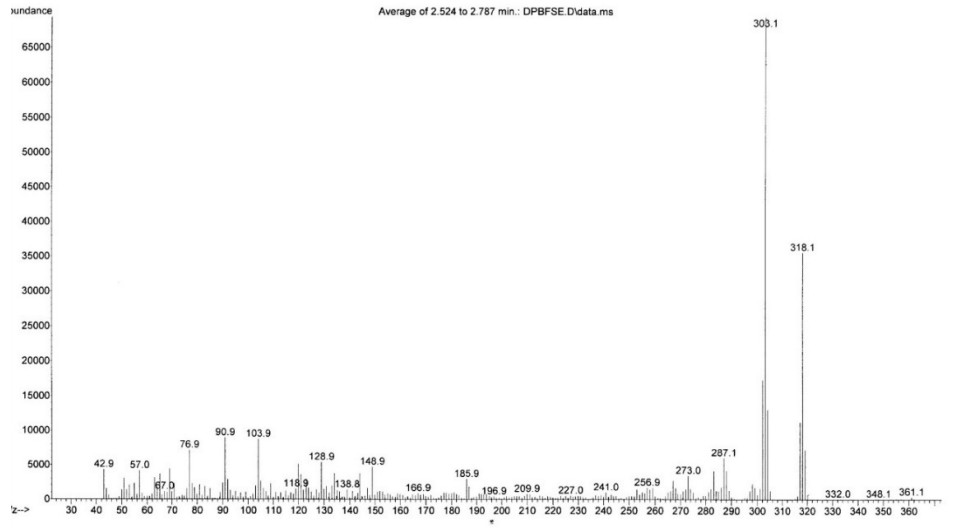

Figure A33 EIMS spectrum of 8-methyl-1, 3, 5, 7- tetramethyl- 2, 6- diethyl- 4, 4-difluoro-4-bora-3a, 4a-diaza-sindacene**, 3.15**

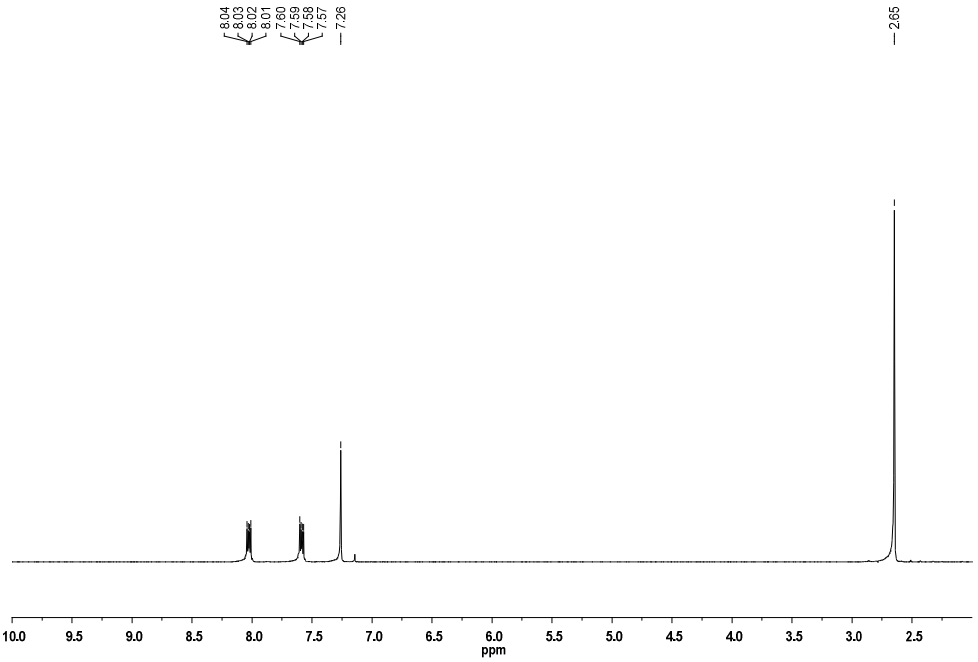

Figure A34 ^{1}H-NMR 1,4-dimethylanthraquinone, **4.3**

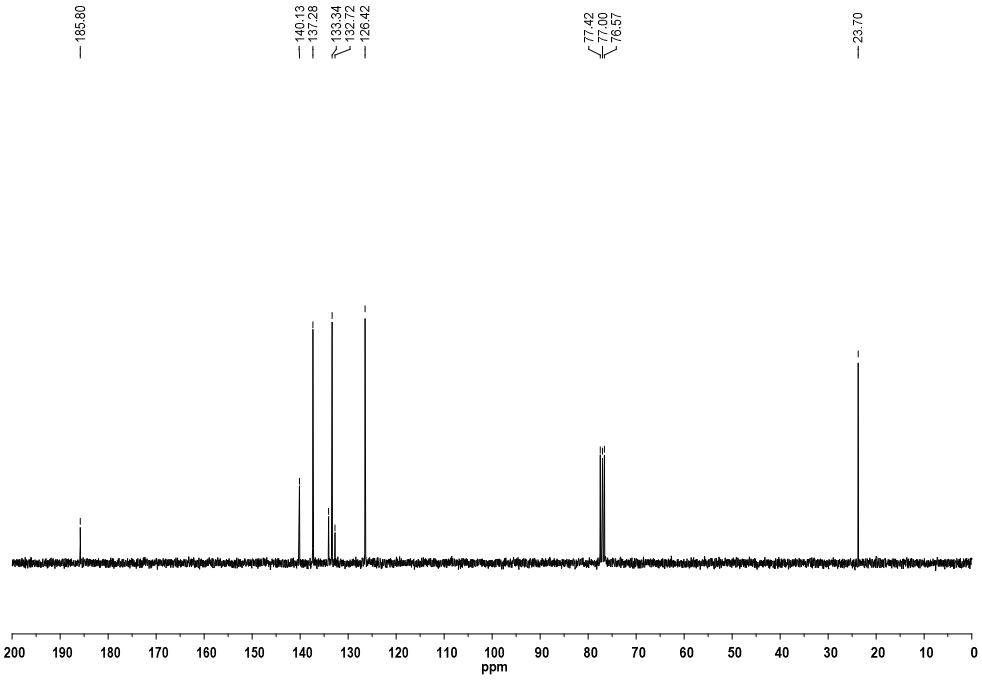

Figure A35 ^{13}C-NMR 1,4-dimethylanthraquinone, **4.3**

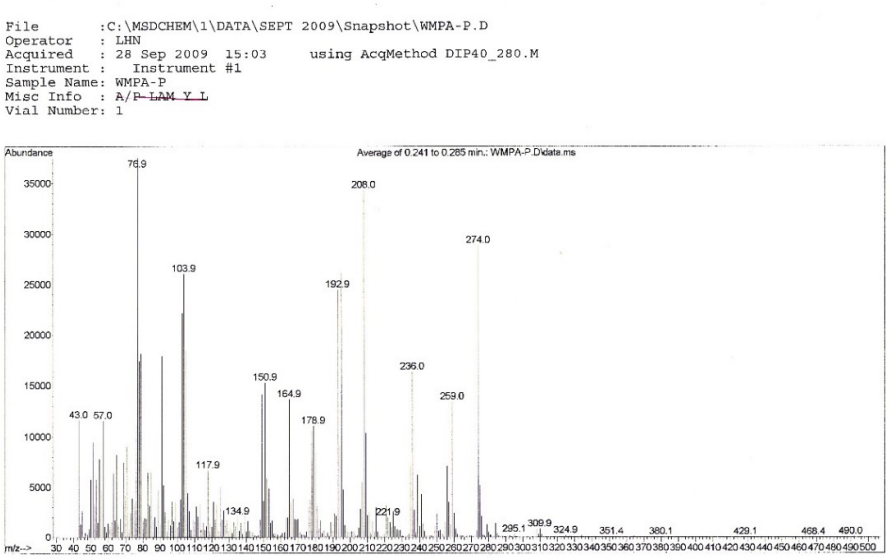

Figure A36 FAB-MS of 1,4-dimethylanthraquinone, **4.3**

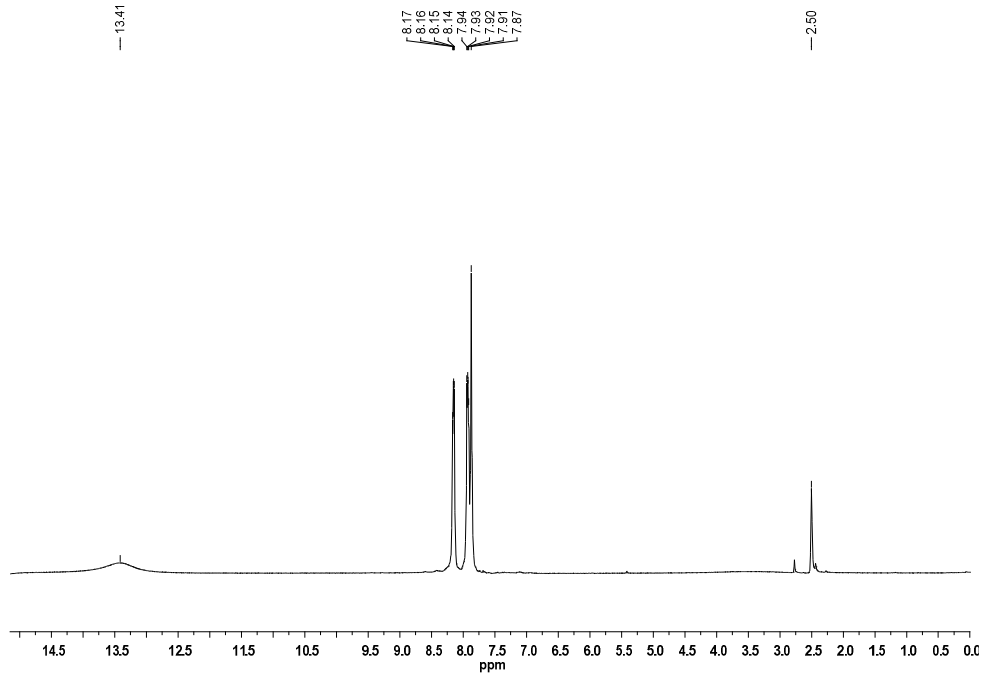

Figure A37 ^{1}H-NMR of 9,10-dioxo-9,10-dihydroanthracene-1,4-dicarboxylic acid, **4.4**

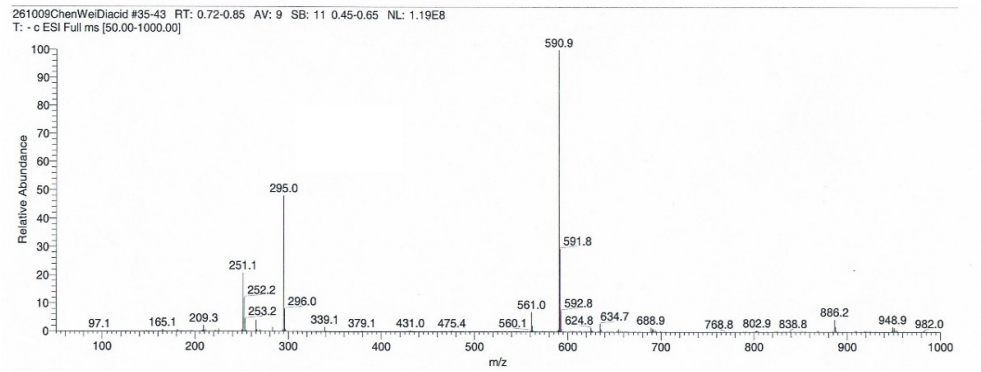

Figure A38 ESI-MS (negative mode) of 9,10-dioxo-9,10-dihydroanthracene-1,4-dicarboxylic acid, **4.4**

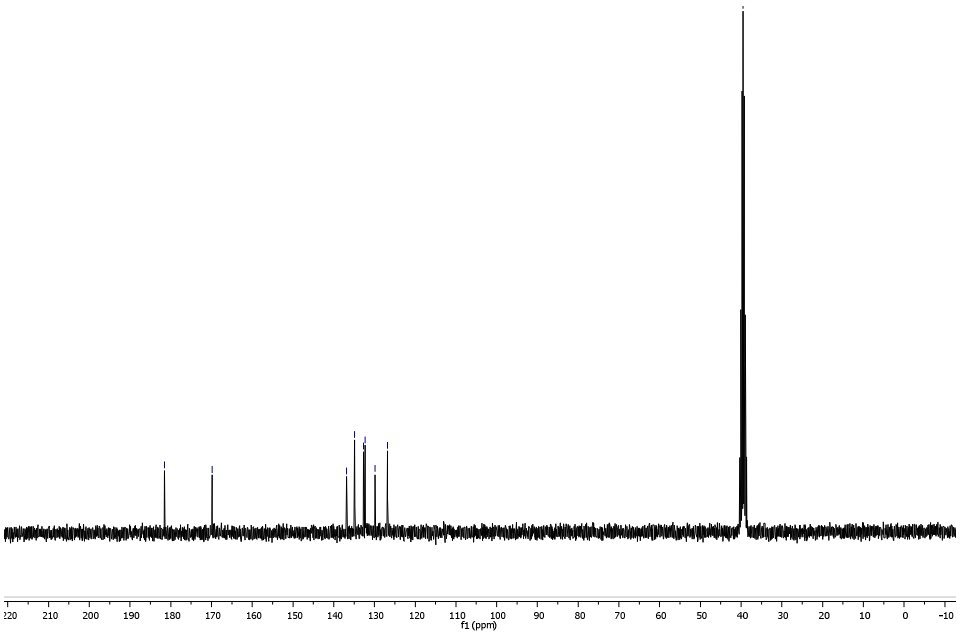

Figure A39 ^{13}C-NMR of 9,10-dioxo-9,10-dihydroanthracene-1,4-dicarboxylic acid, **4.4**

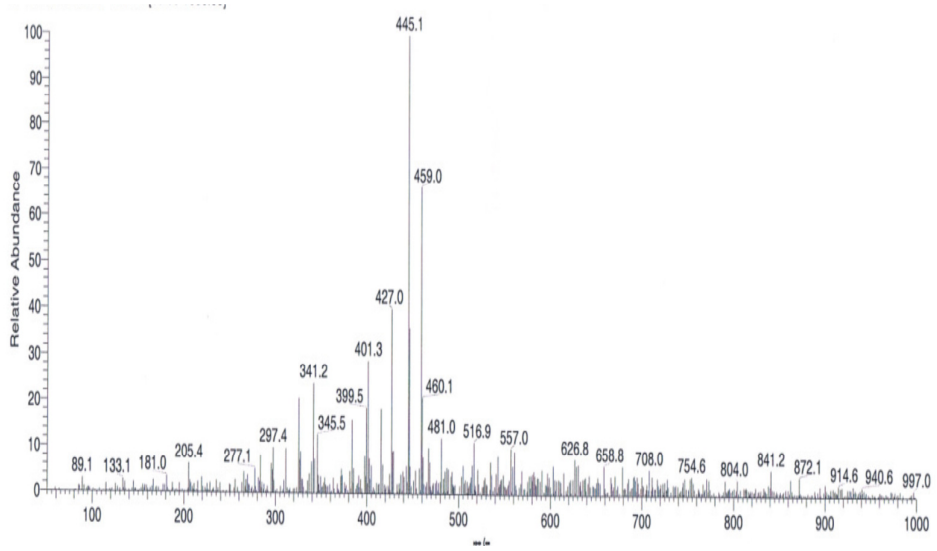

Figure A40 ESI-MS (negative mode) of 9,10-di-*p*-tolylanthracene-1,4-dicarboxylic acid, **4.6**

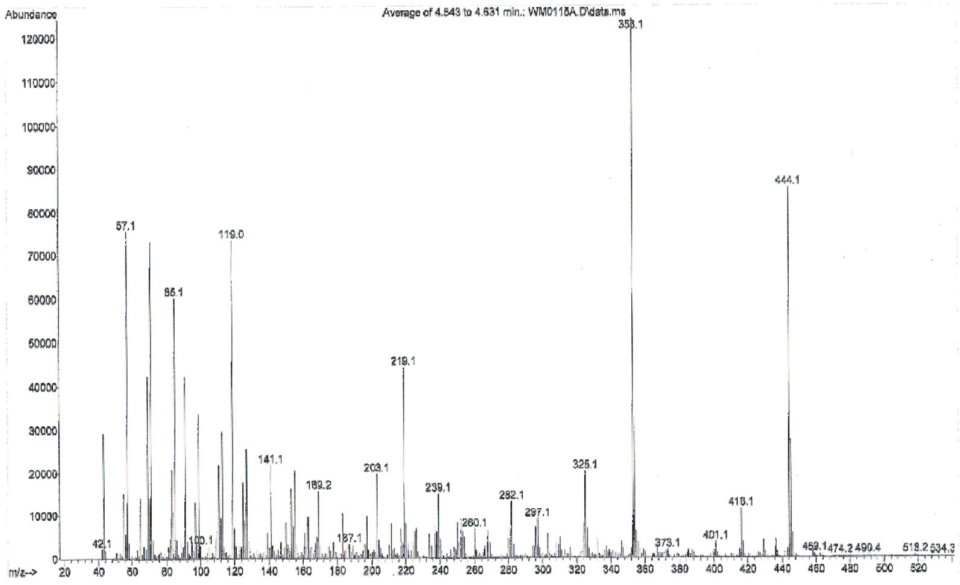

Figure A41 EI-MS of 9, 10-dihydroxy-9,10-di-*p*-tolylanthracene, **4.10**

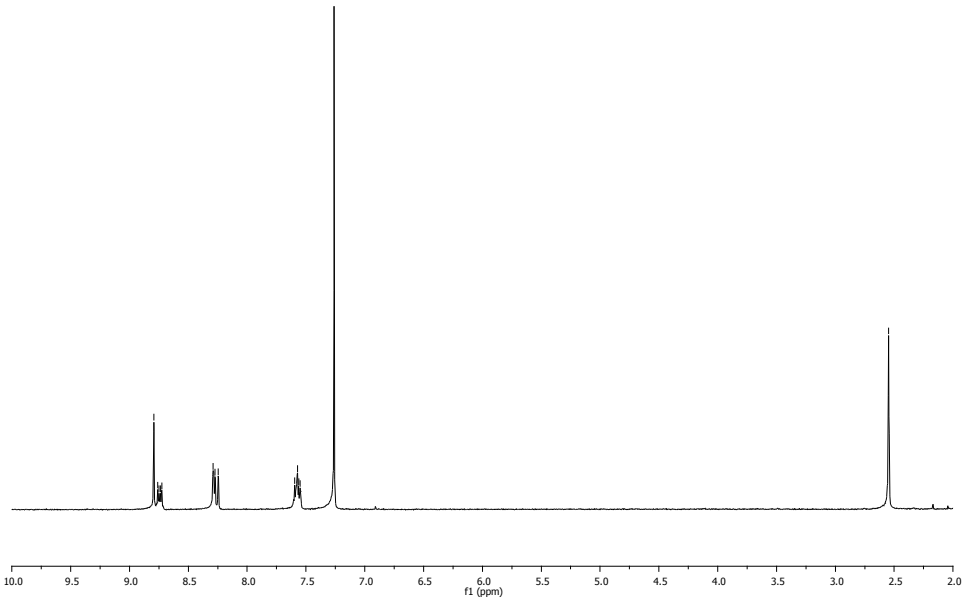

Figure A42 ^{1}H-NMR of HOCD, **4.7**

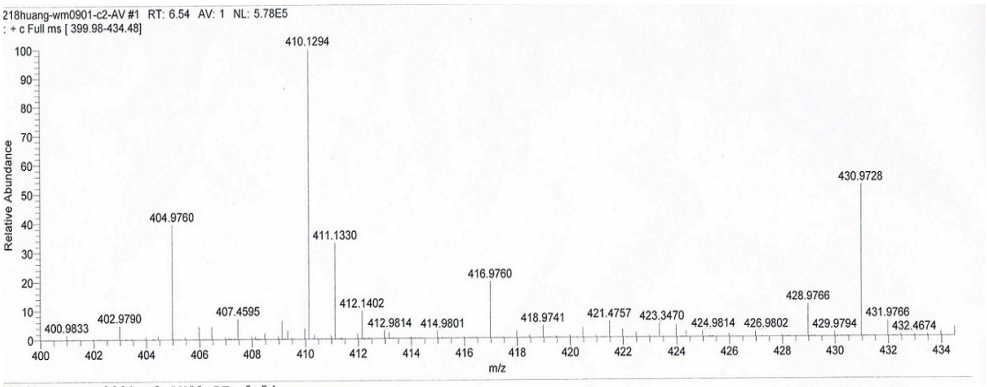

Figure A43 HREIMS of HOCD, **4.7**

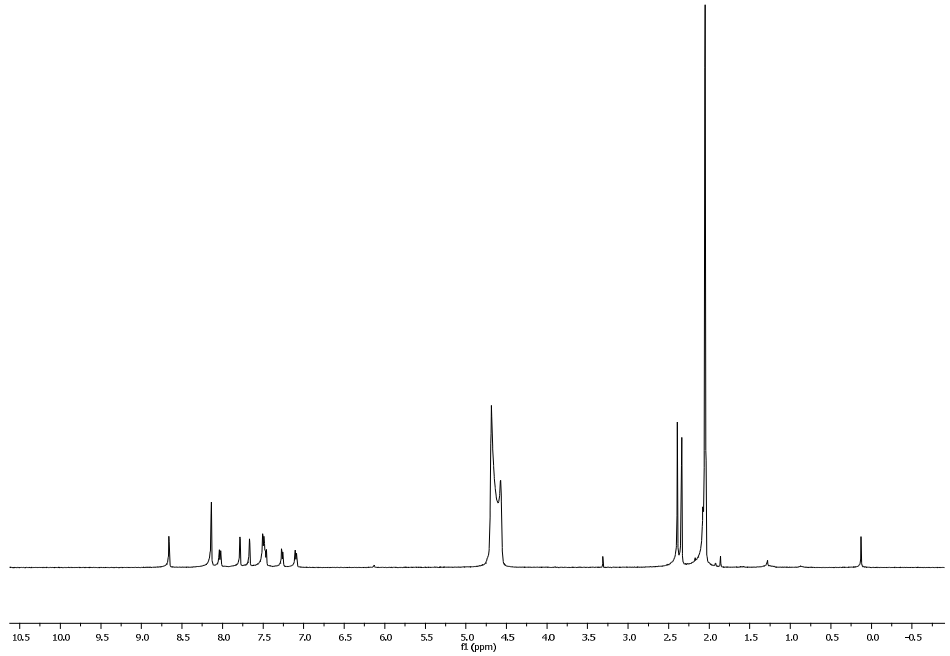

Figure A44 [1]H-NMR of 3,10-dimethyl-5,8-dioxo-5,8-dihydronaphtho[1,2,3,4-rst]pentaphene sulfonic acid, **4.11a**

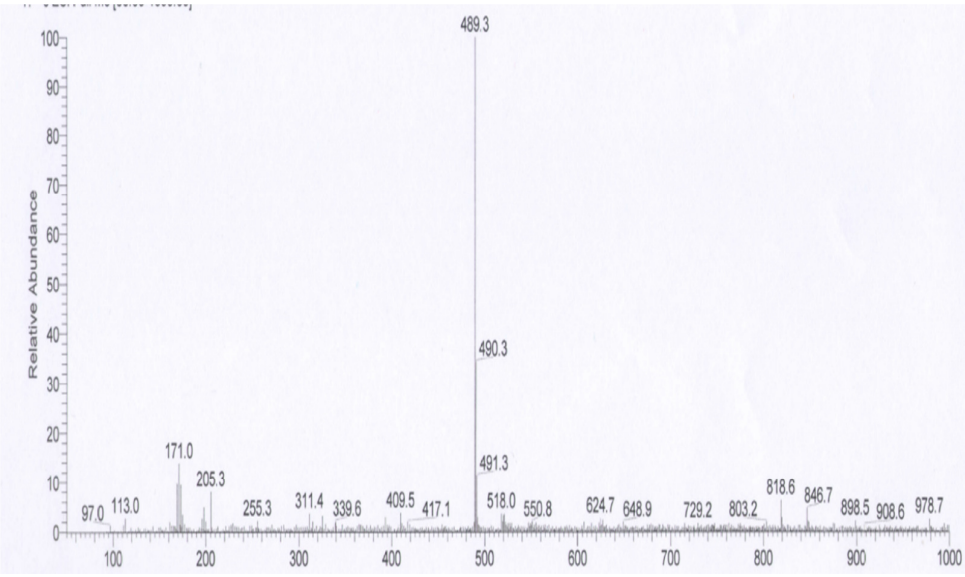

Figure A45 ESI-MS (negative mode) of 3,10-dimethyl-5,8-dioxo-5,8-dihydronaphtho[1,2,3,4-rst]pentaphene sulfonic acid, **4.11a**

Meas. m/z	#	Formula	m/z	err [ppm]	rdb	e⁻ Conf	z
489.0820	1	C 30 H 17 O 5 S	489.0802	-3.7	22.5	even	1-
	2	C 27 H 21 O 5 S 2	489.0836	3.2	17.5	even	

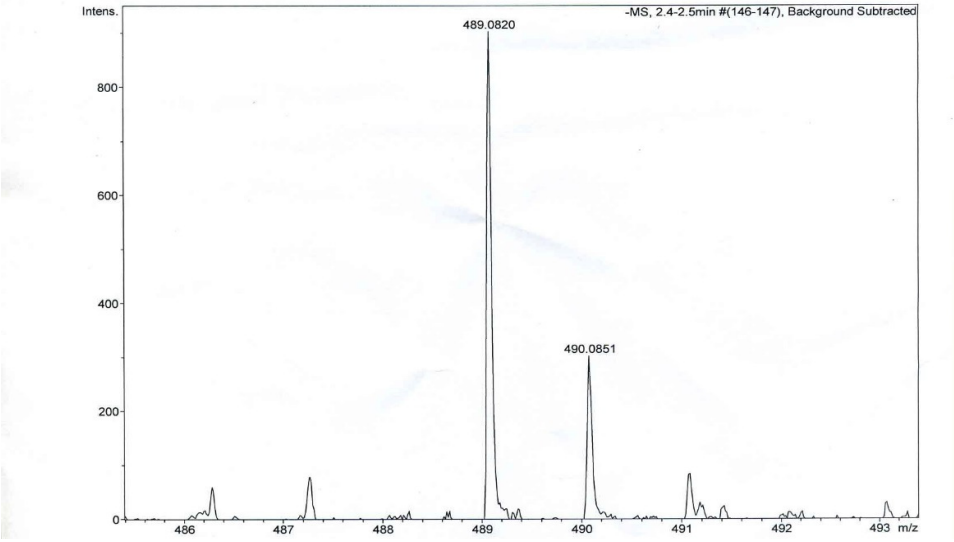

Figure A46 HRESI-MS (negative mode) of **4.11a**

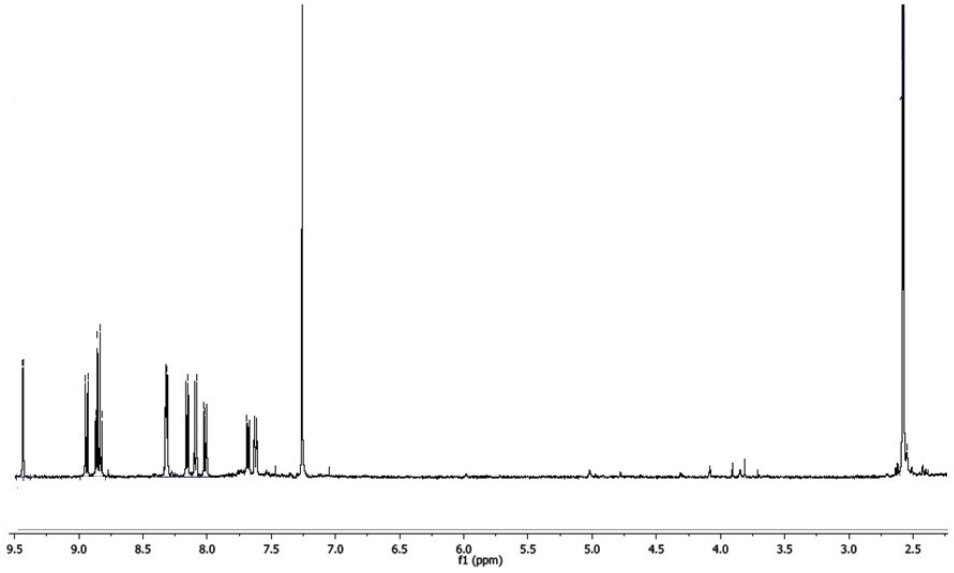

Figure A47 [1]H-NMR of 3,10-dimethyl-5,8-dioxo-5,8-dihydronaphtho[1,2,3,4-rst]pentaphene sulfonic acid, **4.11b**

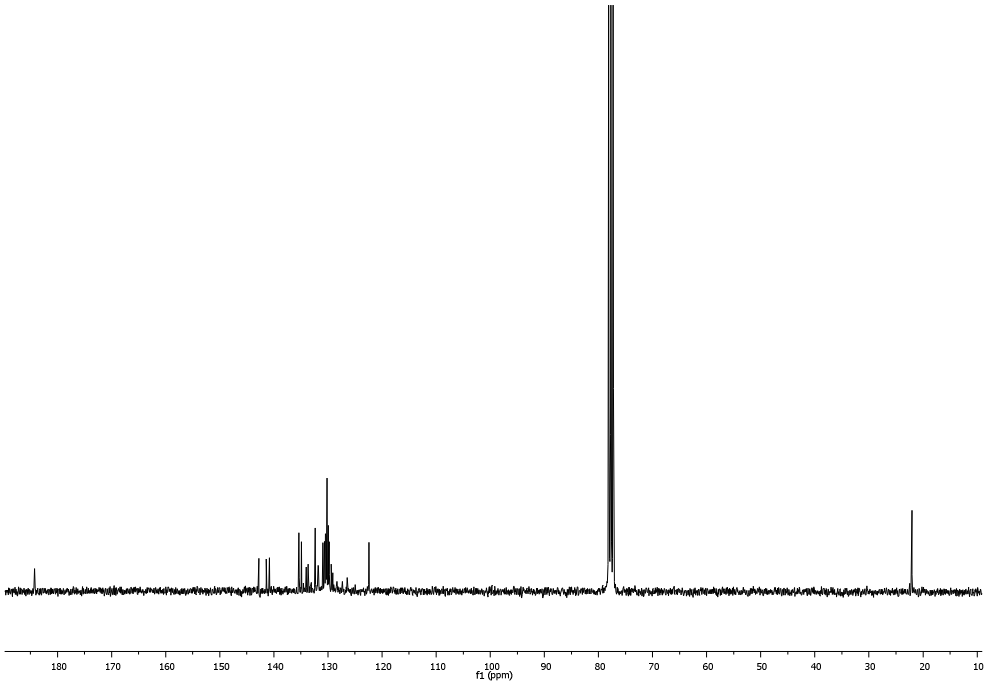

Figure A48 ^{13}C-NMR of 3,10-dimethyl-5,8-dioxo-5,8-dihydronaphtho[1,2,3,4-rst]pentaphene sulfonic acid, **4.11b**

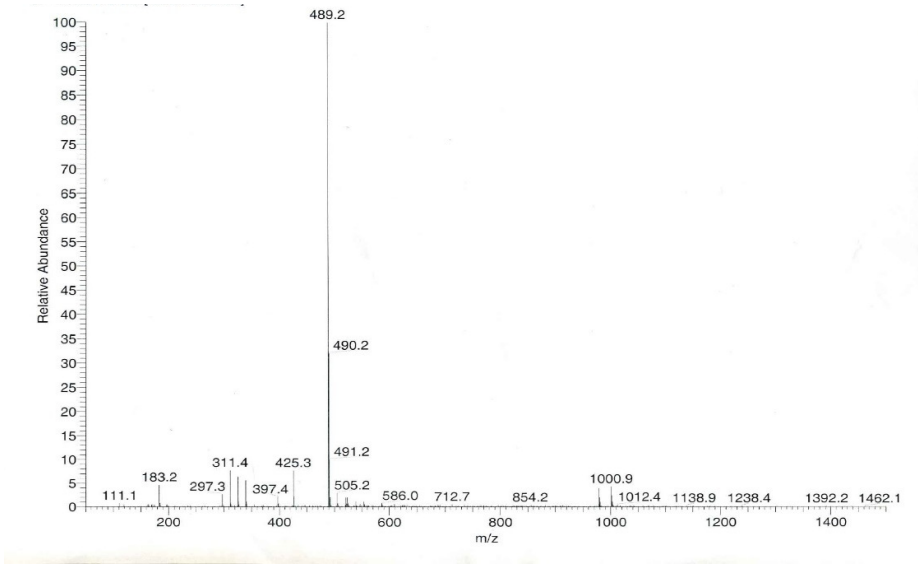

Figure A49 ESI-MS (negative mode) of **4.11b**

Meas. m/z	#	Formula	m/z	err [ppm]	Mean err [ppm]	rdb
489.0795	1	C 30 H 17 O 5 S	489.0802	1.5	2.2	22.5
	2	C 28 H 18 Na O 5 S	489.0778	-3.4	-4.3	19.5
	3	C 26 H 13 N 6 O 3 S	489.0775	-4.0	-4.9	23.5
	4	C 25 H 14 N 4 Na O 6	489.0817	4.5	5.3	20.5
	5	C 23 H 9 N 10 O 4	489.0814	3.9	4.7	24.5

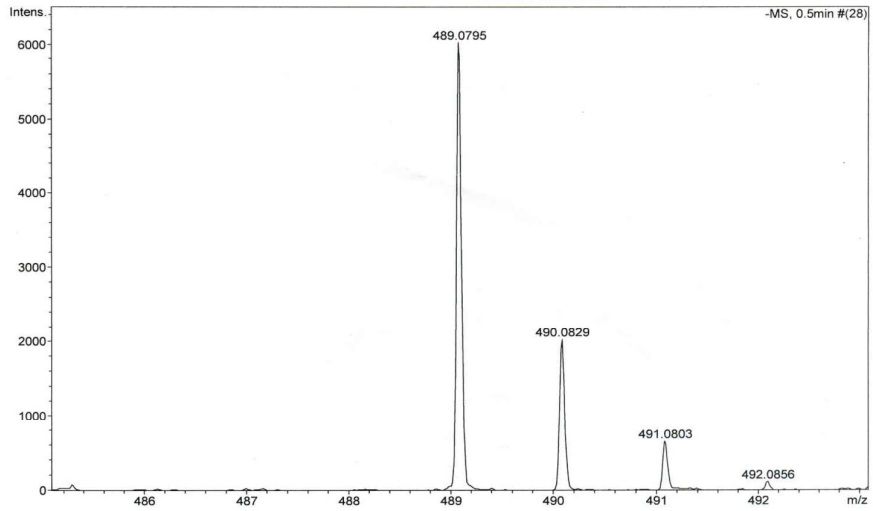

Figure A50 HRESI-MS (negative mode) of **4.11b**

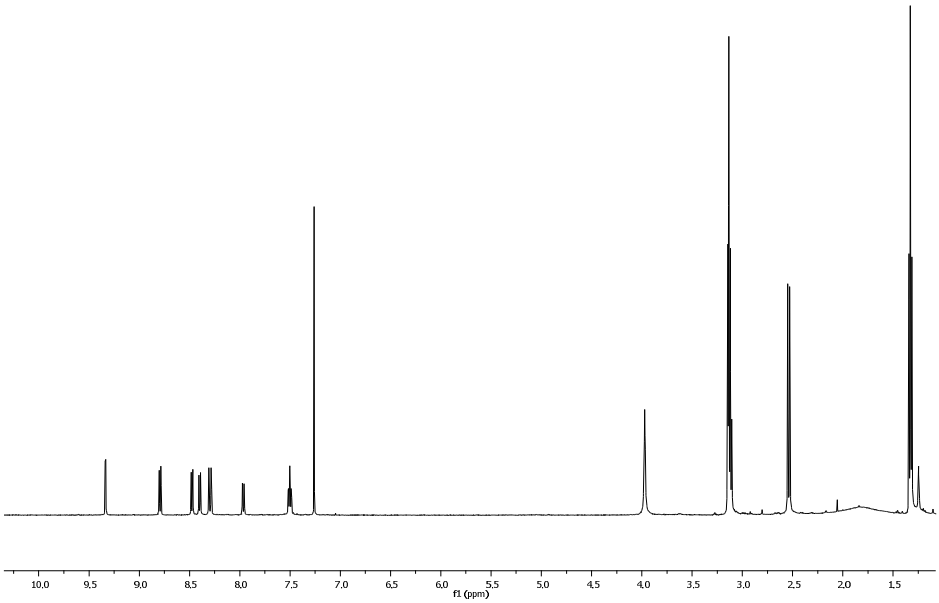

Figure A51 ^{1}H-NMR of **4.16**

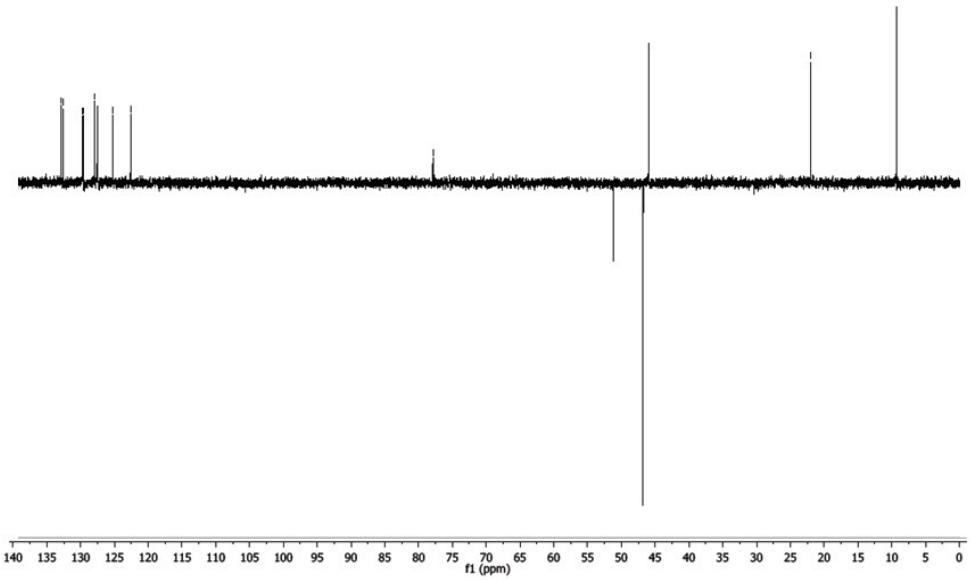

Figure A52 DEPT135-NMR of **4.16**

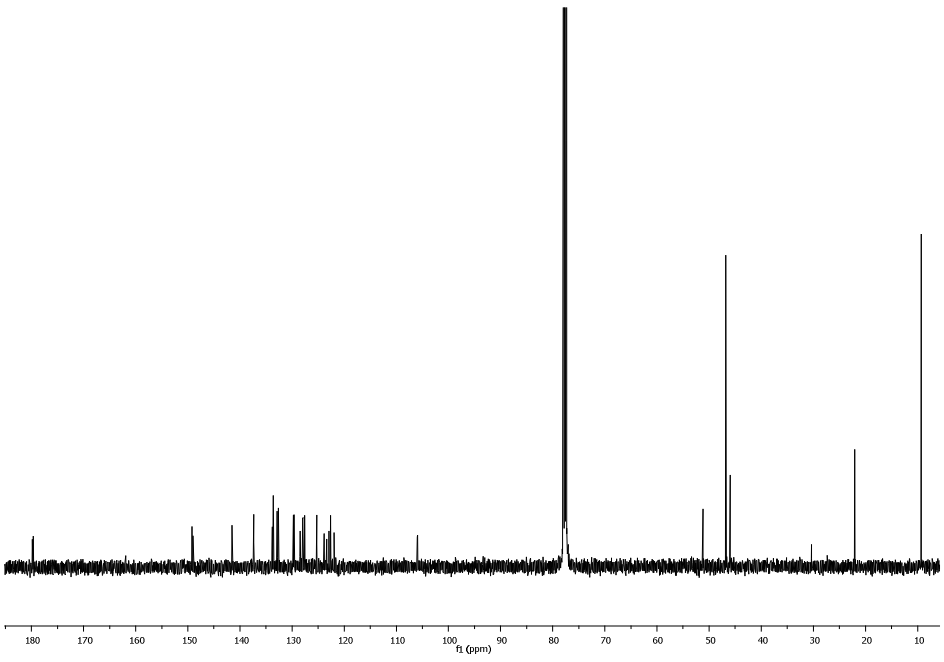

Figure A53 ^{13}C-NMR of **4.16**

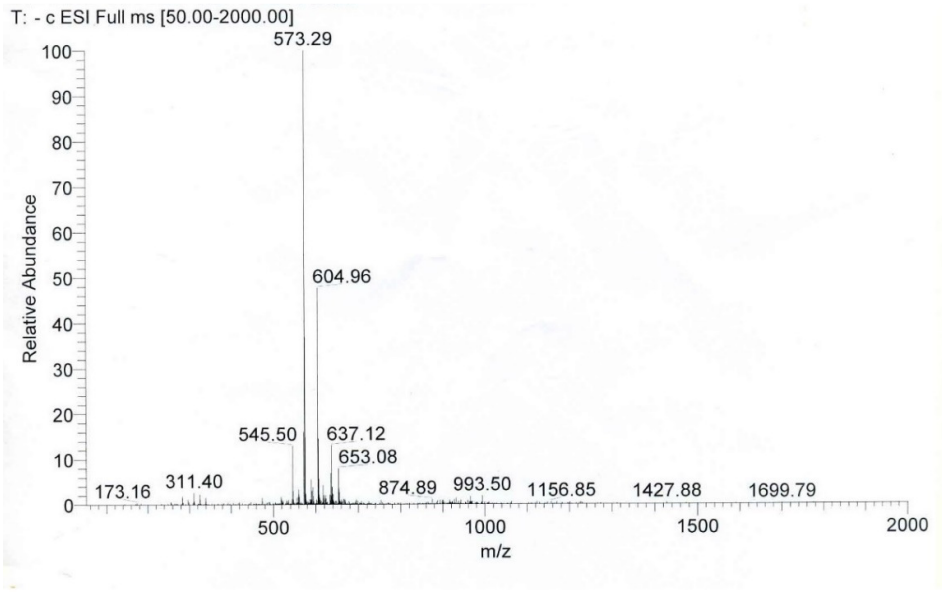

Figure A54 ESI-MS (negative mode) of **4.16**

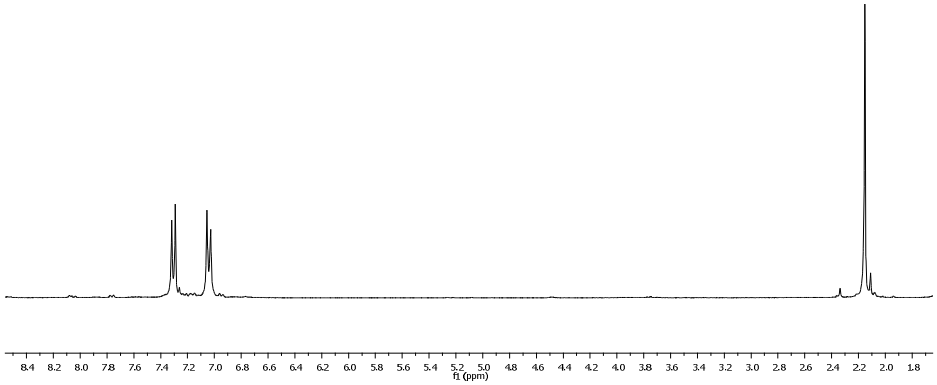

Figure A55 ^{1}H-NMR of **4.17**

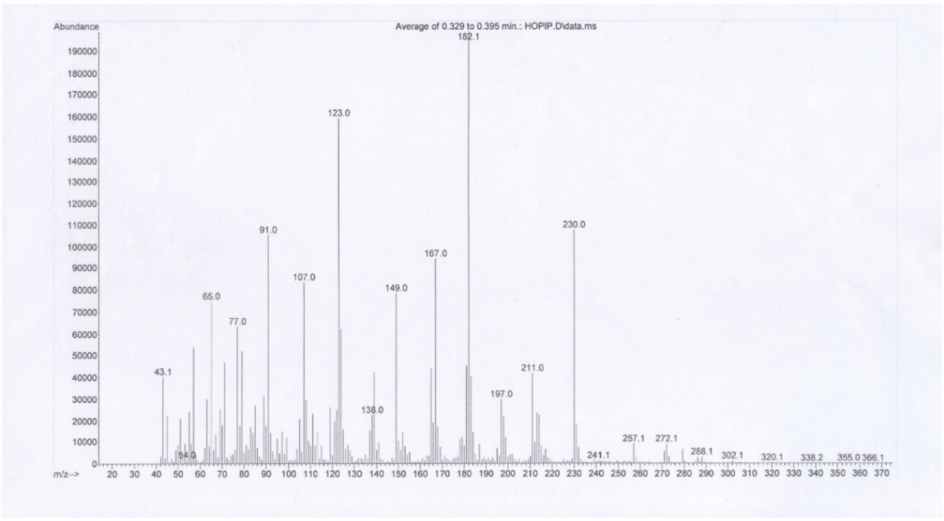

Figure A56 EIMS of **4.17**

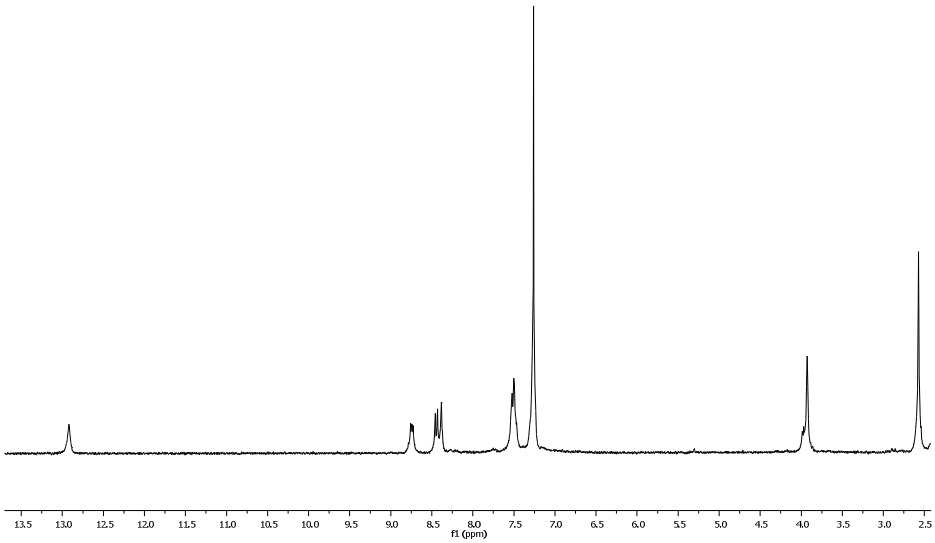

Figure A57 ^{1}H-NMR of **5.1**

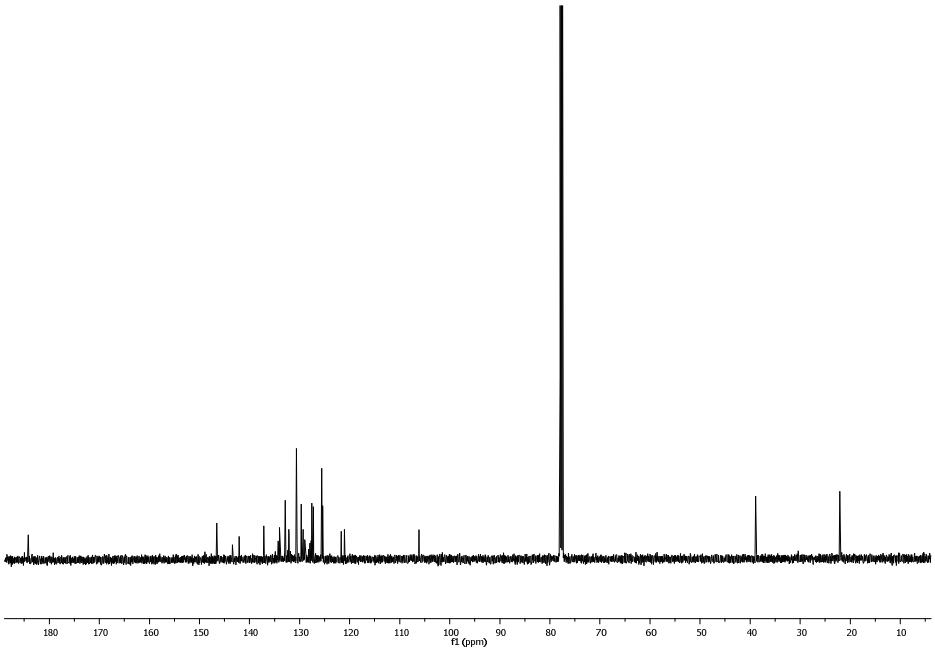

Figure A58 ^{13}C-NMR of **5.1**

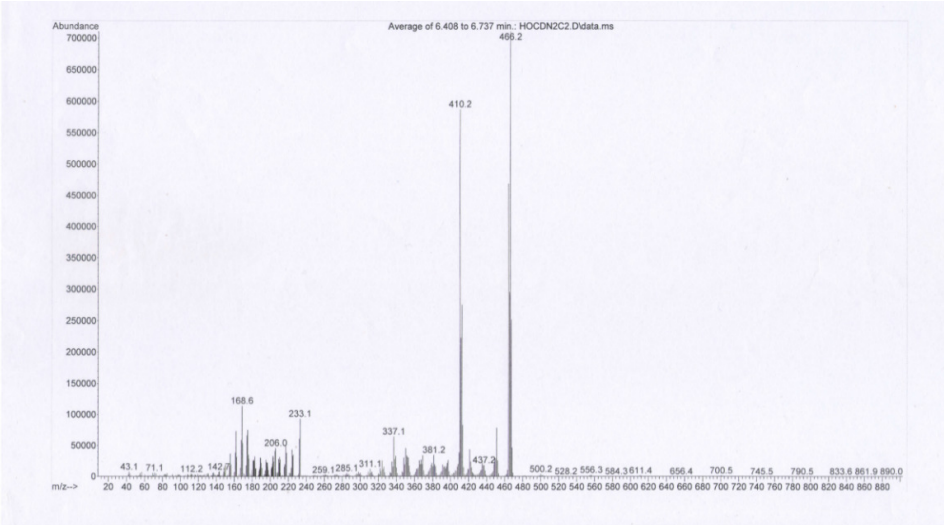

Figure A59 EIMS of **5.1**

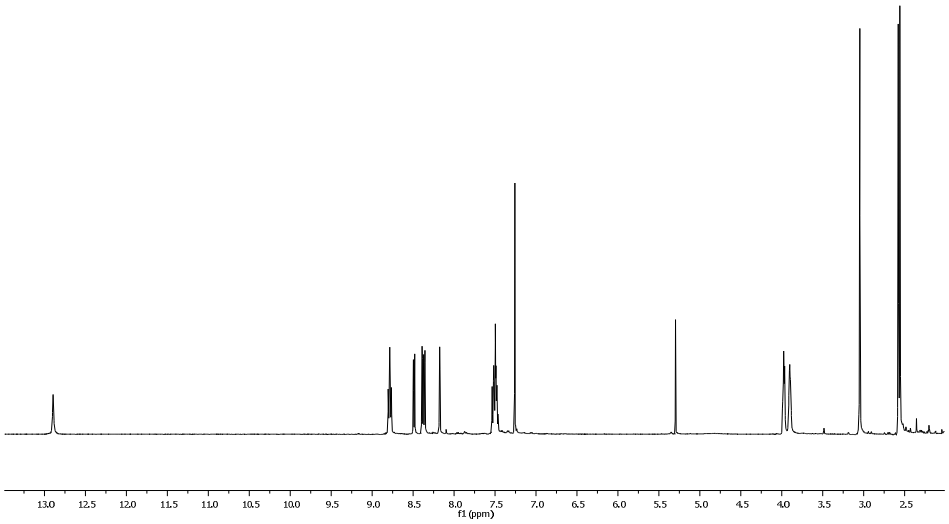

Figure A60 ^{1}H-NMR of **5.2**

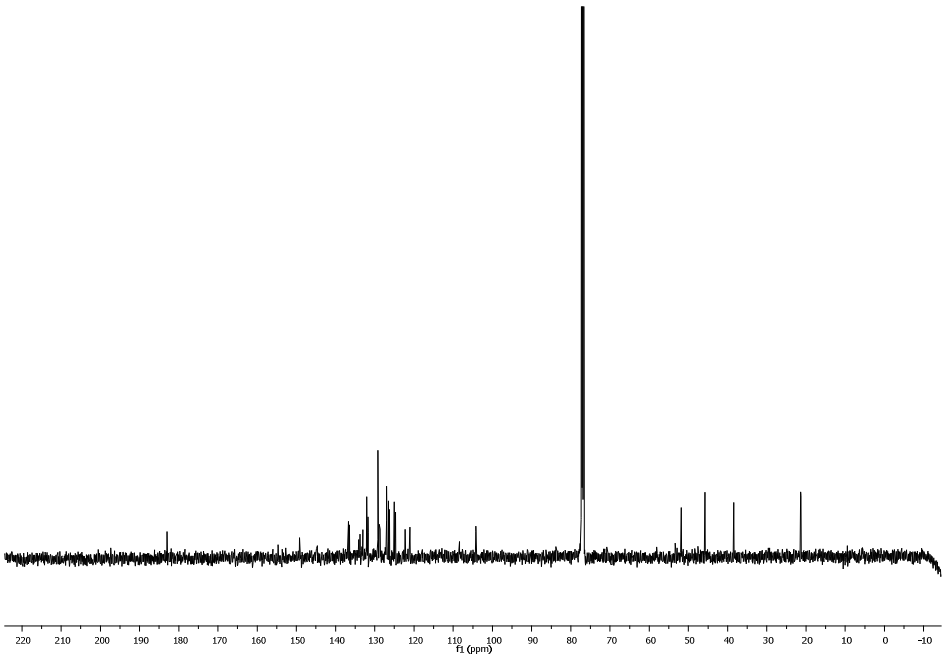

Figure A61 ^{13}C-NMR of **5.2**

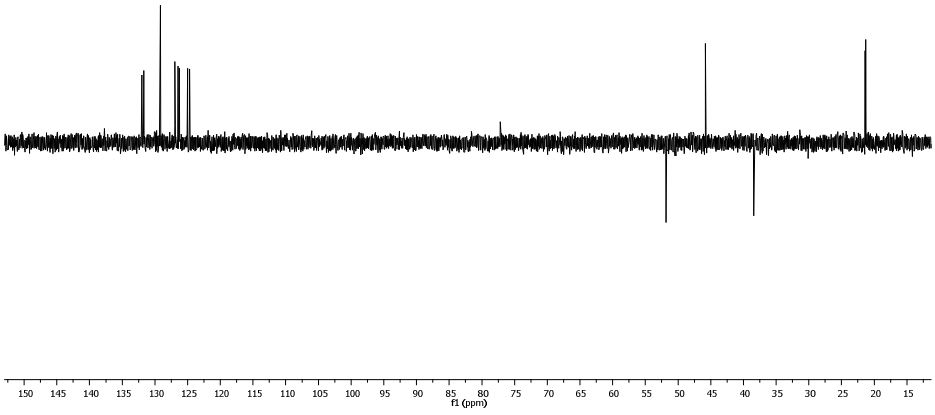

Figure A62 DEPT135-NMR of **5.2**

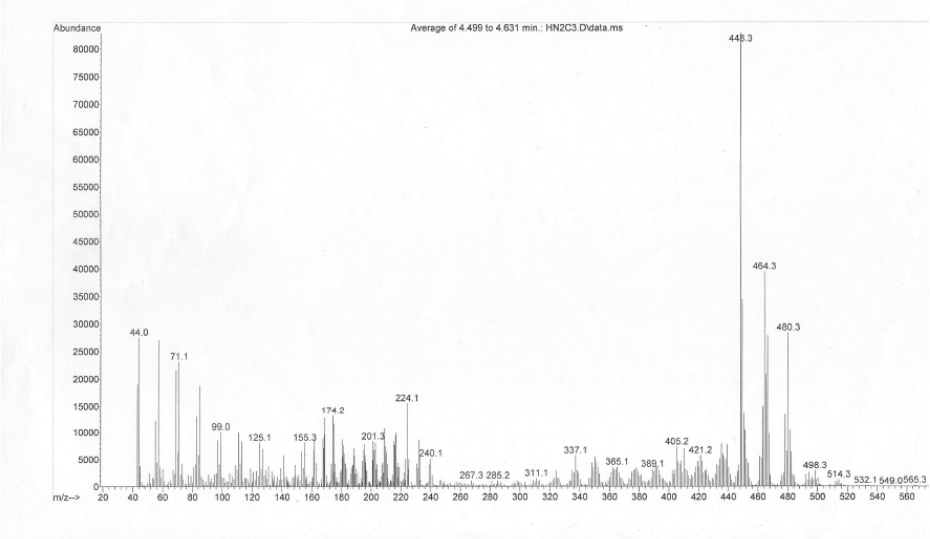

Figure A63 EIMS of **5.2**

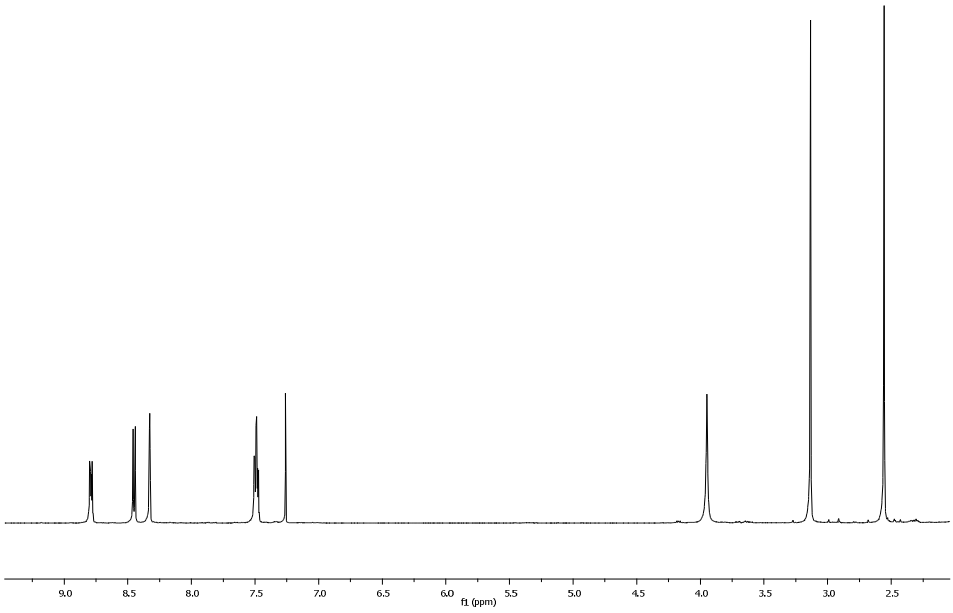

Figure A64 ^{1}H-NMR of **5.3**

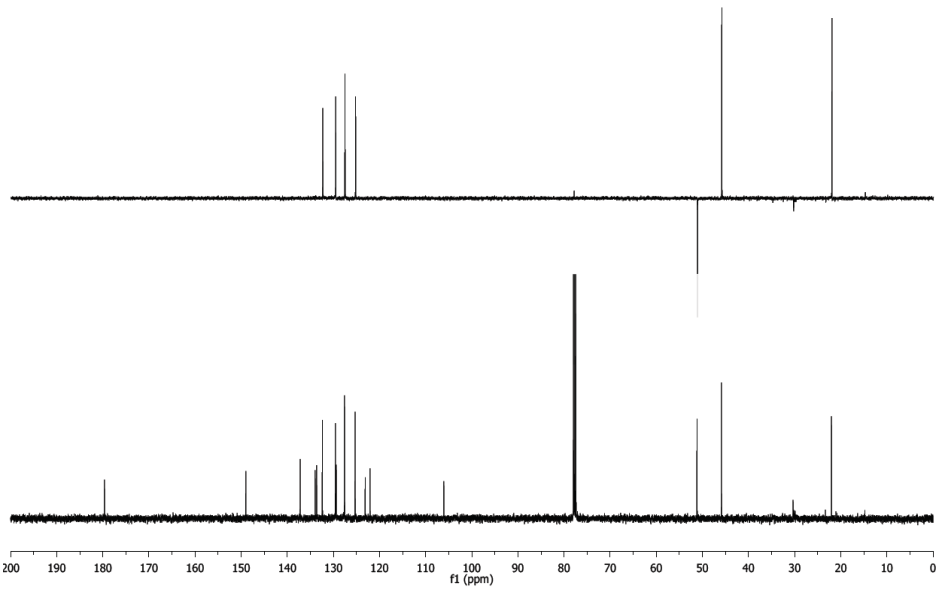

Figure A65 ^{13}C-NMR and DEPT135-NMR of **5.3**

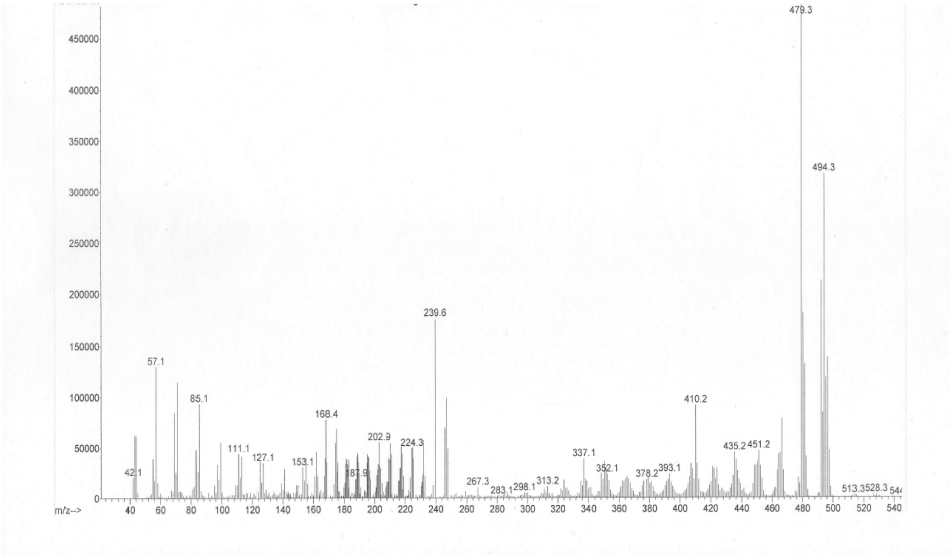

Figure A66 EIMS of **5.3**

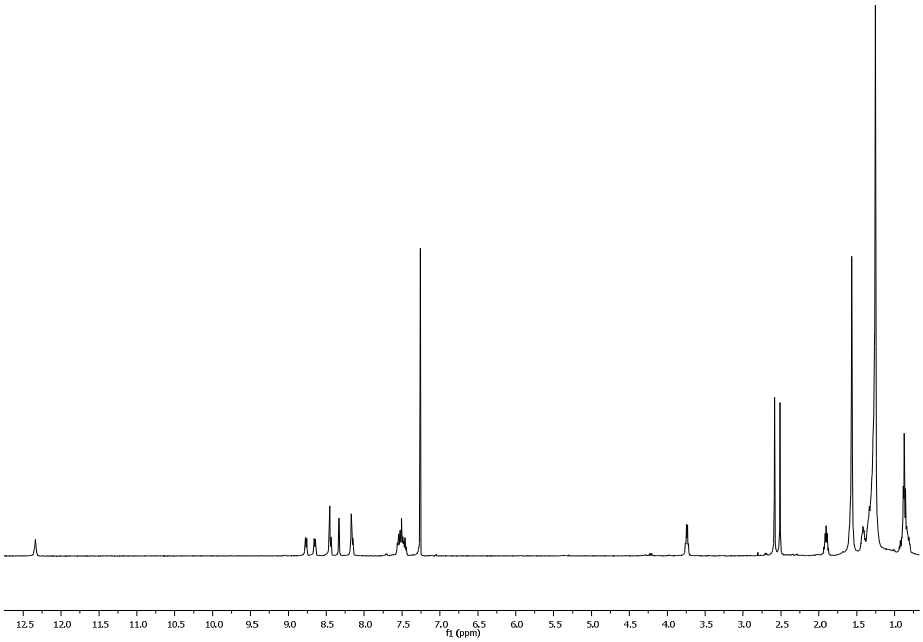

Figure A67 ^{1}H-NMR of **5.4**

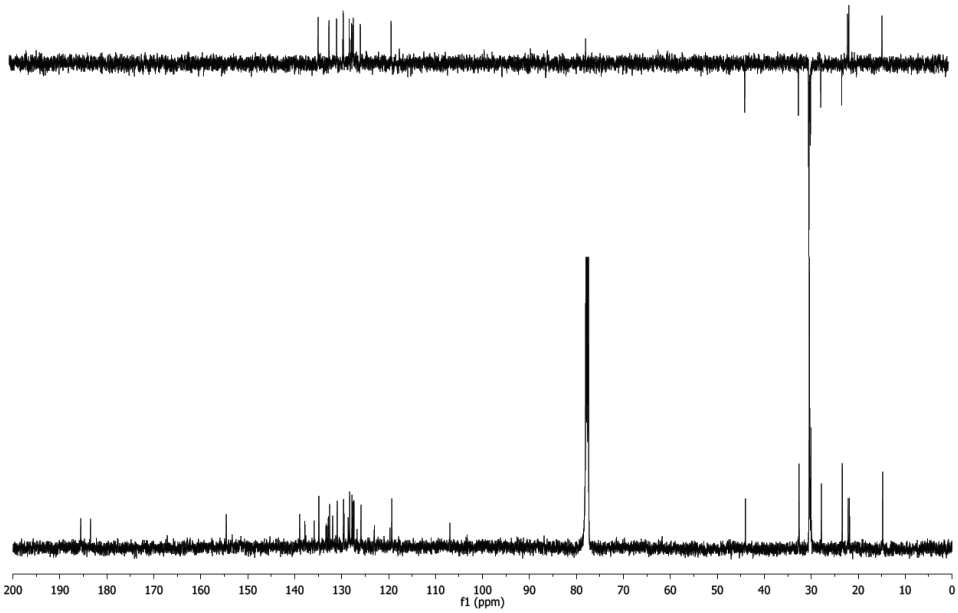

Figure A68 ^{13}C-NMR and DEPT135-NMR of **5.4**

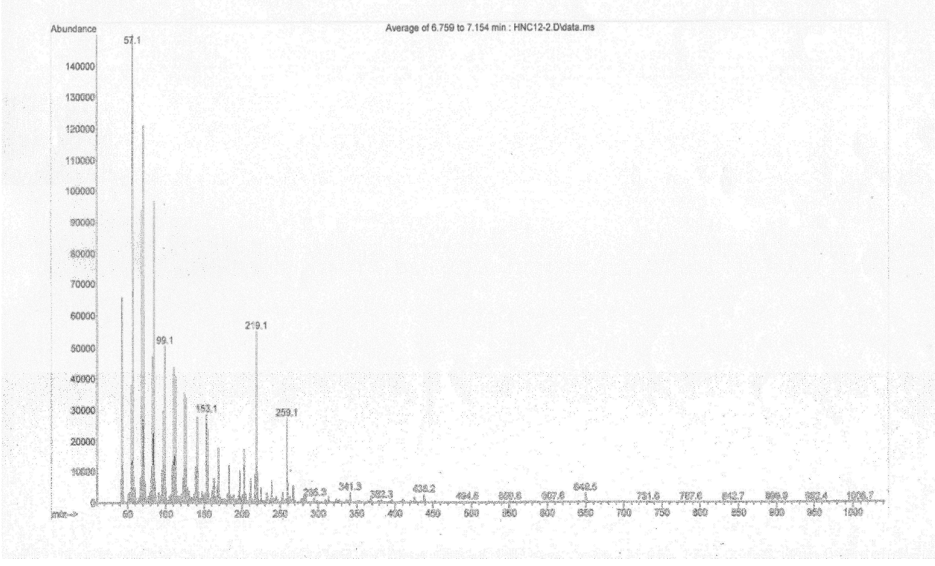

Figure A69 EIMS of **5.4**

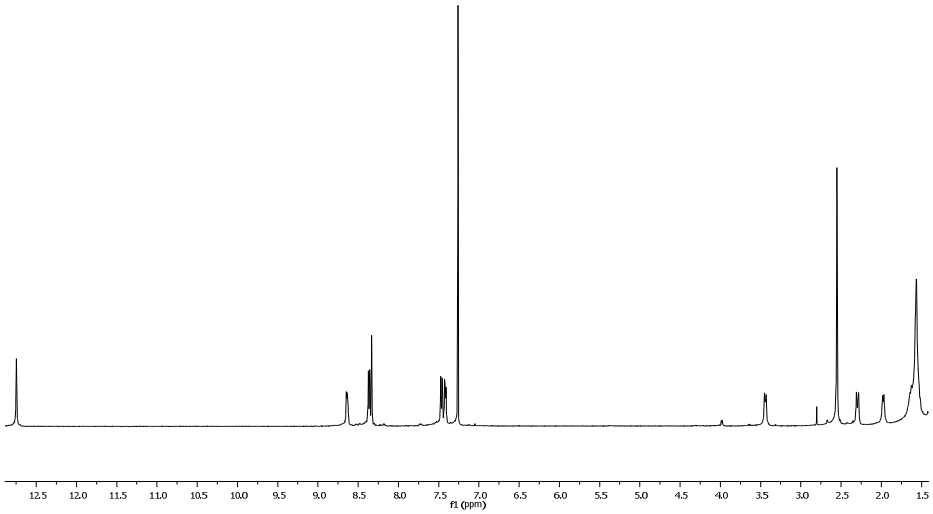

Figure A70 ^{1}H-NMR of **5.5**

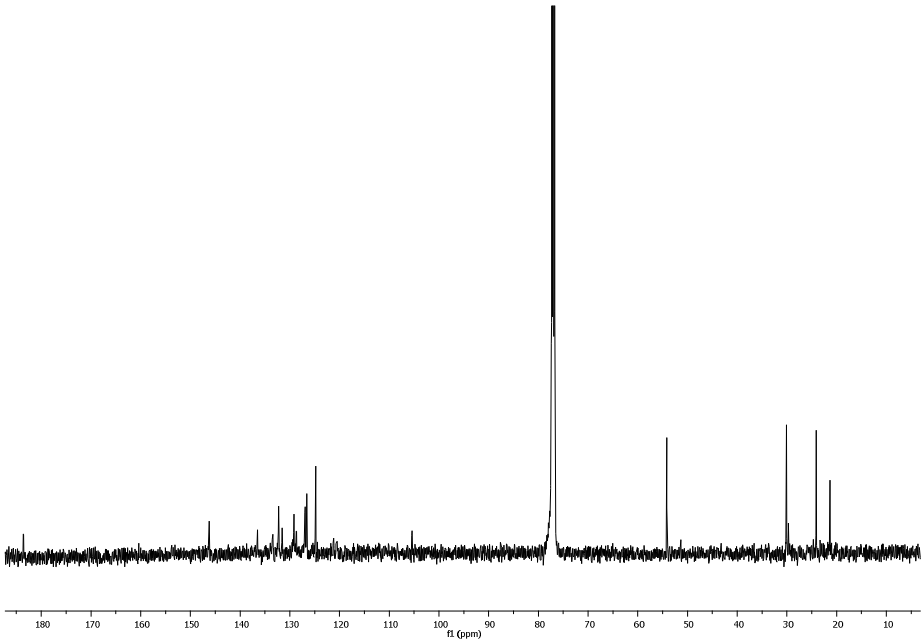

Figure A71 ^{13}C-NMR of **5.5**

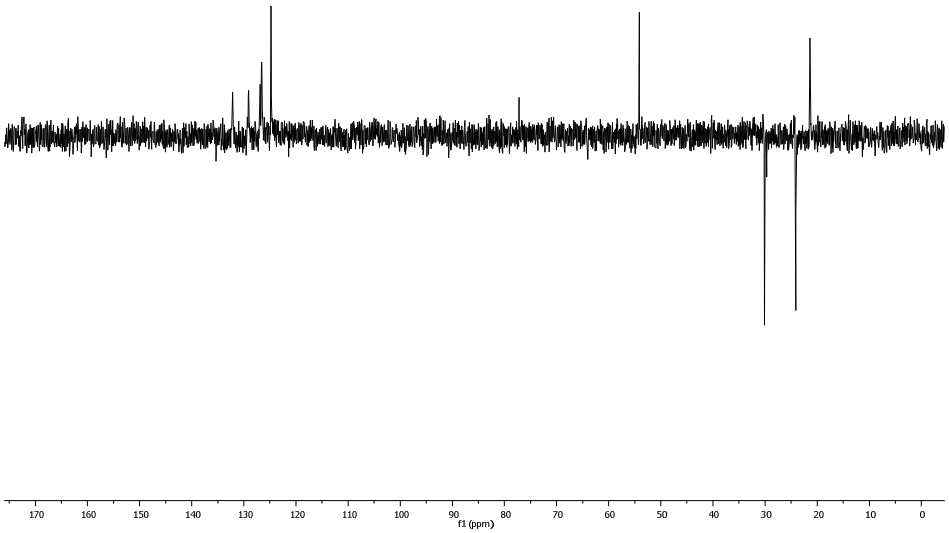

Figure A72 DEPT135-NMR of **5.5**

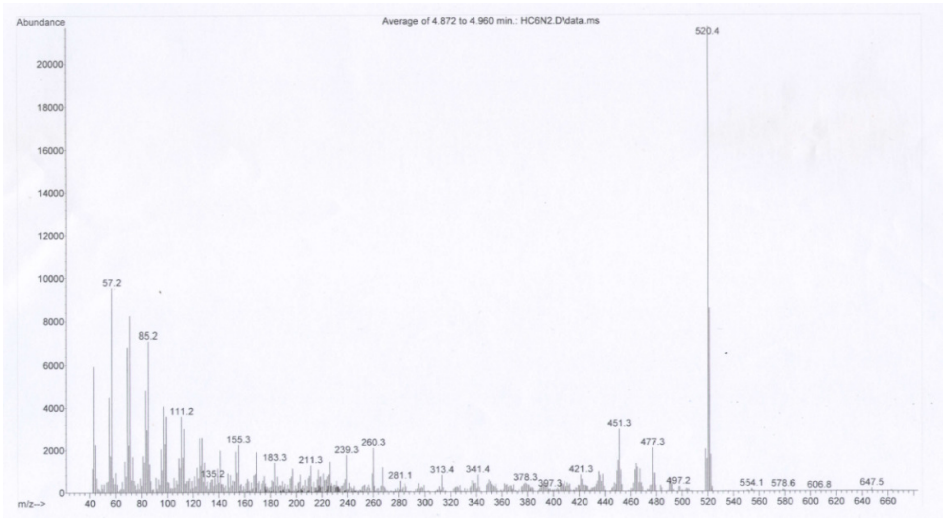

Figure A73 EIMS of **5.5**

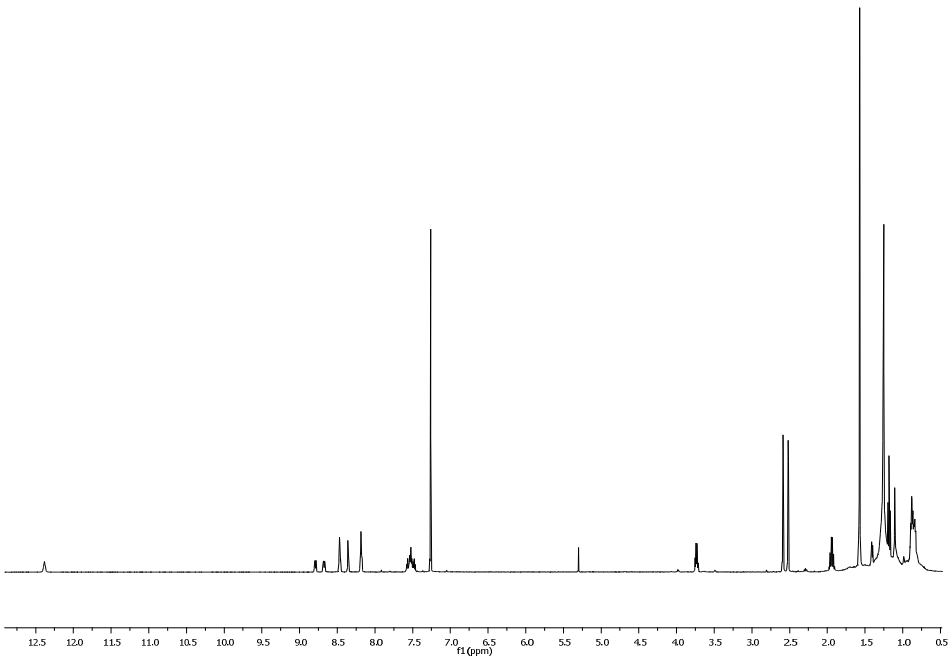

Figure A74 ^{1}H-NMR of **5.6**

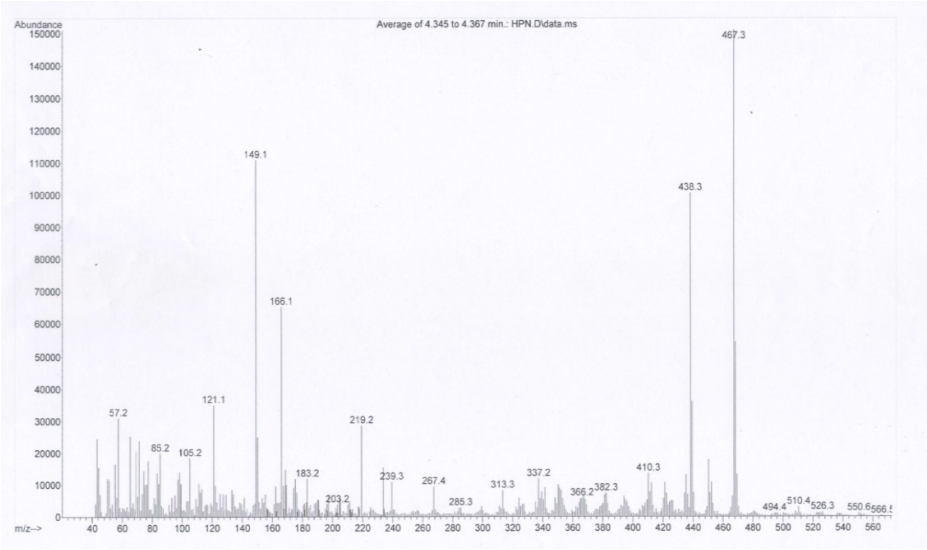

Figure A75 EIMS of **5.6**

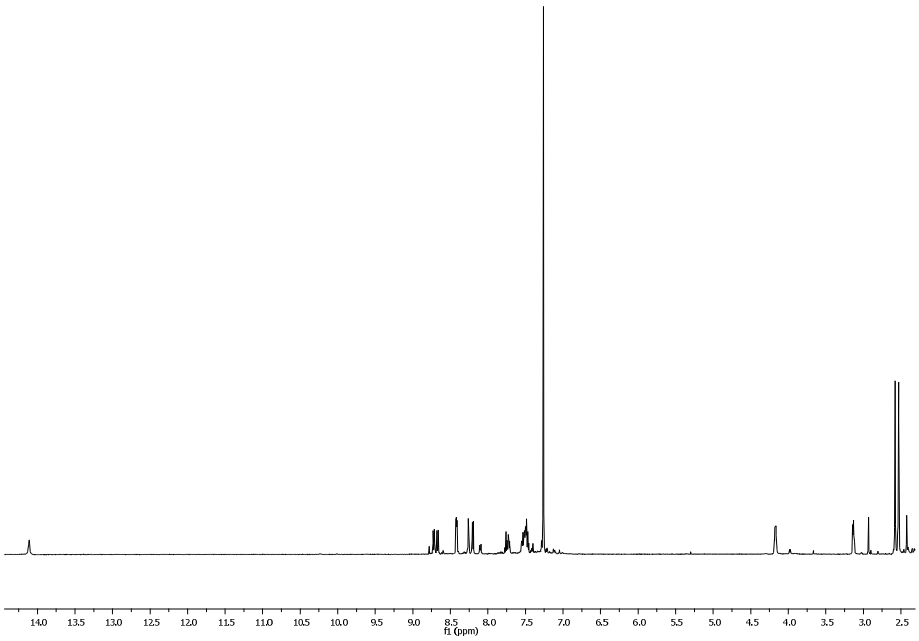

Figure A76 ^{1}H-NMR of **5.7**

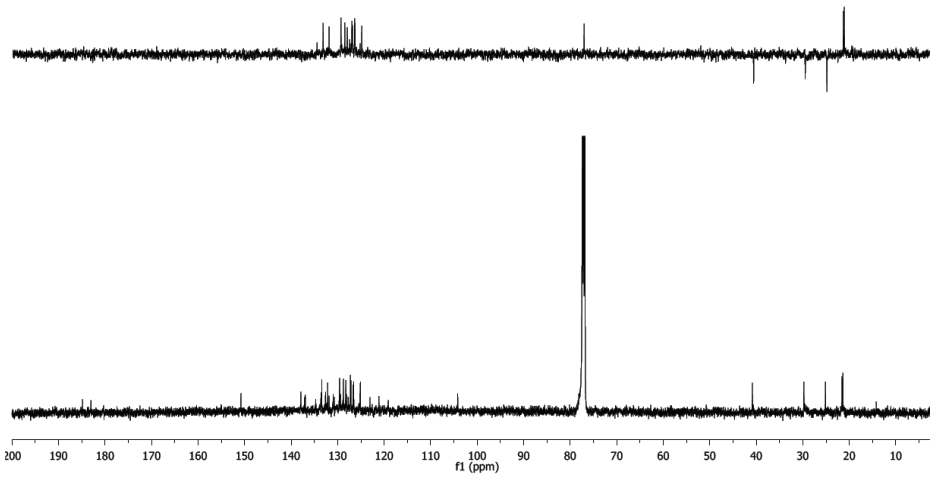

Figure A77 ^{13}C-NMR and DEPT135-NMR of **5.7**

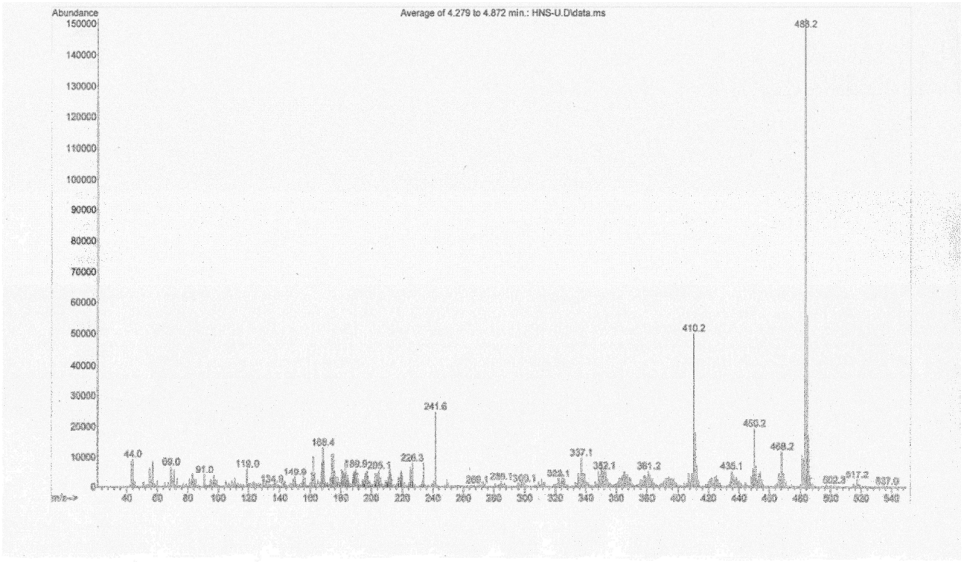

Figure A78 EIMS of **5.7**

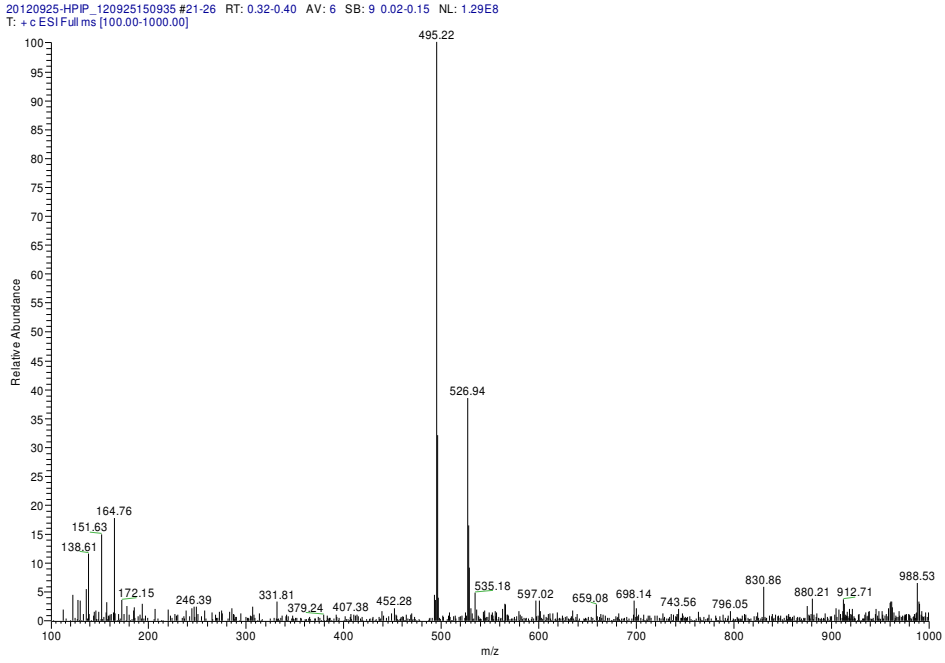

Figure A79 ESIMS (positive mode) of **5.8**

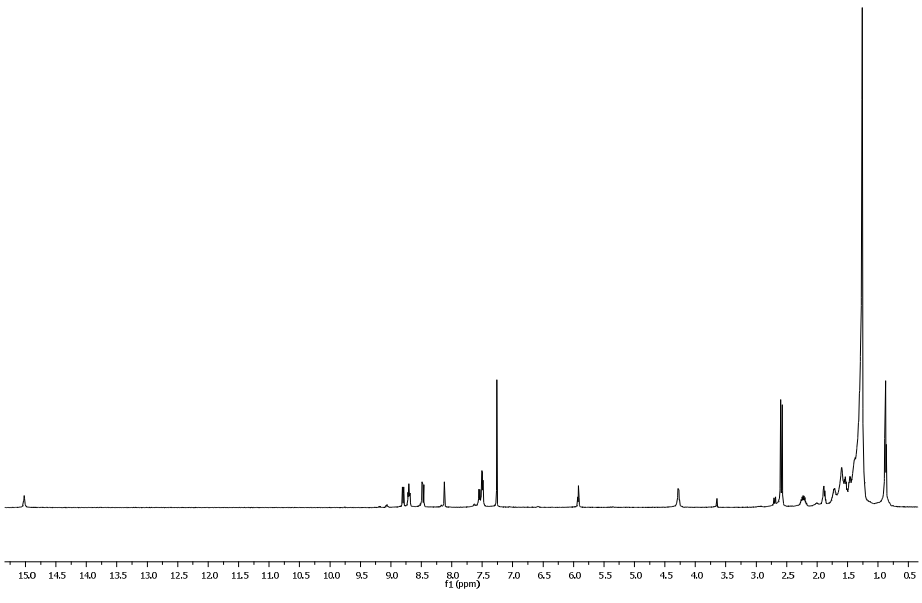

Figure A80 ^{1}H-NMR of **5.9**

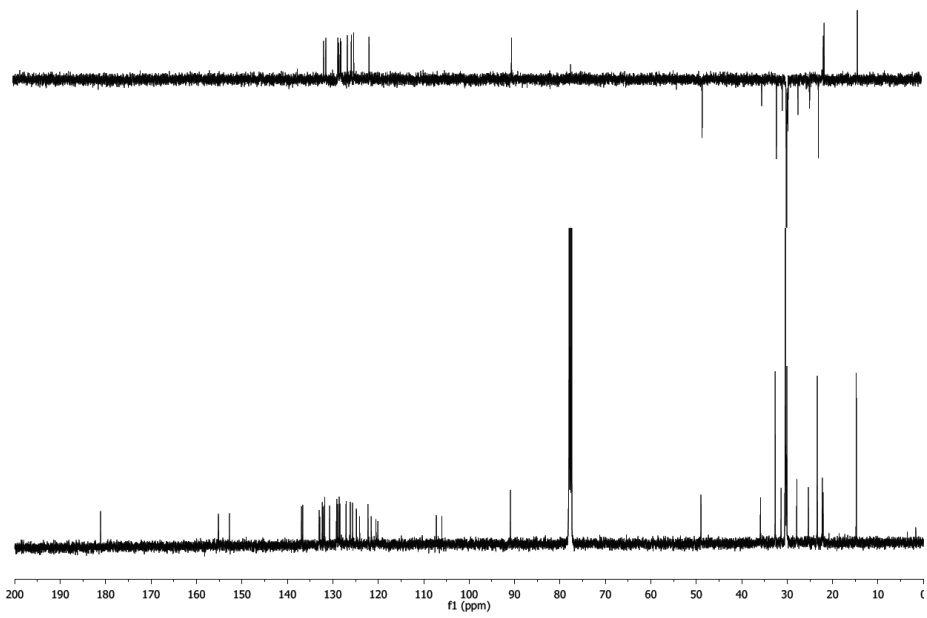

Figure A81 ^{13}C-NMR and DEPT135-NMR of **5.9**

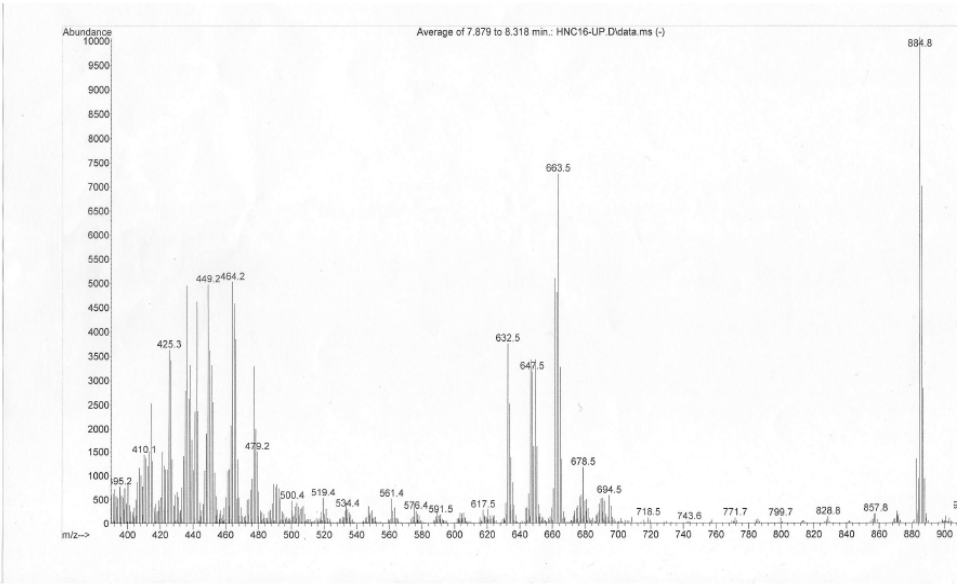

Figure A82 EIMS of **5.9**

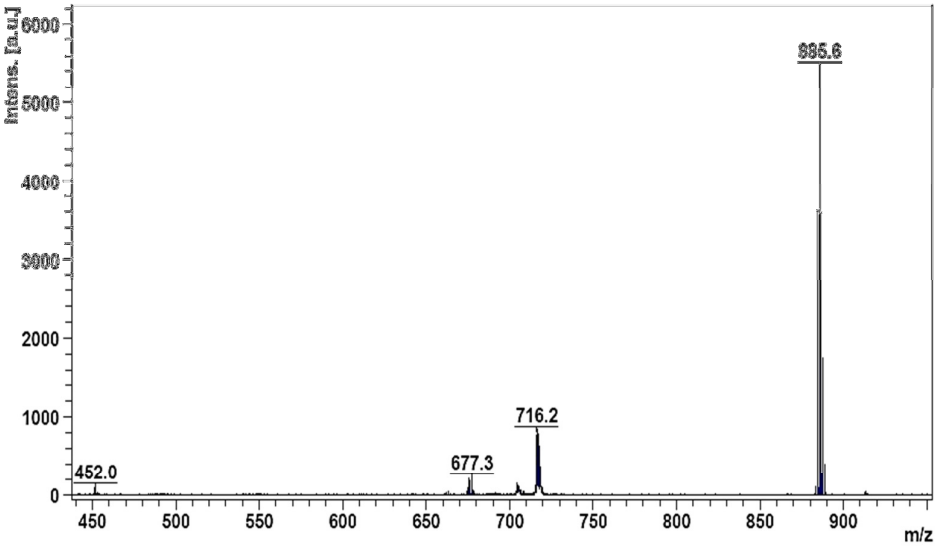

Figure A83 MALDITOF-MS (positive ode) of **5.9**

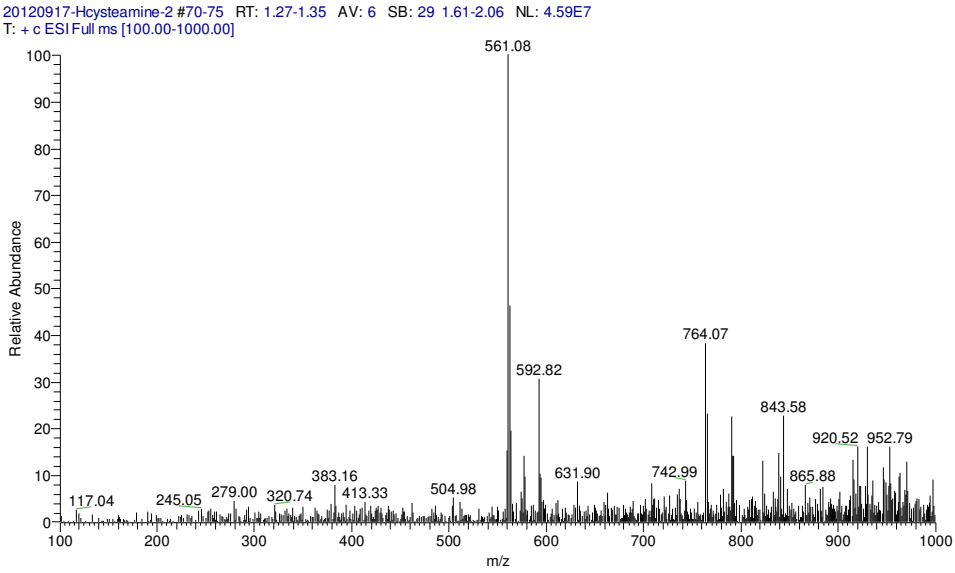

Figure A84 ESIMS (positive mode) of **5.10**